The Dissertation Committee for Mohsen Rezaveisi Certifies that this is the approved version of the following dissertation:

Improvements in Phase Behavior Modeling for Compositional Simulation

Committee:

Kamy Sepehrnoori, Supervisor

Russell T. Johns, Co-Supervisor

Gary A. Pope

Mojdeh Delshad

Kishore K. Mohanty

Improvements in Phase Behavior Modeling for Compositional Simulation

by

Mohsen Rezaveisi, B.E.; M.S.

Dissertation

Presented to the Faculty of the Graduate School of

The University of Texas at Austin

in Partial Fulfillment

of the Requirements

for the Degree of

Doctor of Philosophy

The University of Texas at Austin

May 2015

Dedication

To my family

Acknowledgements

I am extremely grateful to my supervising Professors, Dr. Kamy Sepehrnoori and Dr. Russell T. Johns for their endless support, guidance, inspiration and encouragement throughout these years. I greatly appreciate Dr. Sepehrnoori's brilliant insight and advice and his encouragement for independent thinking that helped me overcome numerous obstacles throughout my research. I am greatly indebted to Dr. Johns for inspiring new ideas, guiding my approach to the research problems, and insightful questions.

I would like to express my deepest gratitude to Dr. Gary A. Pope for countless hours of insightful and instructive discussions. I would have not been able to accomplish my research on capillary equilibrium if it was not for Dr. Pope's advice and guidance. I also deeply appreciate the invaluable comments and feedback from my committee members, Dr. Mojdeh Delshad and Dr. Kishore K. Mohanty. I would also like to thank Dr. Alexander Shapiro for providing his thoughts on some of my questions on capillary equilibrium.

I would like to acknowledge the staff of the Petroleum and Geosystems Engineering Department at The University of Texas at Austin, Dr. Roger Terzian, Tim Guinn, John Cassibry, Frankie Hart, Mary Pettengill, and Glen Baum for their technical and administrative support.

I enjoyed many insightful discussions and feedback from many fellow graduate students and colleagues. In particular, I would like to extend my sincere thanks to Aboulghasem Kazemi Nia Korrani, Saeedeh Mohebbinia, Saeid Khorsandi, Kaveh Ahmadi, Walter Fair, Luiz Schmall, Hamidreza Lashgari, Bahareh Nojabaei, Mojtaba Ghasemi, Reza Ganjdanesh who also provided the fluid model for one of my gas

condensate simulations, and Abdoljalil Varavei. I would also like to thank Alireza Iranshahr and Rustem Zaydullin for answering my questions on CSAT.

I am thankful to my friends Aboulghasem Kazemi Nia Korrani, Javad Behseresht, Saeedeh Mohebbinia, Amir Frooqnia, Amir Kianinejad, Samin Razi Perchikolaee, Walter Fair, Mohammad Rajaei, Rajib Ahsan, Ali Goudarzi, Ali Naderi, Harpreet Singh, Luiz Schmall, Hamidreza Lashgari, Shayan Tavassoli, Mahdi Haddad, Behzad Eftekhari, Morteza Elahi Naraghi, Soheil Ghanbarzadeh, Mohammad Lotfollahi, Ali Abouie, and Alireza Sanaei as well as many other friends that I did not name explicitly for their support and encouragement over the last few years.

I gratefully acknowledge the financial support from Abu Dhabi national oil company, and the member companies of the reservoir simulation joint industry project (RS JIP) at The University of Texas at Austin, and the gas flooding joint industry project at EMS energy institute at Pennsylvania State University.

Improvements in Phase Behavior Modeling for Compositional Simulation

Mohsen Rezaveisi, Ph.D.

The University of Texas at Austin, 2015

Supervisors: Kamy Sepehrnoori

Russell T. Johns

Accurate and reliable phase equilibrium calculations are among the most important issues in compositional reservoir simulation of enhanced oil recovery (EOR) processes especially miscible gas floods. The important challenges in equation of state (EOS)-based compositional simulators are the time-consuming nature of the phase equilibrium calculations, e.g. 30%-50% of the total computational time in the UTCOMP simulator (Chang, 1990), and accuracy as well as robustness of these calculations. Thus, increasing the computational speed and robustness of the phase equilibrium calculations is of utmost importance in IMPEC-type and fully implicit reservoir simulators. Furthermore, most current compositional reservoir simulators ignore the effect of capillary pressure in porous media on the fluid's phase behavior. This assumption may lead to significant errors in performance prediction of tight oil and shale gas reservoirs where the small pore sizes result in very large capillary pressure values.

The "tie-simplex-based (TSB) phase behavior modeling" techniques attempt to speed up phase behavior calculations by skipping stability analysis and preconditioning phase-split calculations. We implemented the compositional space adaptive tabulation (CSAT), a TSB phase behavior modeling method, in UTCOMP and compared the

computational performance of CSAT when used for skipping stability analysis and generating initial estimates for flash calculations, against the standard phase behavior modeling methods in UTCOMP. The results show that the CSAT method as well as a simple heuristic technique, where stability analysis is skipped for single-phase gridblocks surrounded by single phase neighbors, can improve the total computational time by up to 30% compared to the original UTCOMP.

In order to avoid the negative-flash calculations required for adaptive tie-line tabulation during the simulation, a prior set of tie-line tables can be used. We demonstrate that the tie lines from the multiple-mixing-cell (MMC) method are very close to the actual compositional simulation tie lines. Thus, the MMC tie lines were used as prior tie-line tables in three tie-line-based *K*-value simulation methods in order to improve speed and robustness of compositional simulation. Several simulation case studies were performed to compare the computational efficiency of the three MMC-based methods, an extended CSAT method (adaptive *K*-value simulation) and a method based on pure heuristic techniques against the original UTCOMP formulation. The results show that the MMC-based methods and the extended CSAT method can improve the total computational time by up to 50% with acceptable accuracy for the cases studied.

The MMC-based methods, the CSAT method and the heuristic methods were implemented in the natural variable formulation in the fully-implicit General Purpose Adaptive Simulator (GPAS) for speeding up the phase equilibrium calculations. The computational efficiency results for several cases that we studied show that the CSAT method and the MMC-based method improve the computational time of the phase equilibrium calculations by up to 78% in the multi-contact-miscible gas injection cases studied.

Finally, we present a Gibbs free energy analysis of capillary equilibrium and demonstrate that there is a limiting maximum capillary pressure (P_{cmax}) where gas/oil capillary equilibrium is possible and formulate the P_{cmax} limit using the spinodal condition of the phase of smaller pressure in capillary equilibrium. The effect of capillary pressure on phase behavior was implemented in the UTCOMP simulator and several simulation case studies in shale gas and tight oil reservoirs were performed. The simulation results illustrate the effect of capillary pressure on production behavior in shale gas and tight oil reservoirs.

Table of Contents

List of Tables

List of Figures

Chapter 1: Introduction

We first describe the problems that are addressed in this dissertation. We then briefly discuss the detailed objectives of this research. Next, the different chapters in this dissertation are briefly reviewed.

1.1 DESCRIPTION OF THE PROBLEMS

Compositional simulation of enhanced oil recovery (EOR) processes especially gas injection plays a vital role in their performance prediction and design. Compositional simulation of gas injection processes requires coupling of fluid flow equations to thermodynamic phase equilibrium equations. This coupling becomes particularly important when the injected gas and the resident oil develop miscibility upon multiple contacts. Accurate and reliable phase equilibrium calculations are among the most important issues in compositional reservoir simulation especially for miscible gas floods. Current compositional reservoir simulators are designed to use equations of state (EOS) for modeling fluid's phase behavior.

EOSs are a powerful tool for modeling fluids' phase equilibrium in a reservoir simulator because they provide sufficient accuracy, tuning capability, and are rather simple to use. The important challenges posed by EOS-based compositional simulators are the time consuming nature of the phase equilibrium calculations, and accuracy and robustness of these calculations. Millions or even billions of phase equilibrium calculations, i.e. phase stability and phase-split calculations, are performed during a typical reservoir simulation run. A significant fraction of the simulation time is usually spent to perform these calculations, e.g. 30%-50% in UTCOMP (Chang, 1990) which is

implicit in pressure and explicit in composition (IMPEC). These calculations are also most prone to failure due to inadequate initial estimates, convergence to trivial solutions, and calculations close to the phase boundaries or a fluid's critical point. Therefore, it is of utmost importance to develop fast and robust methods and techniques for phase equilibrium calculations.

The standard phase stability test followed by flash calculations (Michelsen, 1982a; 1982b) provides a rather safe method for phase equilibrium calculations. In the standard phase equilibrium calculations procedure, flash calculations are either performed using Gibbs free energy (GFE) minimization (Gautam and Seider, 1979; Trangenstein, 1985; Nichita *et al.*, 2002a; Perschke, 1988; Michelsen, 1982b) or by solving the equations of equality of each component's fugacity in existing phases (Nghiem and Li, 1984; Abhavani and Beamount, 1987; Okuno, 2009). Stability analysis is performed either by finding the values of the tangent plane distance function at its stationary points or by finding the minimum of the tangent plane distance function (Michelsen, 1982a; Trangenstein, 1985; Gautem and Seider, 1979; Perschke, 1988; Chang, 1990; Okuno, 2009).

Increasing the computational speed of phase equilibrium calculations has always been an active research area. The "tie-simplex-based (TSB) phase behavior modeling" techniques attempt to speed up phase behavior calculations by skipping stability analysis and preconditioning phase-split calculations (Voskov and Tchelepi, 2007; 2009a; 2009b; 2009c). The TSB phase behavior modeling is based on parameterization of compositional space in terms of tie lines. The compositional space adaptive tabulation (CSAT) method (Voskov and Tchelepi, 2009a), a TSB method, stores the results of flash calculations in the previous timesteps into a tie-line table and uses them to precondition flash

calculations or to avoid stability analysis in the next timesteps. CSAT is the most promising of the TSB phase equilibrium calculation methods in terms of practicality and computational efficiency. The previous studies on performance of this phase behavior modeling approach were focused on fully implicit reservoir simulators (Voskov and Tchelepi, 2009a; 2009b; 2009c; Iranshahr *et al.*, 2010; Rannou *et al.*, 2013). The computational performance of any phase equilibrium calculations speedup method depends on formulation of the simulator, structure of the code, and the standard phase equilibrium calculations algorithm in the simulator. A comparative study of performance of the TSB phase equilibrium calculations against other methods in general purpose IMPEC-type reservoir simulators is lacking in the literature. Furthermore, investigation of the effect of various parameters of the TSB method is necessary in order to better understand the performance of this method in IMPEC-type reservoir simulators. Moreover, because the TSB approach requires further code development in the current reservoir simulators, it is important to weigh its performance against simpler methods to speed up the phase equilibrium calculations e.g. simple heuristic techniques (Young and Stephenson, 1983; Chang, 1990). This is particularly important in IMPEC-type reservoir simulators because the stability limit (Courant-Friedrichs-Lewy or CFL number) dictates very small timesteps, which results in good phase equilibrium information from the previous timestep.

The tie lines generated in the CSAT method essentially trace the compositional route of the gas injection process. Adaptive tabulation of tie lines in CSAT allows for generating the minimum number of tie-line tables required to approximate the solution to a gas injection problem. However, adaptive tabulation may pose the challenge of possible failure of the required negative flash calculations during tabulation. This is particularly

the case for miscible gas injection where tie-line tabulation has to be performed for near-critical overall compositions. Another challenge with adaptive tabulation is that the solution to the negative flash calculations for a given single-phase overall composition is not necessarily unique. This is because the solution to negative flash calculations is not a physical solution. There are well-documented cases where the tie-line extensions intersect inside the positive compositional space (Ahamdi, 2011) particularly for fluids with bifurcating phase behavior (Ahamdi, 2011; Khorsandi *et al.*, 2014). This is why prior knowledge of the tie lines traversed by the solution of a gas injection problem may translate into valuable information with significant implications for speed and robustness of reservoir simulators (Rezaveisi *et al.*, 2015). Such knowledge of the simulation tie lines for the dispersion-free gas-injection processes can be obtained by use of the method of characteristics (MOC) to obtain the analytical solution (Dindoruk, 1992; Dindoruk *et al.*, 1997; Johns, 1992; Johns and Orr, 1996; Wang and Orr, 1997; Orr, 2007; Ahmadi and Johns, 2011). On the contrary, the solution of actual gas injection processes follows a very complex route due to dispersion, pressure variations, and multi-dimensional flow.

It would be desirable if the solution route of the gas injection process could be determined or approximated before the simulation. We investigate applicability of one variant of the multiple-mixing-cell (MMC) methods that was proposed by Ahmadi and Johns (2011) for such a purpose. This MMC method, originally developed to calculate minimum miscibility pressure (MMP) of a gas injection process, accounts for various levels of mixing of the injected gas and initial oil. For example, infinite contacts correspond to a dispersion-free (infinite Peclet number) process and complete mixing corresponds to only one contact in the MMC method. Ahmadi and Johns (2011) demonstrated that at the limit of infinite number of contacts, the MMC method produces

the key tie lines of the MOC-type gas injection problems. This suggests that application of the tie lines from the MMC method in reservoir simulation may lead to improvements in computational time and robustness of phase equilibrium calculations. We investigate the tie lines from the MMC method and use the MMC tie lines to improve speed and robustness of the TSB method in compositional simulation.

The contribution of phase equilibrium calculations to the total computational time is smaller in fully implicit reservoir simulators compared to the IMPEC-type formulations. Furthermore, even for the same formulation of the simulator this contribution may vary depending on the structure, framework, and complexity of the simulator. The application of the TSB phase equilibrium calculations in fully implicit formulations has been investigated before and very promising performance results have been reported in the literature (Voskov and Tchelepi, 2007; 2009a; 2009b; 2009c; Iranshahr *et al.*, 2010). However, the performance and computational gains from using the TSB methods in fully implicit formulations depends on the standard phase equilibrium calculations algorithm employed in the simulator. It is also important to compare the performance of the original TSB phase equilibrium calculation methods with the improved TSB approach where the MMC tie lines are used. This is because application of the MMC tie lines reduces the possibility of failure of the negative flash calculations during adaptive tabulation. In addition, application of heuristic techniques in fully implicit simulators may also lead to significant improvements in the computational time despite large timesteps. We investigate and compare the performance of these different phase equilibrium calculation methods in the general purpose adaptive simulator, GPAS (Wang *et al.*, 1997), a fully implicit compositional reservoir simulator developed at The University of Texas at Austin.

Current commercial compositional reservoir simulators assume equal pressures for the oil and gas phases in the phase equilibrium calculations. For most conventional reservoirs this assumption is justified because the pore sizes in such reservoirs are on the order of micrometers, which result in small gas/oil capillary pressure values. However, the typical pore sizes for shale gas and tight oil reservoirs are on the order of few nanometers resulting in much larger capillary pressure values (Clarkson *et al.*, 2012; Li *et al.*, 2014b; Javadpour, 2009; Javadpour *et al.*, 2007).

For large gas/oil capillary pressure the properties of each phase, e.g. density and viscosity, must be calculated at its own pressure. Moreover, compositions of the equilibrium phases in the presence of pressure differences across the curved interface are different than the equilibrium compositions without capillary pressure. The phase equilibrium criteria when capillary pressure is included are different from the equilibrium criteria without capillary pressure (Udell, 1982; Firoozabadi, 1999; Tester and Modell, 1997; Shapiro and Stenby, 1997; Shapiro and Stenby, 2001). Furthermore, the traditional stability analysis based on the tangent plane distance criterion (Michelsen, 1982a) cannot be directly applied to the capillary equilibrium problem. A systematic study of the stability and equilibrium concepts across curved interfaces based on the first principles of the classical thermodynamics, in particular based on the GFE analysis, is lacking in the compositional simulation literature.

Few theoretical studies on the capillary equilibrium problem exist in the literature (Shapiro and Stenby, 1997; Shapiro and Stenby, 2001). Prior to this research, the theory of capillary equilibrium has not been applied to the compositional simulation problems in a thermodynamically consistent manner. A particularly important topic related to the capillary equilibrium concept that requires investigation is the capillary condensation

problem in shale gas reservoirs. Several authors investigated the effect of capillary pressure on fluid's phase behavior in tight oil and shale gas reservoirs mostly through standalone flash calculations or black-oil reservoir simulators (Brusilovsky, 1992; Qi *et al.*, 2007; Firincioglu *et al.*, 2012; Nojabaei *et al.*, 2013; Nojabaei *et al.*, 2014; Du and Chu, 2012). However, compositional simulation including the full physics of the problem is required to study the effect of condensation on production behavior. We implement the capillary pressure effects on phase behavior in UTCOMP (Chang, 1990), The University of Texas at Austin's IMPEC-type compositional reservoir simulator for modeling general problems of fluid flow in shale gas and tight oil reservoirs.

1.2 RESEARCH OBJECTIVES

The primary goal of this research is to investigate the performance of various TSB phase equilibrium calculation methods and improve them for better computational speed, accuracy, and robustness in the compositional simulation practice for fully implicit and IMPEC formulations. We also improve compositional simulation when capillary pressure is included in phase equilibrium calculations. The detailed research objectives of this dissertation were to:

1) Study performance of the TSB phase equilibrium calculation methods in UTCOMP as an IMPEC-type compositional reservoir simulator.
2) Compare the computational performance of the TSB phase equilibrium calculation methods with other simpler heuristic techniques in the UTCOMP simulator.
3) Investigate how the performance of the TSB phase equilibrium calculation methods in improving the computational efficiency and robustness depend on the different parameters of the TSB approach.

4) Examine how the MMC tie lines are related to the tie lines obtained during three-dimensional simulation to determine whether the MMC tie lines can be used as prior tie lines in the TSB phase equilibrium calculations.
5) Develop techniques for application of the MMC tie lines in improving speed and robustness of compositional simulation and to improve the traditional TSB phase equilibrium calculation methods through using MMC tie lines as the prior tie lines.
6) Implement the MMC-based phase equilibrium calculation methods in the UTCOMP simulator and to compare the computational performance and robustness of those methods with the traditional TSB phase equilibrium calculation methods.
7) Implement the traditional TSB method and the MMC-based methods of phase equilibrium calculations in GPAS, The University of Texas at Austin's fully implicit compositional reservoir simulator in order to compare their computational performance in fully implicit formulations.
8) Investigate systematically the equilibrium and stability criteria in the presence of curved interfaces using the classical thermodynamics principles and GFE analysis of capillary equilibrium for consistent application in compositional simulation.
9) Implement the effects of capillary pressure on phase behavior in the UTCOMP simulator in order to study the effect of capillary pressure on production performance in tight oil and shale gas reservoirs and to investigate the capillary-equilibrium dominated phenomena such as bubblepoint suppression and capillary condensation.

1.3 DESCRIPTION OF CHAPTERS

Chapter 1 presents an overall introduction to this research, stating the problem and identifying the research objectives.

Chapter 2 provides a background on the topics related to this dissertation. Equilibrium, local stability, and global stability criteria are reviewed. The different formulations of the phase equilibrium calculations and various speedup techniques are discussed. The MMC method and dispersion are also reviewed. The literature related to the capillary equilibrium problem is discussed.

Chapter 3 presents the details of the implementation of the TSB phase equilibrium calculations method in the UTCOMP simulator. The overall computational procedure in UTCOMP and the details of the developed TSB framework are also discussed. Several simulation case studies are performed to compare the computational performance of different heuristic techniques with the TSB method in IMPEC-type simulators.

Chapter 4 investigates applicability of the MMC tie lines for increasing speed and robustness of compositional simulations. First, proximity of the MMC tie lines to the actual three-dimensional simulation tie lines is discussed and demonstrated. Then several techniques for application of the MMC tie lines in compositional simulation are developed and implemented in the UTCOMP simulator. Several simulation case studies are performed to demonstrate the improvements in computational performance and simulation robustness that result from the MMC tie lines.

Chapter 5 discusses the computational efficiency of the TSB and MMC-based phase equilibrium calculation methods in GPAS. The details of the overall computational procedure in GPAS, the natural variable formulation and the phase equilibrium calculations in the natural variable formulation in GPAS are presented. Several

simulation case studies are performed to compare the computational performance of the TSB and MMC-based phase equilibrium calculation methods and two heuristic techniques in GPAS.

Chapter 6 investigates the effect of capillary pressure on phase behavior in compositional reservoir simulators. A GFE analysis of capillary equilibrium criteria is presented. The presence of a limiting maximum capillary pressure where capillary equilibrium is possible is demonstrated. Furthermore, the implementation of capillary pressure effects on phase behavior in the UTCOMP simulator is discussed and several simulation case studies are performed to study the effect of capillary pressure on production behavior in tight gas condensate and tight oil reservoirs.

Chapter 7 summarizes the conclusions of this research and presents several recommendations for future research.

Appendix A presents an introduction to Legendre transforms, which are useful in deriving the various forms of the local stability criteria. Appendix B presents the formulae required for calculation of the GFE and the Helmholtz free energy. Appendix C presents the results of the constant-volume-depletion (CVD) simulations (with and without the effect of capillary pressure on phase behavior) for the two gas condensate fluids that are used in Chapter 6 of this dissertation.

Chapter 2: Background

The goal of this chapter is to provide background on current methods of phase equilibrium calculations in compositional reservoir simulators and the effect of capillary pressure on fluid's phase behavior. We first present the phase equilibrium criteria with and without curved interfaces from the first principles of classical thermodynamics, and then review the literature on traditional stability analysis, phase-split calculations and criteria of thermodynamic stability. Next, different methods of speeding up the phase equilibrium calculations in compositional reservoir simulators are reviewed. Finally, the capillary equilibrium problem in porous media and the related important findings published in the literature are reviewed.

2.1 First and Second Laws of Thermodynamics

Thermodynamics is the study of energy and its transformations, and is built on the first, second, and third laws. These laws are neither proofs nor definitions but are postulates that result from numerous observations that summarize the vast human experience (Firoozabadi, 1999; Tester and Modell, 1997; Michelsen and Mollerup, 2004). The laws exist as postulates because of absence of any contradicting observation. Firoozabadi (1999) presents the five postulates that define the three laws of thermodynamics. The conservation of the system's internal energy denoted by U is postulated as the first law of thermodynamics

$$dU = dQ + dW \ , \tag{2.1}$$

where Q and W represent heat and work, respectively. U is a state function that depends only on a set of state variables and is independent of how we arrive at that particular state while Q and W are not state functions. The second law postulates that a state function

called entropy denoted by *S*, exists such that for a reversible change of state *dS* is given by

$$dS = \frac{dQ_{rev}}{T}, \tag{2.2}$$

where *T* is the absolute temperature and the subscript *rev* designates a reversible process i.e. a process where every intermediate state represents an equilibrium state (Michelsen and Mollerup, 2004). The second law further postulates that the total change in the entropy of the system and surroundings is positive for an irreversible process. For a reversible process the total entropy change of system and surroundings is zero. Since an isolated system does not exchange matter, heat or work with its surroundings, the system's entropy change for any spontaneous process within its boundaries is equal to the total entropy change and thus must be positive. Therefore, for an isolated system the equilibrium state where no spontaneous change of state occurs corresponds to maximum entropy. That is for an isolated system

$$dS \geq 0. \tag{2.3}$$

2.2 EQUILIBRIUM CRITERIA

We first derive the equilibrium criteria in the absence of surface forces and then discuss how the criteria extend to the conditions where curved interfaces exist. The derivations have been presented in many different sources with slight variations in approach. The derivations that follow are adopted from those presented by Michelsen and Mollerup (2004) and Firoozabadi (1999). The fundamental equation for *U* in an open system in the absence of external potential fields is given by

$$U = U\left(S, V, n_1, ..., n_{n_c}, a\right), \tag{2.4}$$

where S is the total entropy, V is the total volume, a is the total surface area of the open system, n_i is the number of moles of component i, and the subscript n_c is the number of components. The differential of U is given by

$$dU = TdS - PdV + \sum_{i=1}^{n_c} \mu_i dn_i + \sigma da\,, \tag{2.5}$$

where P denotes pressure, and μ_i and σ are chemical potential of component i and interfacial tension, respectively. The thermodynamic functions μ_i and σ are defined by

$$\mu_i = (\frac{\partial U}{\partial n_i})_{S,V,n_{j\neq i},a}\,, \tag{2.6}$$

$$\sigma = (\frac{\partial U}{\partial a})_{S,V,n_1,....,n_{n_c}}. \tag{2.7}$$

The σ da term in Eq. (2.5) is the work required to increase the surface area and enters the expression for the dU through the dw term in Eq. (2.1).

At equilibrium the state function S of an isolated system is a maximum for the set of independent variables U, V, n_1,…, n_{nc}. Equivalent equilibrium criteria may be expressed in terms of other independent variables such as T, P, and n_1,…, n_{nc}. Assuming only expansion work and combining the first law, Eq. (2.1) and the second law, Eq. (2.2) for any process we obtain

$$TdS - PdV - dU \geq 0\,. \tag{2.8}$$

The thermodynamic definition for the Gibbs free energy (GFE), denoted by G, is $G = U + PV - TS$. The differential of GFE is given in Eq. (2.9). Combining Eqs. (2.8) and (2.9) results in Eq. (2.10)

$$dG = dU + PdV + VdP - TdS - SdT\,, \tag{2.9}$$
$$dG - VdP + SdT \le 0, \tag{2.10}$$

which shows that a spontaneous change in the state of the isolated system at constant T and P decreases GFE of the system and thus GFE must be a minimum at equilibrium for constant T and P. A similar criterion in terms of the Helmholtz free energy ($A = U - TS$) can be obtained by combining Eqs. (2.11) and (2.8). The equilibrium criterion in terms of Helmholtz free energy is given by Eq. (2.12). Thus, the Helmholtz free energy is a minimum at equilibrium at constant V and T.

$$dA = dU - TdS - SdT\,, \tag{2.11}$$
$$dA + PdV + SdT \le 0. \tag{2.12}$$

To derive the phase equilibrium criteria, we consider an isolated system which consists of several non-reacting phases. Since the system is isolated, the total internal energy, total volume and component mole numbers of the system are fixed i.e. there are n_c+2 constraints on the extensive variables of the system. Assuming the total number of phases is n_p and taking an arbitrary phase α as the reference phase we obtain

$$\sum_{j=1}^{n_p} dU^j = 0 \;\rightarrow\; dU^\alpha = -\sum_{j\neq\alpha} dU^j\,, \tag{2.13}$$
$$\sum_{j=1}^{n_p} dV^j = 0 \;\rightarrow\; dV^\alpha = -\sum_{j\neq\alpha} dV^j\,, \tag{2.14}$$
$$\sum_{j=1}^{n_p} dn_i^j = 0 \;\rightarrow\; dn_i^\alpha = -\sum_{j\neq\alpha} dn_i^j, \qquad i = 1,...,n_c, \tag{2.15}$$

where the subscript i is the component index and the superscript j the phase index. The independent variables are U and V of each phase and mole number of each component in each phase (except phase α) amounting to (n_p-1)(n_c+2) variables. The entropy change of an open system is given by

$$dS = \frac{1}{T} dU + \frac{P}{T} dV - \frac{1}{T} \sum_{i=1}^{n_c} \mu_i dn_i \,. \tag{2.16}$$

since in our isolated system each phase can be considered as an open subsystem, by combining Eq. (2.16) with equilibrium criterion $dS = 0$ we obtain

$$dS = \sum_j \frac{dU^j}{T^j} + \sum_j \frac{P^j}{T^j} dV^j - \sum_j \sum_i \frac{1}{T^j} \mu_i^j dn_i^j = 0. \tag{2.17}$$

Using Eqs. (2.13) through (2.15), we can write Eq. (2.17) in terms of only the independent variables as

$$dS = \sum_{j \neq \alpha} \left(\frac{1}{T^j} - \frac{1}{T^\alpha} \right) dU^j + \sum_{j \neq \alpha} \left(\frac{P^j}{T^j} - \frac{P^\alpha}{T^\alpha} \right) dV^j - \sum_{j \neq \alpha} \sum_i \left(\frac{\mu_i^j}{T^j} - \frac{\mu_i^\alpha}{T^\alpha} \right) dn_i^j = 0. \tag{2.18}$$

Because U^j, V^j, and n_i^j are all independent, in order for the Eq. (2.18) to be satisfied for any variation of the independent variables the coefficients of the independent variations must be zero. In other words, the equilibrium criteria are given by

$$T^j = T^\alpha, \qquad j \neq \alpha, \tag{2.19}$$

$$P^j = P^\alpha, \qquad j \neq \alpha, \tag{2.20}$$

$$\mu_i^j = \mu_i^\alpha, \qquad j \neq \alpha, \text{ and } \quad i = 1, ..., n_c. \tag{2.21}$$

Because the choice of α was arbitrary the above criteria must be valid for all the phases.

We must use the general expression for the internal energy change of an open system in Eq. (2.5) for one (or more) of the equilibrium phases if the equilibrium criteria across curved interfaces are required. Here, we consider an isolated system composed of phase α in equilibrium with a phase β of any shape enclosed by phase α. We consider the interface as part of the bulk phase α (Firoozabadi, 1999). Tester and Modell (1997)

presented another derivation where the interface is considered as the third phase. The final equilibrium criteria are the same with both approaches. We use the internal energy function at constant total entropy, total volume and mole numbers to derive the equilibrium criteria. Firoozabadi (1999) used the Helmholtz free energy to derive the equilibrium criteria. The differential of U of phases α and β treated as open subsystems are given by

$$dU^{\alpha} = T^{\alpha} dS^{\alpha} - P^{\alpha} dV^{\alpha} + \sum_{i=1}^{n_c} \mu_i^{\alpha} dn_i^{\alpha} + \sigma da^{\alpha}, \tag{2.22}$$

$$dU^{\beta} = T^{\beta} dS^{\beta} - P^{\beta} dV^{\beta} + \sum_{i=1}^{n_c} \mu_i^{\beta} dn_i^{\beta} \ . \tag{2.23}$$

The isolated system is constrained by the total entropy, total volume and component mole numbers i.e. Eqs. (2.24) to (2.26)

$$n_i^{\alpha} + n_i^{\beta} = 0, \qquad i = 1, ..., n_c, \tag{2.24}$$

$$V^{\alpha} + V^{\beta} = 0, \tag{2.25}$$

$$S^{\alpha} + S^{\beta} = 0. \tag{2.26}$$

At equilibrium the differential of the internal energy of the isolated system must vanish, thus

$$\begin{aligned} dU &= dU^{\alpha} + dU^{\beta} \\ &= T^{\alpha} dS^{\alpha} - P^{\alpha} dV^{\alpha} + \sum \mu_i^{\alpha} dn_i^{\alpha} + \sigma da^{\alpha} + T^{\beta} dS^{\beta} - P^{\beta} dV^{\beta} + \sum \mu_i^{\beta} dn_i^{\beta} = 0. \end{aligned} \tag{2.27}$$

Using Eqs. (2.24) through (2.26) to express Eq. (2.27) in terms of only the independent variables results in

$$dU = (T^{\alpha} - T^{\beta}) dS^{\alpha} - (P^{\alpha} - P^{\beta}) dV^{\alpha} + \sum_{i=1}^{n_c} (\mu_i^{\alpha} - \mu_i^{\beta}) dn_i^{\alpha} + \sigma da^{\alpha} = 0. \tag{2.28}$$

S^α, V^α, and n_i^α are the independent variables, however the surface area a^α is not independent of V^α (Firoozabadi, 1999; Tester and Modell, 1997). Thus, for Eq. (2.28) to be satisfied for all possible variations of the independent variables the coefficients must be identically zero, which results in the following equilibrium criteria in presence of curved interfaces,

$$T^\alpha = T^\beta, \tag{2.29}$$

$$\mu_i^\alpha = \mu_i^\beta, \qquad i = 1, 2, ...n_c, \tag{2.30}$$

$$P^\beta - P^\alpha = \sigma \frac{da^\alpha}{dV^\alpha}. \tag{2.31}$$

2.3 TRADITIONAL PHASE EQUILIBRIUM CALCULATIONS

Phase equilibrium calculations are performed to determine the number and amount of equilibrium phases and composition of each phase. There are a variety of ways that the problem of phase equilibrium calculations can be stated depending on the specifications of the system under investigation (Michelsen and Mollerup, 2004). The problem of multiphase equilibrium pertinent to compositional reservoir simulation is usually posed as follows: "Given an overall composition vector ($\vec{z}$) and its temperature (T) and pressure (P) what are the number of equilibrium phases and composition and amount (molar fraction) of each phase?" (Chang, 1990; Michelsen 1982a and 1982b; Cao, 2002; Wang *et al.*, 1997; Varavei, 2009; Schmall, 2013). A sequential approach proposed by Michelsen (1982a and 1982b) is usually used to solve this problem: stability analysis followed by flash calculations. The stability analysis determines how many phases exist in equilibrium. Flash calculations determine the amount and composition of each of the equilibrium phases.

Eq. (2.10) is particularly important for multiphase equilibrium calculations in compositional reservoir simulators. It states that a spontaneous change in the state of an isolated system at constant T and P decreases the value of GFE. Thus, at equilibrium the GFE function is at a global minimum with respect to all the possible phase numbers and the component distributions among the phases (Baker *et al.*, 1982; Michelsen, 1982a and 1982b; Perschke, 1988; Chang, 1990). In the previous section, we obtained the equilibrium criteria by imposing the condition that at equilibrium no spontaneous change occurs and thus $dG = 0$. Therefore, the equilibrium criteria given by Eqs. (2.19) through (2.21) or Eqs. (2.29) through (2.31) are only necessary conditions for equilibrium in the absence or presence of curved interfaces. It is possible that more than one solution to Eqs. (2.19) through (2.21) is found for a particular problem. In such cases the true solution is the one that results in a smaller value of GFE. Thus, minimization of GFE is the most fundamental formulation for flash calculations at a given temperature and pressure. In fact, Eq. (2.21) can be derived as a necessary condition for GFE to be a minimum.

2.3.1 Stability Analysis

After the fundamental work of J. W. Gibbs (1878), "On the Equilibrium of Heterogeneous Substances", Baker *et al.* (1982) were the first to systematically investigate the properties of the GFE hypersurface and its implications for multiphase equilibria. Baker *et al.* (1982) state the three requirements that all phase equilibrium solutions must satisfy. First, material balance must be preserved. Second, the chemical potential of each component must be the same in all the phases. Third, the predicted phases at equilibrium must have the lowest possible GFE at the system's temperature and pressure. Based on the GFE analysis of phase equilibrium, they demonstrated different situations where an equation of state (EOS) can predict the incorrect number of phases or

incorrect phase compositions. They suggested that solving a phase equilibrium problem is mathematically equivalent to finding a common tangent hyperplane to the GFE hypersurface. For a stable solution the tangent hyperplane must not be higher than the GFE hypersurface at any point.

Michelsen (1982a) mathematically formulated the tangent plane distance (TPD) criteria and suggested stability analysis as a preliminary step to isothermal flash calculations. Michelsen (1982a) showed that the TPD criterion is the necessary and sufficient condition for stability of a given overall composition ($\vec{z}$) at T and P. The TPD criterion is obtained by comparing the value of GFE of N moles of a homogenous single phase mixture of composition $\vec{z}$ (G^I) with the total GFE where an infinitesimal amount (n moles) of the second phase of composition $\vec{x}$ appears (G^{II}). Taylor series expansion is used to obtain (G^{II}) as follows

$$\begin{aligned} G^{II} &= G(n,T,P) + G(N-n,T,P) = \sum_{i=1}^{n_c} n_i \mu_i(\vec{x},T,P) + G^I - \sum_{i=1}^{n_c} \left(\frac{\partial G}{\partial N_i} \right)_{N_j} n_i \\ &= \sum_{i=1}^{n_c} n_i \mu_i(\vec{x},T,P) + G^I - \sum_{i=1}^{n_c} n_i \mu_i(\vec{z},T,P), \end{aligned} \tag{2.32}$$

$$\Delta G = G^{II} - G^I = \sum_{i=1}^{n_c} n_i [\mu_i(\vec{x},T,P) - \mu_i(\vec{z},T,P)] = n \sum_{i=1}^{n_c} x_i [\mu_i(\vec{x},T,P) - \mu_i(\vec{z},T,P)], \tag{2.33}$$

where n_i is the number of moles of component i in the infinitesimal amount (n moles) of the second phase and N_i is the number of moles of component i in the original mixture. Stability of the original mixture requires that G^I is the global minimum and thus a necessary condition for stability is that $\Delta G > 0$ for all the trial compositions $\vec{x}$. The first term of the summation in Eq. (2.33) is the GFE of the hypothetical single phase of composition $\vec{x}$. The second term is the equation for the tangent hyperplane to the GFE hypersurface at $\vec{z}$. Therefore, from a geometrical point of view, Eq. (2.33) is indeed the

equation of TPD i.e. the distance of the GFE hypersurface at $\vec{x}$ from the tangent hyperplane to the GFE hypersurface at $\vec{z}$ evaluated at $\vec{x}$. The equation for the tangent hyperplane $(T(\vec{x}))$ to the molar GFE hypersurface is obtained by combining Eqs. (2.34) and (2.35). Eq. (2.36) is the tangent hyperplane to the molar GFE hypersurface at a given *T* and *P* and at composition $\vec{z}$ which can be further simplified to obtain Eq. (2.37),

$$T(\vec{x}) = \underline{G}(\vec{z}) + \sum_{i=1}^{n_c-1}\left(\frac{\partial \underline{G}}{\partial x}\right)\Bigg|_{\vec{z}} [x_i - z_i] = \sum_{i=1}^{n_c} z_i \mu_i(\vec{z}) + \sum_{i=1}^{n_c-1}\left(\frac{\partial \underline{G}}{\partial x_i}\right)\Bigg|_{\vec{z}} [x_i - z_i], \tag{2.34}$$

$$\left(\frac{\partial \underline{G}}{\partial x_i}\right)\Bigg|_{\vec{z}} = \mu_i(\vec{z}) - \mu_{n_c}(\vec{z}), \tag{2.35}$$

$$T(\vec{x}) = \sum_{i=1}^{n_c} z_i \mu_i(\vec{z}) + \sum_{i=1}^{n_c-1}\Big(\mu_i(\vec{z}) - \mu_{n_c}(\vec{z})\Big)[x_i - z_i], \tag{2.36}$$

$$T(\vec{x}) = \sum_{i=1}^{n_c} x_i \mu_i(\vec{z}). \tag{2.37}$$

In Eqs. (2.34) and (2.35) $\underline{G}$ is the molar GFE of the mixture and is considered a function of *T*, *P*, and n_c-1 mole fractions. Eq. (2.35) is the expression for the constrained mole fraction derivatives of molar GFE (Firoozabadi, 1999; Tester and Modell, 1997).

Stability analysis is performed either by finding the values of the TPD function at its stationary points or by finding the global minimum of the TPD function. To find a trial composition $\vec{x}$ where the TPD is negative, Michelsen (1982a) solved for the stationary points of the TPD function given by

$$\ln X_i \phi_i(\vec{x}) - \ln z_i \phi_i(\vec{z}) = 0, \qquad i = 1, 2, ..., n_c, \tag{2.38}$$

where

$$X_i = x_i \exp(-k), \tag{2.39}$$

where k is the tangent plane distance and ϕ_i is fugacity coefficient of component i. If the TPD is negative at one of the stationary points the original mixture is unstable. For finding the stationary points, the successive substitution (SS) method combined with second order Newton-like methods may be used (Michelsen, 1982a; Perschke, 1988; Chang, 1990; Okuno, 2009). The alternative approach to answer the global stability question for a given overall composition $\vec{z}$ is to calculate the global minimum of the TPD function constrained to physical compositions (Michelsen, 1982a; Perschke, 1988; Gautem and Seider, 1979; Trangenstein, 1985; Sun and Seider, 1995; Nichita *et al.*, 2002b). Solution techniques for minimization methods are generally second-order convergent in nature (Okuno, 2009; Mohebbinia, 2013).

2.3.2 Flash Calculations

Flash calculations solve for composition and amount of the equilibrium phases after stability analysis has identified the number of equilibrium phases. Flash calculations may be performed using GFE minimization (Trangenstein, 1985; Gautem and Seider, 1979; Nichita *et al.*, 2002a; Perschke, 1988; Michelsen, 1982b) or by applying the equilibrium criteria i.e. equality of chemical potentials of each component in existing phases. The equilibrium criteria in chemical and petroleum engineering applications are usually stated in terms of the thermodynamic function fugacity (f) which is related to chemical potential by (Abott *et al.*, 2001)

$$\mu_i = \Gamma(T) + RT \ln f_i, \tag{2.40}$$

where Γ (T) is a function of temperature and the reference state and R is the universal gas constant. We first consider the flash formulation case where the equilibrium equations are solved. Given an overall composition ($\vec{z}$), temperature T and pressure P, the liquid

composition ($\vec{x}$), gas composition ($\vec{y}$) and liquid and gas molar fractions (l and v) are sought. Thus, for the $2n_c+2$ unknowns, an equal number of independent equations must be chosen. These equations are the equality of fugacity of each component in coexisting phases, the material balance equations and the mole fraction and phase molar fraction constraints given by

$$f_i^l = f_i^v, \qquad i = 1, 2, ..., n_c, \tag{2.41}$$

$$z_i = x_i l + y_i v, \qquad i = 1, 2, ..., n_c, \tag{2.42}$$

$$\sum_{i=1}^{n_c} x_i = 1, \quad \text{or} \quad \sum_{i=1}^{n_c} y_i = 1, \tag{2.43}$$

$$l + v = 1. \tag{2.44}$$

Only n_c+2 of Eqs. (2.42) to (2.44) are independent. A straightforward method of solving these equations is to use K values as the independent variables (Nghiem and Li, 1984; Abhavani and Beamount, 1987; Mohebbinia, 2013). K values are defined as

$$K_i = \frac{y_i}{x_i} \ . \tag{2.45}$$

For a given set of K values one can solve the Rachford-Rice (RR) equation (Rachford and Rice, 1952) given by Eq. (2.46) to obtain l and consequently distribution of components in the equilibrium phases.

$$h(l) = \sum_{i=1}^{n_c} \frac{z_i (K_i - 1)}{1 + l(K_i - 1)} = 0. \tag{2.46}$$

The traditional flash algorithm based on the solution of fugacity equations is the SS method. SS is a robust algorithm and is simple to implement, however, it is linearly convergent and becomes very slow in the near critical region (Michelsen, 1982b). The basic SS algorithm involves solving the RR equation for an initial guess of K values to obtain the phase compositions, calculating the fugacity coefficients (ϕ_i) and updating K values by

$$K_i = \frac{\phi_i^l}{\phi_i^v}, \qquad i = 1, 2, ..., n_c, \tag{2.47}$$

where the superscripts l and v refer to the liquid and gas phases, respectively. Several acceleration methods have been proposed to improve the convergence rate of the SS algorithm. Mehra *et al.* (1983) proposed three algorithms for accelerating the SS method based on analyzing SS as a method of steep descent for energy minimization and choosing an optimal step length. Crowe and Nishio (1975) proposed a general dominant eigenvalue method for promoting the convergence rate of iterative calculations by the SS method. Michelsen (1982b) reported this method as useful for improving computational speed of flash calculations especially in the critical region.

Eqs. (2.41) to (2.45) may also be solved using the Newton method. Newton's method provides faster convergence; however, it requires good initial estimates (Okuno, 2009). This is why the basic SS procedure is commonly used to obtain good initial estimates for higher order methods such as Newton's method. In the Newton method the K values or their logarithms are used as the independent variables and are updated using the Newton step. The primary equations are the equality of fugacity equations, which

means that the Jacobian matrix consists of derivatives of Eqs. (2.41) with respect to the K values.

The solution of the RR equation is also called a constant-K flash. Li and Nghiem (1982) extended the solution of the RR equation to the phase molar fractions that lie outside the physical range. Such flash calculations are called a negative flash. Whitson and Michelsen (1989) showed that the negative flash corresponds to a saddle point in the GFE hypersurface. They identified a window defined by the asymptotes corresponding to the largest and the smallest K values (K_{max} and K_{min}) where the solution to the RR equation results in non-negative phase compositions.

The RR equation shows multiple poles and roots and thus, it is not a trivial task to obtain a robust solution method. Wang and Orr (1997) solved the RR equation for the equilibrium mole fraction of one of the components (x_1) instead of the liquid phase molar fraction in order to improve the convergence of flash calculations in the negative compositional space because x_1 always lies within the physical range regardless of the value of liquid phase molar fraction. Li and Johns (2007) developed a new objective function that provides a smaller convergence window and is near linear inside the window. They showed that the new objective function converges even when performing flash calculations in the near critical region. The method of Li and Johns (2007) is particularly useful for negative flash calculations. Ahmadi (2011) enhanced the Li and Johns (2007) method for a narrower solution window when the overall composition to be flashed lies in the negative compositional space. We used Ahmadi's (2011) enhanced formulation for the negative flash calculations in this dissertation.

Direct minimization of GFE has been widely applied for flash calculations (Gautam and Seider, 1979; Baker *et al.*, 1982; Michelsen, 1982a; Trangenstein, 1985;

Nichita *et al.*, 2002a; Perschke, 1988). The algorithm of Michelsen (1982b) and Perschke *et al.* (1989) based on Newton's method is the standard type of GFE minimization algorithm (Okuno, 2009). Perschke (1988) used a line-search technique with Newton's method in solving the minimization problem. The minimization algorithm is preferred over the Newton method for multiphase equilibria because of the larger number of stationary points of the GFE hypersurface under multiphase equilibrium conditions (Michelsen, 1982b). For the general n_p-phase flash calculations the objective function to be minimized is given by (Chang, 1990)

$$\frac{G}{RT} = \sum_{j=1}^{n_p} \sum_{i=1}^{n_c} n_{ij} \ln f_{ij}, \tag{2.48}$$

$$n_{i1} = N_i - \sum_{j=2}^{n_p} n_{ij}, \qquad i = 1, 2, ..., n_c, \tag{2.49}$$

where n_{ij} and f_{ij} are the number of moles of component i and fugacity of component i in phase j, respectively, and N_i is the total number of moles of component i. The independent variables are n_{ij} for $i = 1, \ldots, n_c$ and for $j = 2, \ldots, n_p$. The necessary conditions for a local minimum are 1) the first order partial derivatives of the objective function with respect to the independent variables must be zero and 2) the Hessian matrix of the objective function must be positive definite. The condition on the first order partial derivatives of the objective function results in the equilibrium constraints given by

$$\frac{\partial}{\partial n_{ij}} \left(\frac{G}{RT} \right) = \ln f_{ij} - \ln f_{i1}, \quad i = 1, ..., n_c \text{ and } j = 2, ..., n_p. \tag{2.50}$$

The Hessian matrix, which is a matrix of the second-order partial derivatives of the objective function, can be obtained analytically. For a three-phase system the Hessian matrix is given by

$$H = \begin{bmatrix} \frac{\partial \ln \overrightarrow{f_1}}{\partial \overrightarrow{n_1}} + \frac{\partial \ln \overrightarrow{f_2}}{\partial \overrightarrow{n_2}} & \frac{\partial \ln \overrightarrow{f_1}}{\partial \overrightarrow{n_1}} \\ \frac{\partial \ln \overrightarrow{f_1}}{\partial \overrightarrow{n_1}} & \frac{\partial \ln \overrightarrow{f_1}}{\partial \overrightarrow{n_1}} + \frac{\partial \ln \overrightarrow{f_3}}{\partial \overrightarrow{n_3}} \end{bmatrix}. \tag{2.51}$$

where the subscript denotes the phase that the vector belongs to. Positive definiteness of the Hessian matrix can be tested by the modified Cholskey decomposition algorithm (Gill and Murray, 1974; Gill *et al.*, 1981; Okuno, 2009). It is important to note that the solution to the above minimization method is a local minimum, and not necessarily the global minimum of GFE.

2.3.3 Local Stability

Local or thermodynamic stability deals with equilibrium states that are stable with respect to physically possible fluctuations. For an isolated system to be at stable equilibrium, the entropy must have a maximum value with respect to any allowed variations. Mathematically, if entropy denoted by *S* is a smoothly varying function of a given set of independent variables, the necessary and sufficient conditions for a maximum in *S* are given by (Tester and Modell, 1997)

$$\delta S = 0, \quad \text{and} \tag{2.52}$$

$$\delta^2 S \leq 0, \quad \text{but if} = 0, \text{ then} \tag{2.53}$$

$$\delta^3 S \leq 0, \quad \text{but if} = 0, \text{ then ..... until } \delta^m S \leq 0, \tag{2.54}$$

where $\delta^m S$ is the lowest order non-vanishing variation of S. The $\delta S = 0$ is the equilibrium criterion stated in terms of entropy. The appropriate inequality from Eqs. (2.53) and (2.54) is the criteria of local or thermodynamic stability. The local stability concept is particularly important when metastable states are involved.

A metastable equilibrium will be destroyed if one perturbs the system e.g. through particles that provide nucleation sites or external disturbances. The limit of local stability also called the spinodal boundary is where the metastable equilibrium ends even in the absence of nucleation sites or external disturbances, and spontaneous homogenous nucleation of a second phase occurs (Tester and Modell, 1997). Therefore, a locally unstable phase cannot physically exist and is not amenable to experimental study (Tester and Modell, 1997). A metastable state can be experimentally achieved or may naturally occur depending on the environment e.g. superheated water.

We note that the stability concept that we discussed in the previous section is a global stability where we investigated if appearance of a second phase of any composition (in the globally possible space) will decrease the GFE of the system (Michelsen, 1982a). This is different from the local stability where we investigate the decrease in the system's GFE with respect to perturbations around the state under investigation. For example, Firoozabadi (1999) in his derivation of the local stability criteria used the Taylor series expansion of the internal energy around the original state to obtain the internal energy of the two hypothetical test phases. A locally stable phase may or may not be (globally) stable with respect to appearance of a second phase. From a physical point of view, nucleation sites such as impurities and rough surface boundaries are always present in porous media and therefore metastable states cannot exist in porous media in the absence of a curved interface (Udell, 1982).

Beegle *et al.* (1974) and Tester and Modell (1997) used the criteria of negativity of the lowest order non-vanishing derivative of S and the properties of the Legendre transforms to obtain the final stability criteria. Firoozabadi (1999) used a different approach to obtain the same criteria. For a general system of n_c components, the necessary and sufficient conditions for local stability are given by (Tester and Modell, 1997)

$$y^{(k-1)}_{(k)(k)} > 0, \qquad k = 1, 2, ..., m-1, \tag{2.55}$$

where $m = n_c + 2$ and n_c is the number of components of the system. The function $y^{(k\text{-}1)}$ is the $(k\text{-}1)$ –th order Legendre transform of the basis function $y^{(0)}$ and the subscript k indicates partial derivatives with respect to the k-th independent variables of $y^{(k\text{-}1)}$. The basis function $y^{(0)}$ can be taken as any of the potential thermodynamic functions of U, S, G, A, and H (enthalpy). The limit of stability (spinodal boundary) is where any of the criteria in Eq. (2.55) is first violated. By use of the properties of the Legendre transforms it is possible to show that if one approaches the limit of stability from an initially stable state then the $y^{(m-2)}_{(m-1)(m-1)}$ is the first to violate the stability criteria (Beegle *et al.*, 1974; Tester and Modell, 1997). Thus, starting from an initially stable state the necessary and sufficient condition for stability is

$$y^{(m-2)}_{(m-1)(m-1)} > 0, \tag{2.56}$$

where $m = n_c + 2$ and the spinodal condition is given by

$$y^{(m-2)}_{(m-1)(m-1)} = 0. \tag{2.57}$$

Eq. (2.57) may be written in terms of any lower order Legendre transforms. An introduction on Legendre transforms is given in Appendix A. A useful relationship between Legendre transforms of different order is given in Eqs. (2.58) and (2.59). Eq. (2.58) is particularly useful when one attempts to express the general local stability criteria in terms of the Helmholtz free energy (the first order Legendre transform of U) or GFE (the second order Legendre transform of U).

$$y_{(m-1)(m-1)}^{(m-2)} = \frac{\eta_i}{\prod_{r=1}^{m-3} y_{(r+1)(r+1)}^{(r)}}, \tag{2.58}$$

$$\eta_i = \begin{vmatrix} y_{(i+1)(i+1)}^{(i)} & y_{(i+1)(i+2)}^{(i)} & \cdots\cdots & y_{(i+1)(m-1)}^{(i)} \\ y_{(i+2)(i+1)}^{(i)} & y_{(i+2)(i+2)}^{(i)} & \cdots\cdots & y_{(i+2)(m-1)}^{(i)} \\ \vdots & \vdots & \vdots & \vdots \\ y_{(m-1)(i+1)}^{(i)} & y_{(m-1)(i+2)}^{(i)} & \cdots\cdots & y_{(m-1)(m-1)}^{(i)} \end{vmatrix}. \tag{2.59}$$

If one approaches the limit of stability from a point inside the stable region then the denominator of Eq. (2.58) remains positive. Thus, the sign of $y_{(m-1)(m-1)}^{(m-2)}$ will be the same as η_i. Therefore, in terms of the i-th order Legendre transform the stability criterion of Eq. (2.56) is

$$\eta_i > 0, \quad \text{where } 0 \le i \le m-2. \tag{2.60}$$

When U as a function of V, S, n_1, …., n_{nc} (the particular order of the independent variables matters) is used as the basis potential function $y^{(0)}$, the stability criteria in terms of the second and the (m-2)-th order Legendre transform of U are given by Eqs. (2.61) and (2.62), respectively (Beegle *et al.*, 1974; Tester and Modell, 1997). Eqs. (2.61) and (2.62) lead to the same results in terms of the limit of stability. However, it is much easier

to apply Eq. (2.61) when using a cubic EOS for the fluid model because the variables that are held constant in the partial derivatives are the ones that we are most experienced with in compositional simulation.

$$\eta_2 = \begin{vmatrix} \left(\frac{\partial^2 G}{\partial n_1^2}\right)_{T,P,n_2,\ldots n_c} & \left(\frac{\partial^2 G}{\partial n_1 \partial n_2}\right)_{T,P,n_3,\ldots n_c} & \ldots\ldots & \left(\frac{\partial^2 G}{\partial n_1 \partial n_{n_c-1}}\right)_{T,P,n_2,\ldots n_c} \\ \left(\frac{\partial^2 G}{\partial n_1 \partial n_2}\right)_{T,P,n_3,\ldots n_c} & \left(\frac{\partial^2 G}{\partial n_2^2}\right)_{T,P,n_1,\ldots n_c} & \ldots\ldots & \left(\frac{\partial^2 G}{\partial n_2 \partial n_{n_c-1}}\right)_{T,P,n_1,\ldots n_c} \\ \vdots & \vdots & \vdots & \vdots \\ \left(\frac{\partial^2 G}{\partial n_1 \partial n_{n_c-1}}\right)_{T,P,n_2,\ldots n_c} & \left(\frac{\partial^2 G}{\partial n_2 \partial n_{n_c-1}}\right)_{T,P,n_1,\ldots n_c} & \ldots\ldots & \left(\frac{\partial^2 G}{\partial n_{n_c-1}^2}\right)_{T,P,n_1,\ldots n_c} \end{vmatrix} > 0, \qquad (2.61)$$

$$y^{(m-2)}_{(m-1)(m-1)} = \left(\frac{\partial \mu_{m-1}}{\partial n_{m-1}}\right)_{T,P,\mu_1,\mu_2,\ldots\ldots,\mu_{m-2},n_{n_c}} > 0\,. \qquad (2.62)$$

We note that in the most general case where knowledge of a previous stable state is not available, i.e. for a given vector of mole numbers, *T*, and *P* without any other information, stability requires that all the *m*-1 criteria in Equation (2.55) be investigated (Tester and Modell, 1997; Heidemann, 1975). In terms of GFE, by successive application of Eq. (2.58) one can show that the necessary and sufficient condition for local stability is that all the principle determinants of η_2 be positive. Of course, in the latter case $y^{(0)}_{(1)(1)}$ and $y^{(1)}_{(2)(2)}$ must also be positive. $y^{(0)}_{(1)(1)}$ is the condition of thermal stability and $y^{(1)}_{(2)(2)}$ is the condition of mechanical stability, which are presumed to be valid in the absence of other information (Heidemann, 1975). Noteworthy, the spinodal condition is also one of the criteria for the critical points (Tester and Modell, 1997; Heidemann, 1975; Firoozabadi,

1999). That is why most of the previous research on the calculation of the spinodal condition can be found in the literature on critical point calculations (Heidemann and Khalil, 1980; Baker and Luks, 1980; Peng and Robinson, 1977). We extensively use the criteria of local stability in Chapter 6 of this dissertation for finding the limit of capillary equilibrium.

2.4 PHASE EQUILIBRIUM CALCULATIONS SPEEDUP

Regardless of the algorithm used, increasing the computational speed of the phase equilibrium calculations has always been an active research area. Part of the research on speeding up the phase equilibrium calculations has been focused on improving the conventional phase equilibrium calculations through employing heuristic methods in reservoir simulators, modifying the traditional algorithms and using fewer number of components (Wang and Stenby, 1994; Young and Stephenson, 1983; Mehra *et al.*, 1983; Crowe and Nishio, 1975; Chang, 1990; Michelsen, 1998; Rasmussen *et al.*, 2006; Pedersen *et al.*, 1985; Egwuenu *et al.*, 2005). Two other main trends in the research on improving the speed of phase equilibrium calculations are using the reduced methods, which solve fewer equations to find the solution to the phase equilibrium problem (Michelsen, 1986; Jensen and Fredenslund, 1987; Hendriks and Van Bergen, 1992; Li and Johns, 2006; Okuno *et al.*, 2010; Okuno, 2009; Mohebbinia *et al.*, 2013; Mohebbinia, 2013; Gorucu and Johns, 2014; Beckner, 2013; Michelsen *et al.*, 2013), and the tie-simplex-based (TSB) phase equilibrium calculations, which use parameterization of compositional space in terms of tie lines (Voskov and Tchelepi, 2007; 2009a; 2009b; 2009c; Iranshahr *et al.*, 2010; 2012; 2013; Fraces *et al.*, 2009; Rannou *et al.*, 2013; Belkadi *et al.*, 2011; Zaydullin *et al.*, 2013; Rezaveisi *et al.*, 2014a; 2015).

Pedersen *et al.* (1985) proposed a characterization method that even with six hydrocarbon fractions produces results possibly as accurate as with 40 components. Their characterization procedure used zero binary interaction coefficients, which is one of the fluid-model's properties that make the reduced method of phase equilibrium calculations more attractive. Egwuenu *et al.* (2005) presented an improved fluid characterization approach where the pseudo-component properties are tuned to the MMP/MME. They showed that a good match of composition profiles and oil recoveries of the unlumped fluid model could be obtained using as few as four components.

Young and Stephenson (1983) proposed a method for reducing the computational time of phase equilibrium calculations in reservoir simulators where with the exception of well gridblocks, stability analysis for a single hydrocarbon phase gridblock is performed only if one of the neighboring gridblocks has two or three hydrocarbon phases. Chang (1990) implemented this heuristic technique in the UTCOMP simulator. Wang and Stenby (1994) proposed a non-iterative approach for speeding up the phase equilibrium calculations. Their approach requires solving only two sets of linear equations based on the phase equilibrium information from the previous timestep to obtain the distribution of component mole numbers. They reported improvements as high as 50% in the computational time with the non-iterative method.

Rasmussen *et al*. (2006) suggested the shadow region method to increase the computational speed of phase equilibrium calculations. The approach tries to avoid performing two sided stability analysis using a "shadow phase." The idea is that performing stability analysis is redundant when the overall composition is far into the single phase region in the previous timestep. Their flash calculation procedure is different from that implemented in UTCOMP. UTCOMP uses sequential stability analysis and

flash calculations but they first perform phase-split calculations. In the shadow method, if the phase-split calculations fail to yield two phases, stability analysis by tangent plane distance minimization is performed. To speed up the flash calculations, for the two-phase region, they correct the initial estimates from the previous timestep and directly proceed to the second order GFE minimization. This strategy for speeding up the flash calculations in the two-phase region is similar to the strategy presented by Michelsen (1998). For the single-phase region inside the shadow phase region, the two-sided stability analysis is abandoned in favor of a one-sided stability analysis. They also use a second order minimization approach from the start. Outside the shadow phase region i.e. far into the single-phase region, any stability analysis is skipped when the overall composition is sufficiently far from the critical point. They presented significant improvements with this method compared to the conventional flash algorithm. The shadow region method as presented by Rasmussen *et al.* (2006) seems to be applicable only for the method of stationary points.

Michelsen (1980) proposed another approach for speeding up flash calculations in the two-phase region in which initial estimates are generated by linearly extrapolating the converged phase compositions of the previous timestep by use of the Jacobian matrix. Rasmussen *et al.* (2006) reported that no significant reduction was found in the computational time using this approach.

For the conventional phase equilibrium calculation methods, regardless of the numerical solution technique, the number of equations required to solve the stability analysis and flash calculation problems directly depends on the number of components (n_c for stability analysis and $n_c \times (n_p\text{-}1)$ for flash calculations). Reduced methods decrease the number of equations needed to be solved for phase equilibrium information by

transforming the variable space. Michelsen (1986) reduced the number of equations to be solved for flash calculations from n_c to three by deriving three reduced parameters. Michelsen's method (1986) assumes zero binary interaction parameters (BIP), which is not always a suitable assumption for compositional reservoir simulation. The method is based on the idea that the fugacity coefficients and compressibility factor from the cubic EOS with Van der Waals mixing rules for the case of zero BIPs can be expressed as a function of only two parameters given by

$$\theta_1 = \sum_{i=1}^{n_c} B_i x_i, \tag{2.63}$$

$$\theta_2 = \sum_{i=1}^{n_c} \sqrt{A_i} x_i, \tag{2.64}$$

where B_i and A_i are the individual component's volume and energy parameters. The third reduced parameter is the molar fraction of one of the phases.

Later research on the reduced method extends to fluid models where one of the components has nonzero BIPs by considering five reduced parameters (Jensen and Fredenslund, 1987). Hendriks and Van Bergen (1992) presented a different reduced method for any number of components with nonzero BIPs using spectral expansion to approximate the BIP matrix. Li and Johns (2006) proposed a two-parameter BIP formula whereby the mixing rule in the equation of state is manipulated so that a flash calculation is a function of only six independent variables regardless of the number of components and the BIP values. The BIPs need to be expressed in terms of a simple quadratic expression in this method. This reduced phase equilibrium calculations method was extended to three-phase flash calculations (Okuno *et al.*, 2010) and four-phase flash calculations (Mohebbinia *et al.*, 2013) and implemented into a compositional reservoir

simulator. Significant speedup and improved robustness were reported especially for a larger number of components and phases (Mohebbinia *et al.*, 2013; Okuno *et al.*, 2010).

Gorucu and Johns (2014) compared eight different reduced methods including the methods based on spectral decomposition and the two-parameter representation of the BIP matrix. They observed that the spectral decomposition methods and its variants are not as fast as the Li and Johns (2006) method and its variants.

Haugen and Beckner (2013) showed that the spectral reduced and conventional phase equilibrium calculation methods can be expressed as a linear transformation of each other and thus, exhibit identical convergence behavior. They reported marginal speedup with this reduced method compared to the highly optimized conventional flash algorithm. Michelsen *et al.* (2013) reported improvements of less than 20% with the spectral decomposition reduced method compared to the conventional flash calculation methods. However, the reduced methods still remain a potential solution to speed up the phase equilibrium calculations and are still an area of active research.

Another attempt to speed up the phase behavior calculations is the tie-simplex-based (TSB) methods proposed by Voskov and Tchelepi (2007; 2009a; 2009b; 2009c). TSB phase behavior modeling is based on parameterization of compositional space in terms of tie lines. Compositional space parameterization (CSP) was inspired by the research on the method of characteristics (MOC) solution of gas injection processes by Orr and co-workers (Dindoruk, 1992; Dindoruk *et al.*, 1997; Johns, 1992; Johns and Orr, 1996; Wang and Orr, 1997; Orr, 2007). The main idea contributing to CSP from MOC is that the solution route in compositional space is determined by structure and properties of tie lines and it can be described using a limited number of key tie lines and the properties of tie lines (Voskov and Tchelepi, 2009a). Although the MOC solutions are under

limiting conditions of dispersion-free, one-dimensional flow of incompressible fluids, the idea of describing real gas injection processes with full degree of complexity in tie-line space seemed plausible. Voskov and Tchelepi (2007) presented a reservoir simulation methodology based on tie-line-based compositional space parameterization and the theoretical background of the parameterization.

The compositional space adaptive tabulation (CSAT) method (Voskov and Tchelepi, 2009a), which falls into the category of TSB methods, stores the results of flash calculations in the previous timesteps into a tie-line table and then uses them to precondition the flash calculations or avoid stability analysis in the next timesteps. When an overall composition is very close to one of the pre-calculated tie lines, the information from that tie line is used. Voskov and Tchelepi (2009a and 2009b) reported significant improvements in the computational time compared to the standard EOS-based compositional simulation. Iranshahr *et al.* (2010) extended the CSAT method to thermal compositional problems and reported an order of magnitude or more improvement in computational efficiency for CSAT compared to that of standard EOS-based reservoir simulation approaches.

Belkadi *et al.* (2011) compared the computational efficiency of the shadow region method and CSAT using a slim-tube simulator at fixed T and P. They also suggested a tie-line distance based approximation (TDBA) method for speeding up flash results in the two-phase region. The TDBA method uses flash results from the previous timestep in the same gridblock. They concluded that the computational time for CSAT increases with the number of tie lines used and the performance of CSAT is highly dependent on the tolerance for tie-line detection and the maximum number of tie lines allowed in the tie-line table. They reported that CSAT with a fixed pre-calculated tie-line table improves

speed as compared with performing flash calculations in all gridblocks, but for small tolerances required for good accuracy the speedup is small. Belkadi *et al.* (2011) reported superior computational efficiency for their TDBA approach using a constant-pressure simulator. Such a simulator may not be applicable to real reservoir problems where pressure changes spatially and with time.

Rannou *et al.* (2013) presented a tie-line-based *K*-value simulation method which employs the CSP concepts including the minimal critical pressure (Voskov and Tchelepi, 2009b) and an interpolation and tabulation framework similar to CSAT. They used the results of one-dimensional simulations to create the initial tie-line tables without performing adaptive tabulation during the simulation. They reported significant improvement in the computational time with good accuracy compared to the conventional simulation technique.

Zaydullin *et al.* (2013) developed an adaptive compositional space parameterization approach where the governing differential equations are cast in the tie-simplex space. The computational efficiency of this EOS-free compositional simulation method was reported to be comparable to that of CSAT. The results of the formulation proposed by Zaydullin *et al.* (2013) is convergent to the EOS-based simulation results as the size of the hypercube of supporting tie-lines and consequently that of the simplexes decreases. This is straightforward to observe as the adaptively created supporting tie lines used in the interpolation are geometrically structured and bound the compositional solution route. We note that the octree data structure used by Zaydullin *et al.* (2013) is highly efficient in finding the simplex to be used for the interpolation. However, with larger number of components (e.g. 20), the required number of supporting tie lines will be significantly larger using the EOS-free formulation. Application of the tie lines from

the multiple-mixing-cell method is potentially helpful in improving the speed and robustness of compositional simulation because we do not expect a significant increase in the number of required tie lines with larger number of components.

Noteworthy, the TSB phase equilibrium calculation methods might also be applicable to the simpler fluid models used in simulation of chemical EOR processes (Lake, 1989; Kianinejad *et al.*, 2015) such as the fluid model used in the four-phase hybrid gas-chemical flood simulator developed by Lashgari *et al.* (2015).

2.5 THE MULTIPLE-MIXING-CELL (MMC) METHOD

The MMC method is a computational method which relies on an EOS description of the reservoir fluid to calculate the minimum miscibility pressure (MMP) of a multi-contact miscible (MCM) gas injection process (Ahmadi and Johns, 2011). A gas injection process is MCM if miscibility is developed in the reservoir after repeated contacts of the injected gas and the initial oil. MMP is defined as the smallest pressure where the gas/oil displacement becomes miscible at a fixed temperature (Ahmadi and Johns, 2011).

Analytical solution of dispersion-free gas-injection processes has been widely used for MMP calculations (Dindoruk, 1992; Dindoruk *et al.*, 1997; Johns, 1992; Johns and Orr, 1996; Wang and Orr, 1997; Orr, 2007; Ahmadi and Johns, 2011; Khorsandi *et al.*, 2014). They considered multiphase transport of an incompressible fluid with constant boundary conditions in porous medium in the absence of dispersion, gravity, and capillary effects. These governing equations result in an eigenvalue problem where the eigenvalues are velocities and the eigenvectors the path directions in compositional space for a given overall composition (Ahmadi and Johns, 2011). Finding the solution involves constructing the composition route that satisfies the velocity constraint, the entropy condition, and the continuity condition among the infinite possible composition paths

(Helfferich and Friedrich, 1981; Johns, 1992; Johns and Orr, 1996; Dindoruk *et al.*, 1997; Orr, 2007; Khorsandi *et al.*, 2014). The key tie lines of the displacement result from the analytical solution, and MMP is defined as the smallest pressure where one of the key tie lines becomes zero length.

MMP calculation using the analytical solution of the dispersion-free gas-injection problem is not a trivial task. Mixing cell or cell to cell methods provide a simpler alternative for MMP calculations. Many authors have proposed various MMC methods for calculating MMP of a gas injection process (Cook *et al.*, 1969; Jaubert *et al.*, 1989; Metcalfe *et al.*, 1973; Pederson *et al.*, 1986; Zhao *et al.*, 2006; Ahmadi and Johns, 2011). In particular, the MMC method of Ahmadi and Johns (2011) is a powerful MMP calculation tool because it can correctly predict miscibility controlled by any cross-over tie line as opposed to single-cell simulation methods, which only predict the correct MMP if miscibility is controlled by the injection gas or initial oil tie lines. Li *et al.* (2014a) extended this MMC method to fluid systems with three hydrocarbon phases. In Ahmadi and Johns' (2011) MMC method, the key tie lines of the displacement are tracked at successively increasing pressures and the MMP is determined by finding the first pressure where one of the key tie lines becomes critical. This MMC method starts by mixing the initial oil and injection gas with a certain mixing ratio in the first contact and performing a PT flash for the resulting overall composition. Then, the equilibrium gas is moved into the next cell to mix with initial oil and the equilibrium oil stays behind to contact the fresh injected gas. Flash calculations are performed for the overall compositions of the second contact and the calculations continue by moving the equilibrium gas ahead of the equilibrium oil to the next contacts. Thus, the MMC method accounts for various levels of mixing of the injection gas and initial oil. For example,

infinite contacts correspond to a dispersion-free process and complete mixing corresponds to only one contact in the MMC method. The MMC tie lines traverse the analytical solution of the dispersion-free gas-injection problem at the limit of infinite number of contacts, thus this method is consistent with the theory of gas injection processes. Therefore, we hypothesize that the MMC tie lines must be very close to the actual simulation tie lines even in presence of non-idealities resulting from dispersion, multi-dimensional flow, heterogeneity, and pressure variations in the reservoir.

2.6 DISPERSION IN COMPOSITIONAL SIMULATION

Physical dispersion is defined as the mixing that occurs during miscible displacements as a result of molecular diffusion, heterogeneity, and mechanical mixing within the pores (Bear, 1972; Lake, 1989). Dispersion results in dilution of the injected fluid at the displacement front and hence degradation of miscibility. Dispersivity (α) is defined as the proportionality constant between the dispersion coefficient and velocity and is usually used to quantify physical dispersion (Adepoju, 2013). Dispersivity is conventionally measured by fitting the solution of the one-dimensional convection-diffusion equation (CDE) to the effluent concentrations of a coreflood (Adepoju *et al.*, 2013; Adepoju, 2013). In order to obtain better performance prediction of gas floods, standard reservoir engineering practice is to approximate the expected physical dispersion resulting from heterogeneity with the numerical dispersion by selecting an optimum number of gridblocks (Haajizadeh *et al.*, 1999 and 2000; Jerauld *et al.*, 2008; Garmeh and Johns, 2010; Adepoju *et al.*, 2013; Adepoju, 2013). The gridblock sizes are adjusted to obtain a cell Peclet number (*Pe*) given by Eq. (2.65) that is equal to physical Peclet number given by Eq. (2.66)

$$Pe\big|_{cell} = \frac{2L}{\Delta x\left(1+\frac{v_i \Delta t}{\Delta x}\right)} \cong 2N_B, \tag{2.65}$$

$$Pe\big|_{physical} = \frac{v_i L}{D_L} = \frac{L}{\alpha_L}, \tag{2.66}$$

where N_B is the number of gridblocks, v_i is the interstitial velocity, Δt is the timestep size, Δx is the gridblock size, L is total length of the linear model, D_L is the longitudinal dispersion coefficient, and α_L is the longitudinal dispersivity.

Numerical dispersion partly results from the truncation error of the finite difference representation of the governing equations and partly from the finite cell sizes that will allow the fluid to move faster than the normal flow (or the analytical solution) would allow (Jessen *et al.*, 2004). Many authors have addressed the effect of numerical dispersion on the performance predictions of reservoir simulators (Stalkup, 1990; Haajizadeh *et al.*, 1999 and 2000; Walsh and Orr, 1990; Jessen *et al.*, 2004; Johns *et al.*, 2002). Stalkup (1990) studied the impact of numerical dispersion on the recovery predictions through numerical sensitivity studies and argued that the most realistic prediction is obtained by extrapolating the oil recovery to gridblock sizes of zero. Johns *et al.* (2002) studied the effect of dispersive mixing on the displacement efficiency and the displacement mechanism of four- and 12-component systems. They found that the rate of increase in the recovery with enrichment above the MME is larger than below the MME at the typical mixing levels of reservoirs.

Jessen *et al.* (2004) introduced the concept of "dispersive distance" as the distance between the dilution line and the critical tie line (or the midpoint of the shortest key tie line) of the composition path calculated from the analytical solution of the dispersion-free gas-injection problem. They demonstrated that the quantitative difference between the oil

recoveries predicted from the coarse-grid numerical simulation and the values from the analytical solution of the dispersion-free gas-injection problem correlate well with the dispersive distance.

In this dissertation we are interested in the effect of dispersion on the solution route and consequently on the tie lines of the numerical simulations of the gas injection processes. Dispersion has been shown to drive the compositional route of the gas injection processes towards the dilution line and thus result in loss of miscibility (Walsh and Orr, 1990; Jessen *et al.*, 2004). Because the solution route is driven towards the dilution line in presence of dispersion, simulation tie lines may initially be close to the tie lines for a few contacts of the MMC method when several different mixing ratios are used. Furthermore, some displacements are rather insensitive to numerical (or physical) dispersion as demonstrated by Jessen *et al.* (2004) and Haajizadeh *et al.* (1999 and 2000) because their dispersive distance is small. In such cases the compositional route of the actual simulation is close to the analytical solution of the gas injection problem and application of the MMC tie lines for approximating the simulation tie lines becomes even more attractive.

We note that in gravity-stable gas injection processes (Kulkarni, 2005; Rezaveisi *et al.*, 2010) where frontal velocities are small and the gravity force is dominant, the physical and numerical dispersion effects are smaller compared to pattern gas floods. The critical velocity required for a gravity-stable flood when the injected and in situ fluids are near miscible, e.g. in near-miscible up-dip gas injection or in gravity-stable surfactant floods, is essential to the success of the EOR process (Kulkarni, 2005; Tavassoli, 2014; Tavassoli *et al.*, 2014). In gravity-stable gas injection and pattern gas floods, the compositional route and thus the tie lines depend on the choice of the relative

permeability function. Multiphase relative permeability is a function of saturation and flow history (Sahni *et al*., 1998; DiCarlo *et al.*, 2000; Kianinejad *et al*., 2014) especially in cyclic processes such as the water-alternating-gas injection as demonstrated by Kianinejad *et al.* (2014).

2.7 CAPILLARY PRESSURE EFFECTS ON PHASE BEHAVIOR

Almost all current commercial compositional general purpose reservoir simulators ignore the effects of capillary pressure on phase behavior. This is because these simulators were designed to model fluid transport and equilibrium in conventional reservoirs where the gas/oil capillary pressure values are small. For example, for a pore radius of 1 μm the value of capillary pressure per unit interfacial tension (IFT), in dynes/cm, is only 0.29 psia from the Laplace equation (for contact angle of zero). On the other hand, for a pore radius of 10 nm the capillary pressure value per unit IFT (in dynes/cm) is 29 psia. Presence of nanopores in shale reservoirs has been verified by techniques such as ultra-high-pressure mercury injection, back-scattered scanning electron microscopy and atomic force microscopy (Javadpour, 2009; Javadpour e*t al.*, 2007; Katsube, 2000). The smallest pore sizes in shale gas reservoirs typically found in the organic matter and clays are often between 2 to 50 nm in diameter (mesopore) or even less than 2 nm (micropore) while the largest pore sizes can be larger than 50 nm in diameter (macropore) (Clarkson *et al.*, 2012; Li *et al.*, 2014b). These small pore sizes are the reason why the capillary pressure effect on phase behavior in shale gas and tight oil reservoirs could be important.

2.7.1 Theory of Capillary Equilibrium

The Kelvin equation is the first attempt to describe dependency of phase behavior on capillary pressure. It relates the vapor pressure of a pure component in presence of a curved interface to the vapor pressure without capillary pressure effects, assuming the vapor phase is an ideal gas and the liquid phase is incompressible. The Kelvin equation for the condition where the liquid phase is the wetting phase is given by

$$P^{\alpha} = P_{vp} \exp(\frac{2\sigma V^{\beta}}{rRT}), \tag{2.67}$$

where P^{α} is the vapor pressure in the presence of capillarity, P_{vp} is vapor pressure without the capillary effect, r is radius of the cylindrical pore, σ is IFT, V^{β} is molar volume of the liquid phase, T is temperature, and R is the universal gas constant. Several different approaches can be used to derive the Kelvin equation (Tester and Modell, 1997; Firoozabadi, 1999; Shapiro and Stenby, 1997; Ruthven, 1984).

Shapiro and Stenby (1997) extended the Kelvin equation to non-ideal multicomponent mixtures and proved that capillary condensation is possible only for the case where the liquid phase is the wetting phase. They note that their generalization of the Kelvin equation is approximate and is valid only in the vicinity of the true dewpoint.

The presence of curved interfaces results in fewer mechanical equilibrium constraints in the capillary equilibrium problem and thus more degrees of freedom (Li, 1994). For the two-phase capillary equilibrium problem the number of degrees of freedom is one more than the degrees of freedom of the phase equilibrium without capillarity. In the most general case, the phase rule for equilibrium in presence of curved interfaces when the curvature of the interface is not very large is given by (Firoozabadi, 1999)

$$F = n_c + 1, \tag{2.68}$$

where F is the number of degrees of freedom and n_c is the number of components. Larger degrees of freedom results from the fact that for an n_p-phase capillary equilibrium system, $n_p - 1$ of the phases require specification of $n_c + 2$ independent intensive variables to determine their intensive state. This is because for $n_p - 1$ of the phases the interface must be counted as part of the bulk phase. When the interface is counted as part of the phase the Gibbs-Duhem theorem is given by (Firoozabadi, 1999)

$$SdT - VdP + ad\sigma + \sum_{i=1}^{n_c} n_i d\mu_i = 0. \tag{2.69}$$

Udell (1982) analyzed the thermodynamics of single-component vapor-liquid equilibria in presence of curved interfaces using the expression for chemical potential of the liquid and vapor phases from the Van der Waals' EOS. Udell (1982) concluded that both the liquid and vapor phases in capillary equilibrium are in a superheated state. Furthermore, the superheated liquid phase, whose intensive state corresponds to a metastable state in the absence of capillary pressure, is unconditionally stable when capillary pressure is imposed.

Shapiro and Stenby (2001) analyzed the capillary equilibrium problem in the space of intensive variables T, P, $\mu_1,\ldots, \mu_{nc}$ and made valuable conclusions on the significance of the spinodal boundary. By use of the phase surface geometry concepts and the local stability criteria they proved that 1) for any phase, capillary equilibrium is possible only between the true equilibrium point and the spinodal point. Therefore, the boundary for capillary equilibrium coincides with the spinodal boundary. 2) The phase of lower pressure is always a metastable phase and the phase of larger pressure is always a

stable phase at their respective pressures. Figure 2-1 from Shapiro and Stenby (2001) demonstrates the above two conclusions in the case of a single-component fluid at a given temperature. In Figure 2-1a, *GG'* is the gas branch of the *V-P* diagram, *E* is the point of true equilibrium, and *EG'* is the metastable section of the gas branch. *L'L* is the liquid branch of the *V-P* diagram and *EL'* is the metastable section of the liquid branch. The *L'G'* branch is the thermodynamically unstable or the locally unstable section of the *V-P* diagram. Points *G'* and *L'* are the spinodal points. Figure 2-1b is obtained from Figure 2-1a through integrating the relation $d\mu = VdP$ at constant temperature. In the absence of capillary pressure, the degree of freedom for a single component system with two phases is one. However, the number of degrees of freedom for the capillary equilibrium problem of a single component fluid is two. Any horizontal line that intersects both the liquid and gas' chemical potential (μ) curves in Figure 2-1b corresponds to a possible capillary equilibrium state. Another important point in Figure 2-1b is that capillary equilibrium is possible for a larger range of capillary pressure when the gas phase is at the lower pressure. This corresponds to a gas-wet system, which is not the case in petroleum reservoirs. Noteworthy, the natural wettability of the rock may be altered by chemical EOR processes such as surfactant/alkali floods (Goudarzi *et al.*, 2015).

2.7.2 Experimental and Modeling Studies

Sigmund *et al.* (1973) performed a theoretical and experimental study of the effect of porous media on phase behavior of binary hydrocarbon systems. The authors concluded that equilibrium compositions and pressures would not be disturbed except for very large values of curvature, which are unlikely in hydrocarbon reservoirs because the very fine pores (if present) will be occupied by the connate water. Sigmund *et al.*'s

(1973) measured dewpoint and bubblepoint pressures were found to be independent of the presence of porous media composed of 30 to 40 US mesh glass-bead packs. On the other hand, Firoozabadi (1999) and Brusilovsky (1992) refer to the experimental study of Trebin and Zadora (1968) where the latter authors reported that the dewpoint pressures of gas condensate mixtures in a porous media can be 10% or 15% higher than those observed in conventional PVT cells.

Brusilovsky (1992) numerically studied the effects of porous media on phase behavior of multicomponent systems and dewpoint and bubblepoint pressures by use of a new EOS designed for better volumetric and vapor-liquid-equilibrium predictions at high pressures. This author concluded that when the surface curvature is increased the bubblepoint pressure decreases and the dewpoint pressure increases; thus, in porous media the bubblepoint and dewpoint are first achieved in the larger and smaller pores, respectively. The author further noted that at high pressures (>20 MPa) the influence of porous media on the bubblepoint and dewpoint pressures is small.

Ping *et al.* (1996) suggested a mathematical model that accounts for capillary pressure and adsorption effects on phase behavior. They showed that capillary pressure and adsorption both increase the dewpoint pressure and their effect becomes more pronounced as the porosity and permeability decrease. These authors suggest that their theory possibly explains the differences in the reported experimental results on the effect of capillary pressure on phase behavior.

Qi *et al.* (2007) proposed a new method for considering the capillary pressure effects and reservoir deformation on gas/oil equilibrium in deep gas condensate reservoirs. They concluded that these two parameters make retrograde condensation appear at higher pressure and consequently, accentuate the formation damage, which

decreases the well production rate faster than usual. In their phase behavior model, they use the vacancy solution multicomponent adsorption model and the single-component Kelvin equation for predicting the dewpoint pressure, which is not necessarily applicable to multicomponent mixtures at high pressure.

Firincioglu *et al.* (2012) extended the phase equilibrium calculations to account for capillary forces using the Peng-Robinson (PR) EOS (Peng and Robinson, 1976). They investigated the relative contribution of capillary and surface Van der Waals forces for three oil samples assuming an initial stable gas bubble. Their results suggest that the surface forces are insignificant compared to the capillary forces for pore sizes larger than 1 nm. The authors also showed that bubblepoint pressure suppression affects the saturated portion of the oil formation volume factor and extends the under saturated portion of the curve.

Nojabaei *et al.* (2013) numerically modeled the capillary pressure effect on phase behavior for several binary mixtures and Bakken reservoir's oil. They investigated the capillary pressure effect on the entire phase diagram as well as on the oil phase's density, viscosity, and interfacial tension. They concluded that the small pores decrease the bubblepoint pressure and either increase or decrease the dewpoint pressure depending on the part of the phase diagram being investigated. These authors further note that a good history match of the gas production rates and flowing bottomhole pressure in the middle Bakken was possible only after adjusting the PVT properties to account for the bubblepoint suppression resulting from the capillary pressure effect on phase behavior.

Nojabaei *et al.* (2014) developed a compositionally-extended black oil model where the black oil data are considered a function of gas content of the oleic phase and the capillary pressure. In their fully implicit variable bubblepoint formulation, the flash

calculations are based on *K* values explicitly calculated from the black oil data and thus are noniterative. Their input fluid data to the black oil simulator are pre-calculated using the PR EOS as a function of pressure at several pore sizes. Interpolation in the pre-calculated table is then performed during the simulation to obtain fluid properties such as IFT, viscosity, formation volume factor, and density for a given pressure and effective pore size. Their novel black oil model was verified against Penn State University's in-house fully-implicit compositional simulator that also included the effect of capillary pressure on phase behavior. Furthermore, the authors showed that the simulated oil recoveries of Bakken reservoir can be 10% larger when the effect of pore size distribution on phase behavior is considered. Even though their formulation is novel and is a major step in considering the capillary pressure effect on phase behavior, a black oil model may not be accurate enough for complex compositional processes.

Du and Chu (2012) adjusted the black oil input PVT tables of several Bakken-reservoir's fluid models to account for the capillary pressure effect on phase behavior. They used the modified black oil PVT data to simulate the effect of capillary pressure on phase behavior by use of a standard reservoir simulator and concluded that high capillary pressure increases production.

Wang *et al.* (2013) developed a tight oil compositional simulator that models the effect of capillary pressure in nanopores on fluid properties using the PR EOS. They used the Leverett *J*-function (Leverett, 1941) as the capillary pressure model. They extended the traditional stability analysis criterion i.e. the TPD to the capillary equilibrium problem, which does not seem applicable. Furthermore, from their description of the phase equilibrium calculations, their simulator appears to only be applicable to tight oil reservoirs; thus, their compositional model is not general.

We implement the capillary pressure effects on phase behavior in the UTCOMP simulator for the general compositional simulation problems including compositional modeling of gas condensate and tight oil reservoirs.

2.7.3 Other Effects of Nanopores on Fluid's Phase Behavior

The effect of confinement on phase behavior of hydrocarbon fluids is still an area of active research. Different authors have presented evidence that the thermodynamic properties such as critical temperature and pressure, density, and surface tension inside the nanoscale (< 10 nm) systems deviate significantly from their values in an unconfined state, as a result of increased influence of pore walls on the molecules, increased interaction of the molecules, and smaller number of molecules present in the pore (Singh *et al.*, 2009; Hamada *et al.*, 2007; Devegowda *et al.*, 2012; Zarragoicoechea and Kuz, 2004; Ortiz *et al.*, 2005; Morishige *et al.*, 1997; Sapmanee, 2011). Devegowda *et al.* (2012) presented a critical review of the previously published research on modeling the changes in critical properties under confinement in nanopores.

Zarragoicoechea and Kuz (2004) derived an equation for the shift in the critical temperature under confinement from a generalized Van der Waals EOS characterized only by the Lennard-Jones size parameter.

Singh *et al.* (2009) conducted grand-canonical transition-matrix Monte Carlo numerical simulations to study thermophysical properties (including critical properties) of methane, ethane, propane, n-butane, and n-octane in slit pores with widths smaller than five nm.

Devegowda *et al.* (2012) extended the numerical simulation data of Singh *et al.* (2009) in two-, four-, and five-nm pores to other hydrocarbons on the basis of their molar mass. Devegowda *et al.* (2012) applied a simple correlation-type model of pore proximity

effect (in sub-10 nm pores) to gas condensate fluids in order to investigate condensate banking, a phenomenon that adversely affects well productivity in conventional reservoirs (Pope *et al.*, 2000; Fevang and Whitson, 1996). These authors concluded that condensate banking in the near-wellbore region is significantly alleviated in low-permeability shale gas reservoirs because of favorable modification of fluid properties under confinement (Sapmanee, 2011; Devegowda *et al.*, 2012).

Ma and Jamili (2014) used the simplified local-density theory of single-component fluids coupled with a modified PR EOS to predict density profiles in confined pores. They showed that the density is greater near the wall than in the center of the pore. These authors used the molecular simulation results of Singh (2009) to validate their model. Li *et al.* (2014b) used their engineering density functional theory (DFT) combined with the PR EOS to study adsorption and phase behavior of pure substances and their mixtures in nanopores and in nanoporous media. They concluded that for pure hydrocarbons in nanopores, heavier components are more susceptible to capillary condensation and hysteresis at lower temperatures and in smaller pores. However, for mixtures, capillary condensation and hysteresis may still occur above the cricondentherm.

Teklu *et al.* (2014) included both the capillary pressure and confinement effect on their standalone phase equilibrium calculations using the PR EOS. In order to model the confinement effect on phase behavior, they used the critical temperature and pressure shifts (ΔT_c and ΔP_c, respectively) given in Eqs. (2.70) and (2.71) based on Singh's (2009) results

$$\Delta T_c = \frac{T_{cb} - T_{cp}}{T_{cb}} = 0.9409 \frac{\sigma_{LJ}}{r_p} - 0.2415 \left(\frac{\sigma_{LJ}}{r_p} \right)^2, \qquad (2.70)$$

$$\Delta P_c = \frac{P_{cb} - P_{cp}}{P_{cb}} = 0.9409 \frac{\sigma_{LJ}}{r_p} - 0.2415 \left(\frac{\sigma_{LJ}}{r_p} \right)^2, \quad (2.71)$$

$$\sigma_{LJ} = 0.244 \sqrt[3]{\frac{T_{cb}}{P_{cb}}}, \quad (2.72)$$

where r_p is the pore throat radius, σ_{LJ} is the collision diameter, and T_c and P_c are critical temperature and pressure, and the additional subscripts *b* and *p* refer to bulk and confined conditions, respectively. The authors concluded that when the confinement effects are included, the bubblepoint decreases significantly, the upper dewpoint increases and the MMP of Bakken oil with pure CO_2 decreases. They further note that the confinement effect on phase behavior for pore radii greater than 20 nm is marginal. Their reported phase envelopes of the Bakken oil with only the capillary pressure effect on phase behavior do not seem to be entirely correct because the phase envelopes at different pore radii must converge at the critical point when only capillary pressure effects are considered.

Shapiro and Stenby (1999) used the potential theory of adsorption to analyze the adsorption of multicomponent mixtures at high pressure. They derived an analytical solution to the thickness of the multicomponent film, which can be regarded as a first order approximation. Al-rub and Datta (1998) attributed the inadequate predictions of the liquids' vapor-pressure reduction in capillaries (especially for radii>1 μm) obtained from the Kelvin equation to the long range surface forces on the liquid. They developed theory that simultaneously accounts for the effects of curvature and the long range surface forces on the vapor pressure. Moreover, the same authors (Al-rub and Datta, 1999) developed a semi-empirical model to account for the effect of long range surface forces on phase equilibrium of mixtures in porous media.

The fluid transport mechanisms in nanoscale pores in shale gas reservoirs are different from the continuum-type flow mechanism, i.e. the Darcy flow, applied in conventional reservoirs. This is because in such small pores the mean free path of the gas molecules is comparable to the size of the pores resulting in high Knudsen-number flow, where continuum-type transport models are not applicable (Javadpour *et al.*, 2007). Gas flow mechanisms in shale gas reservoirs is an area of active research (Javadpour *et al.*, 2007; Singh *et al.*, 2014; Rezaveisi *et al.*, 2014b; Naraghi and Javadpour, 2015). For example, Singh *et al.* (2014) proposed a nonempirical apparent permeability model that applies to gas flow with Knudsen number less than unity. The apparent permeability model can be used in reservoir simulators to account for Knudsen diffusion and slip flow when modeling shale gas reservoirs (Javadpour *et al.*, 2007; Singh *et al.*, 2014; Rezaveisi *et al.*, 2014b; Naraghi and Javadpour, 2015).

In this dissertation we only investigate the effects of capillary pressure on phase equilibrium in nanopores. We assume that the phase behavior can be described by bulk-phase thermodynamics, which is a reasonable assumption for pores larger than about 10 nm. For pore sizes smaller than 10 nm the interaction between the pore wall and the fluid molecules and the effects of surface forces on fluid behavior result in a heterogeneous distribution of molecules in the pores. Thus, the fluid cannot be modeled by the assumption of bulk-phase thermodynamics and other fluid models such as statistical-thermodynamic-based models are needed in pores smaller than about 10 nm (Li *et al.*, 2014b).

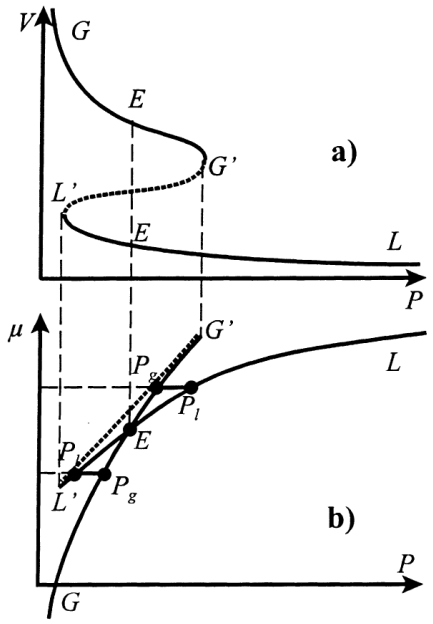

Figure 2-1: Single-component fluid's vapor-liquid equilibrium under the effect of capillary pressure from Shapiro and Stenby (2001) a) *V-P* diagram b) μ-*P* diagram.

Chapter 3: Tie-Simplex-Based (TSB) Phase Behavior Modeling in IMPEC-Type Compositional Reservoir Simulators

The goal of this chapter is to study performance of the TSB phase behavior modeling in IMPEC-type compositional reservoir simulators. We use UTCOMP (Chang, 1990), The University of Texas at Austin's in house IMPEC-type compositional reservoir simulator for that purpose. We first present the overall computational procedure and the phase behavior algorithm in UTCOMP. Then we present the details of the TSB phase behavior modeling algorithm employed in this research and demonstrate how this algorithm fits in the overall computational procedure in UTCOMP. The TSB phase behavior modeling method that we implemented in UTCOMP is compositional space adaptive tabulation (CSAT). Next, we perform several simulation case studies where we compare the computational performance of the standard phase behavior modeling methods in the UTCOMP simulator against that of the TSB phase behavior modeling algorithm.

3.1 COMPUTATIONAL PROCEDURE IN UTCOMP

IMPEC-type reservoir simulators are based on explicit treatment of the saturation and concentration-dependent terms in the discretized form of the governing partial differential equations. This type of formulation is prevalent throughout the petroleum industry. The IMPEC-type simulators are easier to develop than the fully implicit simulators, and they lead to smaller computational intensity over a single timestep. Furthermore, this type of simulator offers a framework where additional physics could be implemented easier than in the fully implicit formulations. The IMPEC-type formulations also in general lead to less numerical dispersion and more accuracy compared to the fully

implicit formulations. The disadvantage of the IMPEC-type simulators is that they are only conditionally stable. Often, this stability limit leads to very small timesteps for problems with large variations of physical properties e.g. for the multi-contact-miscible (MCM) gas injection problems.

In this chapter we use UTCOMP (Chang, 1990) for testing the performance of different phase behavior calculations algorithms.

3.1.1 Overall Computational Procedure in UTCOMP

In UTCOMP the pressure equation is derived on the premise that the pore volume must be equal to the total fluid volume

$$V_t(P,\vec{N}) = V_p(P), \tag{3.1}$$

where V_t is the total fluid volume, V_p is pore volume, P is pressure, and $\vec{N}$ is the vector of component mole numbers. Differentiating Eq. (3.1) with respect to time and expanding the resulting derivatives with respect to their independent variables using the chain rule gives

$$\left(\frac{\partial V_t}{\partial P}\right)_{\vec{N}}\left(\frac{\partial P}{\partial t}\right) + \sum_{i=1}^{n_c+1}\left(\frac{\partial V_t}{\partial N_i}\right)_{P,N_{k(k\neq i)}}\left(\frac{\partial N_i}{\partial t}\right) = \left(\frac{dV_p}{dP}\right)\left(\frac{\partial P}{\partial t}\right), \tag{3.2}$$

where the subscripts i and k denote component index, t is time, n_c is the number of components and $\left(\frac{\partial V_t}{\partial N_i}\right)_{P,N_{k(k\neq i)}}$ is the partial derivative of total fluid volume with respect to number of moles of component i and is denoted by $\overline{V_{ti}}$. The partial derivative of the number of moles of component i with respect to time is obtained from the mass conservation equation given by

$$\frac{\partial N_i}{\partial t} + V_b \vec{\nabla}.\left(\sum_{j=1}^{n_p} \xi_j x_{ij} \overrightarrow{u_j} - \phi \xi_j S_j \overline{\overline{K_{ij}}} \nabla x_{ij} \right) - q_i = 0, \tag{3.3}$$

where V_b is bulk volume of the gridblock, ξ is molar density, $\vec{u}$ is velocity vector, ϕ is porosity, S is saturation, the subscript j denotes phase index, x_{ij} and $\overline{\overline{K_{ij}}}$ are respectively the mole fraction and dispersion tensor of component i in phase j, q_i is molar flow rate of component i (due to the source term), and n_p is the total number of phases. The final form of the pressure equation is given by

$$\begin{aligned} &\left(V_p^0 c_f - \frac{\partial V_t}{\partial P} \right) \left(\frac{\partial P}{\partial t} \right) - V_b \sum_{i=1}^{n_c+1} \overline{V_{ti}} \vec{\nabla}. \sum_{j=1}^{n_p} \overline{\overline{k}} \lambda_{rj} \xi_j x_{ij} \nabla P = \\ &\qquad V_b \sum_{i=1}^{n_c+1} \overline{V_{ti}} \vec{\nabla}. \sum_{j=1}^{n_p} \overline{\overline{k}} \lambda_{rj} \xi_j x_{ij} \left(\nabla P_{c2j} - \gamma_j D \right) + \\ &\qquad V_b \sum_{i=1}^{n_c+1} \overline{V_{ti}} \vec{\nabla}. \sum_{j=1}^{n_p} \phi \xi_j S_j \overline{\overline{K_{ij}}} \nabla x_{ij} + \sum_{i=1}^{n_c+1} \overline{V_{ti}} q_i, \end{aligned} \tag{3.4}$$

where V_p^0 is pore volume of the gridblock at the reference pressure, c_f is the formation compressibility, $\overline{\overline{k}}$ is the permeability tensor, λ_{rj} is the relative mobility of phase j, P_{c2j} is capillary pressure between phase 2 (the reference phase) and phase j, γ is specific weight and D is depth of the gridblock.

Eq. (3.4) is discretized over the simulation grid and solved for pressure. All of the terms are treated explicitly (values from the previous timestep are used) except for pressure. $\overline{V_{ti}}$ is obtained from the thermodynamic equilibrium constraints. After solving the pressure equation, the mass conservation equation, Eq. (3.3), is used to explicitly calculate the total moles of hydrocarbon components and water in each gridblock. Stability analysis and phase-split calculations are then performed in each gridblock to determine the number of equilibrium phases and composition of each phase. Further

details of discretization of the governing equations and the physical model are given in Chang (1990). The overall computational procedure in UTCOMP is summarized in Figure 3-1. UTCOMP is sufficiently flexible to enable modeling of various EOR processes. For example, Korrani *et al.* (2014) coupled UTCOMP with IPhreeqc known as a comprehensive geochemical package (Charlton and Parkhurst, 2011), towards a multiphase reactive-transport simulator that enables mechanistic modeling of low-salinity waterflooding in UTCOMP.

It is worth to note that the phase equilibrium calculations are not coupled with the other calculations in the simulator e.g. pressure matrix calculations. Therefore, modifying the existing phase equilibrium calculation methods in UTCOMP is straightforward.

3.1.2 Phase Behavior Computations in UTCOMP

A sequential procedure is used for the phase equilibrium calculations in UTCOMP. Phase stability analysis is first performed for the overall composition of the gridblock. A two-phase flash calculation is performed if stability analysis indicates unstable mixture. A further stability analysis is performed for one of the resulting phases of the two-phase flash to determine whether a three-phase flash calculation is required. Several methods of phase stability analysis and flash calculations have been implemented in UTCOMP. The stationary point location method using a combination of successive substitution (SS) and Newton methods is one of the stability analysis options in UTCOMP. The other phase stability analysis method in UTCOMP is minimization of Gibbs free energy (GFE) with respect to the trial phase composition. There are also two phase-split calculation methods in UTCOMP. The first one uses only accelerated successive substitution (ASS) to solve the equality of fugacity equations. The second one combines a GFE minimization algorithm with the ASS.

During simulation of MCM gas floods, it is possible that overall mole fraction of a component becomes zero in some gridblocks. To avoid singularity problems in the phase equilibrium calculations, the components with the overall mole fraction smaller than a pre-specified value (e.g. 10^{-12}) are excluded from the phase equilibrium calculations. This step slightly adds to the number of operations in UTCOMP as the fluid properties of the excluded components should also be excluded from the fluid properties arrays.

In a compositional reservoir simulator the results of the phase equilibrium calculations in the previous timestep can be utilized to initialize the calculations of the next timestep. In IMPEC-type reservoir simulators the timesteps are inherently small and thus the phase-equilibrium results of the previous timestep provide very good information for equilibrium calculations of the next timestep. There are two simple heuristic methods in UTCOMP for improving the speed and robustness of phase equilibrium calculations solely from equilibrium information of the previous timestep.

The first heuristic method in UTCOMP is to use the results of flash calculations in the previous timestep in a given gridblock to skip stability analysis and also as initial estimates of equilibrium ratios (*K* values) for the flash calculation at the next timestep for the same gridblock (Chang, 1990). This method is applicable only if a gridblock had two phases in the previous timestep. This is particularly effective in an IMPEC-type simulator where timesteps are inherently small and compositions do not change rapidly over a timestep. Two conditions must be satisfied before the *K* values from previous flash results are used (Perschke, 1988). The first condition checks whether a physically meaningful solution to the Rachford-Rice (RR) equation (Rachford and Rice, 1952) exists and is given by

$$\sum_{i=1}^{n_c} z_i^{n+1} K_i^n \geq 1 \text{ and } \sum_{i=1}^{n_c} \frac{z_i^{n+1}}{K_i^n} \geq 1, \tag{3.5}$$

where z_i^{n+1} is the overall mole fraction of component *i* in the next timestep and K_i^n is the equilibrium ratio of component *i* resulting from flash calculations in the previous timestep. The second condition is that the GFE of the two-phase mixture after solving the RR equation using K_i^n values must be less than the GFE of the single-phase mixture of composition $\vec{z}^{n+1}$. This condition is given by

$$\sum_{j=1}^{2} \sum_{i=1}^{n_c} l_j x_{ij} [\ln x_{ij} + \ln \phi_{ij}(\overrightarrow{x_j})] \leq \sum_{i=1}^{n_c} z_i [\ln z_i + \ln \phi_i(\vec{z})]. \tag{3.6}$$

where l_j is molar fraction of phase *j*, ϕ_{ij} is fugacity coefficient of component *i* in phase *j*, $\overrightarrow{x_j}$ is composition vector of phase *j* and $\vec{z}$ is the overall composition vector. These conditions guarantee that for the overall composition $\vec{z}^{n+1}$, a two-phase mixture exists that satisfies the material balance equations and its GFE is lower than the single-phase GFE. Hence, the single-phase mixture of composition $\vec{z}^{n+1}$ is unstable, and the stability analysis calculations can be avoided. The procedure also provides good *K*-value estimates for the next flash calculation (Perschke, 1988). At this point, flash calculations will converge very quickly to the solution in a few iterations using SS or ASS. This heuristic method is by default used in all the simulations with UTCOMP and will be referred to as Heuristic Method 1 (HM1) hereafter in this chapter. The TDBA method (Belkadi *et al.*, 2011) is closely related to this strategy in UTCOMP, except that in TDBA the flash results from the previous timestep are accepted within certain accuracy and further calculations are avoided. Thus, TDBA may introduce inaccuracy into the flash calculation results for displacements with significant pressure variations. We investigate and report the range of the imparted inaccuracies in the TDBA method in Chapter 4 of this dissertation.

The second heuristic method for skipping stability analysis and improving the computational time in UTCOMP is applicable when many gridblocks are in the single-phase region during the simulation. When this method is used, the simulator skips stability analysis and flash calculations for the single-phase gridblocks surrounded by single-phase neighbors in the previous timestep. The only exceptions are well gridblocks for which stability analysis is always performed (Chang, 1990). This heuristic method will be referred to as Heuristic Method 2 (HM2) hereafter in this chapter. Different combinations of the two heuristic methods can be applied for a particular reservoir simulation problem. Our implementation of CSAT allows application of both methods, individually or in combination, with CSAT. The flowchart for the phase equilibrium calculations in UTCOMP is given in Figure 3-2. We may replace the whole flowchart with the TSB phase equilibrium calculations method (CSAT) to compare CSAT with the original phase equilibrium calculations. We can also use CSAT to entirely replace or only precede the steps of the flowchart that are enclosed in the dashed blue box. We used the latter method for implementation of the TSB phase equilibrium calculation methods in UTCOMP. The flowchart given in Figure 3-2 is for two-phase hydrocarbon systems. The general phase-equilibrium calculations algorithm in UTCOMP, which includes three-phase hydrocarbon systems, is given in Chang (1990).

3.2 TSB PHASE BEHAVIOR MODELING

TSB phase behavior modeling is based on parameterization of compositional space in terms of tie lines. Compositional space parameterization (CSP) was inspired by the research on the method of characteristic (MOC) solution of gas injection processes by Orr and co-workers (Orr, 2007; Dindoruk, 1992; Dindoruk *et al.*, 1997; Johns, 1992; Johns and Orr, 1996; Wang and Orr, 1997). The main idea contributing to CSP from

MOC is that the solution route in compositional space is determined by structure and properties of tie lines and it can be described using a limited number of key tie lines and the properties of tie lines (Voskov and Tchelepi, 2009a). Although the MOC solutions apply only to the limiting conditions of dispersion-free and one-dimensional flow of incompressible fluids, the idea of describing the complex real gas-injection processes in the tie-line space is very appealing. Voskov and Tchelepi (2007) presented a reservoir simulation methodology based on TSB compositional space parameterization and the theoretical background of the parameterization.

The methodology is built on solution invariance (for special cases) or near-invariance of the gas injection processes in the tie-line space rather than the traditional compositional space. For a system of n_c components, the overall mole fraction of the i-th component z_i in terms of the oil and gas mole fractions, x_i and y_i, is given by

$$z_i = x_i l + y_i (1-l), \qquad i = 1, 2, ..., n_c - 1, \tag{3.7}$$

solving for l using the equation for one of the components e.g. component one and substituting the resulting expression (of l) in the rest of the equations in Eqs. (3.7) yields

$$z_i = A_i z_1 + B_i, \qquad i = 2, ..., n_c\text{-}1,$$
$$\text{where } A_i = \frac{x_i - y_i}{x_1 - y_1}, \qquad B_i = y_i - y_1 \frac{x_i - y_i}{x_1 - y_1}, \tag{3.8}$$

Eq. (3.8) parameterizes the compositional space in terms of the parameters A_i and B_i, which are constant for a given tie line. It is possible to write A_i and B_i in terms of n_c - 2 tie-line parameters denoted by γ_i. Thus, Eq. (3.8) allows for expressing any overall composition in terms of n_c - 2 tie-line parameters and overall mole fraction of one of the components. The tie-line parameters must uniquely represent a tie line for a rigorous

parameterization. The uniqueness of parameterization may seem trivial considering the phase equilibrium constraints (equality of component fugacities) however it remains a very challenging problem for general two-phase multicomponent systems (Khorsnadi *et al.*, 2014; Durta, 2009). For convenience the n_c - 2 center-point coordinates of a tie line are used as the tie-line parameters (Iranshahr *et al.*, 2013). Even though the n_c - 2 center-point coordinates might not uniquely parameterize the tie lines under general conditions, they are adequate for practical simulation purposes. Zaydullin *et al.* (2013) developed an EOS-free compositional simulation framework in the tie-line space using the center-point coordinates as the tie-line parameters. They used the phase equilibrium constraints to retrieve the equilibrium compositions from the tie-line parameters in general compositional problems. For simple systems and under limiting conditions, the equilibrium compositions can be expressed as polynomial functions of γ_i (Entov *et al.*, 2001).

One can show that the above parameterization splits the solution of the gas injection problem into hydrodynamic and thermodynamic parts in special cases. The mass conservation equations for the one-dimensional dispersion-free two-phase flow in dimensionless form are given by

$$\frac{\partial z_i}{\partial \tau} + \frac{\partial F_i}{\partial \psi} = 0, \qquad i = 1, 2, ..., n_c, \tag{3.9}$$

where F_i is the overall fractional flow of component i, τ is dimensionless time, and ψ is dimensionless distance. Substituting the conventional composition variables with the parameterized form yields

$$\frac{\partial z_1}{\partial \tau} + \frac{\partial F_1}{\partial \psi} = 0, \tag{3.10}$$

$$\frac{\partial (A_i z_1 + B_i)}{\partial \tau} + \frac{\partial (A_i F_1 + B_i)}{\partial \psi} = 0, \qquad i = 2, ..., n_c - 1. \tag{3.11}$$

Entov *et al.* (2001) showed that under certain conditions the A_i and B_i must satisfy the auxiliary Riemann problem given by

$$\frac{\partial A_i}{\partial \tau} + \frac{\partial B_i}{\partial \chi} = 0, \qquad i = 2, ..., n_c - 1. \tag{3.12}$$

The solution to Eq. (3.12) is only a function of thermodynamic behavior of the system and is independent of the hydrodynamic properties. Therefore the solution route in the tie-line space is invariant. This is equivalent to the MOC solution of the dispersion-free gas-injection processes with the shock jump assumption between each two consecutive key tie lines. Such a system is also known as a fully self-sharpening system. In such MOC-type problems the calculated MMP and the compositional route depend only on the thermodynamic behavior of the system as long as the system remains fully self-sharpening. The near-invariance of the solution in the actual multi-dimensional gas injection problems in the tie-line space was demonstrated using numerical examples by Voskov and Tchelepi (2007) and Rannou *et al.* (2013).

The idea of CSP and its application in reservoir simulation has been the topic of active research for the last few years (Voskov and Tchelepi, 2007; 2008; 2009a; 2009b; 2009c; Iranshahr *et al.*, 2010; 2012; 2013; Fraces *et al.*, 2009; Rannou *et al.*, 2013; Belkadi *et al.*, 2011; Zaydullin *et al.*, 2013; Rezaveisi *et al.*, 2014a; 2015). The theory and practical application of the method have matured in recent years. The idea moved from preconditioning standalone flash calculations to skipping stability analysis in immiscible gas injection processes and then to miscible gas injection processes through

parameterizing the critical surface of tie lines. Later Iranshahr *et al.* (2010; 2013) extended the approach to thermal simulation problems and provided theoretical derivation of the continuity of tie simplexes and uniqueness of parameterization. The previous research on applicability of the TSB methods in compositional reservoir simulators was almost entirely focused on fully implicit reservoir simulators. The only authors that applied the method in an IMPEC-type reservoir simulator were Belkadi *et al.* (2011) who applied the TSB methods in a slim-tube simulator at constant pressure and temperature. Thus, we implemented the TSB phase equilibrium calculation methods in UTCOMP, a comprehensive IMPEC-type reservoir simulator in order to compare their performance against the traditional phase equilibrium calculations in UTCOMP.

In their earlier works, Voskov and Tchelepi (2009a) referred to constructing the phase diagram at several different pressure values and then parameterizing the phase diagram using a finite number of tie lines before starting the simulation as CSP. They suggested that for any given pressure (P) and overall composition ($\vec{z}$), the following minimization problem can be solved to find the closest tie line at P_L and P_U where P_L and P_U are the immediate lower and upper pressures that bound the pressure of interest ($P \in [P_L, P_U]$). That is, one must find

$$\min_{\gamma}\left(\sum_{i=1}^{n_c}(A_i(\gamma)z_1 + B_i(\gamma) - z_i)^2\right). \tag{3.13}$$

This specific method of the CSP approach for compositional simulation however requires a large number of tie lines to solve a high-dimensional optimization problem, e.g. for more than five components. Therefore, it is not practical in the compositional simulation context.

Compositional space tabulation (CST) begins with CSP but with a fewer number of pre-tabulated tie lines. To implement CST in a reservoir simulator one needs to select a set of overall composition vectors and a pressure range for a particular gas injection problem. Flash calculations are then performed for those overall composition vectors at the discrete pressure values and the results are stored in tie-line tables. Tie lines that extend through the initial reservoir composition and injection composition are obvious candidates for tie-line tabulation (Voskov and Tchelepi, 2009a). For a given overall composition of interest, the information in the pre-calculated tables are used if a matching tie line can be found, otherwise a regular flash calculation will be performed. Linear interpolation of x_i and y_i from the tie lines at P_L and P_U are used to find a new tie line (x_i and y_i) at the pressure of interest for each of the existing tables. To check if the overall composition ($\vec{z}$) is close to any of the pre-stored tie lines the following equations are used (Voskov and Tchelepi, 2009a)

$$l = \frac{z_i - y_i}{x_i - y_i}, \tag{3.14}$$

$$\text{Error} = \sqrt{\sum_{j=1}^{n_c} \left(x_j l + y_j (1-l) - z_j \right)^2} \le \varepsilon, \tag{3.15}$$

In Eq. (3.15), the error is the distance of the overall composition of interest from the interpolated tie line, which should be less than a certain tolerance value called the tie-line detection tolerance (ε). If the overall composition $\vec{z}$ is close to the phase boundary, it may be incorrectly assigned as single or two phase based on the interpolated tie line (Voskov and Tchelepi, 2009a). This misidentification leads to a discontinuity of physical properties in an IMPEC reservoir simulator and consequently to small timestep sizes using UTCOMP's automatic timestep selection algorithm. In fully implicit simulators it

will lead to oscillatory behavior in the global Newton iterations (Voskov and Tchelepi, 2009b). Voskov and Tchelepi (2009b) proposed using the minimum acceptable distance to the phase boundary (DMIN) based on the interpolated tie line as a criterion to decide whether $\vec{z}$ is sufficiently far from the phase boundary or not. For example, when $\vec{z}$ is close to the liquid boundary, the distance (d) of the overall composition of interest from the boundary is given by

$$d = \sqrt{\sum_i \left(z_i - x_i\right)^2}, \tag{3.16}$$

where x_i is the equilibrium liquid phase composition of the interpolated tie line.

When the number of components is large, CST requires a very large number of tie-line tables if a comprehensive table is to be built or leaving a significant part of the compositional space out of the region of coverage of the tie lines. This is a potential problem because it is not known which part of the compositional space needs to be parameterized a priori. This problem is more pronounced as the number of components increases. Furthermore, if the injection composition changes with time e.g. due to recycling of the produced gas, the CST method which uses a fixed table of tie lines will likely become more inefficient. It is possible to run one-dimensional simulations to obtain the prior tie lines of the CST approach or other tie-line based methods (Rannou *et al.*, 2013). However, the tie lines from one-dimensional simulations depend on the specified transport properties e.g. relative permeabilities and viscosities. In Chapter 4, we propose a more elegant approach for finding the prior tie-line tables of a particular gas injection problem from the multiple-mixing-cell (MMC) method.

As a modification of the CST strategy, the CSAT method has been proposed by Voskov and Tchelepi (2009a) where the tabulated tie lines are created adaptively as

needed during the simulation. In CSAT the simulation starts with a set of tie-line tables and new tie-line tables are generated as needed during the simulation. The CSAT method may be employed for generating initial estimates for flash calculations and for skipping stability analysis. CSAT is the most promising of the TSB methods in terms of practicality in compositional reservoir simulation mainly because it creates most of the tie-line tables based on the actual composition route. The tie lines produced by adaptive tabulation provide complete coverage of the solution route of the gas injection problem. Adaptive tabulation however is prone to failure as negative flash calculations might be performed in challenging areas of the phase diagram.

There is no tie line or tie-line extension in the supercritical region of the phase diagram. Thus, for the MCM gas injection processes where the compositional route will traverse the supercritical region, the CSAT approach as described above must be modified with a method for determining whether a composition is supercritical or subcritical. Otherwise, the search for finding a matching tie line and calculation of the new tie-line table for the supercritical overall compositions will fail (Voskov and Tchelepi, 2009b).

Voskov and Tchelepi (2009b) suggested an adaptive super-critical state criterion (SSC) where the critical tie-line surface is adaptively parameterized to solve this problem. In adaptive SSC, critical tie lines are calculated and tabulated in a separate critical tie-line table when needed during the simulation. Essential to the applicability of SSC is the concept of Minimal Critical Pressure (MCP), which is defined as the minimum pressure at which an overall composition is intersected by a critical tie line (Voskov and Tchelepi, 2009b). During the regular CSAT tabulation for an overall composition, whenever the length of the tie line is smaller than a predetermined

tolerance, the procedure reverts to calculation of the critical tie line and the corresponding MCP. The criterion for a critical tie line is that its length is limited by the ε_1 and ε_2 tolerances i.e.

$$\varepsilon_1 \le TL = \sqrt{\sum_i \left(x_i - y_i\right)^2} \le \varepsilon_2, \tag{3.17}$$

where *TL* is the tie-line length. The critical tie lines and their MCPs are tabulated in critical tie-line tables. The critical tie-line tables parameterize the critical surface of tie lines. The MCP values of critical tie lines are different; therefore, the critical surface is parameterized at different pressure values. If a matching critical tie line is found for a given overall composition ($\vec{z}$) in the existing table of critical tie lines, the pressure of the mixture is compared with the MCP of the matching tie line. If the mixture's pressure is larger than the MCP value, the mixture is in supercritical state, otherwise the mixture is subcritical. Calculation of the critical tie line and the MCP for a given overall composition requires performing negative flash calculations for a tie line that is going to become critical. In this region, the calculations become sensitive to the choice of the critical tie-line length tolerances. It is worth to note that there is question as to whether the critical tie-line parameterization for an overall composition is unique or not because it is not the actual critical pressure of $\vec{z}$ that is being calculated. Instead, we calculate a critical tie line that extends through $\vec{z}$. For some fluid systems e.g. systems with bifurcating phase behavior (Ahmadi, 2011), the overall composition of interest may lie on extension of two critical tie lines with different MCPs. Thus, MCP is a concept that is based on structure of tie lines and facilitates parameterizing the critical surface. This method of parameterizing the critical surfaces of tie lines was successfully applied to practical MCM gas injection problems (Voskov and Tchelepi, 2009b).

3.3 IMPLEMENTATION OF TSB PHASE BEHAVIOR MODELING IN UTCOMP

In this section we discuss the details of our implementation of CSAT, a TSB phase behavior modeling method in UTCOMP. We first discuss our negative flash calculations algorithm for adaptive tabulation. Then we present the flowchart and computational procedure for our implementation of CSAT in UTCOMP.

3.3.1 Negative Flash Calculations for Adaptive Tabulation

A robust negative flash calculations core is required for successful adaptive tabulation in CSAT. The negative flash calculations is required because the simulation overall compositions that are used for adaptive tabulation might be in the single-phase region. We have developed a robust two-phase negative flash calculations method that calculates the tie line extending through a given overall composition ($\vec{z}$) using various sets of initial estimates for *K* values. A negative flash calculation is similar to conventional flash calculations except that the liquid phase molar fraction is not bounded by the physical limits of [0, 1].

We used a modified version of the Li and Johns' (2007) constant *K*-value flash (Ahmadi, 2011) to replace the RR equation in our negative flash calculations. The Li and Johns' constant *K*-value flash is especially superior for the calculation of gas tie line in gas injection processes. This method always includes the heaviest component in the negative flash calculations even when its overall mole fraction is zero. Even though the injection gas usually contains only the light hydrocarbon components, the equilibrium compositions of the heaviest component of the gas tie line are usually non-zero. The Wilson's correlation is usually used for the initial *K*-value guess in the phase equilibrium calculations. However the negative flash calculations using Wilson's initial estimates sometimes fail especially for the injection gas tie line. Therefore, we use a second set of

initial estimates of *K* values whenever the tie-line calculation fails using the first set of initial estimates.

We use SS followed by the Newton method to solve the equality of fugacity constraints in our negative flash calculations. The Newton method always properly chooses the direction of change in the independent variables however the step length might be excessive and lead to a larger norm of the residuals vector. In this case our negative flash code cuts the step length. If cutting the step length does not lead to a smaller value of the norm of the residuals vector, the Newton iterations are stopped and the SS iterations are resumed.

3.3.2 Computational Procedure for Implementation of CSAT in UTCOMP

The general CSAT implementation for both miscible and immiscible gas injection problems includes two tie-line table search algorithms; subcritical tie-line table search and critical tie-line table search. Two tie-line table generation functions are also required; subcritical and critical tie-line table generation functions. When the compositional route is not passing through the supercritical region and the overall compositions do not lead to critical tie lines within the pressure range of tabulation, the critical tie-line tables are not created and the total tie-line table search collapses to only a subcritical table search.

The subcritical tie-line table generation function is called when a matching tie line is not found for an overall composition $\vec{z}$ among the pre-existing tie-line tables. Figure 3-3 illustrates the subcritical tie-line tables in our implementation of CSAT in UTCOMP. A set of discrete pressure levels is specified for tabulation before starting the simulation. The specified pressure levels are based on the expected pressure range of the gas injection displacement. For example, for a simulation problem with only one injector and one producer at constant bottomhole pressures, the pressure range of tabulation must at

least cover the wells' bottomhole pressures. Figure 3-3 shows that table #1 has been generated for the overall composition vector $\vec{z}_1$, and it contains the results of several flash calculations (i.e. tie lines) for $\vec{z}_1$ at different values of pressure in the pressure range of interest. For any tie-line table (table #*N*), the program calculates the tie lines for the corresponding overall composition vector ($\vec{z}_N$) from the lowest tabulation pressure and continues to higher pressures. At each pressure level, the length of the generated tie line is calculated and compared with critical tie-line length criterion (ε_2 in Eq. (3.17)). If the tie-line length is smaller than ε_2, the critical tie-line generation function for that overall composition ($\vec{z}_N$) is called. The critical tie-line tabulation function finds and stores the MCP and the corresponding critical tie line for $\vec{z}_N$. Once the critical tie-line tabulation function is called for $\vec{z}_N$ at a certain pressure level, flash calculations at higher pressure levels are skipped in the corresponding subcritical table.

The critical tie-line table search is performed before the subcritical tie-line table search. This search looks for a matching critical tie line for the overall composition of interest ($\vec{z}$) in the existing critical tie-line tables. If a matching critical tie line is found, its MCP value is compared with pressure (*P*) of the mixture. If *P* > MCP, $\vec{z}$ is supercritical single-phase and stability analysis and flash calculations are skipped; however, if *P* < MCP then $\vec{z}$ is subcritical and the program proceeds to the subcritical tie-line table search. If no matching critical tie line is found, the algorithm proceeds to subcritical tie-line table search as well. The flowchart given in Figure 3-4 illustrates the critical tie-line table search algorithm implemented in UTCOMP. In this flowchart, "Error" is the distance of $\vec{z}$ from the critical tie line, which is calculated from Eqs. (3.14) and (3.15).

The flowchart given in Figure 3-5 shows the subcritical tie-line table search algorithm implemented in UTCOMP. The "Error" in this flowchart is also calculated

from Eqs. (3.14) and (3.15). The test for proximity to the phase boundary is performed using Eq. (3.16). The distance (d) in this equation should be greater than DMIN before stability analysis can be skipped. When a new tie-line table is generated for an overall composition, an interpolation is performed for the pressure of interest based on the new table and the error is calculated. The error is almost always less than the tie-line detection tolerance (ε) because this table has been generated for the same overall composition for which interpolation is being performed. If for any reason this error does not satisfy the tolerance criterion (Error < ε), the program proceeds to regular stability analysis and flash calculations, i.e. for a given overall composition, the tie-line table generation is performed only once. Linear interpolation according to Eqs. (3.18) and (3.19) is performed to interpolate a tie line at pressure P between P_L and P_U entries of table # I. That is,

$$x_{i(P)} = x_{i(P_L)} + \frac{x_{i(P_U)} - x_{i(P_L)}}{P_U - P_L}\left(P - P_L\right), \qquad i = 1, 2, ..., n_c, \tag{3.18}$$

$$y_{i(P)} = y_{i(P_L)} + \frac{y_{i(P_U)} - y_{i(P_L)}}{P_U - P_L}\left(P - P_L\right), \qquad i = 1, 2, ..., n_c, \tag{3.19}$$

where x and y represent the equilibrium liquid and gas mole fractions of the tie line and the subscripts P_U and P_L indicate whether they belong to the upper or lower limiting pressure in the table.

3.4 SIMULATION CASE STUDIES

Several simulation cases were performed to compare the computational efficiency of CSAT with that of the original UTCOMP. Most of the case studies are similar to the simulations that were performed for comparing computational efficiency of CSAT with that of the standard phase behavior algorithm in a fully implicit reservoir simulator

(Voskov and Tchelepi, 2009a and 2009b). All the simulation case studies were performed using the automatic timestep selection mode in UTCOMP. The timestep selector automatically selects the timestep size to avoid numerical instability (Chang, 1990). The timesteps are selected so that the relative changes in pressure, saturation, volume error and component mole numbers do not exceed predetermined values (0.008, 0.01, 0.01 and 0.01, respectively) and are always constrained between the minimum timestep size (typically 1.0×10^{-6} days) and the maximum allowed timestep size (0.5 days). Robustness of the implementation of CSAT in UTCOMP becomes very important while using the automatic timestep selector because rapid and discontinuous changes in the variables controlling the timestep sizes lead to the timestep size reaching the minimum value for several iterations. It is also important to recognize that for each case study, different methods do not exactly lead to the same number of timesteps due to small differences in the results of flash calculation algorithms.

The simulation results with different methods for each case study presented below were found to be numerically the same (at least up to the fifth decimal digits in saturation values), unless otherwise stated. The simulation cases are displacement of oil by gas where up to two hydrocarbon phases may form. There is no mobile water phase. The relative permeability model for all the cases is the Corey model (Corey, 1986) given by

$$k_{rj} = k_{rj}^{0}\left(\frac{S_j - S_{jr}}{1-\sum_{l=1}^{n_p} S_{lr}}\right)^{e_j}, \qquad j = 1,2,...,n_p, \tag{3.20}$$

where k_{rj} is the relative permeability of phase j, k_{rj}^{0} and e_j are respectively the endpoint relative permeability and Corey exponent of phase j, S_j is saturation of phase j, S_{lr} is the residual saturation of phase l, and n_p is the number of phases. The relative permeability

parameters of the gas and oil phases are given in Table 3-1. Capillary pressure was assumed to be zero in all the simulations.

For each case study we run at least four simulations, two simulations with the original UTCOMP phase behavior algorithms and two with CSAT. The first simulation with original UTCOMP is performed using only HM1. The other original UTCOMP simulation uses both HM1 and HM2. These two heuristic methods in original UTCOMP were selected because the first one is by default UTCOMP's standard flash algorithm and the second one is employed when many gridblocks are in the single-phase region throughout the simulation. Furthermore, we presume that most reservoir simulators use the results of the previous flash calculations as an initial estimate for the next timestep. Not using the heuristic methods will definitely lead to more computational time (as reported for the first case study) but this is not the common practice because HM1 is almost always used.

Additional simulations for each case study use CSAT for the phase equilibrium calculations. One CSAT simulation uses CSAT only for skipping stability analysis (represented by CSAT(SA)) and another one uses CSAT for skipping stability analysis and generating initial estimates for flash calculations (represented by CSAT(SA/Flash)). All CSAT(SA) cases use HM1 and all the CSAT(SA/Flash) cases do not use the heuristic methods, unless otherwise stated. In all the simulations Peng-Robinson (PR) EOS (Peng and Robinson, 1976) has been used for phase behavior modeling. The simulations were performed on dedicated CPU nodes with 2.73 GHz CPU and 15.86 GB of memory (RAM). In our table search we use a partial sorting, which brings the most recently hit tie-line table one step forward in the search order if its number of successful hits is greater than that of the prior tie-line table in the search order. We found this partial

sorting more efficient than no sorting of the tie-line tables. Belkadi *et al.* (2011) used the same partial sorting in their implementation of CSAT in a slim-tube simulator.

3.4.1 Case 1

Case 1 is similar to case 1 in Voskov and Tchelepi (2009a). It is a quarter of a five-spot pattern with 10×10×5 gridblocks where the injector and producer are in opposite corners. The reservoir is homogenous with $k_x = k_y = 100$ md and $k_z = 50$ md. Initial composition of the reservoir fluid is 4% C_1, 16% C_4-C_6, 20% C_{7+1}, and 60% C_{7+2}. Injected fluid is pure C_1. Injection pressure is 600 psia and production pressure is 400 psia. Initial reservoir pressure is 500 psia. Total simulation time is 7,500 days and reservoir temperature is 100°F. The fluid properties are taken from the SPE 3 comparative solution problem (Kenyon and Behie, 1987). The fluid components for this case study are a subset of the nine-component model in Case 3 whose properties required for fluid modeling are given in Table 3-2. Because the entire simulation shows a variation of only 200 psia in pressure, five pressure levels were used for tie-line tabulation. The value of minimum miscibility pressure (MMP) calculated from the MMC method of Ahmadi and Johns (2011) for this gas injection process is 4,142 psia suggesting an immiscible displacement. No critical tie-line table was created indicating that the composition route does not pass through the supercritical region. The criterion length for calling the critical tie-line tabulation function was 1.0×10^{-5} ($\varepsilon_2 = 1.0\times10^{-5}$). The computational efficiency results for simulations of this case are given in Table 3-3. The reported MMP calculations were performed using the PennPVT toolkit.

CSAT(SA) improves the total CPU time by 17.96% and 0.94% compared to the (original UTCOMP) simulations with only HM1 and with both HM1 and HM2, respectively. The corresponding improvements in the phase behavior calculations time

are 34.3% and 0.05% compared to the simulation with only HM1 and the simulation with both HM1 and HM2, respectively. The phase behavior calculations time includes both stability and flash calculations. Although, CSAT offers significant computational advantage over using HM1, its benefits compared to using both HM1 and HM2 are insignificant.

For the simulation with both HM1 and HM2, 1,410,000 stability analyses were performed while in CSAT(SA) 82,000 stability analyses were performed. CSAT(SA) reduced the number of stability analyses performed by 94.1%. The total time spent on table search, table generation and other operations required for CSAT(SA) is 11.94 *sec*. This extra time is offset by the time needed for performing approximately 1,330,000 additional stability analyses for the simulation with both HM1 and HM2 and that is why the total computational time for these two cases is almost the same. CSAT(SA) skipped 98.4% of stability analyses compared to the simulation with only HM1, but the total time savings compared to using only HM1 are small because of the small contribution of stability analysis to the total computational time (24.2% of the total computational time). When both HM1 and HM2 are used in the simulation, CSAT is not superior compared to the original UTCOMP's phase behavior calculations algorithm for this case. The small number of tie-line tables generated (5 for CSAT(SA)) leads to small tie-line table generation time.

CSAT(SA) performs better compared to CSAT(SA/Flash) where heuristic methods are not employed and CSAT is used for both generating initial estimates for flash calculations and skipping stability analysis. Performance of the original UTCOMP simulation without HM1 and HM2 is also reported in Table 3-3. CSAT has improved the computational time by 30% compared to this simulation case. However, this is not the

common simulation practice where prior estimates are used as initial guesses for the next timestep. To test the effect of ε and DMIN on performance of CSAT for this simulation case, two additional simulations were performed. The first one is a CSAT(SA) simulation that uses ε = 0.1 and DMIN = 0.001, which are not as strict for tie-line detection and skipping stability analysis. For this case, the simulation timesteps become very small, which indicates rapid changes in number and properties of the phases resulting from incorrectly assigning a single-phase to a two-phase mixture (or vice versa). The same problem occurs late in the simulation for the other CSAT(SA) case when ε = 0.1 and DMIN = 0.01 is used. Another CSAT(SA) case was run with ε = 0.01 and DMIN = 0.01 with 20 pressure levels of tabulation. The results do not show any significant difference in computational efficiency compared to the case where five pressure levels are used (CPU time is 132.06 *sec*).

Table 3-3 also shows the relative speed of each simulation compared to the simulation with HM1 and HM2. The overall compositions for which the tie-line tables were generated during the simulation with CSAT(SA) are given in Table 3-4. The number of hits for each tie-line table is also reported in Table 3-4. Table 3-4 shows that the solution route traverses a small region of the compositional space. Figure 3-6 and Figure 3-7 show the cumulative oil recovery and the saturation profile at 2,400 days respectively for different simulations. The simulation results are the same.

3.4.2 Case 2

Case 2 is a three-dimensional reservoir model with 10×10×5 gridblocks. The reservoir is homogenous with $k_x = k_y$ = 300 md and k_z = 50 md. Initial composition of the reservoir fluid is 30% C_1, 3% C_3, 7% C_6, 20% C_{10}, and 40% C_{15}. Injected fluid is pure C_1. Injection pressure is 3,000 psia and production pressure is 1,000 psia. These wells are at

opposite corners in a quarter of a five-spot pattern. Initial reservoir pressure is 2,000 psia and reservoir temperature 160°F. Total simulation time is 3,400 days. This case is similar to Case 6 in Voskov and Tchelepi (2009a) and the fluid properties are taken from the SPE 5 comparative solution problem (Killough and Kossack, 1987). The fluid model properties are given in Table 3-5. Twenty equally spaced pressure levels were used in tie-line tabulation for the CSAT simulations. The computational results for the simulations for this case are given in Table 3-6.

The MMP from the MMC method is 5,794 psia for this displacement. No critical tie-line tables were generated in CSAT since the reservoir pressure is smaller than the MMP. CSAT(SA) improves the total computational time by 23.7% and 1.1% compared to the simulations with only HM1 and with both HM1 and HM2, respectively. The improvement in phase equilibrium time is 40.54% and 3.14 % compared to using only HM1 and using both HM1 and HM2, respectively. The stability analysis time is 27.9% of the total computational time in the original UTCOMP simulation with only HM1. We could improve the stability analysis time by using CSAT(SA) or using HM2 to achieve a reduction in computational time of 23.7% and 22.6%, respectively. This is because CSAT decreases the number of stability analyses actually performed by 99.1% compared to the simulation with only HM1. Comparably, when HM2 is used, 81.4% of stability analyses are skipped without any need for table search. Therefore, computational efficiency of CSAT(SA) depends on the original phase equilibrium calculations algorithm being compared and it does not offer significant advantage over using both HM1 and HM2 for this simulation case. CSAT(SA)'s computational advantage over the original UTCOMP's flash algorithm with only HM1 is significant (23.7%) even though it is somehow smaller than the results reported by Voskov and Tchelepi (2009b) for fully implicit and adaptive

implicit formulations. This also indicates that formulation of the reservoir simulator is important in evaluating performance of new methods of phase behavior modeling. UTCOMP is an IMPEC simulator and the timesteps determined by the automatic timestep selector are inherently small. Therefore, previous flash results will provide very good initial estimates for the next flash calculations. Consequently, computational advantages of CSAT are smaller for an IMPEC-type simulator in the cases studied.

The computational time of CSAT(SA/Flash) is larger than that of CSAT(SA) because of the larger number of tables generated (10) and larger table search time. For both CSAT(SA) and CSAT(SA/Flash) the tie-line table generation time is less than 0.01 *sec*, which is insignificant. Relative speed of different simulations compared to the best original UTCOMP simulation is given in the last row of the Table 3-6, which supports the above discussion. Figure 3-8 shows the cumulative oil recovery curves for different simulations reported in Table 3-6. Figure 3-8 also shows that the same results are obtained for different simulations of this case.

For this specific fluid system, the total CPU time with CSAT(SA) using ε = 0.1 and DMIN = 0.001 is 178.44 *sec* and a total number of 1,300 stability analyses were actually performed (3,603,000 skipped). For this large ε, only one tie-line table corresponding to the initial reservoir composition is generated. Although the computational time in this case is better than that reported in Table 3-6, the above discussion is still valid. The simulation results (saturation profiles and recovery curves) with ε = 0.1 are very close to the other cases. Even if CSAT(SA) is run with ε = 1, a similar total computational time and number of SA skipped is obtained as that of ε = 0.1. This indicates that performance of CSAT also depends on the specific gas injection

problem being considered. For Case 1, CSAT(SA) with these values of ε failed to complete the simulation.

3.4.3 Case 3

Case 3 is a one-dimensional reservoir model with 500 gridblocks. The reservoir is homogenous with k_x = 100 md. Initial composition of the reservoir fluid is 1.3% CO_2, 1.9% N_2, 16% C_1, 8.7% C_2, 5.9% C_3, 9.7% C_{4-6}, 4.7% C_{7+1}, 11.5% C_{7+2}, and 40.3% C_{7+3}. Injected fluid is 90% N_2 and 10% C_1. Injection pressure is 2,000 psia and production pressure is 500 psia. Injector and producer are in opposite ends of the reservoir. Initial reservoir pressure is 1,200 psia and reservoir temperature is 120°F. Total simulation time is 1,500 days. This case is similar to Voskov and Tchelepi's (2009a) example and the fluid properties are taken from the SPE 3 problem (Kenyon and Behie, 1987). The fluid properties required for EOS modeling are given in Table 3-2. The computational efficiency results for this case are given in Table 3-7. The simulation results for the simulations reported in Table 3-7 occasionally differ in saturation by a maximum value of 0.0001 at the front of the injected gas, but recovery curves are generally the same. The value of MMP obtained from the MMC method for the injection gas and initial oil is 9,889 psia demonstrating an immiscible displacement.

CSAT(SA) improves computational time and phase behavior time by 14.81% and 20.7% respectively compared to the simulation with only HM1. The number of stability analysis has been reduced by 99% compared to using only HM1. The source of this large number of skipped stability analysis is the gridblocks in the single-phase region at the initial timestep and the gridblocks away from the front of the injected gas in the later timesteps that have remained single-phase from the beginning of the simulation. Computational advantage of CSAT(SA), however, disappears compared to the simulation

with both HM1 and HM2, and it does even better than CSAT(SA) in terms of computational time and the number of stability analysis skipped. A one-dimensional reservoir with many gridblocks in the single-phase region favors applicability of HM2 in the simulation for this case. The computational time for CSAT(SA/Flash) is the largest compared to other simulations for this case. The tie-line table generation time is still insignificant for the CSAT simulations.

One CSAT(SA) simulation case using ε = 0.1 and DMIN = 0.0001 with ten pressure levels in the tie-line tables was performed. The computational time for this case was 1500.33 *sec*, where 13,077,680 stability analyses were skipped. The larger computational time for this case compared to CSAT(SA) with ε = 0.01 and DMIN = 0.01 with more strict CSAT tolerance parameters is because of smaller timestep sizes due to occasional failure of CSAT(SA) in correctly obtaining flash calculation results. Reduced timestep size was confirmed by comparing the total number of timesteps of the two CSAT(SA) cases (83,433 for CSAT(SA) with ε = 0.1 compared to 82,125 for CSAT(SA) with ε = 0.01). This result is not the same as what we observed for Case 2 where increasing the CSAT tolerance parameters slightly improved the computational time, further indicating that the results of CSAT(SA) depend on the specific gas injection problem under investigation. The results for CSAT(SA) using ε = 0.1 and DMIN = 0.0001 are the same as the other simulation cases in Table 3-7 but a maximum error value of 0.0016 is observed in saturation profiles. The cumulative oil recovery curves show only negligible differences. Only two tie-line tables were generated for this CSAT(SA) case.

One CSAT(SA/Flash) simulation was run using only HM1, which resulted in 1471.86 *sec* of computational time. Even using HM1 in CSAT(SA/Flash) did not lead to

better performance compared to CSAT(SA) for this case. Using HM1 only leaves 1143 overall composition values whose initial estimates for flash is obtained from CSAT.

3.4.4 Case 4

Case 4 is a three-dimensional reservoir model, with 50×50×5 gridblocks. The reservoir is homogenous with $k_x = k_y = 100$ md and $k_z = 50$ md. Initial composition of the reservoir fluid is 1.3% CO_2, 1.9% N_2, 16% C_1, 8.7% C_2, 5.9% C_3, 9.7% $C_{4\text{-}6}$, 4.7% C_{7+1}, 11.5% C_{7+2}, and 40.3% C_{7+3}. Injected fluid is 80% N_2, 10% C_1, and 10% C_2. An injection well with injection pressure of 2,000 psia is placed in the center and four production wells each producing at 1,000 psia are at the corners. Initial reservoir pressure is 1,300 psia. Total simulation time is 2,200 days and reservoir temperature is 120°F. This case is similar to Voskov and Tchelepi's (2009a) Case 4 and the fluid properties are taken from the SPE 3 problem. The value of MMP calculated from the MMC method for the injection and initial fluid composition is 9,875 psia. The simulation performance results for this case are given in Table 3-8.

For this case, 84.6% of the phase behavior time and 39.8% of the total computational time is spent on stability analysis in the simulation with only HM1. This rather significant contribution of stability analysis to the computational time is because the initial conditions of the reservoir are single phase in all gridblocks and also because the simulation was terminated just before breakthrough of gas. CSAT(SA) improves the computational time and the phase behavior time by 29.1% and 71.3% compared to the simulation with only HM1, respectively. For this case with a large number of single-phase gridblocks the total reduction in the computational time obtained by CSAT(SA) is significant. Comparably, under these conditions the efficiency of the simulation with both HM1 and HM2 also improves and its computational performance becomes very close to

that of CSAT(SA). For this case, using both HM1 and HM2 performs slightly better than CSAT(SA). The CSAT(SA/Flash) reported for this case in Table 3-8 was performed using HM1, which explains why its performance is close to CSAT(SA).

3.4.5 Case 5

Case 5 is a one-dimensional reservoir model with 100 gridblocks. The reservoir is homogenous with k_x =100 md. Initial composition of the reservoir fluid is 1.3% CO_2, 1.9% N_2, 16% C_1, 8.7% C_2, 5.9% C_3, 9.7% C_{4-6}, 4.7% C_{7+1}, 11.5% C_{7+2}, and 40.3% C_{7+3}. The injected fluid is 90% CO_2 and 10% C_3. An injection well with injection pressure of 3,000 psia is placed in one end and a production well with bottomhole production pressure of 1,000 psia is in the other end of the reservoir. Initial reservoir pressure is 2,000 psia and reservoir temperature is 120°F. Total simulation time is 500 days. This case is similar to Voskov and Tchelepi (2009b)'s example case. The computational time comparisons for this case are given in Table 3-9.

The improvements in computational time and phase behavior time obtained by CSAT(SA) compared to the simulation with only HM1 are 10.9% and 19.1%, respectively. For this case, the simulation with both HM1 and HM2 performs slightly better than CSAT(SA). The general observations for previous cases hold for this near-miscible case as well; large number of stability analysis have been skipped by CSAT(SA) and a noticeable improvement to the computational time has been made. For CSAT(SA/Flash) the minimum timestep size was taken to be 0.001 days because it would not complete the simulation with a minimum timestep size of 0.00001 days. For CSAT(SA/Flash), 11 critical tie lines were created whereas for CSAT(SA) no critical tie line was generated. This is because of the slightly different solution routes that CSAT(SA/Flash) and CSAT(SA) experience. In CSAT(SA/Flash) no use is made of the

flash calculation results of the previous timestep. Therefore, more compositions are prone to tabulation and, hence, potentially generating critical tie lines in CSAT(SA/Flash). For all the critical tie lines, the MCP was higher than the pressure of the corresponding overall composition for which critical tie-line tabulation was performed. The critical tie lines experienced only 361 hits during the simulation, which means only a small number of near-critical compositions occurred during the simulation. The value of MMP from the MMC method is 3,656 psia, which is consistent with the small number of near-critical overall compositions throughout the simulation.

Another simulation for this case was made with CSAT(SA) using ε = 0.1 and DMIN = 0.001. The total CPU time for this case is 131.84 *sec* (phase equilibrium time is 54.43 *sec*) and nine critical tie-line tables were generated. The total number of stability analysis actually performed is 66,180 (3,304,500 skipped). Despite improved computational time, the simulation results for this case are noticeably different from the results of original UTCOMP. Performing this CSAT(SA) simulation with the above values of ε and DMIN was only possible when a minimum timestep size of 0.001 was used. If the values of all the parameters are retained and only DMIN is changed to 0.01, the simulation results are still similar. The computational time is improved to 138.41*sec*.

3.4.6 Case 6

Case 6 is a two-dimensional areal reservoir model with 20×20 gridblocks. The reservoir is homogenous with $k_x = k_y$ = 113 md. Initial composition of the reservoir fluid is 0.77% CO_2, 20.25% C_1, 11.8% $C_{2\text{-}3}$, 14.84% $C_{4\text{-}6}$, 28.63% $C_{7\text{-}14}$, 14.9% $C_{15\text{-}24}$, 2.95% $C_{25\text{-}28}$, 1.96% $C_{29\text{-}32}$, 1.305% $C_{33\text{-}36}$, 0.869% $C_{37\text{-}40}$, 0.5781% $C_{41\text{-}44}$, and 1.1505% C_{45+}. Injected fluid is 1% CO_2, 65% C_1, 30% $C_{2\text{-}3}$, and 4% $C_{4\text{-}6}$. The component properties required for phase behavior modeling are given in Table 3-10. An injection well with

injection pressure of 4,600 psia is placed in one corner and a production well with bottomhole production pressure of 4,100 psia is placed in the other corner of the reservoir. Initial reservoir pressure is 4,550 psia and reservoir temperature is 260°F. This case is adopted from Okuno (2009). The value of MMP calculated from the MMC method is 3,217 psia, which is significantly lower than the injection and production pressures indicating a MCM displacement. The total simulation time is 1,100 days. The computational efficiency results are given in Table 3-11.

Using CSAT(SA) with the given set of parameters in Table 3-11 does not improve the computational time compared to the simulation with only HM1. This is because of the large number of tie-line tables that were generated by CSAT(SA), which gives a large table search time. The simulation with both HM1 and HM2, on the other hand, improves the computational and phase behavior time of the simulation with only HM1 by 45.7% and 89.4%, respectively.

The computational time of CSAT(SA) for this case can be improved by using ε = 0.1, DMIN = 0.001, and $\varepsilon_{critical}$ = 0.0005. For these parameters, the total computational time with CSAT(SA) is 117.61 *sec* (39.93 *sec* for phase equilibrium time), and only 320 stability analyses were performed (3,848,900 skipped). For ε = 1, DMIN = 0.001 and $\varepsilon_{critical}$ = 0.5, the total CPU time of CSAT(SA) is 93.32 *sec*, which leads to much better CPU time but it is still less efficient than the simulation with both HM1 and HM2. For the latter CSAT(SA) simulation only subcritical tie-line tables were generated.

The simulation results (recovery curves and saturation profiles) with both HM1 and HM2 are the same as the simulation results with only HM1, however, small variations in oil recovery curves between the CSAT(SA) results and the results of the simulation with only HM1 are observed.

3.5 SUMMARY AND CONCLUSIONS

We implemented CSAT, a TSB phase behavior modeling method, in UTCOMP. We performed several simulation case studies to compare the computational performance of CSAT against the standard phase behavior modeling methods in UTCOMP. The simulation results for the cases that we studied, using the CSAT parameters that we used, show that the computational advantage of CSAT over the standard phase equilibrium calculation methods depends on the standard method that is being compared with CSAT. CSAT substantially reduces the number of stability analysis performed compared to original UTCOMP where only initial estimates from the flash calculation results from previous timesteps are used (with only HM1). Reductions as high as 99.9% were observed in the number of stability analyses, however, the contribution to the total computational time is less than 30% for most cases. This is because in UTCOMP, an IMPEC-type simulator, the contribution of stability analysis to the total computational time is small when flash results from the previous timestep are used to avoid stability analysis. Furthermore, the flash results from the previous timestep provide good initial estimates for performing flash calculations. The table search time reduces the computational efficiency of CSAT when the number of tie-line tables is large. For all of the cases performance of CSAT when used to skip both stability analysis and generate initial estimates for flash calculations is inefficient compared to CSAT when used only to skip stability analysis, and for some cases it is even less efficient than the simulation with only HM1. This is due to the small timesteps used in the IMPEC simulators, which favor using previous flash results with no table search.

Computational advantages of CSAT for the above reported cases are smaller as another option (simulation with both HM1 and HM2) is activated in UTCOMP where

stability analysis for single-phase gridblocks surrounded by single-phase neighbors is skipped. In several cases, the simulation with both HM1 and HM2 even performs better than CSAT. When the fraction of gridblocks in the single-phase region increases, the computational advantages of CSAT and the simulations with both HM1 and HM2 will improve. Thus, there is little advantage to use CSAT in an IMPEC-type simulator over other simpler schemes such as the ones described here to avoid stability analysis for the type of simulation cases that we have performed. We note that in this chapter we used CSAT only to skip stability analysis and to generate initial estimates for flash calculations, but not to approximate the flash results. Even though for other simulation cases or other implementation methods, the computational efficiency of CSAT might be larger compared to our simulation cases, it is reasonable to conclude that in IMPEC-type simulators using the equilibrium and phase-state information from the previous timesteps in each gridblock leads to performance improvements that are comparable to CSAT.

Performance of CSAT for the UTCOMP simulator was also found to be dependent on the value of several parameters (ε, DMIN, $\varepsilon_{critical}$). For several cases, ε values of 0.1 or greater led to simulation failure, however for all of our cases the simulations were successful with ε = 0.01 and DMIN = 0.01. Using smaller values for these parameters improves accuracy, but leads to unacceptably large table search time. For most of our cases, the tie-line table generation time was insignificant. Performance of CSAT also depends on the specific gas injection problem being considered. Under ideal conditions where a significant portion of the gridblocks are in the single-phase region, CSAT leads to good computational gains (see Case 4), but it may also lead to small computational gains compared to the base case original UTCOMP where stability analysis is skipped using a very simple algorithm.

Table 3-1: Corey's relative permeability parameters of oil and gas phases for the simulation case studies.

$k_{rg}^{0} = 0.85$	$k_{ro}^{0} = 0.75$
$S_{gr} = 0.15$	$S_{or} = 0.15$
$e_{gas} = 4$	$e_{oil} = 3.5$ *

* k_{rg}^{0} and k_{ro}^{0} are respectively the gas and oil endpoint relative permeabilities, e_{gas} and e_{oil} are respectively the gas and oil Corey exponents, and S_{or} and S_{gr} are the residual oil and gas saturations, respectively.

Table 3-2: Component properties for simulations in Cases 1, 3, 4, and 5 (Kenyon and Behie, 1987).

	P_c (psia)	T_c (R)	V_c (ft^3/lbmol)	MW	ω
CO_2	1071.34	547.56	1.505	44.01	0.225
N_2	492.32	227.16	1.433	28.01	0.04
C_1	670.14	335.88	1.585	16.04	0.013
C_2	708.35	549.72	2.370	30.07	0.098
C_3	616.3	665.7	2.5	44.1	0.1524
C_{4-6}	498.19	713.16	4.156	67.28	0.234
C_{7+1}	376.22	1030.5	7.709	110.9	0.332
C_{7+2}	245.42	1134.36	12.322	170.9	0.495
C_{7+3}	124.92	1552.68	29.305	282.1	0.833

Table 3-3: Computational efficiency results for Case 1 (similar to Case 1 in Voskov and Tchelepi, 2009a).

	HM1*	HM1 and HM2	WO HM1 and HM2	CSAT (SA) $\varepsilon = 0.01$ DMIN = 0.01	CSAT (SA/Flash) $\varepsilon = 0.01$ DMIN = 0.01
CPU time (*sec*)	159.71	132.27	185.69	131.02	143.18
Phase equilibrium time (*sec*) (SA** time)	82.94 (38.74)	54.52 (10.57)	114.74	54.49	72.44
No. of SA performed (skipped)	5,190,430	1,410,950	8,132,000	82,540 (5,107,890)	86,400
CSAT time (*sec*) /No. of tie-line tables	-	-	-	11.94 /5	24.34/24
Total tie-line table generation time (*sec*)	-	-	-	0.002	0.011
Relative speed to simulation with HM1 and HM2	0.828	1	0.712	1.009	0.924

* HM1: The original UTCOMP simulation that only uses HM1 (uses flash results from the previous timestep in the same gridblock).

HM1 and HM2: The original UTCOMP simulation that uses both HM1 (uses flash results from the previous timestep in the same gridblock) and HM2 (skips stability analysis for single-phase gridblocks surrounded by single-phase neighbors in the previous timestep).

WO HM1 and HM2: The original UTCOMP simulation without any of the heuristic methods (HM1 and HM2). This is not the usual simulation practice with UTCOMP.

CSAT(SA): The simulation uses CSAT only for skipping stability analysis. It also uses HM1.

CSAT(SA/Flash): The simulation uses CSAT for skipping stability analysis and generating initial estimates for flash calculations.

** SA : Stability analysis.

Table 3-4: Overall compositions for which tie-line tables were generated for Case 1.

$\vec{z}_1$	$\vec{z}_2$	$\vec{z}_3$	$\vec{z}_4$	No. of tie-line hits
0.04	0.16	0.2	0.6	5,020,863
0.150635	0.138577	0.177717	0.533072	77,752
0.156338	0.131695	0.177992	0.533976	14,866
0.165026	0.124543	0.177433	0.532997	11,747
0.188411	0.115417	0.174005	0.522168	310

Table 3-5: Component properties for the simulations in Case 2 (Killough and Kossack, 1987).

	P_c (psia)	T_c (R)	V_c (ft^3/lbmol)	MW	ω
C_1	670.14	335.88	1.585	16.04	0.013
C_3	616.3	665.7	2.5	44.1	0.1524
C_6	436.9	913.4	4.7828	86.18	0.3007
C_{10}	304	1111.8	9.66	142.29	0.4885
C_{15}	200	1270	12	206	0.65
C_{20}	162	1380	19.96	282	0.85

Table 3-6: Computational efficiency results for Case 2 (similar to Case 6 in Voskov and Tchelepi, 2009a).

	HM1	HM1 and HM2	CSAT(SA) $\varepsilon = 0.01$ DMIN = 0.01	CSAT (SA/Flash) $\varepsilon = 0.01$ DMIN = 0.01
CPU time (*sec*)	239.84	184.91	182.82	220.32
Phase equilibrium time (*sec*) (SA time)	143.16 (67.05)	87.87 (11.12)	85.11	127.52
No. of SA performed (skipped)	3,604,340	669,370	32,212 (3,572,120)	13,980 (3,593,060)
CSAT time (*sec*) /No. of tie-line tables	-	-	9.35/3	32.13/10
Total tie-line table generation time (*sec*)	-	-	0.0039	0.011
Relative speed to simulation with HM1 and HM2	0.771	1	1.011	0.839

Table 3-7: Computational efficiency results for Case 3 (similar to example case in Voskov and Tchelepi, 2009a).

	HM1	HM1 and HM2	CSAT (SA) $\varepsilon = 0.01$ DMIN = 0.01	CSAT(SA/Flash) $\varepsilon = 0.01$ DMIN = 0.01
CPU time (*sec*)	1,710.82	1,463.26	1,469.92	1,941.13
Phase equilibrium time (*sec*) (SA time)	1,143.99 (262.45)	897.79 (21.53)	906.98	1,360.94
No. of SA performed (skipped)	12,707,298	121,500	123,500 (12,590,870)	334,030 (12,376,340)
CSAT time (*sec*) /No. of tie-line tables	-	-	44.18 / 11	443.41 / 245
Total tie-line table generation time (*sec*)	-	-	0.015	0.303
Relative speed to simulation with HM1 and HM2	0.855	1	0.995	0.754

Table 3-8: Computational efficiency results for Case 4 (similar to Case 4 in Voskov and Tchelepi, 2009a).

	HM1	HM1 and HM2	CSAT(SA) $\varepsilon = 0.01$ DMIN = 0.01	CSAT * (SA/Flash) $\varepsilon = 0.01$ DMIN = 0.01
CPU time (*sec*)	15,119.31	10,037.02	10,719.83	10,723.13
Phase equilibrium time (*sec*) (SA time)	7,119.36 (6,023.36)	1,335.43 (206.10)	2,045.69	2,038.43
No. of SA performed (skipped)	335,304,070	11,040,840	170,920 (335,170,720)	168,800 (335,170,720)
CSAT time (*sec*) /No. of tie-line tables	-	-	890.35/17	889.80/17
Total tie-line table generation time (*sec*)	-	-	0.022	0.03
Relative speed to simulation with HM1 and HM2	0.664	1	0.936	0.936

* This CSAT case uses HM1.

Table 3-9: Computational efficiency results for Case 5 (similar to example case in Voskov and Tchelepi, 2009b).

	HM1	HM1 and HM2	CSAT (SA) $\varepsilon = 0.01$ DMIN = 0.01 $\varepsilon_{critical} = 0.0005$ $\varepsilon_2 = 0.00005$	CSAT (SA/Flash) $\varepsilon = 0.01$ DMIN = 0.01 $\varepsilon_2 = 0.005$ DTMIN=0.001
CPU time (*sec*)	170.248	140.57	151.64	174.175
Phase equilibrium time (*sec*) (SA time)	81.60 (35.51)	49.337 (2.43)	65.98	95.64
No. of SA performed (skipped)	3,832,240	131,640	1,424,560 (2,403,240)	190,750 (3,165,400)
CSAT time (*sec*) /No. of tie-line tables	-	-	8.14/ 231 subcritical and no critical	28.12/ 380 subcritical and 11 critical
Total tie-line table generation time (*sec*)	-	-	0.61	1.125
Relative speed to simulation with HM1 and HM2	0.826	1	0.927	0.807

Table 3-10: Component properties for simulations in Case 6 (Okuno, 2009).

	P_c (psia)	T_c (R)	V_c (ft^3/lbmol)	MW	ω
CO_2	1071.34	547.56	1.505	44.01	0.225
C_1	670.14	335.88	1.585	16.04	0.013
C_{2-3}	653.37	618.88	2.84	38.40	0.130
C_{4-6}	485.94	839.87	5.01	72.82	0.244
C_{7-14}	315.54	1085.86	8.85	135.82	0.600
C_{15-24}	261.51	1321.15	11.59	257.75	0.903
C_{25}-C_{28}	147.038	1421.87	21.04	368.30	0.955
C_{29}-C_{32}	128.362	1479.91	23.97	424.40	1.053
C_{33}-C_{36}	113.681	1532.36	26.79	480.51	1.140
C_{37}-C_{40}	101.852	1580.73	29.48	536.61	1.218
C_{41}-C_{44}	92.1141	1626.06	32.05	592.72	1.290
C_{45+}	71.2558	1750.73	38.88	760.47	1.464

Table 3-11: Computational efficiency results for Case 6.

	HM1	HM1 and HM2	CSAT(SA) $\varepsilon = 0.01$ $\varepsilon_{critical} = 0.0005$ $\varepsilon_2 = 0.00005$ DMIN = 0.01	CSAT (SA/Flash) $\varepsilon = 0.01$ $\varepsilon_2 = 0.0005$ DMIN = 0.01
CPU time (*sec*)	155.16	84.12	156.63	156.94
Phase equilibrium time (*sec*) (SA time)	79.75 (72.78)	8.445 (0.439)	80.23	80.18
No. of SA performed (skipped)	3,849,201	19,640	4,030 (3,845,171)	4,030 (3,845,170)
CSAT time (*sec*) /No. of tie-line tables	-	-	71.92/ 265 subcritical and 255 critical tie-line tables	72.12/ 265 subcritical and 255 critical tie-lines
Total tie-line table generation time (*sec*)	-	-	2.26	2.245
Relative speed to simulation with HM1 and HM2	0.54	1	0.54	0.54

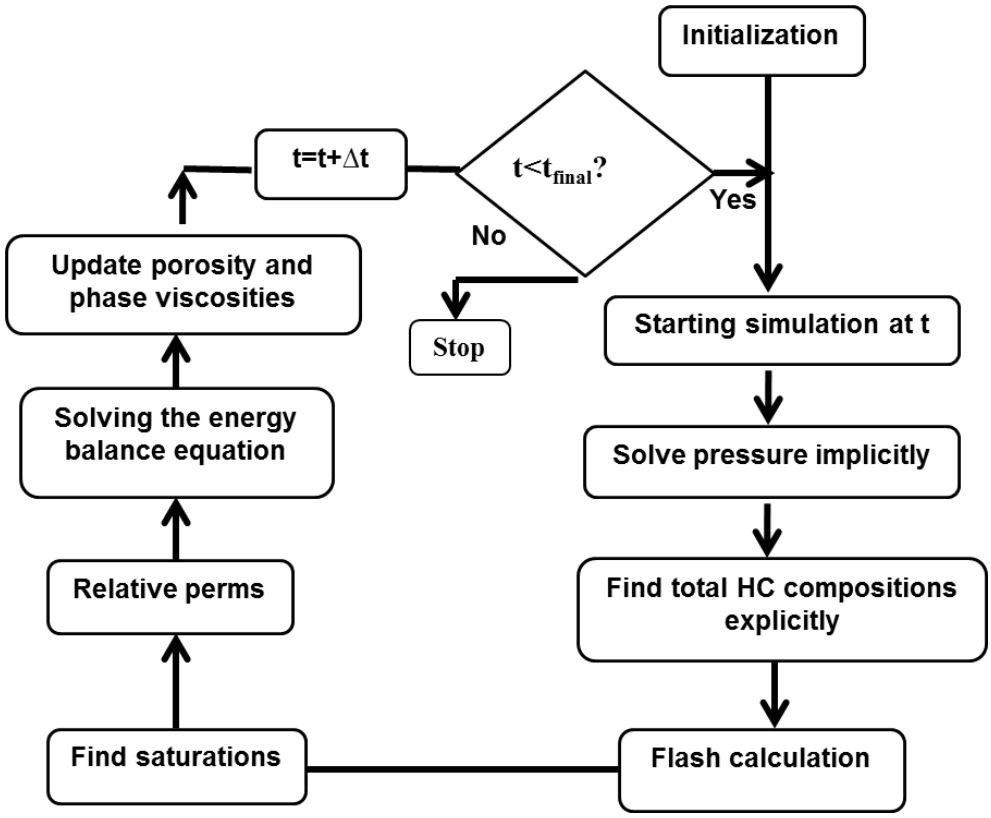

Figure 3-1: The overall computational procedure in UTCOMP (from Korrani, 2014).

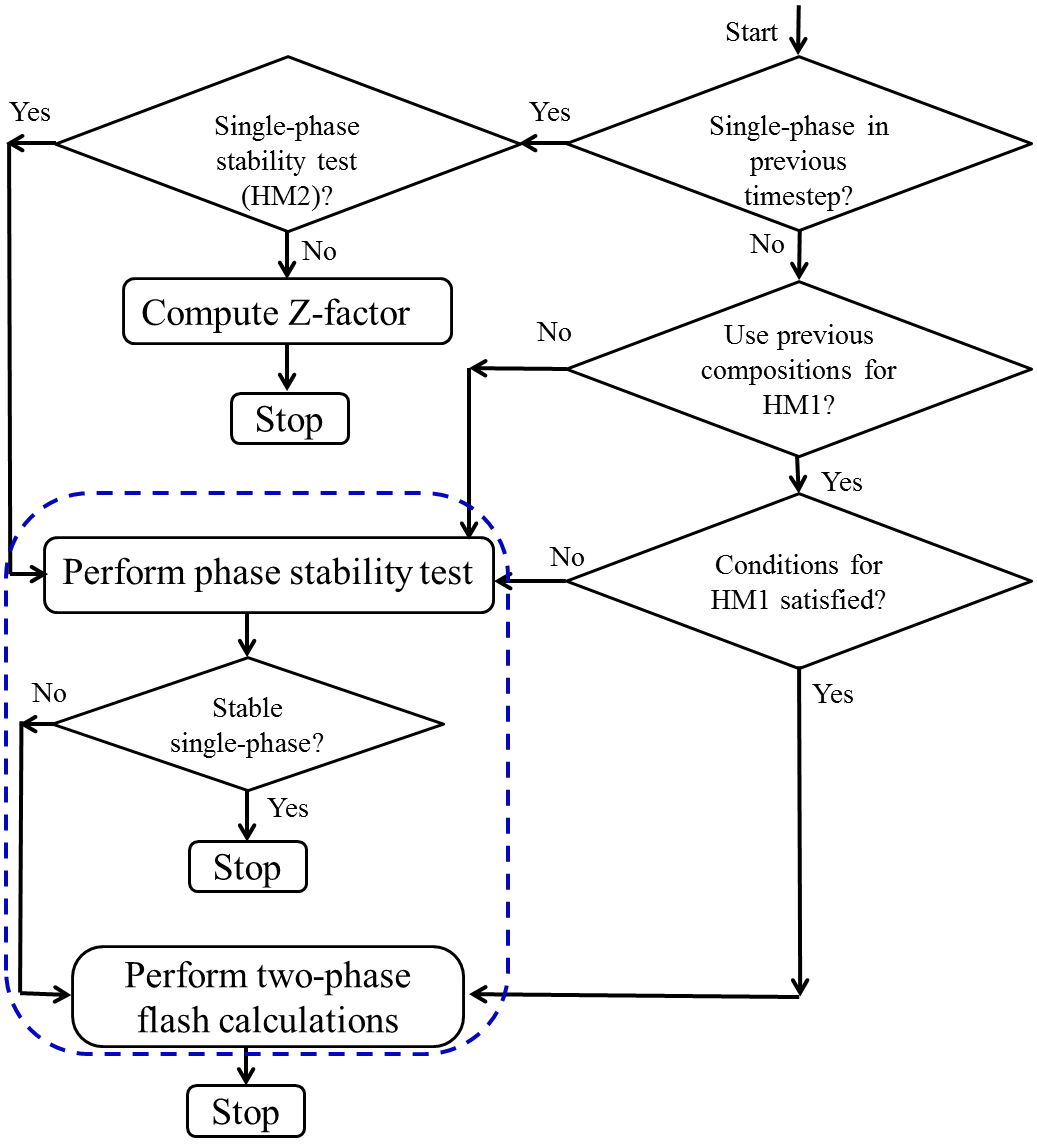

Figure 3-2: Flowchart of phase equilibrium calculations (two hydrocarbon phases) in UTCOMP.

Table 1	
Z_{i1}	
P = 1700 psia	$x_1, x_2, \ldots$
	$y_1, y_2, \ldots$
P = 1800 psia	$x_1, x_2, \ldots$
	$y_1, y_2, \ldots$
P = 2000 psia	$x_1, x_2, \ldots$
	$y_1, y_2, \ldots$
…	…

Table N	
Z_{iN}	
P = 1700 psia	$x_1, x_2, \ldots$
	$y_1, y_2, \ldots$
P = 1800 psia	$x_1, x_2, \ldots$
	$y_1, y_2, \ldots$
P = 2000 psia	$x_1, x_2, \ldots$
	$y_1, y_2, \ldots$
…	…

Figure 3-3: Illustration of subcritical tie-line tables in our implementation of CSAT in UTCOMP.

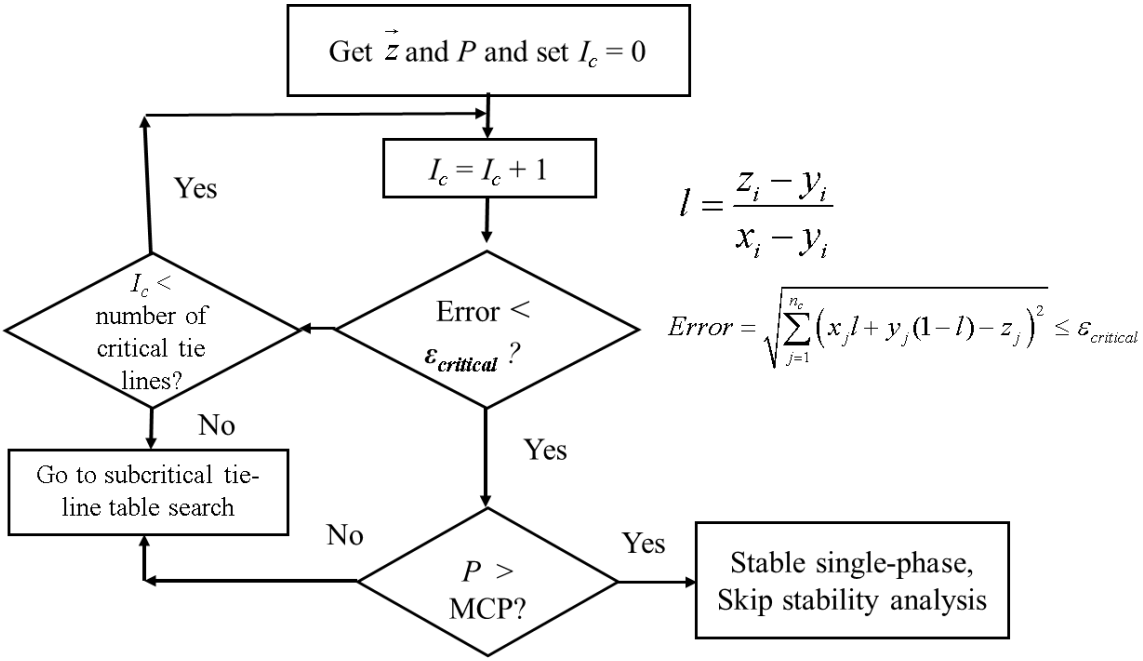

Figure 3-4: The flowchart for critical tie-line table search implemented in UTCOMP.

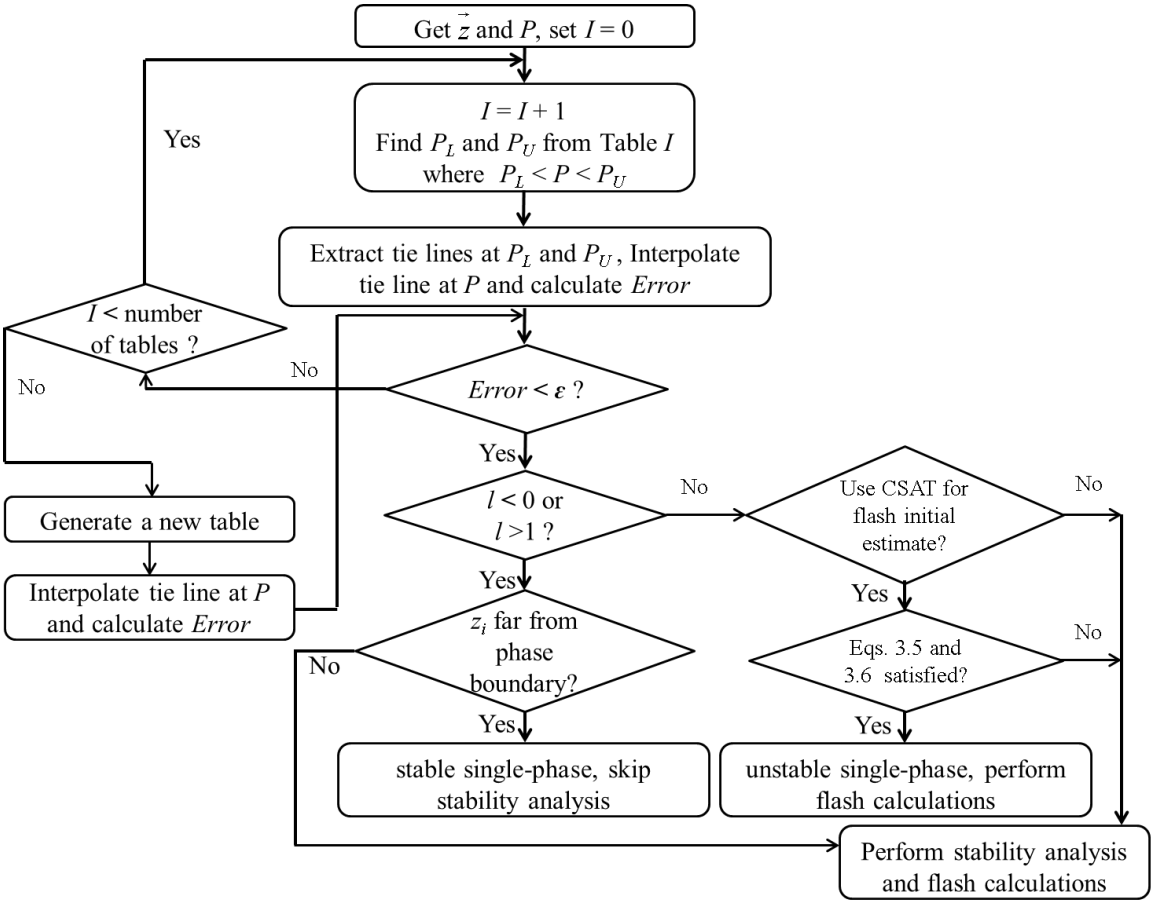

Figure 3-5: The flowchart for subcritical tie-line table search implemented in UTCOMP.

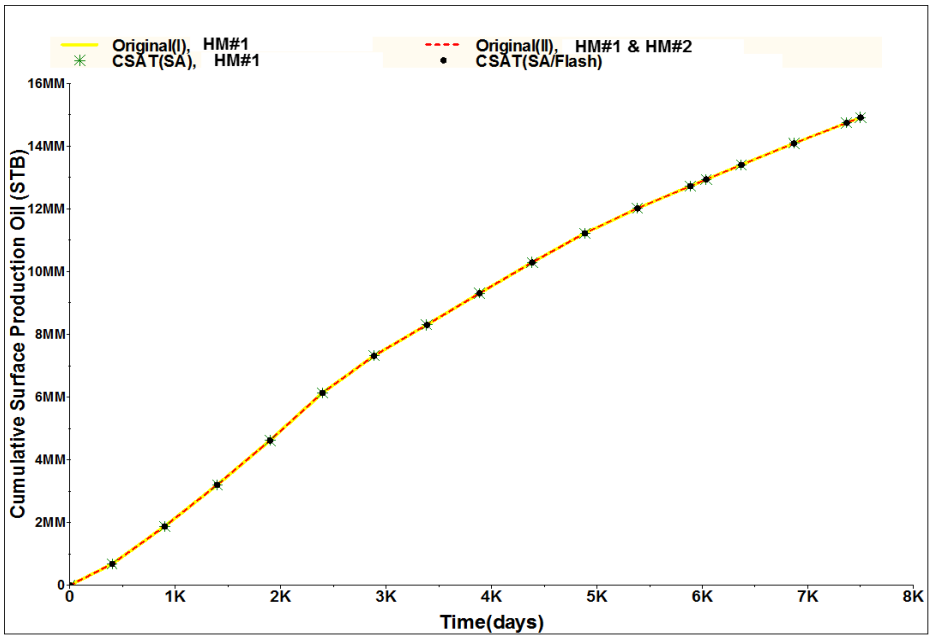

Figure 3-6: Cumulative oil recovery for different simulations in Case 1.

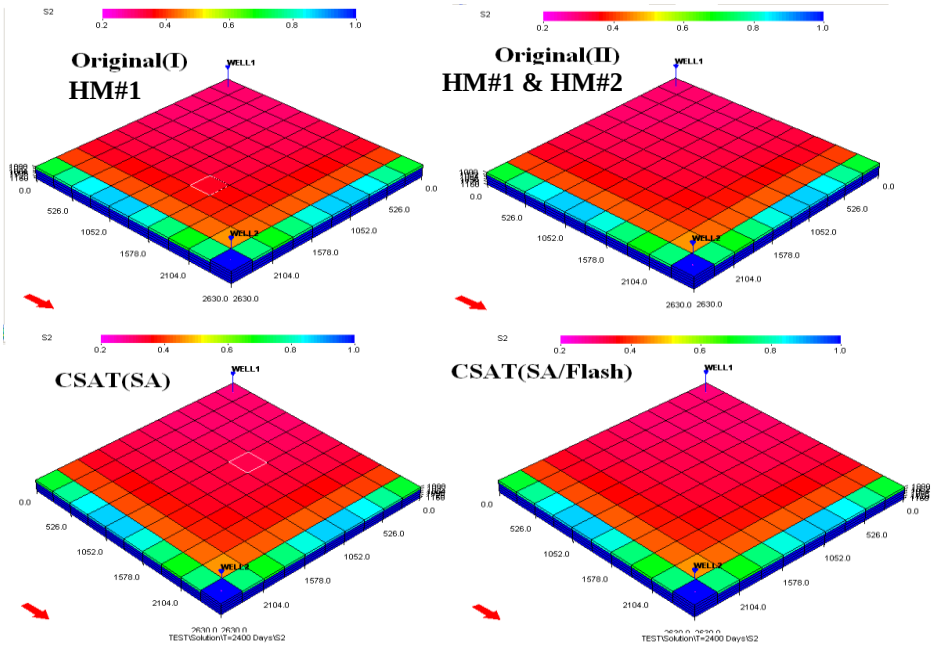

Figure 3-7: Saturation profiles for different simulations at 2,400 days in Case 1.

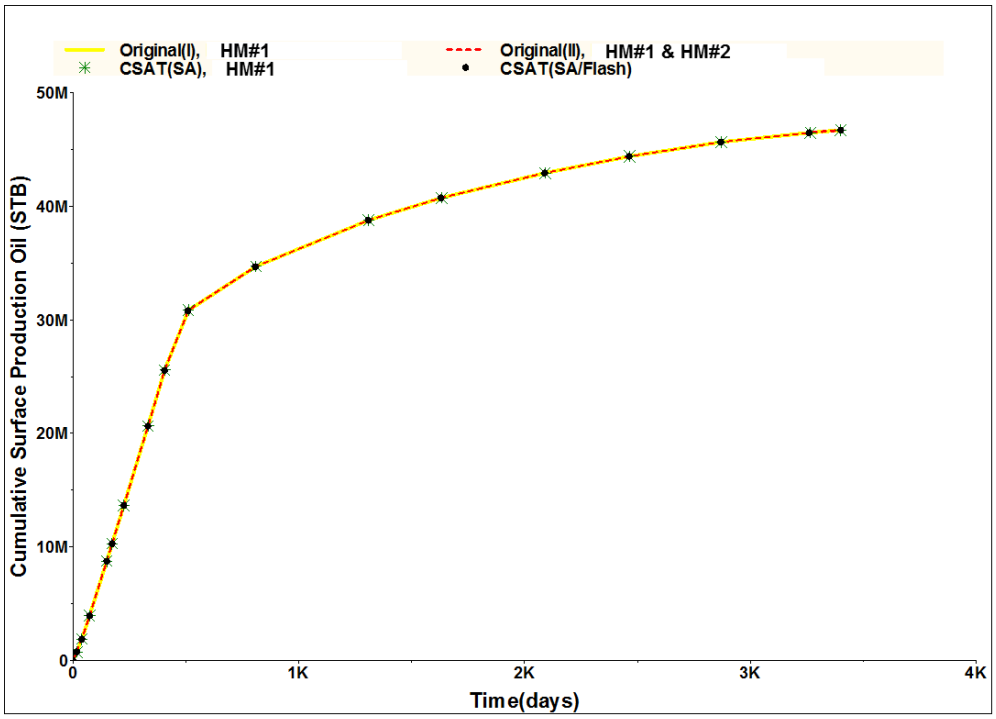

Figure 3-8: Cumulative oil recovery for different simulations in Case 2.

Chapter 4: Application of Multiple-Mixing-Cell (MMC) Method in Compositional Simulation

In this chapter we investigate application of the MMC method in improving speed and robustness of compositional reservoir simulation. We demonstrate that the MMC tie lines represent a significant fraction of the actual compositional simulation tie lines and provide excellent coverage of the simulation compositional route. We developed a robust MMC simulation code which performs MMC simulations of a gas injection problem at various pressure levels, processes the resulting tie lines and outputs the processed tie lines in a format that can be read as initial tie-line tables in the CSAT framework developed in Chapter 3. We suggest three tie-line-based *K*-value simulation methods for application of MMC tie lines in reservoir simulation. In two of the tie-line-based *K*-value simulation methods, we examine tabulation and interpolation of MMC tie lines in a framework similar to the compositional space adaptive tabulation (CSAT). In the third method, we perform *K*-value simulations based on inverse distance interpolation of *K* values from MMC tie lines. The MMC-based methods are then compared to the computational time using other methods of phase equilibrium calculations including a modified application of CSAT (an adaptive tie-line-based *K*-value simulation), a method utilizing only heuristic techniques, and the standard method in UTCOMP, The University of Texas at Austin's in house IMPEC-type reservoir simulator.

4.1 Motivation For Tie-Simplex-Based (TSB) Simulation

The TSB simulation techniques were inspired by the method of characteristic (MOC) solutions of dispersion-free gas-injection processes (Voskov and Tchelepi, 2009a). The MOC solutions apply under limiting conditions of one-dimensional,

dispersion-free gas injection under Riemann boundary condition and at constant pressure. The solution to MOC-type problems is self-similar, that is each concentration wave travels at a constant velocity (Johns, 1992; Johns and Orr, 1996; Dindoruk *et al.*, 1997; Orr, 2007). Consequently, if fine-grid numerical simulation is used to obtain the solution to an MOC-type problem, the history of the overall compositions and hence the tie lines experienced at different spatial points or gridblocks are the same. For example, in a fully self-sharpening n_c-component system where all the key tie lines are connected by shocks (Johns, 1992; Johns and Orr, 1996), only n_c-1 tie lines are sufficient to fully describe the analytical solution. Hence, the complete phase equilibrium information required for numerical simulation of the same problem is present in n_c-1 tie lines, if numerical dispersion effects could be eliminated. Under numerical dispersion, smeared shock fronts form, which may be represented by a few tie lines between the corresponding key tie lines. For MOC systems that are not fully self-sharpening, rarefactions occur along non tie-line paths which in turn cross the tie lines forming ruled surfaces between the corresponding key tie lines. The section of the ruled surfaces of tie lines between any two key tie lines can be represented by a finite number of tie lines with a pre-specified tolerance, demonstrating that the numerical solution of an MOC-type problem only requires a finite number of tie lines.

The solution of actual gas injection processes, however, follows a very complex route mainly due to dispersion. Dispersion is defined as the mixing that occurs during miscible displacement as a result of diffusion, velocity gradients along pores, heterogeneity, and mechanical mixing within pores (Bear, 1972). Numerous studies investigate the influence of dispersion on miscible displacements and attempt to quantify the influence of various mixing mechanisms on gas injection processes (Walsh and Orr,

1990; Johns *et al*., 1994; Jessen *et al.*, 2004; Johns and Garmeh, 2010; Shojaei *et al.*, 2012; Adepoju *et al.*, 2013). Heterogeneity, pressure variations, multi-dimensional flow, variations in the injection rate and composition, and multiple production/injection wells further complicate the compositional route of the actual gas injection processes. However, portions of the solution are still similar to the MOC solution e.g. oil and gas tie lines are always part of the solution. Numerical and physical dispersion drive the solution route towards the dilution line instead of following the MOC route (Walsh and Orr, 1990; Jessen *et al.*, 2004). Even under these complexities, a few tie lines may cover a significant fraction of the compositional route within a certain distance tolerance. CSAT adaptively tabulates the simulation tie lines. However, adaptive tabulation may be susceptible to failure and it may lead to a large number of tables for small distance tolerances. It might be more desirable to look for the closest tie line in a preexisting set of tie-line tables than to perform the adaptive tabulation. Thus, gaining prior knowledge of the tie lines traversed by the solution of a gas injection problem before starting the simulation could be very valuable to improve robustness (provide good initial guess of K values for subsequent flash calculations and identify trivial solutions from a flash calculation), avoid stability analysis altogether, and potentially decrease the flash calculations time. Furthermore, the prior tie lines can be utilized to supplement adaptive tabulation. We use the MMC method in this paper to obtain a representative set of prior tie lines for a simulation displacement without using adaptive tabulation.

4.2 THE MMC METHODS

Several MMC methods have been proposed for calculating MMP of a gas injection process (Cook *et al.*, 1969; Jaubert *et al.*, 1989; Metcalfe *et al.*, 1973; Pederson *et al.*, 1986; Zhao *et al.*, 2006; Ahmadi and Johns, 2011). We use the MMC method that

was proposed by Ahmadi and Johns (2011) in this dissertation. This method is based on performing only PT flash calculations and moving the injected and equilibrium gas ahead of the equilibrium liquid in each cell. The MMC method uses a variable number of cells, and it is independent of gas-oil ratio, cells' volume, the amount of gas injected and transport specific functions. MMC calculations begin with only two cells where the injection gas is located in the upstream cell and the reservoir fluid in the downstream cell (Ahamadi and Johns, 2011). The reservoir oil (x^o) and injection gas (y^g) are then mixed in a specified mixing ratio α (e.g. α = 0.5) in the first contact and the resulting overall composition ($z = x^o + \alpha\ (y^g - x^o)$) is flashed to yield an equilibrium liquid (x) and equilibrium vapor (y) phase (Figure 4-1a). The first contact produces one tie line (*TL#*1) that always intersects the dilution line between the initial oil and injection gas. The location of the intersection point and orientation of *TL#*1 with respect to the gas and oil tie lines is controlled by α. The second contact contains both an upstream and a downstream contact. The upstream contact mixes the equilibrium liquid (x) with fresh injection gas (y^g) and produces *TL#*2. The downstream contact mixes the equilibrium gas (y) with fresh oil (x^o) and produces the *TL#*3. *TL#*2 is positioned in the space between *TL#*1 and the injection gas tie line. Similarly, *TL#*3 is positioned in the space between *TL#*1 and the initial oil tie line. Figure 4-1b shows the oil and gas tie lines, the MMC tie lines of the first two contacts (*TL#*1, *TL#*2, and *TL#*3) and the related dilution lines for injection of 65% C_1 and 35% C_3 into an oil reservoir with initial composition of 20% C_1, 40% C_6, and 40% C_{16} on a quaternary diagram (P = 2,000 psia, T = 200ºF, and α = 0.5). This example was adopted from Johns (1992). The component properties required for phase behavior modeling are given in Table 4-1. The next contact consists of six cells and produces three tie lines. The tie lines from the third contact are positioned in the space

between the oil and gas tie lines and the tie lines from the second contact. Additional cell-to-cell contacts are made based on moving the equilibrium gas ahead of the equilibrium liquid phase in the next contacts. The n-th contact produces n new tie lines and the total number of created tie lines after n contacts is $n(n+1)/2$.

4.2.1 MMC and Simulation Tie Lines

Ahmadi and Johns (2011) demonstrated that with sufficient number of contacts the same set of key tie lines is obtained using the MMC method compared to the analytical MOC solution. The tie lines of an actual simulation displacement, however, deviate from the MOC solution due to physical and numerical dispersion and mixing effects resulting from multi-dimensional flow. The MMC method accounts for various levels of mixing of the injected gas and initial oil. The tie lines that are formed in the early contacts are most likely to represent the tie lines of an actual simulation due to mixing between oil and gas, and therefore bound all tie lines developed during the simulation. We first investigate the tie lines that are formed after different numbers of contacts are taken using the MMC method. We compare the MMC tie lines from different number of contacts with the simulation tie lines. We demonstrate applicability of the MMC tie lines in the context of reservoir simulation before applying the method in a reservoir simulator.

We performed one-dimensional gas injection displacements at constant pressure with different levels of grid refinement and collected all the simulation overall compositions (compositional route). The compositions were then compared to the MMC tie lines to find the fraction of the compositional route that lies on the MMC tie lines within a pre-specified tolerance. The fluid model examined in this section consists of nine components and is taken from the SPE 3 problem (Kenyon and Behie, 1987). The initial

reservoir fluid is composed of 1.3% CO_2, 1.9% N_2, 16% C_1, 8.7% C_2, 5.9% C_3, 9.7% C_{4-6}, 4.7% C_{7+1}, 11.5% C_{7+2}, and 40.3% C_{7+3} and the injection gas is 90% C_1 and 10% C_3. The component properties required for phase behavior modeling are given in Table 3-2. Reservoir temperature is 120°F and initial reservoir pressure is 3,500 psia. The injection and production pressures are 3,525 and 3,475 psia, respectively. The small pressure drop of 50 psia between the injector and the producer was imposed to mimic a constant pressure displacement. The total simulation time is 2,000 days. The length of the linear system (L) is 2,500 ft. We performed the simulations with a wide range of number of gridblocks from 5 to 10,000 to impose different levels of numerical dispersion in order to approximate various levels of dispersion possible in real simulation problems.

The cell Peclet number was used as a dimensionless measure of dispersion. The Peclet number describes the ratio of convective to dispersive transport. Fanchi (1983) derived the expression for numerical dispersion when the finite difference scheme is explicit in time and uses backward spatial difference (equivalent to the upstream weighting of concentrations in reservoir simulation). The cell Peclet number (Pe) was calculated from

$$Pe = \frac{v_i L}{D_L} = \frac{v_i L}{\frac{v_i \Delta x}{2}\left(1 + \frac{v_i \Delta t}{\Delta x}\right)} \approx \frac{2L}{\Delta x}, \qquad (4.1)$$

where v_i is interstitial velocity, L is length of the linear model, D_L is the longitudinal dispersion coefficient, Δx is the gridblock size, and Δt is the timestep size.

Figure 4-2 shows the percentage of simulation overall compositions which lie on the MMC tie lines collected from a different number of contacts at various values of cell Peclet number for a mixing ratio of 0.5. The distance tolerance of 0.01 was used to

indicate a matching tie line. The horizontal axis indicates how many contacts of the MMC were used to match the simulation overall compositions. For example, 10 contacts indicate that 55 tie lines from the first 10 contacts were used for comparison against the simulation tie lines. Figure 4-2 shows that for each Peclet number, the percentage of tie-line hits increases with increasing number of MMC contacts until it stabilizes at a maximum value. For each Peclet number, there is a specific contact number at which the maximum tie-line hits occur and further increase in the number of contacts does not increase the tie-line hits significantly. The expected Peclet number in practical reservoir simulation problems roughly varies from 20 to 2,000 depending on the scale of the displacement. Figure 4-2 shows that the number of contacts required to achieve the maximum tie-line hits for this range of Peclet number is smaller than 200. In fact, the MMC tie lines from only 20 contacts contribute to more than 75% of tie-line hits for the expected range of Peclet number in actual simulation problems.

As the Peclet number increases the maximum fraction of simulation overall compositions that lie on the MMC tie lines increases but larger number of contacts are required to obtain the maximum tie-line hits. This is expected because it takes an infinite number of contacts in the MMC method to achieve the MOC solution exactly (the dispersion-free limit). For MMC tie lines with mixing ratios of 0.2 and 0.8 similar trends are obtained but the maximum number of tie lines hit slightly changes. Figure 4-3 shows the maximum percentage of tie lines hit and the number of MMC contacts required for the maximum hits versus Peclet number for different mixing ratios. There are small differences among the maximum hits for various Peclet numbers and different mixing ratios but the results for different mixing ratios generally show the same trends. Figure 4-3 confirms that for small Peclet numbers encountered in reservoir simulation, a small

number of contacts are sufficient to obtain the maximum number of tie-line hits. The MMC tie lines in the early contacts are different for different mixing ratios. Using 200 contacts and three mixing ratios (0.2, 0.5 and 0.8) collectively, the percentage of tie-line hits significantly increases to 98%, 99%, 92%, and 89.1% for the Peclet numbers of 2000, 200 and 20, and 10, respectively. Therefore, using additional mixing ratios increases the number of tie-line hits at a given contact number.

To demonstrate applicability of the MMC tie lines under multi-dimensional flow problems, a similar comparative study was performed for a three-dimensional reservoir model. We performed simulations for a five-component fluid model in a quarter of a five-spot pattern with two levels of grid refinement (10×10×5 and 20×20×10). The initial oil composition is 30% C_1, 3% C_3, 7% C_6, 20% C_{10}, and 40% C_{15}. The injection gas is pure C_1. The fluid properties required for phase behavior modeling are given in Table 3-5. The injector and producer bottomhole pressures are 3,000 psia and 1,000 psia, respectively and reservoir temperature is 160ºF. The compositional route of the displacement at 1,700 ± 25 psia was compared to the MMC tie lines for two distance tolerances of 0.01 and 0.001. Figure 4-4 shows the percentage of simulation compositional route that lies on the MMC tie lines for different number of contacts. Similar to the one-dimensional displacements, the tie-line hits increase with increasing number of contacts. The number of contacts required to obtain the maximum tie-line hits is very small because of the increased level of mixing and more dispersion compared to the one-dimensional simulations. Interestingly, for the 10×10×5 gridblock model, the compositional route of the simulation is completely covered by the MMC tie lines for only 10 contacts within a distance tolerance of 0.01 at the investigated pressure. For one level of refinement, the maximum percentage of tie-line hits is 97% with MMC tie lines of only 15 contacts. The

above results for one and three-dimensional simulations suggest that the MMC tie lines represent a significant fraction of the simulation tie lines and cover almost the entire compositional route within a reasonable distance tolerance.

4.2.2 MMC and MOC Tie Lines

The MMC tie lines at small number of contacts were shown to closely approximate the simulation tie lines. The MMC tie-lines at large number of contacts will approach the dispersion-free MOC solution route and may not be as influential in reservoir simulation with significant dispersion. We demonstrate that for sufficiently large number of contacts (at the limit of an infinite number of contacts) the MMC tie lines generate ruled surfaces of tie lines which are the same as the ruled surfaces and the shock surfaces traversed by the MOC solution route. In fact, for a fully self-sharpening system with only four components and constant *K* values, it is easy to verify that the MMC tie lines create the planes that define the MOC's cross-over tie line. For such a system, the cross-over tie line intersects both the oil and gas tie lines generating two planes which contain the MMC tie lines when a large number of contacts have occurred. Intuitively, at an infinite number of contacts an infinite number of tie lines are to be positioned between the initial oil and the injected gas tie lines in the compositional space. This will require each tie line to intersect its immediate adjacent tie line separated by infinitesimal distance in order to create a continuous transition from the oil tie line to the gas tie line. This is consistent with the concept of ruled surfaces of tie lines in the MOC solution (Johns, 1992). Figure 4-5 shows the MMC tie lines (red lines) of the 100th contact for the injection of 65% C_1 and 35% C_3 into an oil reservoir with initial composition of 20% C_1, 40% C_6, and 40% C_{16} at 2,000 psia and 200ºF. This example was adopted from Johns (1992). The injection gas, initial oil and the cross-over tie lines from

the MOC solution are also given. The MMC tie lines between the cross-over and the gas tie lines lie close to the plane that these two key tie lines create. Figure 4-6 superimposes a portion of the solution route of the three-dimensional simulation (10×10×3 gridblocks) of the same displacement problem on the MMC tie lines of the 100th contact. Figure 4-6 shows that the solution route is close to the MMC tie lines. Where the solution route deviates from the MMC tie lines, it tends to disperse in the quadrant (formed by ruled tie-line surfaces containing the cross-over tie line) that contains the dilution line between the injection gas and initial oil. Interestingly, the first MMC tie line in the first contact is obtained for a point on the dilution line, and the later contacts develop and move the MMC tie lines toward the MOC ruled surfaces. Therefore, it is reasonable to expect that the MMC tie lines with different mixing ratios provide a good coverage of the composition route of the three dimensional simulations.

Figure 4-7 shows the three-dimensional-simulation tie lines of the four-component displacement (pink circles) and the MMC tie lines of the first contact (red squares) and the 100th contact (blue squares) for different mixing ratios in the tie-line space ($\gamma_i = (x_i + y_i)/2$). The MMC tie lines of 12 different mixing ratios were used. Figure 4-7 shows that the simulation tie lines of the four-component displacement are bounded by the MMC tie lines of the first and 100th contact when several different mixing ratios are used. The oil, gas and cross-over tie lines are also specified in Figure 4-7. Figure 4-8 shows the MMC tie lines of the first contact, the intermediate contacts (second to 99th) and the 100th contact for 12 different mixing ratios. The MMC tie lines of the intermediate contacts occupy the same space that the simulation tie lines do, which further corroborates application of the MMC tie lines in approximating simulation tie lines. Even though such an approximation is usually sufficient for practical simulation

purposes, one cannot conclude that the approximation error will go to zero upon using MMC tie lines from infinitely many mixing ratios and infinite number of contacts.

4.3 Application of MMC Method in Compositional Simulation

The tie lines obtained at small number of contacts of the MMC method fit in the compositional space between the oil and gas dilution line and the MOC solution. The portion of the space between the dilution line and the MOC solution that is filled with the MMC tie lines depends on the mixing ratio. Therefore, using MMC tie lines with several mixing ratios is expected to produce tie lines that are sufficiently close to the simulation tie lines. This observation suggests that MMC tie lines can be utilized in an interpolation scheme similar to CSAT in order to improve speed and robustness of the reservoir simulators. We investigate this idea in the context of an IMPEC-type reservoir simulator. We investigate three possible methods for employing the MMC tie lines in reservoir simulation and present the methodology for tabulation of the MMC tie lines.

4.3.1 Tie-line Tabulation Using MMC Method

The multiple contacts in the MMC method suggested by Ahmadi and Johns (2011) are performed at a constant pressure and temperature. In actual simulation problems pressure varies in time and space coordinates. We divide the expected pressure range of the simulation into several discrete pressure levels and perform individual MMC simulations at the different pressure levels. The MMC simulations can be performed up to any number of contacts however we do not perform the simulations beyond 20 contacts. The results of the previous examples demonstrate that only a few contacts provide acceptable tie lines for an actual simulation problem and benefits of using tie lines from more contacts are minimal. We use two different strategies for grouping MMC

tie lines at different pressures depending on the interpolation technique employed in the simulation problem. First, we group the corresponding tie lines from different pressure levels into individual tie-line tables similar to the CSAT tabulation. For example, all the tie lines obtained in the first contact at different pressure levels are grouped into one tie-line table. If the tie-line length is smaller than a pre-specified tolerance (0.005) at a certain pressure, it is marked as a critical tie line and the corresponding pressure is used as its minimal critical pressure (MCP). The second method is to group all the tie lines collected at each pressure level into one table. After only a few contacts, many repeated tie lines are encountered within a tolerance of 0.01 or 0.001. We eliminated the repeated tie-line tables from the collected tables. One may perform the MMC simulations with several different mixing ratios to obtain more comprehensive tie-line tables if tie lines from one mixing ratio are deemed insufficient.

Although the oil and gas tie lines tend to develop after a few contacts in the MMC simulations, we always calculate the exact oil and gas tie lines and use them as the first and second tie-line tables in the initial search order. We used the PennPVT toolkit (PennPVT toolkit, 2010; Ahmadi and Johns, 2011) to validate our MMC code and tie-line table calculations. In our MMC simulation code we used the negative-flash calculations core that was discussed in Chapter 3. The MMC simulation code performs MMC simulations of a specific gas injection process at various pre-specified pressure levels, eliminates the repeated tie lines within a tolerance at each pressure level, and outputs the remaining tie lines in the specific format that is readable by each of the MMC-based simulation methods. We describe the various MMC-based-simulation methods in the next section.

4.3.2 Simulation Techniques Using MMC Tie lines

We investigate three possible methods for employing the MMC tie lines in reservoir simulation. Other variants might be possible, but we limit our investigation to these three methods in order to demonstrate the potential of using MMC tie lines in reservoir simulation. The first two MMC methods are tie-line-based *K*-value simulation methods using an interpolation framework similar to CSAT but without any adaptive tabulation. The first method retrieves a matching tie line from the initial table only if the required distance tolerance is met while the second method always retrieves either a matching tie line or the closest tie line. The third method uses inverse distance interpolation of all the MMC tie lines at the pressure of interest to obtain the *K* values used in the *K*-value simulation. These methods were implemented in UTCOMP. We compare the computational efficiency of the above MMC-based methods with standard UTCOMP simulation and two other phase behavior modeling speedup methods namely a modified CSAT (an adaptive *K*-value simulation) and pure heuristic techniques. The detailed description of the methods used in the comparative study is as follows:

1. **UTCOMP 1**: This method uses UTCOMP's phase equilibrium calculations algorithm which always attempts to avoid stability analysis calculations using flash results in the previous timestep in the same gridblock, and to generate initial estimates for flash calculations if a single-phase mixture is determined to be unstable. We examine accuracy and speed of the other methods compared to this method. The detailed description of phase equilibrium algorithms in UTCOMP are given in Perschke (1988).
2. **UTCOMP 2**: This method employs two additional heuristic techniques to speed up phase equilibrium calculations in addition to those described for UTCOMP 1. First,

stability analysis for a gridblock is skipped if it is surrounded by single-phase neighbors of the same phase number in the previous timestep. Second, if the overall composition is sufficiently close to the previous tie line in the same gridblock, the *K* values from that tie line are adopted and a Rachford-Rice (RR) calculation (Rachford and Rice, 1952) is performed to obtain the equilibrium compositions and molar fractions. This technique is called tie-line distance based approximation (TDBA) and was suggested by Belkadi *et al*. (2011).

3. **CSAT**: Because of the stability limit in IMPEC-type simulators, the phase equilibrium results from the previous timestep provide very good information on the equilibrium state in the next timestep. Therefore, in the context of IMPEC-type reservoir simulators, using CSAT or the MMC-based methods to skip stability analysis and precondition flash calculations is not as efficient as what has been reported in the literature for fully implicit simulators (Rezaveisi *et al.*, 2014a). Hence, in this chapter we use CSAT to approximate flash results in addition to skipping stability analysis and preconditioning flash calculations. That is, once an overall composition is determined to be in the two-phase region by the interpolated tie line from CSAT, we accept the *K* values from that tie line and perform a RR calculation to obtain phase compositions and molar fractions. This is basically an adaptive *K*-value simulation based on CSAT tie lines. This approximation will lead to loss of accuracy but we show that significant improvements in the computational time are obtained with acceptable errors compared to the UTCOMP 1 simulation. This modification in implementation of CSAT and the MMC-based methods was necessary to obtain percentage improvements in the computational time that allow obvious distinction between computational performances of different techniques. In our experience, a

distance tolerance of 0.01 is sufficiently accurate for skipping stability analysis using CSAT; however, applying the same criterion for approximating flash results may produce inaccurate results. Therefore, we use two different distance tolerances for skipping stability analysis and approximating flash results. The rest of the implementation details of CSAT in UTCOMP are given in Chapter 3 of this dissertation and in Rezaveisi *et al.* (2014a).

4. **MMC1**: In the simulations with this method we use the above CSAT framework with only the MMC tie lines i.e. without adaptive tabulation. Adaptive tabulation offers the obvious advantage of adaptively parameterizing the compositional route of the gas injection process and hence always producing sufficiently close tie lines to the compositional route. A fixed initial table of tie lines, on the other hand, offers the advantage of eliminating the possibility of failed tie-line tabulation calculations. The distance tolerances for skipping stability analysis and approximating flash results, and the number of contacts used in the MMC method are the parameters that may vary in different simulation runs using MMC1. Flash calculations and/or stability analysis are performed in MMC1 when the tolerances are not met, but these new flash calculations are not saved in the tables.
5. **MMC2**: This method is a tie-line-based *K*-value simulation where *K* values are interpolated from the MMC tie lines. The tabulation format of the MMC tie lines for this method is the same as that of CSAT. This approach is very similar to the tie-line-based *K*-value method presented by Rannou *et al.* (2013). However, they used one-dimensional simulations to create the tie-line tables used in the *K*-value interpolation. Furthermore, Rannou *et al.* (2013) always find the closest two tie lines to perform inverse distance interpolation of the *K* values for subcritical compositions. We use the

K values from the first MMC tie line that satisfies a pre-specified distance tolerance. If a matching tie line within the required tolerance is not found from any of the MMC tie lines, *K* values are interpolated from the closest two tie lines by inverse distance interpolation. If the interpolated *K* values for an overall composition indicate existence of a two-phase mixture, a RR calculation is performed to obtain phase compositions and molar ratios. The rest of the implementation details of this method are similar to MMC1. We note that the MMC2 method always retrieves a matching tie line from the tie-line tables, while MMC1 may revert to regular phase equilibrium calculations if the required distance tolerance is not met.

6. **MMC3**: This method is also a *K*-value simulation based on the MMC tie lines. In this method all the MMC tie lines obtained for each pressure level are grouped into separate tables. For a given overall composition and pressure, the MMC tie lines are first interpolated to the pressure of interest and then an inverse distance interpolation of *K* values from all the tie lines is performed. The *K* values are then used to decide if the mixture is single-phase or two-phase. A RR calculation is performed to obtain the phase equilibrium information if existence of a two-phase mixture is determined.

4.4 SIMULATION CASE STUDIES

Several simulation cases were studied to compare the computational efficiency of the above methods including those that only use the MMC tie lines. The simulations were performed using constant timestep sizes to ensure that the simulations with different methods go through the same timesteps. Because of the approximations applied to obtain the phase equilibrium information, the simulation results of different methods are not numerically the same. Therefore, we report the mean and maximum value of the relative error in oil rates as well as the mean absolute error in oil saturation for all gridblocks, and

for each method compared to the simulation with UTCOMP 1. All of the simulations were performed using the Peng-Robinson (PR) EOS (Peng and Robinson, 1976) for the phase equilibrium calculations.

The simulation cases considered are two-phase gas injection into oil reservoirs. There is no mobile water phase. Corey model (Corey, 1986) was used for the oil and gas relative permeability using the parameters given in Table 4-2. Capillary pressure was assumed to be zero in all the simulations.

The simulations were performed on dedicated CPU nodes with 2.73 GHz CPU and 15.86 GB of memory (RAM). In our table search, we used a partial sorting strategy, which brings the most recently hit tie-line table one step forward in the search order if its number of successful hits is greater than that of the prior tie-line table in the search order. We also tested a neighbor-based algorithm for table search, where we keep track of the index of the last tie line that was successfully used in each gridblock. In the search for finding the matching tie line in later timesteps, the indexes corresponding to the last successful tie lines in the same gridblock and its neighbors supersede our regular partial-sorting-based search order. In other words, to find a matching tie line we first test the last tie-line tables that were successfully used in the same gridblock or its neighbors in the previous timesteps. If a matching tie line within the required tolerance is not found, then the rest of the tie-line tables are tested in the order of their successful number of hits. For the current grid model, we did not observe significant improvement in computational time using the neighbor-based search algorithm probably because of the small number of gridblocks. However, for very large number of gridblocks it is possible that such a search algorithm will be more efficient.

One of the main computational kernels in the simulations with UTCOMP is setting up the pressure-equation matrix using explicit saturation/composition-dependent terms and solving the resulting linear system of equations. After solving the pressure equation, the total number of moles of each component in each gridblock is calculated using the discretized mass conservation equations with forward differencing in time. These calculations do not involve iterations and are computationally inexpensive. The other computational kernel in the UTCOMP simulator is the thermodynamic equilibrium calculations i.e. stability analysis and flash calculations. The contribution of this part of the calculations to the total computational time depends on various parameters including the number of gridblocks, number of fluid components, number of hydrocarbon phases, and complexity of the fluid model. Usually the stability analysis calculations are computationally less demanding than phase-split calculations. In our simulation cases, the thermodynamic equilibrium calculations contribute to approximately 60% of the total computational time; however, for other problems this contribution may vary from 30% to 60%. The main computational kernel in the thermodynamic equilibrium calculations using CSAT, MMC1, and MMC2 is the table search for finding the matching tie-line. The tie-line table generation time is insignificant for these methods. Inverse-distance interpolation of the approximating tie line is the main operation that needs to be performed in the MMC3 method. The RR calculation of a two-phase mixture is the other computational kernel of all the tie-line-based *K*-value simulation methods.

We used a three dimensional grid model with 20×20×6 gridblocks and a heterogeneous stochastic permeability field for all the simulations. The permeability field was populated using a Dykstra-Parsons coefficient of 0.1 for the simulation Cases 1 to 4

and 0.8 for the simulation Cases 5 to 7. The mean of the log-normal permeability field is 30 md. The correlation length in each direction was 50% of the length of the medium.

4.4.1 Case 1

Case 1 is high pressure N_2 injection into an oil reservoir in a quarter of a five-spot pattern. Initial composition of the reservoir fluid is 1.3% CO_2, 1.9% N_2, 16% C_1, 8.7% C_2, 5.9% C_3, 9.7% C_{4-6}, 4.7% C_{7+1}, 11.5% C_{7+2}, and 40.3% C_{7+3}. Injected fluid is 90% N_2 and 10% C_1. Injection pressure is 11,000 psia and production pressure is 10,000 psia. Injector and producer are in opposite corners of the reservoir. Initial reservoir pressure is 10,500 psia and reservoir temperature is 120°F. Total simulation time is 600 days, which will lead to injection of 2.8 PV of gas into the reservoir. The fluid properties are taken from the SPE 3 problem (Kenyon and Behie, 1987). The fluid properties required for EOS modeling are given in Table 3-2. The computational efficiency results for this case are given in Table 4-3. A constant timestep size of 0.25 days was used. This timestep size was selected by trial and error to produce the same results as that of UTCOMP simulation with more conservative timesteps in the automated timestep selection mode.

We run several simulations with different values of the relevant parameters for all the methods. For each method, the computational performance of the fastest simulation that produces sufficiently accurate simulation results is reported in Table 4-3. All of the simulations reported in Table 4-3 produce oil rates and saturation fields that are close to the base UTCOMP simulation. We report the maximum and mean value of the relative errors in oil rate among all the timesteps and the mean absolute error in oil saturation for all gridblocks at 150 and 550 days for each simulation method.

The phase equilibrium calculations comprise 58.7% of the computational time in UTCOMP 1 simulation where 1,231,460 stability analyses and 4,533,341 phase-split

calculations are performed. Using the heuristic techniques to skip stability analysis and approximate flash results in the UTCOMP 2 method leads to 33.0% improvement in the computational time with reasonable accuracy. This improvement in computational time is obtained through skipping 1,023,356 stability analyses and approximating the results of 3,368,231 phase-split calculations using *K* values from the previous tie line in the same gridblock. This improvement is significant considering simplicity of the heuristic techniques. The distance tolerance for using the previous tie line to approximate the flash results was 5×10^{-5}, which is smaller than the required tolerance for the same accuracy using CSAT or the MMC-based methods. This is because in the UTCOMP 2 method the *K* values of the previous tie line are accepted without any correction for the pressure change during the timestep while in CSAT and MMC-based methods the *K* values are obtained from an interpolated tie line at the pressure of interest. The mean absolute error in oil saturation at 150 and 550 days are 0.00034 and 0.00277, respectively. The mean and maximum relative errors in oil rates are 2.71% and 14.04%, respectively. Using a larger value for the distance tolerance led to less accurate results and using a smaller tolerance (1×10^{-5}) gives slightly more accurate results at the expense of fewer allowed approximations and hence less improvement in the computational time.

The simulation with CSAT leads to 45.6% improvement in computational time, which results from skipping almost all of the stability analyses and approximating all the phase-split calculations using *K* values interpolated from CSAT tie lines. We reiterate that in Chapter 3 of this dissertation we used CSAT only to skip stability analysis and generate initial estimate for flash calculations not to approximate flash results using *K* values from CSAT. The distance tolerance for skipping stability analysis and approximating flash results was 0.01. The distance tolerance of 0.01 usually worked well

for skipping stability analysis with CSAT but a more strict tolerance may be required to produce sufficiently accurate results while approximating flash results. Adaptive tabulation produced 43 tie-line tables and two critical tie lines. The mean absolute error in oil saturation at 150 and 550 days are 0.0027 and 0.0039, respectively. The mean and maximum relative errors in oil rate are 0.78% and 15.9%, respectively. CSAT simulations with more strict distance tolerances produced slightly more accurate results at the expense of less improvement in the computational time.

The simulation with the MMC1 method leads to 45.4% improvement in the computational time, which is very close to the time improvement obtained using CSAT. Almost all of the stability analyses were skipped and approximations were made for all of the flash results for a distance tolerance of 0.01. For this simulation 120 tie-line tables (four critical tie lines) were collected from 20 contacts of three MMC simulations with mixing ratios of 0.2, 0.5, and 0.8. Only 44 tie-line tables were used for interpolation during the simulation. The oil and gas tie lines were placed as the first and second tie lines in the initial search order. The gas tie line contributed to 21.13% of the subcritical tie-line hits. The oil tie line becomes critical at a pressure of 10,391.80 psia and it contributes to 99.3% of the critical tie-line hits. The distance between the liquid and vapor compositions of the oil and gas tie lines are 0.866 and 1.0687, respectively. The computational performance of the MMC1 tie-line interpolation method with a fixed tie-line table confirms that the MMC tie lines represent a significant fraction of the simulation tie lines. The mean absolute errors in oil saturation at 150 and 550 days are 0.0039 and 0.0062, respectively. The mean and maximum relative errors in oil rate are 1.04% and 9.49%, respectively. We repeated this simulation with MMC tie lines from 20 contacts for a mixing ratio of 0.5. The improvement in the computational time compared

to the simulation with UTCOMP 1 was 44.2% due to slightly fewer matching tie lines. The MMC1 simulation with tie lines from only 10 contacts leads to 42.8% improvement in the computational time. The improvements obtained in the computational time are not very sensitive to the number of mixing ratios employed in MMC simulations for this specific injection and initial fluid.

The simulations with the MMC2 method leads to 47.1% improvement in computational time compared to the UTCOMP 1 simulation. Similar to the simulation with MMC1, the MMC tie lines from 20 contacts of three mixing ratios were used. In this method the matching tie line for an overall composition is obtained by inverse distance interpolation of the closest two tie-lines. If during the search for the closest two tie lines, the distance of the overall composition to a tie line is found to be less than a pre-specified tolerance (0.01 in this case), that tie line is taken as the matching tie line. The values of mean absolute error in oil saturation at 150 and 550 days are 0.0029 and 0.0061, respectively. The values of mean and maximum relative error in oil rate are 0.98 % and 6.68%, respectively. Most of the simulation overall compositions were closer than the required tolerance (0.01) to the MMC tie-lines. The farthest subcritical simulation overall composition from the MMC tie lines used distances of 0.0119 and 0.0103 from the closest two tie lines for the *K*-value approximation. MMC2 simulation with MMC tie lines from 20 contacts and with a mixing ratio of 0.5 improves the computational time by 46.5%.

The simulation with MMC3 method using 35 tie lines from 10 contacts leads to 24.06% decrease in the computational time. The inverse distance interpolation was performed with distance exponent of two. The mean absolute error in oil saturation at 150 and 550 days are 0.0022 and 0.00535, respectively. The mean and maximum values of

relative error in oil rate are 1.33% and 11.1%, respectively. If only 11 tie-line tables from MMC simulation are employed the computational improvements compared to the UTCOMP 1 simulation increase to 41.3%. However, the mean and maximum relative errors in oil rate increase to 11.0% and 66.4%, respectively. This method is of less accuracy compared to the other methods even though it also improves the computational time significantly.

For this case study most of the tested methods improve the computational time significantly with acceptable accuracy. The MMC1 and MMC2 methods with no adaptive tabulation perform very well in terms of computational time and are comparable to the CSAT method.

4.4.2 Case 2

Case 2 is injection of 90% CO_2, 1% N_2, and 9% C_1 into an oil reservoir with the same initial composition as Case 1. The model is a quarter of a five-spot pattern. The injection pressure is 5,500 psia and the production pressure is 4,000 psia. Initial reservoir pressure is 4,500 psia. Reservoir temperature is 120°F. A constant timestep size of 0.125 days was used. The simulation performance results for this case are given in Table 4-4. The simulation results with this case are more sensitive to the distance tolerances used in approximating flash results compared to Case 1 because of more complexity of the phase behavior with CO_2-rich injected fluid.

The phase equilibrium calculations comprise 60% of the computational time in the UTCOMP 1 simulation where 1,363,644 stability analyses and 5,361,159 phase-split calculations are performed. The simulation with the UTCOMP 2 method and a distance tolerance of 3×10^{-5} for approximating flash results, improves the computational time by 30.29% compared to the UTCOMP 1 simulation. This improvement in the computational

time is obtained by skipping 1,008,553 additional stability analyses and approximating the results of 3,833,809 phase-split calculations. The mean absolute errors in oil saturation at 100 and 200 days are 0.0007 and 0.0033, respectively; and the mean and maximum relative errors in oil rate are 5.78% and 19.71%, respectively. Increasing the distance tolerance used in approximating flash results leads to more speed at the expense of accuracy and vice versa.

The simulation with CSAT yields 45.6% improvement in the computational time compared to the UTCOMP 1 simulation. A distance tolerance of 0.005 for skipping both stability analysis and flash calculations was used. Almost all of the flash calculations and stability analysis were skipped by CSAT. The adaptive tabulation in CSAT offers the advantage of finding a matching tie line (either by generating a new table or using an existing one) no matter how small the distance tolerance is, even though small tolerances can produce large numbers of tie-line tables. The values of mean absolute error in oil saturation at 100 and 200 days are 0.00379 and 0.00383, respectively and the mean and maximum relative errors in oil rate are 2.25% and 10.70%, respectively. For this distance tolerance, 170 tie-line tables were generated. Performing the CSAT simulation with a distance tolerance of 0.01 will improve the computational speed by 47.74% compared to the UTCOMP 1 simulation, but at the expense of accuracy.

The simulation with MMC1 leads to 38.1% improvement in the computational time, which is less than that of CSAT with adaptive tabulation. The distance tolerance for skipping flash and stability analysis was 0.005. The mean absolute error in oil saturation at 100 and 200 days are 0.00303 and 0.0047, respectively, and the values of mean and maximum relative error in oil rate are 3.4% and 13.1%, respectively. The tie lines from five contacts of MMC simulations with 11 different mixing ratios were used. 93.9% of all

the simulation overall compositions were hit by the MMC tie lines for the distance tolerance of 0.005. The oil and gas tie lines contribute to 70% of the total number of tie-line hits and 99% of the total number of tie-line hits are due to 28 tie-line tables. Analysis of the tie-line hits showed that 67 tie-line tables did not experience any hits. These extra tie lines only contribute to failed table searches. This is why MMC1 does not perform as efficiently as CSAT in terms of computational time. Future implementations may try to alleviate this problem by removing the MMC tie-line tables that are not hit after a certain time (e.g. 10% of the simulation time) from the search order. However, even in that case we do not expect the MMC1 to outperform adaptive tabulation because adaptive tabulation provides the complete coverage of the compositional route of the simulation with a minimum number of tie-line tables.

If distance tolerance of 0.01 is used instead of 0.005, the improvement in computational time increases to 45.5%. The values of mean absolute error in oil saturation at 100 and 200 days are 0.0084 and 0.01 and the mean and maximum values of relative error in oil rate are 5.2% and 15.48%, respectively which are less accurate than the results with the distance tolerance of 0.005. For this distance tolerance, 99.2% of the simulation overall compositions lie on the MMC tie lines. This shows that upon selecting appropriate number of contacts, the MMC tie lines are sufficiently close to all of the simulation overall compositions.

The best simulation with MMC2, improves the computational time by 44.7%. A distance tolerance of 0.005 was used to stop the search for the closest tie lines. The MMC tie lines from five contacts with 11 mixing ratios were used. The mean absolute error in oil saturation at 100 and 200 days are 0.00412 and 0.00528, respectively. The mean and maximum relative errors in oil rate are 3.45% and 13.2%, respectively. If MMC tie lines

from five mixing ratios are used instead of 11 mixing ratios, 45.4% improvement in computational time is obtained compared to the UTCOMP 1 simulation. However, some accuracy is lost as the mean and maximum relative errors in oil rate increase to 4.15% and 29.4%, respectively. Using MMC tie lines from 11 contacts of three mixing ratios, improves the computational time by 43.9% with approximately the same level of accuracy.

The fastest acceptable simulation with MMC3 leads to 40.2% improvement in computational time compared to the UTCOMP 1 simulation. MMC tie lines from five contacts of the MMC simulation with a mixing ratio of 0.5 were used for this simulation (16 tie-line tables). The mean absolute error in oil saturation at 100 and 200 days are 0.0127 and 0.0113, respectively. The mean and maximum relative errors in oil rates are 4.52% and 49.6%, respectively. The accuracy of the MMC3 method with these parameters is less than the other MMC-based methods. If 38 MMC tie-line tables from six contacts with three mixing ratios are used, the improvement in the computational time decreases to 24.9%. The results are more accurate compared to using tie lines from only one mixing ratio. The mean absolute errors in oil saturation at 100 and 200 days decrease to 0.0082 and 0.0070, respectively. The mean and maximum relative errors in oil rate also decrease to 1.85% and 29.3%, respectively.

4.4.3 Case 3

Case 3 is also a quarter of a five-spot pattern. Initial composition of the reservoir fluid is 0.77% CO_2, 20.25% C_1, 11.8% C_{2-3}, 14.84% C_{4-6}, 28.63% C_{7-14}, 14.9% C_{15-24}, 2.946% C_{25-28}, 1.961% C_{29-32}, 1.305% C_{33-36}, 0.869% C_{37-40}, 0.5781% C_{41-44}, and 1.1505% C_{45+}. Injected fluid is 10% CO_2, 65% C_1, 20.0% C_{2-3}, and 5% C_{4-6}. The component properties required for phase behavior modeling are given in Table 3-10. An

injection well with injection pressure of 3,900 psia is placed in one corner and a production well with bottomhole production pressure of 3,300 psia is placed in the other corner of the reservoir. Initial reservoir pressure is 3,750 psia and reservoir temperature is 260°F. This case is adopted from Okuno (2009). Total simulation time is 350 days leading to injection of 2.5 pore volumes of gas. A constant timestep size of 0.1 days was used. The computational efficiency results for this case are given in Table 4-5.

For this case, 61.7% of the computational time is spent on phase equilibrium calculations in the simulation with UTCOMP 1. The number of stability analyses and phase equilibrium calculations performed are 5,292,812 and 3,113,108, respectively. The simulation with UTCOMP 2 using a distance tolerance of 1×10^{-5} produces nearly identical results compared to the UTCOMP 1 simulation while improving the computational time by 12.4%. None of the other methods could reduce the simulation time for the same level of accuracy. This improvement in computational time is obtained by skipping 4,418,053 stability analyses (main contribution) and 180,133 phase-split calculations. If a distance tolerance of 1×10^{-4} is used, the improvement in the computational time increases to 39.95%. Only 970,167 stability analyses were performed and 2,149,181 phase-split calculations were skipped. The mean absolute errors in oil saturation at 100 and 200 days are 0.0172 and 0.0346, respectively and the mean and maximum relative errors in oil rate are 3.68 % and 17.24%, respectively.

The simulation with CSAT using a distance tolerance of 0.01 improves the computational time by 51.4%. Almost all of the stability analyses and flash calculations are skipped using this distance tolerance and only 24 tie-line tables were generated. Only 25,363 flash calculations were actually performed. The mean absolute errors in oil saturation are 0.0282 and 0.0441 at 100 and 200 days, respectively. The mean and

maximum relative errors in oil rate are 2.9447% and 29.068%, respectively. This CSAT simulation was performed using the neighbor-based search algorithm. The improvement in the computational time using the partial sorting search algorithm was 50.05% with slightly less accurate oil rate results. Using the neighbor-based search algorithm suppresses the slight oscillations observed in oil rate for this case. If a distance tolerance of 0.005 is used in the CSAT simulation with neighbor-based search algorithm, 51.6% improvement in the computational time is obtained while producing more accurate results. Only 5,676 stability analyses and 4,011 flash calculations were actually performed, which is why the computational performance slightly improves despite more tables compared to the CSAT simulation using tolerance of 0.01. The mean absolute error in oil saturation at 100 and 200 days were 0.016535 and 0.022779, respectively. The mean and maximum relative errors in oil rate were 2.33% and 16.59%, respectively.

The simulation with MMC1 using a distance tolerance of 0.01 and neighbor-based search algorithm, improves the computational time by 51.35%. Only 32,324 stability analyses and 11,442 phase-split calculations were performed using MMC1. The mean absolute error in oil saturation at 100 and 200 days are 0.0367 and 0.0371, respectively. The mean and maximum relative errors in oil rate are 4.25% and 44.38%, respectively. The simulation with MMC1 is slightly less accurate compared to the CSAT simulation with the same distance tolerance. For this simulation, 38 tie-line tables were collected from 20 contacts of MMC simulation with a mixing ratio of 0.5. The percentage of the simulation overall compositions that were hit by the MMC tie lines is 99.7%. If the MMC1 simulation is performed using a distance tolerance of 0.005, then 94.49% of all the overall compositions are hit by the MMC tie lines and the improvements in the computational time reduce to 44.36%, which is less than CSAT with the same tolerance.

This is because for this distance tolerance 480,904 stability analyses and 145,519 flash calculations are performed. For this simulation, the mean absolute error in oil saturation at 100 and 200 days are 0.0138 and 0.0199, respectively. The mean and maximum relative errors in oil rate are 1.572% and 13.61%, respectively.

The simulations with MMC2 using a distance tolerance of 0.005 results in 48.98% improvement in the computational time. Tie lines from 20 MMC contacts with a mixing ratio of 0.5 were used. The mean absolute error in oil saturation at 100 and 200 days are 0.0146 and 0.0153, respectively. The mean and maximum relative errors in oil rate are 2.84% and 22.59%, respectively. This method provides more accurate results compared to the CSAT simulation in Table 4-5 with comparable computational efficiency. If the tie lines (51 tie-line tables) from 20 contacts with three mixing ratios are used, the improvements in the computational time decrease slightly to 48.42%. The mean absolute error in oil saturation does not change significantly (0.0146 and 0.0159 at 100 and 200 days, respectively). The mean and maximum relative errors in oil rate, however, decrease to 1.1681% and 13.97%, respectively.

The simulation with MMC3 improves the computational time by 31.86%. MMC tie lines (29 tie-line tables) from 16 contacts with a mixing ratio of 0.5 were used for the inverse distance interpolation of K values. The mean absolute error in oil saturation at 100 and 200 days are 0.038 and 0.037, respectively. The mean and maximum relative errors in oil rate were 5.25% and 37.00%, respectively.

4.4.4 Case 4

Case 4 is simultaneous injection of two different gas streams through two injectors into an oil reservoir with the same initial composition as Case 1. The injection gas composition of the first injector is 90% CO_2, 1% N_2, and 9% C_1 and the injection gas

composition of the second injector is 9% CO_2, 1% N_2, and 90% C_1. The model is a line-drive with two producers on the opposing side of two injectors in a square-shaped reservoir. The injectors and producers operate at constant bottomhole pressures of 5,500 psia and 4,000 psia, respectively. Initial reservoir pressure is 4,500 psia and reservoir temperature is 120°F. A constant timestep size of 0.125 days was used. The simulation performance results for this case are given in Table 4-6.

For this case, the phase equilibrium calculations contribute to 58.9% of the computational time in the UTCOMP 1 simulation where 2,334,088 stability analyses and 4,390,569 phase-split calculations are performed, respectively. The simulation with the UTCOMP 2 method and a distance tolerance of 5×10^{-5} for approximating flash results, improves the computational time by 30.7% compared to the UTCOMP 1 simulation. This improvement in the computational time is obtained by skipping 1,841,038 additional stability analyses and approximating the results of 3,268,785 phase-split calculations. The mean absolute errors in oil saturation at 100 and 200 days are 0.0006 and 0.0030, respectively; and the mean and maximum relative errors in oil rate are 2.15% and 8.33%, respectively. If a distance tolerance of 1×10^{-4} is used the improvement in the computational time increases to 36.5% and the results are less accurate. For this distance tolerance, the mean absolute errors in oil saturation at 100 and 200 days are 0.0018 and 0.0080, respectively. The mean and maximum relative errors in oil rate are 3.2% and 12.8%, respectively.

The best simulation with CSAT results in 45.2% improvement in the computational time compared to the UTCOMP 1 simulation. The neighbor-based search algorithm was used in this CSAT simulation. A distance tolerance of 0.01 for skipping both stability analysis and flash calculations was used. The flash calculations and stability

analysis were almost entirely skipped by CSAT. Adaptive tabulation generated 565 tie-line tables. The oil tie line and the two injection gas tie lines contribute to 50% of the total tie-line hits and 90% of the total tie-line hits are due to only 30 tie lines. The values of mean absolute error in oil saturation at 100 and 200 days are 0.0067 and 0.0044, respectively and the mean and maximum relative errors in oil rate are 0.76% and 4.33%, respectively. Performing the CSAT simulation without the neighbor-based search algorithm and using the same distance tolerance yields 35.1% improvements in the computational time. The corresponding values of mean absolute error in oil saturation at 100 and 200 days are 0.0036 and 0.0042, respectively and the mean and maximum relative errors in oil rate are 0.62% and 5.41%, respectively. 581 tie-line tables are generated without the neighbor-based search algorithm.

The simulation with MMC1 leads to 35.3% improvement in the computational time. The distance tolerance for skipping flash and stability analysis was 0.01. The number of stability analyses and flash calculations performed are 408,870 and 165,196, respectively. The mean absolute error in oil saturation at 100 and 200 days are 0.0012 and 0.0086, respectively, and the values of mean and maximum relative error in oil rate are 0.96% and 4.68%, respectively. Individual MMC simulations with the two injection gases were performed to obtain the prior tie line tables. The tie lines from five contacts of MMC simulations with five different mixing ratios for each injection gas were used (122 tie line tables). 94.2% of all the simulation overall compositions were hit by the MMC tie lines for the distance tolerance of 0.01. The oil and gas tie lines contribute to 54.1% of the total number of tie-line hits and 90% of the total number of tie-line hits are due to 22 tie-line tables. 56 tie-line tables did not contribute to any hits. Regular phase equilibrium

calculations were performed for the 5.8% of the simulation overall compositions that were not hit by the MMC tie lines.

Some of the un-hit overall compositions result from mixing of the two injection gases which is not explicitly accounted for in the prior tie line tables. The CSAT method with the same distance tolerance leads to a large number of tie line tables because CSAT finds or creates a matching tie line for each simulation overall composition. Some simulation tie lines are not frequently encountered during the simulation and their tabulation only adds to the computational overhead with CSAT depending on the table-search algorithm. It might be computationally more beneficial to perform regular flash calculations for those tie lines (their corresponding overall compositions) instead of tabulating them; however, it is not possible to identify those overall compositions before the simulation.

If distance tolerance of 0.005 is used instead of 0.01 in simulation with MMC1, the improvement in computational time decreases to 14.8%. The number of stability analyses and flash calculations performed are 1,133,149 and 592,527, respectively. Only 83.3% of the simulation overall compositions are hit by the MMC tie lines in this case.

The simulations with MMC2 using a distance tolerance of 0.01 results in 39.3% improvement in the computational time. MMC simulations using the two injection gases and their mixture were performed to obtain the prior tie line tables. 168 tie-line tables from five contacts with five different mixing ratios were used. The mean absolute error in oil saturation at 100 and 200 days are 0.0025 and 0.0052, respectively. The mean and maximum relative errors in oil rate are 0.72% and 9.20%, respectively. If a distance tolerance of 0.005 is used instead of 0.01 the improvement in the computational time decreases to 29.3%, and the results are more accurate.

The simulation with MMC3 improves the computational time by 23.33%. MMC simulations with both injection gases and their mixture were performed to obtain the prior tie-line tables. MMC tie lines (29 tie-line tables) from 5 contacts with a mixing ratio of 0.5 were used for the inverse distance interpolation of *K* values. The mean absolute error in oil saturation at 100 and 200 days are 0.0047 and 0.0058, respectively. The mean and maximum relative errors in oil rate are 1.60% and 21.8%, respectively.

4.4.5 Case 5

For this case study, all the simulation parameters are similar to Case 1 except for the permeability field. The permeability field was populated using a Dykstra-Parsons coefficient of 0.8. The computational efficiency results for this case are given in Table 4-7.

The phase equilibrium calculations contribute to 42.5% of the computational time in UTCOMP 1 simulation where 2,817,165 stability analyses and 2,947,056 phase-split calculations are performed. Using the heuristic techniques to skip stability analysis and approximate flash results in the UTCOMP 2 method leads to 31.6% improvement in the computational time. This improvement in computational time results from skipping 2,077,516 stability analyses and approximating the results of 2,260,817 phase-split calculations using *K* values from the previous tie line in the same gridblock. The simulation of the same case (Case 1) with the more homogeneous permeability field leads to similar improvement in the computational time. The distance tolerance for using the previous tie line to approximate the flash results was 5×10^{-5}. The mean absolute error in oil saturation at 150 and 550 days are 0.00015 and 0.0013, respectively. The mean and maximum relative errors in oil rates are 0.29% and 1.20%, respectively. Similar to the

other simulation cases, using a larger value for the distance tolerance leads to less accurate results and more improvement in the computational time.

The simulation with CSAT results in 42.8% improvement in computational time, which is obtained through skipping almost all of the stability analyses (2,817,265) and approximating 2,942,096 phase-split calculations using *K* values interpolated from CSAT tie lines. The distance tolerance for skipping stability analysis and approximating flash results was 0.01. Adaptive tabulation produced 33 tie-line tables and two critical tie lines. The mean absolute error in oil saturation at 150 and 550 days are 0.0006 and 0.0012, respectively. The mean and maximum relative errors in oil rate are 0.13% and 0.99%, respectively. The critical oil tie line contributes to 98% of the total critical tie-line hits. The exact oil and gas tie lines contribute to 5% of the total subcritical tie-line hits and 22.9% of the total subcritical tie-line hits are due to a tie line that is very close to the gas tie line.

The simulation with the MMC1 method leads to 42.1% improvement in the computational time. By use of a distance tolerance of 0.01, almost all of the stability analyses were skipped and approximations were made for almost all of the flash results. Similar to Case 1, for this simulation 120 tie-line tables (four critical tie lines) were collected from 20 contacts of three MMC simulations with mixing ratios of 0.2, 0.5, and 0.8. The gas tie line contributed to 9.5% of the subcritical tie-line hits. The critical oil tie line contributes to 97.9% of the critical tie-line hits. The computational performance of the MMC1 method in this case is similar to the performance of MMC1 simulation in Case 1 with a less heterogeneous permeability field. The mean absolute errors in oil saturation at 150 and 550 days are 0.0020 and 0.0037, respectively. The mean and maximum relative errors in oil rate are 0.90% and 3.2%, respectively.

The simulations with the MMC2 method leads to 43.2% improvement in computational time compared to the UTCOMP 1 simulation. Similar to the MMC1 simulation, the MMC tie lines from 20 contacts of three mixing ratios were used. The distance tolerance for stopping the search for the closest tie line was 0.01. The values of mean absolute error in oil saturation at 150 and 550 days are 0.0020 and 0.0036, respectively. The values of mean and maximum relative error in oil rate are 0.91 % and 3.25%, respectively. Similar to the MMC2 simulation in Case 1, most of the simulation overall compositions were closer than the required tolerance to the MMC tie-lines. The farthest subcritical simulation overall composition from the MMC tie lines used distances of 0.013 and 0.012 from the closest two tie lines for the *K*-value approximation.

The simulation with MMC3 method decreases the computational time by 16.7% compared to the simulation with UTCOMP1. The MMC tie lines from 10 contacts of the MMC simulation with a mixing ratio of 0.5 were used (35 tie-line tables). The inverse distance interpolation was performed with distance exponent of two. The mean absolute error in oil saturation at 150 and 550 days are 0.0019 and 0.0034, respectively. The mean and maximum values of relative error in oil rate are 0.91% and 4.12%, respectively.

4.4.6 Case 6

The simulation parameters for this case are the same as Case 2 except for the more heterogeneous permeability field taken from Case 5. The simulation performance results for this case are given in Table 4-8.

The phase equilibrium calculations comprise 60.1% of the computational time in the UTCOMP 1 simulation where 2,902,304 stability analyses and 3,822,037 phase-split calculations are performed. The simulation with the UTCOMP 2 method and a distance tolerance of 3×10^{-5} for approximating flash results, improves the computational time by

31.4% compared to the UTCOMP 1 simulation. The number of additional stability analyses skipped is 1,975,375 and approximations were made for the results of 2,830,096 phase-split calculations. The mean absolute errors in oil saturation at 100 and 200 days are 0.0052 and 0.0057, respectively and the mean and maximum relative errors in oil rate are 1.21% and 4.15%, respectively.

The simulation with CSAT yields 44.6% improvement in the computational time compared to the UTCOMP 1 simulation. A distance tolerance of 0.01 for skipping both stability analysis and flash calculations was used. Almost all of the stability analysis and flash calculations were skipped. Only 104,095 stability analyses and 9,913 phase-split calculations were actually performed. The values of mean absolute error in oil saturation at 100 and 200 days are 0.0064 and 0.0053, respectively and the mean and maximum relative errors in oil rate are 1.44% and 10.76%, respectively. For this distance tolerance, 50 tie-line tables were generated. Performing the CSAT simulation with a distance tolerance of 0.005 will improve the computational speed by 41.8% compared to the UTCOMP 1 simulation while more accurate results are obtained. The values of mean absolute error in oil saturation at 100 and 200 days are 0.0030 and 0.0029, respectively. The mean and maximum relative errors in oil rate are 0.65% and 6.81%, respectively. For this distance tolerance 141 tie-line tables were created by adaptive tabulation.

The simulation with MMC1 results in 43.1% improvement in the computational time. The distance tolerance for skipping both flash calculations and stability analyses was 0.01. The mean absolute error in oil saturation at 100 and 200 days are 0.0032 and 0.0031, respectively and the values of mean and maximum relative error in oil rate are 0.69% and 5.67%, respectively. 122 tie line tables from five contacts of MMC simulations with 11 different mixing ratios were used. 97.5% of all the simulation overall

compositions were hit by the MMC tie lines for the distance tolerance of 0.01. The oil and gas tie lines contribute to 42.4% of the total number of tie-line hits and 99% of the total number of tie-line hits are due to 32 tie-line tables. Analysis of the tie-line hits showed that 55 tie-line tables did not experience any hits.

If distance tolerance of 0.005 is used instead of 0.01, the improvement in computational time decreases to 30.0%. The values of mean absolute error in oil saturation at 100 and 200 days are 0.0018 and 0.0017 and the mean and maximum values of relative error in oil rate are 0.47% and 4.02%, respectively, which are slightly more accurate than the results with the distance tolerance of 0.01. For this distance tolerance, 86.1% of the simulation overall compositions lie on the MMC tie lines. This shows that even with small distance tolerances the MMC tie lines are sufficiently close to most of the simulation overall compositions if appropriate number of contacts are selected. The oil and gas tie lines contribute to 39.7% of the total subcritical tie-line table hits.

The best simulation with MMC2, improves the computational time by 40.91%. A distance tolerance of 0.005 was used to stop the search for the closest tie line. The tie lines from five contacts of the MMC simulations with five different mixing ratios were used (58 tie-line tables). The mean absolute error in oil saturation at 100 and 200 days are 0.0020 and 0.0019, respectively. The mean and maximum relative errors in oil rate are 0.65% and 6.4%, respectively. If 122 MMC tie lines from 11 mixing ratios are used instead of five mixing ratios, 37.5% improvement in computational time is obtained compared to the UTCOMP 1 simulation. The simulation results are slightly more accurate, as the mean and maximum relative errors in oil rate decrease to 0.51% and 4.53%, respectively. The mean absolute error in oil saturation at 100 and 200 days are 0.0019 and 0.0018, respectively.

The simulation with MMC3 leads to 38.04% improvement in computational time compared to the UTCOMP 1 simulation. Similar to the MMC3 simulation in Case 2, MMC tie lines from five contacts of the MMC simulation with a mixing ratio of 0.5 were used for this simulation. The mean absolute error in oil saturation at 100 and 200 days are 0.0068 and 0.0056, respectively. The mean and maximum relative errors in oil rates are 1.75% and 12.5%, respectively. The results of the MMC3 simulation are less accurate compared to the MMC1 and MMC2 simulations. If 38 MMC tie-line tables from six contacts with three mixing ratios are used, the improvement in the computational time decreases to 20.75%. The results are more accurate compared to using tie lines from only one mixing ratio. The mean absolute errors in oil saturation at 100 and 200 days decrease to 0.0019 and 0.0020, respectively. The mean and maximum relative errors in oil rate also decrease to 0.41% and 6.05%, respectively.

4.4.7 Case 7

The simulation parameters for this case are the same as Case 3 except for the permeability field which is more heterogeneous and is taken from Case 5. The simulation performance results for this case are given in Table 4-9.

In the simulation with UTCOMP 1, 62.7% of the computational time is spent on the phase equilibrium calculations. The number of stability analyses and phase equilibrium calculations performed are 5,914,543 and 2,489,519, respectively. The simulation with UTCOMP 2 using a distance tolerance of 1×10^{-5} improves the computational time by 21.1% compared to the UTCOMP1 simulation while producing sufficiently accurate results. This improvement in computational time is obtained through skipping 3,817,129 stability analyses (main contribution) and 823,303 phase-split calculations. The mean absolute error in oil saturation at 100 and 200 days are 0.00008

and 0.0024, respectively. The mean and maximum relative errors in oil rate are 0.43% and 4.95%, respectively. If a distance tolerance of 1×10^{-4} is used, the improvement in the computational time increases to 35.99%. Only 2,255,715 stability analyses were actually performed and 2,102,990 phase-split calculations were skipped. The mean absolute errors in oil saturation at 100 and 200 days are 0.011 and 0.025, respectively and the mean and maximum relative errors in oil rate are 2.65% and 11.67%, respectively.

The simulation with CSAT using a distance tolerance of 0.01 improves the computational time by 51.6%. Almost all of the stability analyses and flash calculations were skipped using this distance tolerance and only 17 tie-line tables were generated. The mean absolute errors in oil saturation are 0.013 and 0.021 at 100 and 200 days, respectively. The mean and maximum relative errors in oil rate are 2.48% and 9.38%, respectively. Similar to the CSAT simulation in Case 3, this CSAT simulation was performed using the neighbor-based search algorithm. If a distance tolerance of 0.005 is used in the CSAT simulation with the neighbor-based search algorithm, 51.49% improvement in the computational time is obtained while producing slightly more accurate results. Only 11,584 stability analyses and 9,501 flash calculations are actually performed and 46 tie-line tables are generated. The mean absolute error in oil saturation at 100 and 200 days are 0.0100 and 0.0165, respectively. The mean and maximum relative errors in oil rate are 2.04% and 9.46%, respectively.

The simulation with MMC1 using a distance tolerance of 0.01 and the neighbor-based search algorithm, improves the computational time by 51.3%. The mean absolute error in oil saturation at 100 and 200 days are 0.0131 and 0.0226, respectively. The mean and maximum relative errors in oil rate are 3.41% and 11.37%, respectively. The simulation with MMC1 is slightly less accurate compared to the CSAT simulation with

the same distance tolerance. Similar to the MMC1 simulation in Case 3, for this simulation, 38 tie-line tables were collected from 20 contacts of MMC simulation with a mixing ratio of 0.5. The percentage of the simulation overall compositions that were hit by the MMC tie lines is 99.4%. The exact oil and gas tie lines contribute to 33.2% and 2.83% of the total tie-line table hits.

The simulations with MMC2 using a distance tolerance of 0.005 results in 47.3% improvement in the computational time. The tie lines from 20 MMC contacts with a mixing ratio of 0.5 were used (38 tie-line tables). The mean absolute error in oil saturation at 100 and 200 days are 0.0078 and 0.0153, respectively. The mean and maximum relative errors in oil rate are 1.91% and 10.95%, respectively. If 51 tie-line tables from 20 contacts with three mixing ratios are used, the improvements in the computational time decrease slightly to 46.79%. The mean absolute error in oil saturation does not change significantly (0.0078 and 0.0153 at 100 and 200 days, respectively). The mean and maximum relative errors in oil rate are 1.92% and 10.94%, respectively.

The simulation with MMC3 improves the computational time by 31.97%. Similar to the MMC3 simulation in Case 3, 29 tie-line tables from 16 contacts of the MMC simulation with a mixing ratio of 0.5 were used for the inverse distance interpolation of K values. The mean absolute error in oil saturation at 100 and 200 days are 0.0097 and 0.017, respectively. The mean and maximum relative errors in oil rate were 1.89% and 9.81%, respectively.

4.5 SUMMARY AND CONCLUSIONS

We demonstrated using several examples that the MMC tie lines cover almost the entire compositional route of one-dimensional and three-dimensional displacements solved with an IMPEC compositional simulator. Only a small number of tie lines from

the first few contacts of the MMC method are required to encompass most of the simulation compositional route. The MMC tie lines were placed in tie-line tables prior to performing simulation. Three tie-line-based *K*-value simulation methods were used. Computational efficiency of different methods indicates that the MMC-based methods and the CSAT (adaptive *K*-value simulation) can improve the total computational time by up to 50% with acceptable accuracy for the cases studied. The CSAT method resulted in 45.6%, 45.5%, 51.40%, 45.2%, 42.8%, 44.6%, and 51.6% improvement in the computational time for the seven cases studied. This decrease was possible only when the phase-split calculations were entirely replaced by approximations from the interpolated tie lines. Two of the MMC-based methods use the CSAT framework, but without adaptive tabulation. These two MMC methods use two different tie-line interpolation techniques and perform very similar to CSAT in terms of speed and accuracy. The first method uses only a distance tolerance criterion for retrieving a matching tie line and results in a decrease of 45.4%, 38.1%, 51.35%, 35.3%, 42.1%, 43.1%, and 51.3% in the computational time for the cases studied. The second method retrieves either a matching tie line within a distance tolerance or the closest tie line and improves the computational time by 47.1%, 44.7%, 48.98%, 39.3%, 43.2%, 40.9%, and 47.3% for the cases studied.

Using the CSAT framework with only MMC tie lines provides almost complete coverage of the compositional simulation route; however, it may be slightly less efficient than CSAT because of a larger number of tie-line tables. It is likely, however, that further improvements to the MMC-based method can be made to reduce the number of tie-line tables used.

The results also show that using very simple heuristic techniques improves the computation time significantly with the same level of accuracy as the more complicated

techniques. Improvements of 33.00%, 30.29%, 39.95%, 30.7%, 31.6%, 31.4%, and 21.1% in the total computational time were obtained for the cases studied using our IMPEC-type simulator. The tie-line table generation time for both CSAT and MMC-based methods is negligible compared to the total computational time. We also demonstrated that at the limit of an infinite number of contacts the MMC tie lines produce the ruled surfaces of tie lines that the MOC solution traverses.

The MMC approach may offer an advantage over adaptive tie-line tabulation in terms of robustness. This advantage stems from the fact that the MMC approach uses prior contacts as initial guesses of K values for successive contacts. Furthermore, the MMC approach does not require relative permeabilities, and therefore is independent of phase labeling and identification. Phase identification problems are numerous around critical points, and also when three hydrocarbon phases form. The MMC approach to compositional simulation therefore may be very useful to provide initial K-value guesses when three hydrocarbon phases are present in both IMPEC and fully-implicit simulators.

Table 4-1: Component properties for the four-component simulations (from Johns, 1992).

	P_c (psia)	T_c (°F)	V_c (ft^3/lbmol)	MW	ω
C_1	667.8	-116.63	1.5899	16.04	0.0104
C_2	707.8	90.09	2.3768	30.07	0.0990
C_3	615.8	205.85	3.2534	44.087	0.1530
C_6	430.6	453.63	5.9299	86.18	0.2990
C_{16}	205.7	830.91	15.000	226.448	0.7420

Table 4-2: Corey's relative permeability parameters of oil and gas phases for the simulation case studies.

$k_{rg}^{\ 0} = 0.85$	$k_{ro}^{\ 0} = 0.75$
$S_{gr} = 0.15$	$S_{or} = 0.15$
$e_{gas} = 4$	$e_{oil} = 3.5$

Table 4-3: Computational efficiency results for Case 1.

	UTCOMP 1	UTCOMP 2	CSAT	MMC1	MMC2	MMC3
CPU time (*sec*)	4,050.03	2,713.1	2,202.45	2,213.04	2,142.37	3,075.50
Phase equil. time (*sec*)	2,375.67	1,048.26	519.38	530.5	468.46	1,398.51
No. of SA performed	1,231,460	221,986	2,933	780	0	0
No. of phase split performed	4,533,341	1,165,120	867	220	0	0
Mean and max. relative error in oil rate	-	2.71%, 14.04%	0.78%, 15.9%	1.04%, 9.49%	0.98%, 6.68%	1.33%, 11.1%
Mean error in oil saturation at 150 and 550 days	-	0.0003, 0.0028	0.0027, 0.0039	0.0039, 0.0062	0.0029, 0.0061	0.0022, 0.0054
Improvement in computational time (%)	-	33	45.6	45.4	47.1	24.06

Table 4-4: Computational efficiency results for Case 2.

	UTCOMP 1	UTCOMP 2	CSAT	MMC1	MMC2	MMC3
CPU time (*sec*)	4,916.23	3,427.15	2,672.09	3,044.34	2,717.75	2,940.98
Phase equil. time (*sec*)	2,953.29	1,457.36	686.62	1,064.71	738.28	963.35
No. of SA performed	1,363,644	380,467	240,402	338,349	0	0
No. of phase split performed	5,361,159	1,471,915	1,821	135,650	0	0
Mean and max. relative error in oil rate	-	5.78%, 19.71%	2.25%, 10.70%	3.44%, 13.10%	3.45%, 13.22%	4.52%, 49.6%
Mean error in oil saturation at 100 and 200 days	-	0.0007, 0.0033	0.0038, 0.0038	0.0030, 0.0047	0.0041, 0.0053	0.0127, 0.0113
Improvement in computational time (%)	-	30.29	45.6	38.1	44.7	40.2

Table 4-5: Computational efficiency results for Case 3.

	UTCOMP 1	UTCOMP 2	CSAT	MMC1	MMC2	MMC3
CPU time (*sec*)	7,712.80	4,631.43	3,748.11	3,752.34	3,953.54	5,255.48
Phase equil. time (*sec*)	4,758.45	1,765.30	872.05	860.0	1,011.38	2,349.78
No. of SA performed	5,291,812	970,167	25,363	32,324	0	0
No. of phase split performed	3,113,108	501,696	18,416	11,442	0	0
Mean and max. relative error in oil rate	-	3.68%, 17.24%	2.95%, 29.07%	4.25%, 44.38%	2.84%, 22.59%	5.25%, 37.00%
Mean error in oil saturation at 100 and 200 days	-	0.0172, 0.0346	0.0282, 0.0441	0.0367, 0.0371	0.0146, 0.0153	0.0380, 0.0370
Improvement in computational time (%)	-	39.95	51.4	51.35	48.98	31.86

Table 4-6: Computational efficiency results for Case 4.

	UTCOMP 1	UTCOMP 2	CSAT	MMC1	MMC2	MMC3
CPU time (*sec*)	4,475	3,100	2,452	2,894	2,718	3,431
Phase equil. time (*sec*)	2,634	1,259	590	1,035	859	1,581
No. of SA performed	2,334,088	530,305	52,559	408,870	0	0
No. of phase split performed	4,390,569	1,117,722	5,212	165,196	0	0
Mean and max. relative error in oil rate	-	2.15%, 8.33%	0.76%, 4.33%	0.96%, 4.68%	0.72%, 9.20%	1.60%, 21.8%
Mean error in oil saturation at 100 and 200 days	-	0.0006, 0.0030	0.0067, 0.0044	0.0012, 0.0086	0.0025, 0.0052	0.0047, 0.0056
Improvement in computational time (%)	-	30.7	45.2	35.3	39.3	23.33

Table 4-7: Computational efficiency results for Case 5.

	UTCOMP 1	UTCOMP 2	CSAT	MMC1	MMC2	MMC3
CPU time (*sec*)	3,405.40	2,329.98	1,949.16	1,971.16	1,935.97	2,837.86
Phase equil. time (*sec*)	1,956.33	879.32	491.37	507.34	475.023	1,386.78
No. of SA Performed	2,817,165	750,045	3,040	5,583	0	0
No. of phase split performed	2,947,056	685,743	1,618	1,275	0	0
Mean and max. relative error in oil rate	-	0.29%, 1.20%	0.13%, 0.99%	0.90%, 3.20%	0.91%, 3.25%	0.91%, 4.12%
Mean error in oil saturation at 150 and 550 days	-	0.0002, 0.0013	0.0006, 0.0012	0.0020, 0.0037	0.0020, 0.0037	0.0019, 0.0034
Improvement in computational time (%)	-	31.6	42.8	42.1	43.2	16.7

Table 4-8: Computational efficiency results for Case 6.

	UTCOMP 1	UTCOMP 2	CSAT	MMC1	MMC2	MMC3
CPU time (*sec*)	4,402.89	3,020.23	2,437.94	2,504.62	2,601.59	2,728.06
Phase equil. time (*sec*)	2,646.66	1,273.67	674.79	735.82	842.38	982.69
No. of SA performed	2,902,304	967,252	104,095	116,633	0	0
No. of phase split performed	3,822,037	967,795	9,913	10,259	0	0
Mean and max. relative error in oil rate	-	1.21%, 4.15%	1.44%, 10.76%	0.69%, 5.67%	0.65%, 6.47%	1.75%, 12.45%
Mean error in oil saturation at 100 and 200 days	-	0.0052, 0.0057	0.0064, 0.0053	0.0032, 0.0031	0.0020, 0.0019	0.0068, 0.0056
Improvement in computational time (%)	-	31.4	44.6	43.1	40.9	38.0

Table 4-9: Computational efficiency results for Case 7.

	UTCOMP 1	UTCOMP 2	CSAT	MMC1	MMC2	MMC3
CPU time (*sec*)	7,454.53	5,883.57	3,604.76	3,633.21	3,931.88	5,070.97
Phase equil. time (*sec*)	4,673.51	3,104.44	845.87	886.64	1,145.23	2,323.98
No. of SA performed	5,914,543	2,147,947	11,383	69,524	0	0
No. of phase split performed	2,489,519	1,642,851	8,270	14,732	0	0
Mean and max. relative error in oil rate	-	0.43%, 4.95%	2.48%, 9.38%	3.41%, 11.37%	1.91%, 10.95%	1.89%, 9.81%
Mean error in oil saturation at 100 and 200 days	-	0.0001, 0.0024	0.0131, 0.0218	0.0131, 0.0226	0.0078, 0.0153	0.0097, 0.0170
Improvement in computational time (%)	-	21.1	51.6	51.3	47.3	31.97

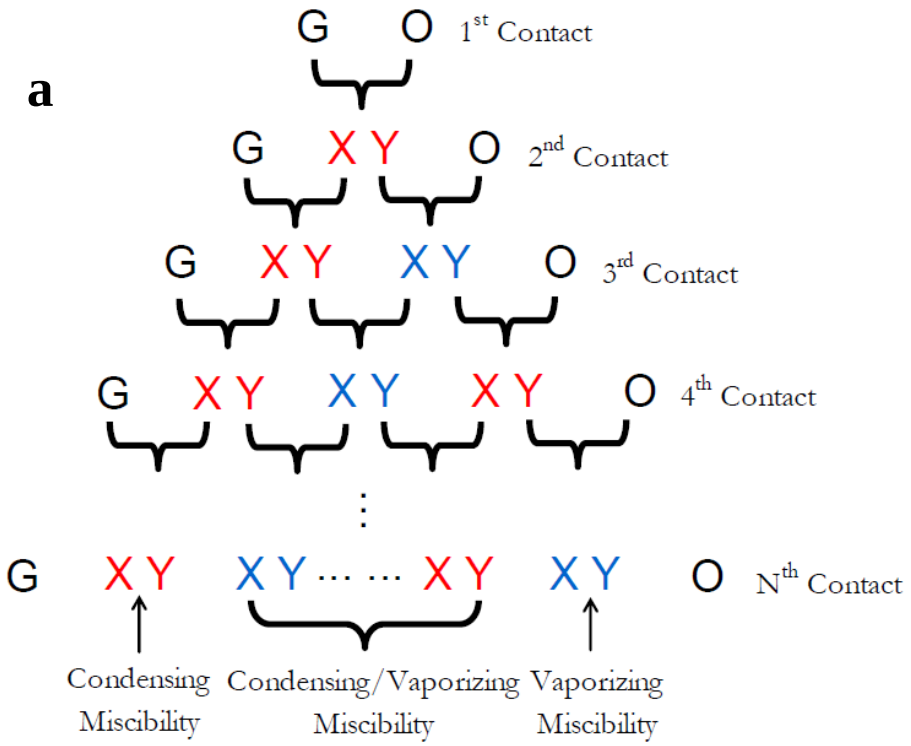

Figure 4-1: continued next page.

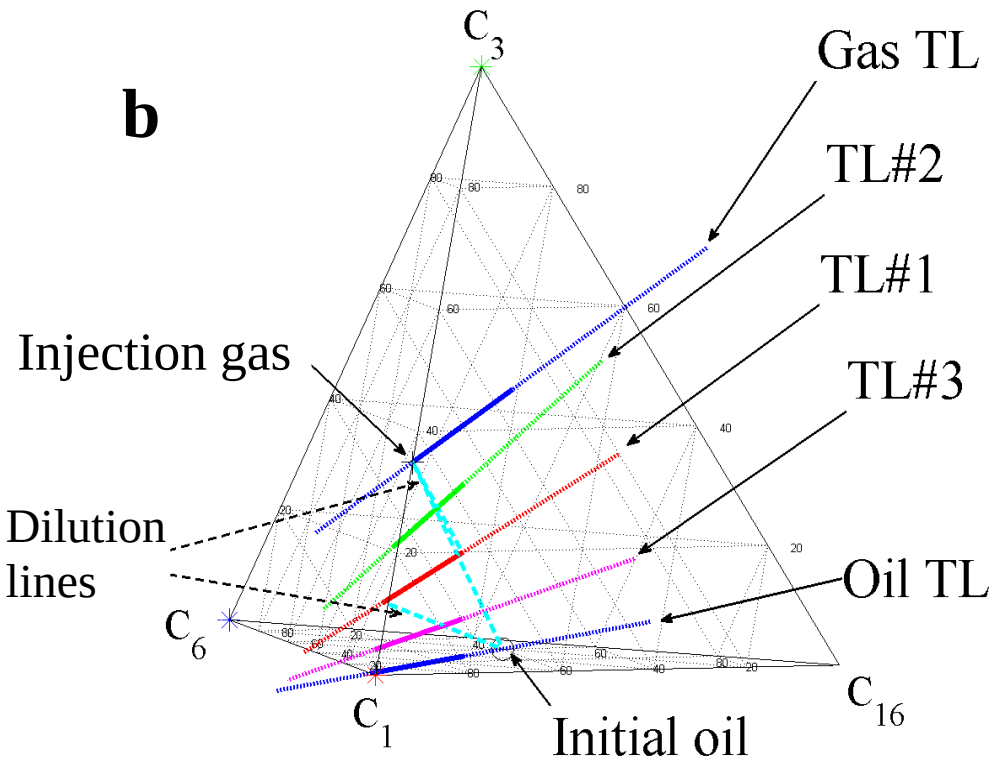

Figure 4-1: a) Illustration of repeated contacts in the MMC method (from Ahmadi and Johns, 2011) b) Schematic representation of the injection gas composition, initial oil composition, oil tie line, gas tie line, the MMC tie lines of the first two contacts (TL#1, TL#2, and TL#3) and the related dilution lines for a four-component displacement (phase behavior model from Johns (1992)).

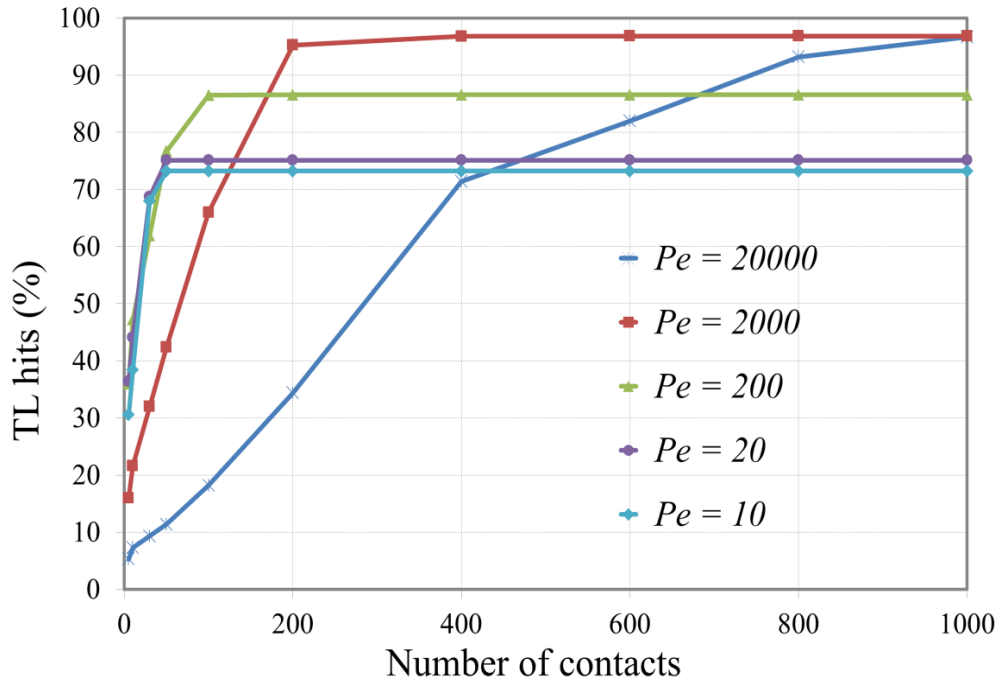

Figure 4-2: Percentage of simulation overall compositions hit by the MMC tie lines collected for different number of contacts at various Peclet numbers (*Pe*) for one-dimensional displacements of the nine-component fluid.

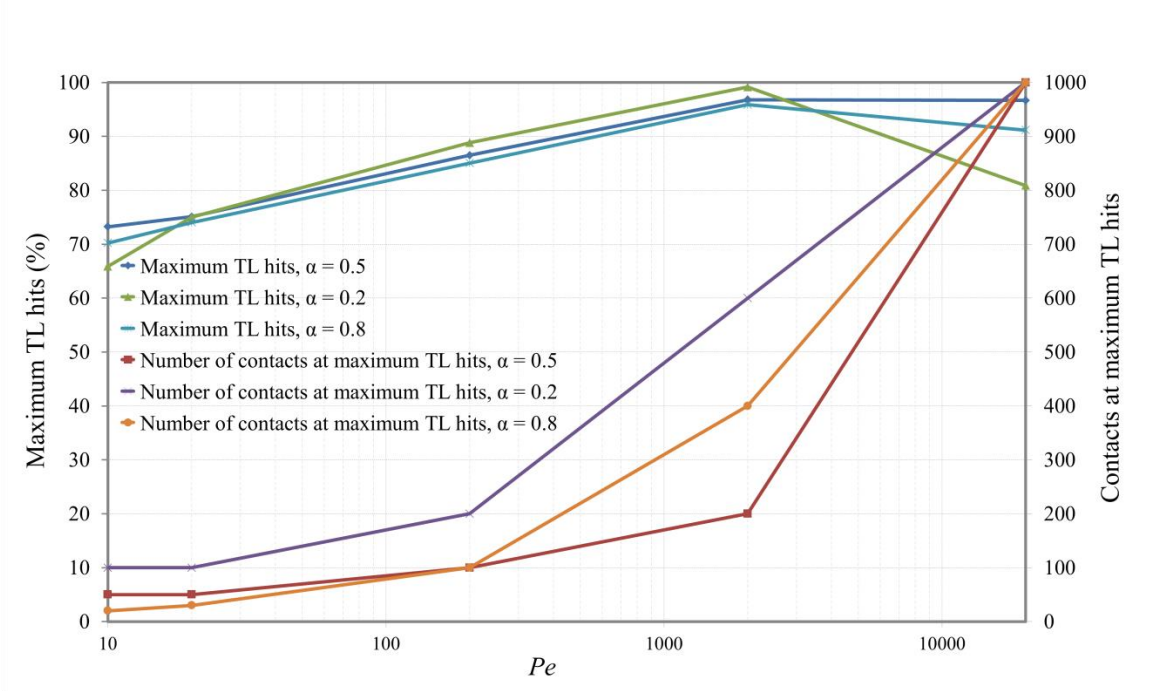

Figure 4-3: Maximum percentage of tie-line hits and the number of MMC contacts required for the maximum hits versus *Pe* for different mixing ratios (α).

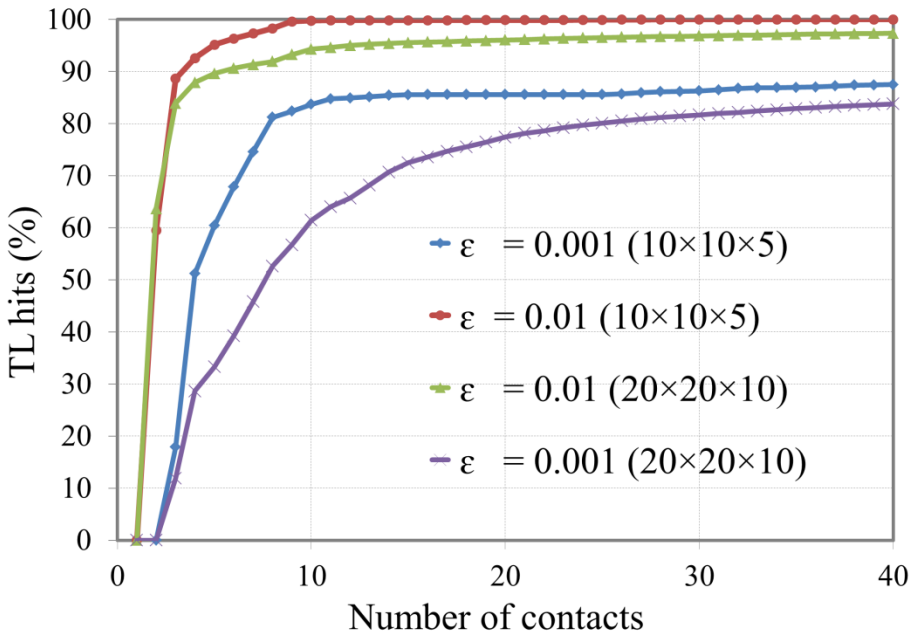

Figure 4-4: Percentage of compositional route that lies on the MMC tie lines versus number of contacts for three-dimensional five-component simulations.

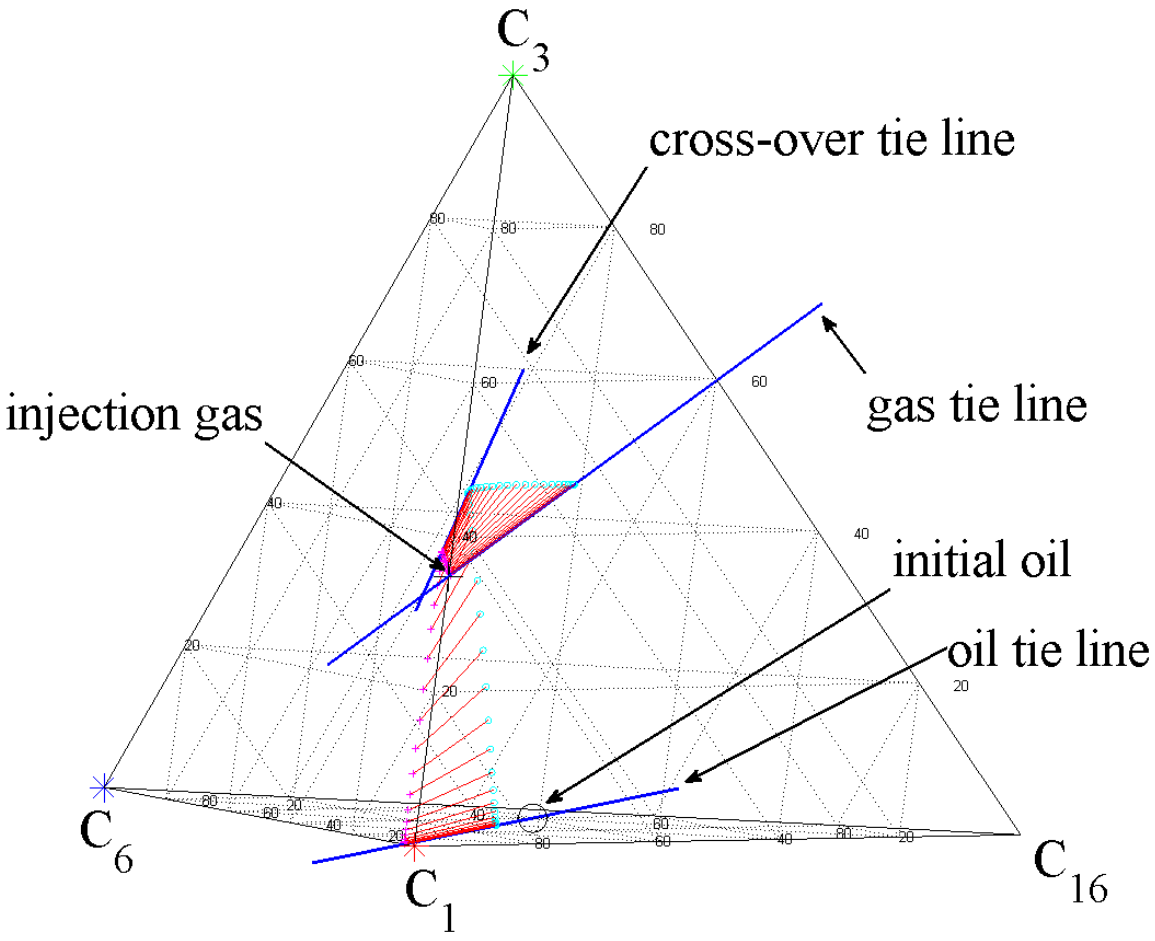

Figure 4-5: MMC tie lines after 100 contacts (red lines) and key tie lines of the MOC solution (blue lines) for a four-component displacement (phase behavior model from Johns (1992)).

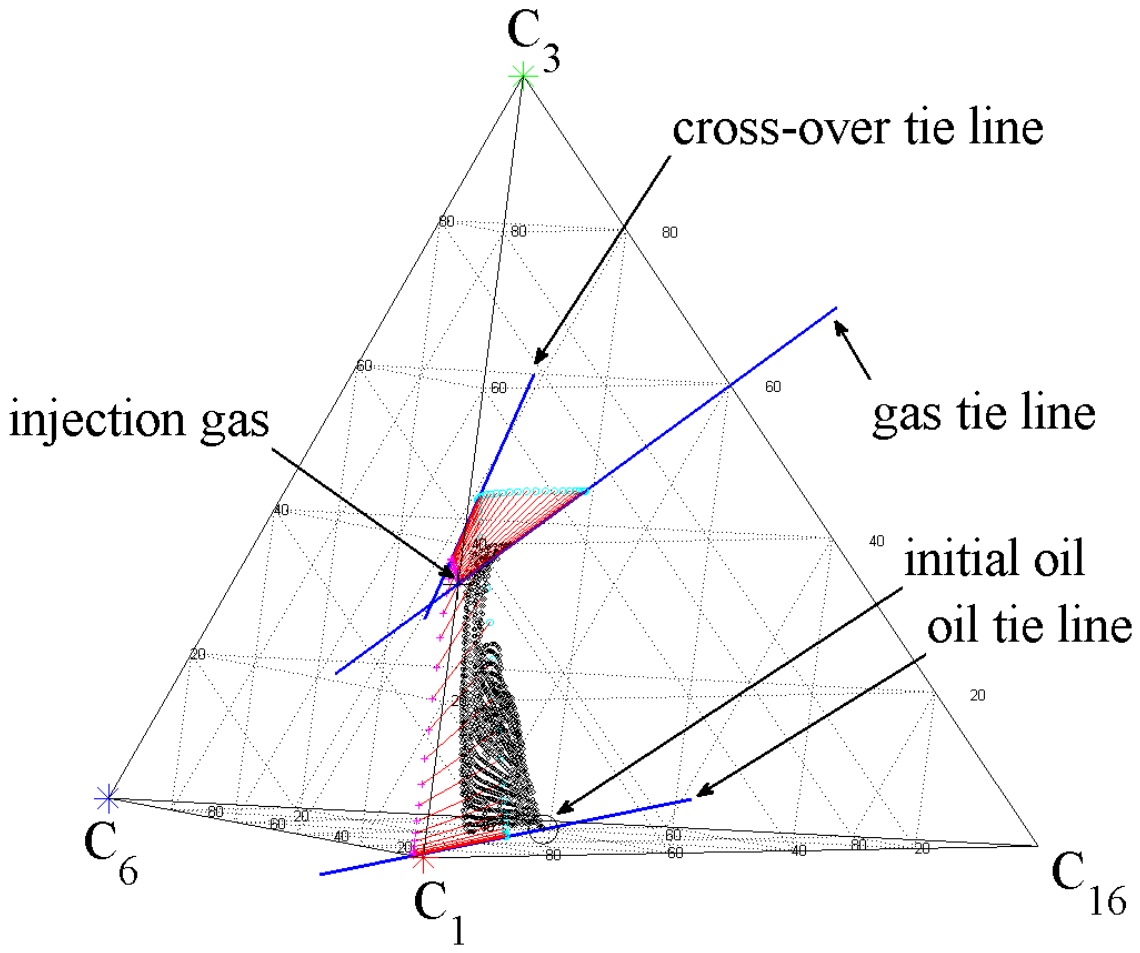

Figure 4-6: MMC tie lines after 100 contacts (red lines), key tie lines of the MOC solution (blue lines) and a portion of the three-dimensional solution route (black circles) for a four-component displacement (phase behavior model from Johns (1992)).

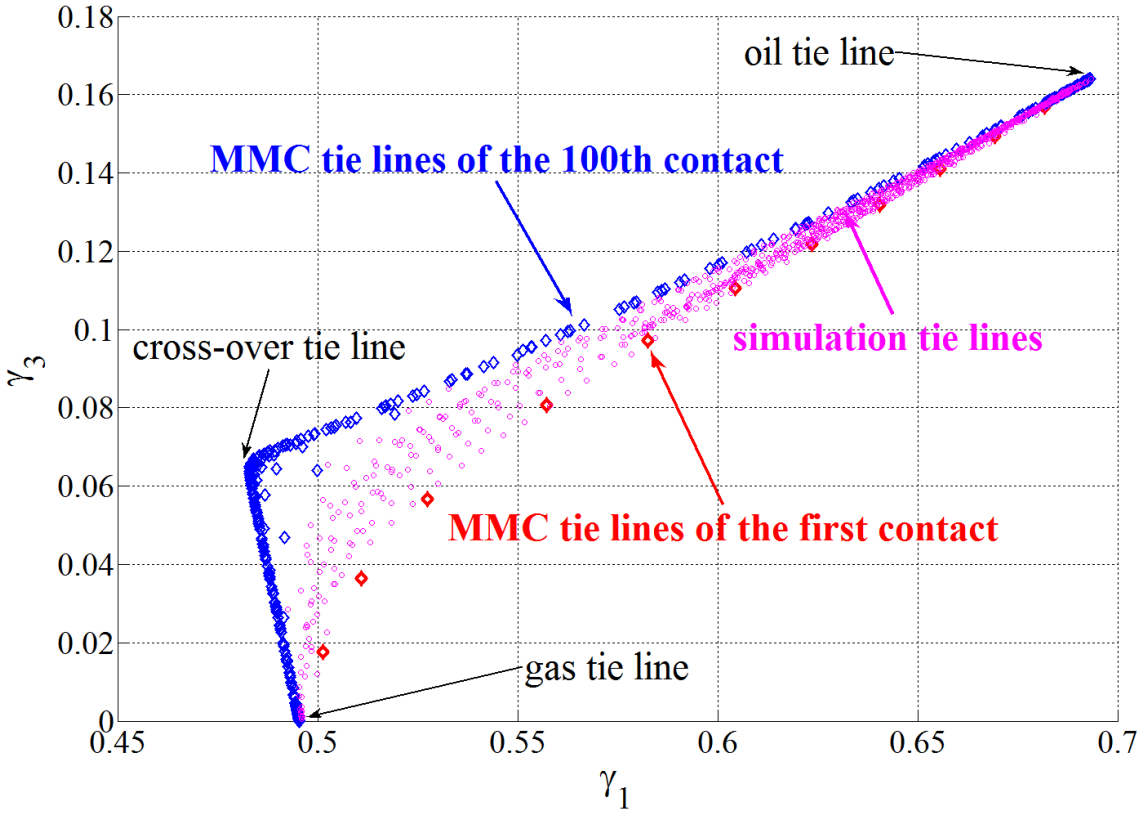

Figure 4-7: Three-dimensional simulation tie lines of the four-component displacement (pink circles) and the MMC tie lines of the first contact (red squares) and the 100th contact (blue squares) in the tie-line space ($\gamma_i = (x_i + y_i)/2$) (phase behavior model from Johns (1992)).

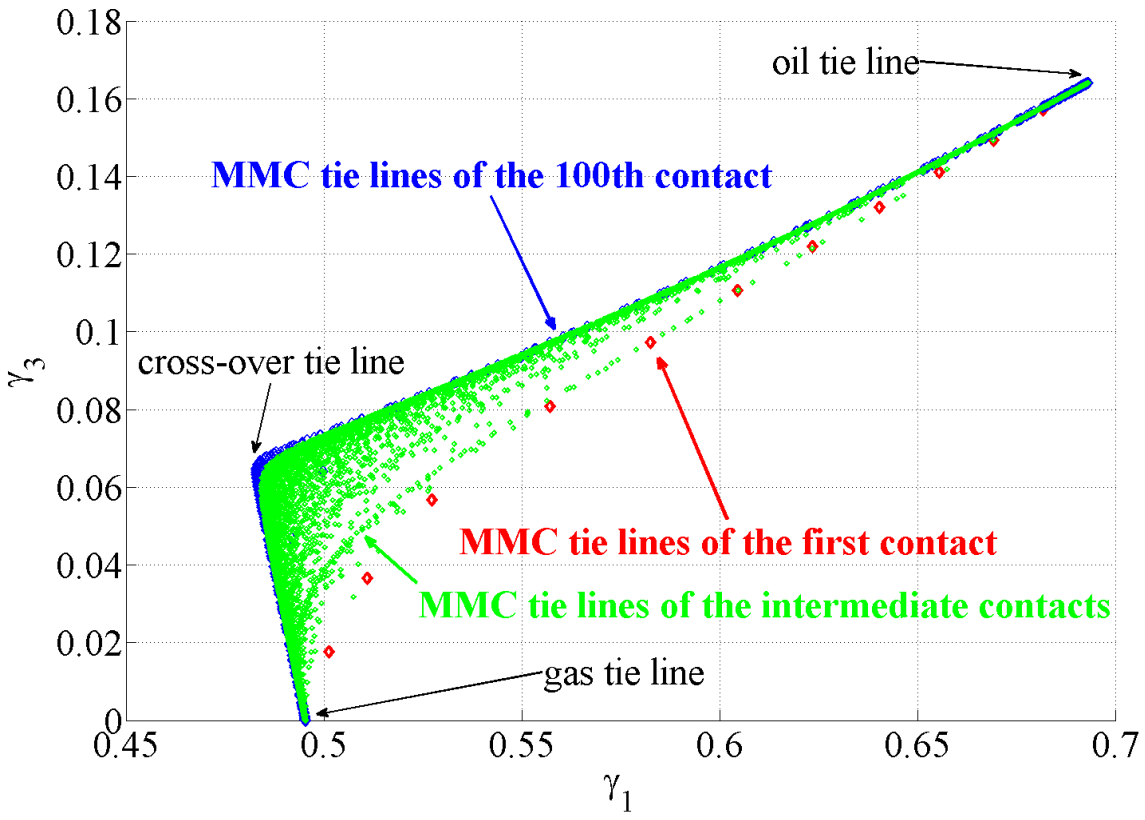

Figure 4-8: MMC tie lines of the first contact (red squares), the 100th contact (blue squares) and the intermediate contacts in the tie-line space ($\gamma_i = (x_i + y_i)/2$) for the four-component displacement (phase behavior model from Johns (1992)).

Chapter 5: Tie-Simplex-Based (TSB) Phase Behavior Modeling in Fully Implicit Compositional Reservoir Simulators

In this chapter we investigate the computational efficiency of the TSB phase equilibrium calculations method in a fully implicit reservoir simulator. We use the natural variable formulation as the simulation framework for comparing different phase equilibrium calculation methods. The overall computational procedure in The University of Texas at Austin's fully implicit general purpose adaptive simulator (GPAS) is presented first. Next, the details of the natural variable formulation in GPAS are discussed. Then we illustrate the phase behavior calculations in the natural variable formulation and how the TSB method can be utilized in this formulation. Finally, we perform several simulation case studies and compare the computational performance of various phase equilibrium calculation methods using the natural variable formulation in GPAS.

5.1 COMPUTATIONAL FRAMEWORK OF GPAS

GPAS is a fully implicit, compositional, equation of state (EOS) reservoir simulator specifically designed for large-scale parallel reservoir simulations. GPAS has been developed at the Center for Petroleum and Geosystems Engineering (CPGE) at The University of Texas at Austin (Wang *et al.*, 1997). GPAS was developed under the framework called Integrated Parallel Accurate Reservoir Simulator (IPARS), which was also developed at The University of Texas at Austin (Gropp *et al.*, 1996; Parashar *et al.*, 1997; Wheeler *et al.*, 1999). Through the IPARS framework, the physical model development in GPAS is separated from the code involving parallel processing, which substantially facilitates development of new physical models by researchers with limited

background in parallel processing. A variety of reservoir simulation problems for the multiphase multi-dimensional flow are supported by the IPARS framework. The IPARS framework provides functions which perform input/output processing, memory allocation for FORTRAN arrays, domain decomposition, well management, table lookup and interpolation, and message parsing between processors for updating ghost-layers' parameters. GPAS uses the Newton method to linearize the governing partial differential equations. The linear system of equations is solved using the linear solvers form Portable Extension Toolkit for Scientific Computation (PETSc) package developed at the Argonne National Laboratory (ANL) (Balay *et al.*, 1998).

The EOS compositional model (Wang *et al.*, 1997) is only one of the physical models developed under the GPAS framework. Thermal EOS compositional modeling (Varavei, 2009; Varavei and Sepehrnoori, 2009), a chemical flood model (Han *et al.*, 2005), unstructured gridding (Marcondes and Sepehrnoori, 2010), a full-tensor dual porosity model (Tarahhom, 2008; Tarahhom *et al.*, 2009), a geo-mechanical coupling (Pan, 2009; Pan *et al.*, 2007) and various fully implicit formulations (Schmall, 2013; Schmall *et al.*, 2014) are also implemented in GPAS. The reader is referred to GPAS's Technical Documentation and User's Guide for further details regarding the overall computational procedure under the IPARS framework.

5.2 THE FULLY IMPLICIT FORMULATION IN GPAS

The reservoir simulator solves the equations that mathematically describe the known physical laws that govern the physical model under consideration. The governing equations are mass conservation equations, thermodynamic equilibrium constraints, and the volume balance constraint. We use the natural variable formulation that was developed and implemented by Schmall (2013) as the framework for comparing the

performance of various phase equilibrium calculation methods. The following assumptions were made in the development of this mathematical model (Schmall, 2013):

- isothermal system
- multiphase Darcy's law
- instantaneous local equilibrium
- inert rock
- absence of any chemical reactions between the reservoir fluids
- diagonal permeability tensor
- slightly compressible porous media

When the maximum number of hydrocarbon phases is two and in the presence of an aqueous phase that is immiscible with the hydrocarbon phases, the governing differential equations are as follows:

a) n_c mass conservation equation for each hydrocarbon component

$$V_b \frac{\partial}{\partial t}\left(\phi N_i\right) - V_b \vec{\nabla} \cdot \sum_{j=1}^{n_p} \left(\frac{\bar{\bar{k}} k_{rj}}{\mu_j} \xi_j x_{ij} \left(\vec{\nabla} P_j - \gamma_j \vec{\nabla} D \right) - \phi \xi_j S_j \bar{\bar{K}} \vec{\nabla} x_{ij} \right) - q_i = 0 \,, \qquad (5.1)$$

where

$n_c =$ number of hydrocarbon components

$V_b =$ bulk volume

$\phi =$ porosity

$N_i =$ total number of moles of component *i*

$t =$ time

$\bar{\bar{k}} =$ permeability tensor

k_{rj} = relative permeability of phase *j*

μ_j = viscosity of phase *j*

ξ_j = molar density of phase *j*

x_{ij} = mole fraction of component *i* in phase *j*

n_p = number of phases

P = pressure

γ_j = specific weight of phase *j*

D = depth of the gridblock

S_j = saturation of phase *j*

$\overline{\overline{K}}$ = dispersion tensor

q_i = molar flow rate of component *i*.

b) The mass conservation equation for the water component

$$V_b \frac{\partial}{\partial t}\left(\phi N_w\right) - V_b \vec{\nabla} \cdot \sum_{j=1}^{n_p} \left(\frac{\overline{\overline{k}} k_{rw}}{\mu_w} \xi_w \left(\vec{\nabla} P_w - \gamma_w \vec{\nabla} D \right) \right) - q_w = 0 \ , \tag{5.2}$$

where the subscript *w* designates the water phase or the water component.

c) n_c thermodynamic equilibrium constraints expressed as equality of fugacity of each component in the oil and gas phases. For the gridblocks that contain only one hydrocarbon phase, the thermodynamic equilibrium constraints are not part of the governing equations.

$$f_i^o - f_i^g = 0, \qquad i = 1, 2, \ ...., n_c. \tag{5.3}$$

d) Two mole fraction constraints for the oil (j = 2) and gas (j = 3) phases

$$\sum_{i=1}^{n_c} x_{ij} = 1\,, \qquad j = 2,3. \tag{5.4}$$

e) One volume constraint equation

$$\sum_{j=1}^{n_p} S_j = 1 \text{ or } \sum_{j=1}^{n_p} \frac{N_j}{\xi_j} = 1\,. \tag{5.5}$$

The above system of equations forms $2n_c + 4$ equations in each gridblock for a given timestep. One possible full set of unknowns in each gridblock is oil composition (x_1, x_2, …., x_{nc}), gas composition (y_1, y_2, …., y_{nc}), pressure of one phase e.g. water pressure, and phase saturations. If capillary pressure is nonzero, then capillary pressure-saturation relations are used to obtain pressure of the other phases during Newton iterations.

Through thermodynamic arguments one can show that only n_c+1 equations need to be solved simultaneously in a fully implicit system (Cao, 2002; Aziz and Wong, 1988). These $n_c + 1$ equations solved implicitly are referred to as primary equations and the remaining, solved subsequently, are secondary equations. Various choice of primary equations and primary variables leads to different formulations e.g. the natural variable formulation also called Coats formulation (Coats, 1980), Collins formulation (Collins, *et al.*, 1992), and Branco and Rodriguez formulation (Branco and Rodriguez, 1996). Eqs. (5.1) and (5.2) often constitute the set of primary equations, and are discretized using an implicit finite difference scheme and upstream weighting of the transmissibility terms. At the solution, the residuals of all of the nonlinear governing equations must be (approximately) zero. In general, the residuals vector ($\vec{R}$) consists of the finite difference form of Eqs. (5.1) and (5.2), and the Eqs. (5.3) through (5.5). The residuals vector ($\vec{R}$) is a function of the unknown vector or the vector of independent variables ($\vec{X}$). $\vec{X}$ is

considered as a solution vector at the new time level if it satisfies $\vec{R}(\vec{X}) \approx \vec{0}$. The Newton method to obtain a solution vector at the new time level starts by assuming a guess value for the solution vector $\vec{X}^{k=0}$, where *k* denotes the iteration level. Then the guessed solution vector is used to evaluate all the dependent variables, physical properties, and the residuals vector ($\vec{R}^{k=0}$). If the convergence criteria are not satisfied at this point, the solution vector needs to be updated using $\vec{X}^{k+1} = \vec{X}^{k} + \Delta\vec{X}^{k}$, where $\Delta\vec{X}^{k}$ is the solution to the linear system in Eq. (5.6). The last two steps are repeated until the convergence criteria are satisfied.

$$J(\vec{X}^{k})\Delta\vec{X}^{k} = -\vec{R}^{k}. \tag{5.6}$$

The matrix *J* called the Jacobian matrix is comprised of sub-matrices J_{IK} which are derivatives of the residuals vector in gridblock *I* with respect to the unknown variables of gridblock *K*. Eq. (5.7) is the expanded form of Eq. (5.6) in terms of the sub-matrices of each gridblock.

$$\begin{pmatrix} J_{1,1} & J_{1,2} & \dots & J_{1,N_B} \\ J_{2,1} & J_{2,2} & \dots & J_{2,N_B} \\ \vdots & & & \vdots \\ J_{N_B,1} & J_{N_B,2} & \dots & J_{N_B,N_B} \end{pmatrix} \begin{pmatrix} \Delta\vec{X}_1 \\ \Delta\vec{X}_2 \\ \vdots \\ \Delta\vec{X}_{N_B} \end{pmatrix} = -\begin{pmatrix} \vec{R}_1 \\ \vec{R}_2 \\ \vdots \\ \vec{R}_{N_B} \end{pmatrix}, \tag{5.7}$$

where N_B is the number of gridblocks.

5.3 THE NATURAL VARIABLE FORMULATION

In the natural variable formulation, also called the Coats formulation (Coats, 1980), the primary equations are the hydrocarbon components and water mass conservation equations (Eqs. (5.1) and (5.2)). These are selected as the primary equations

because they include variables of the same gridblock and also the neighboring gridblocks. The equality of fugacity equations and the other constraint equations are the secondary equations. The secondary equations of each gridblock do not include variables of the neighboring gridblocks, and are used to eliminate the secondary variables from the primary equations.

The primary variables in each gridblock depend on the number of hydrocarbon phases and the phase state in the gridblock. Table 5-1 shows the primary variables in the presence of different hydrocarbon phases.

Schmall (2013) implemented the natural variable formulation in GPAS. The overall computational procedure for obtaining the solution vector ($\vec{X}$) over one timestep in the natural variable formulation in GPAS is shown in Figure 5-1. Schmall (2013) used the procedure proposed by Cao (2002) to decouple the primary equations from the secondary variables. In this procedure, first the secondary unknown variables are eliminated from the primary equations using the secondary equations. Then, the primary variables and subsequently the secondary variables are solved for. Explicit stability analysis and phase-split calculations are performed only for the single-phase gridblocks after updating the solution vector at the end of a Newton iteration (the box denoted by asterisk in Figure 5-1). For the two-phase gridblocks, the phase-split equations are part of the global Jacobian matrix and solved during the global Newton iterations. Eq. (5.8) illustrates a diagonal sub-matrix of the Jacobian matrix and the corresponding right-hand side implemented in the natural variable formulation in GPAS (Schmall, 2013). R_{mi}, R_{mw}, R_{fi}, R_x, and R_y are residuals of the mass conservation equation of component *i*, mass conservation equation of water, fugacity constraint of component *i*, and the mole fraction

constraints in oil and gas phases, respectively and S_o and S_g are the oil and gas saturations, respectively.

$$\begin{bmatrix} \begin{bmatrix} \frac{\partial R_{m1}}{\partial S_o} & \frac{\partial R_{m1}}{\partial S_g} & \frac{\partial R_{m1}}{\partial y_3} & \cdots & \frac{\partial R_{m1}}{\partial y_{nc}} & \frac{\partial R_{m1}}{\partial P} \\ \frac{\partial R_{m2}}{\partial S_o} & \frac{\partial R_{m2}}{\partial S_g} & \frac{\partial R_{m2}}{\partial y_3} & \cdots & \frac{\partial R_{m2}}{\partial y_{nc}} & \frac{\partial R_{m2}}{\partial P} \\ \vdots & \vdots & \vdots & \cdots & \vdots & \vdots \\ \frac{\partial R_{mnc}}{\partial S_o} & \frac{\partial R_{mnc}}{\partial S_g} & \frac{\partial R_{mnc}}{\partial y_3} & \cdots & \frac{\partial R_{mnc}}{\partial y_{nc}} & \frac{\partial R_{mnc}}{\partial P} \\ \frac{\partial R_{mw}}{\partial S_o} & \frac{\partial R_{mw}}{\partial S_g} & \frac{\partial R_{mw}}{\partial y_3} & \cdots & \frac{\partial R_{mw}}{\partial y_{nc}} & \frac{\partial R_{mw}}{\partial P} \end{bmatrix} & \begin{bmatrix} \frac{\partial R_{m1}}{\partial y_1} & \frac{\partial R_{m1}}{\partial y_2} & \frac{\partial R_{m1}}{\partial x_1} & \cdots & \frac{\partial R_{m1}}{\partial x_{nc}} \\ \frac{\partial R_{m2}}{\partial y_1} & \frac{\partial R_{m2}}{\partial y_2} & \frac{\partial R_{m2}}{\partial x_1} & \cdots & \frac{\partial R_{m2}}{\partial x_{nc}} \\ \vdots & \vdots & \vdots & \cdots & \vdots \\ \frac{\partial R_{mnc}}{\partial y_1} & \frac{\partial R_{mnc}}{\partial y_3} & \frac{\partial R_{mnc}}{\partial x_1} & \cdots & \frac{\partial R_{mnc}}{\partial x_{nc}} \\ \frac{\partial R_{mw}}{\partial y_1} & \frac{\partial R_{mw}}{\partial y_2} & \frac{\partial R_{mw}}{\partial x_1} & \cdots & \frac{\partial R_{mw}}{\partial x_{nc}} \end{bmatrix} \\ \begin{bmatrix} \frac{\partial R_{f1}}{\partial S_o} & \frac{\partial R_{f1}}{\partial S_g} & \frac{\partial R_{f1}}{\partial y_3} & \cdots & \frac{\partial R_{f1}}{\partial y_{nc}} & \frac{\partial R_{f1}}{\partial P} \\ \frac{\partial R_{f2}}{\partial S_o} & \frac{\partial R_{f2}}{\partial S_g} & \frac{\partial R_{f2}}{\partial y_3} & \cdots & \frac{\partial R_{f2}}{\partial y_{nc}} & \frac{\partial R_{f2}}{\partial P} \\ \vdots & \vdots & \cdots & \cdots & \vdots & \vdots \\ \frac{\partial R_{fnc}}{\partial S_o} & \frac{\partial R_{fnc}}{\partial S_g} & \frac{\partial R_{fnc}}{\partial y_3} & \cdots & \frac{\partial R_{fnc}}{\partial y_{nc}} & \frac{\partial R_{fnc}}{\partial P} \\ \frac{\partial R_x}{\partial S_o} & \frac{\partial R_x}{\partial S_g} & \frac{\partial R_x}{\partial y_3} & \cdots & \frac{\partial R_x}{\partial y_{nc}} & \frac{\partial R_x}{\partial P} \\ \frac{\partial R_y}{\partial S_o} & \frac{\partial R_y}{\partial S_g} & \frac{\partial R_y}{\partial y_3} & \cdots & \frac{\partial R_y}{\partial y_{nc}} & \frac{\partial R_y}{\partial P} \end{bmatrix} & \begin{bmatrix} \frac{\partial R_{f1}}{\partial y_1} & \frac{\partial R_{f1}}{\partial y_2} & \frac{\partial R_{f1}}{\partial x_1} & \cdots & \frac{\partial R_{f1}}{\partial x_{nc}} \\ \frac{\partial R_{f2}}{\partial y_1} & \frac{\partial R_{f2}}{\partial y_2} & \frac{\partial R_{f2}}{\partial x_1} & \cdots & \frac{\partial R_{f2}}{\partial x_{nc}} \\ \vdots & \vdots & \vdots & \cdots & \vdots \\ \frac{\partial R_{fnc}}{\partial y_1} & \frac{\partial R_{fnc}}{\partial y_2} & \frac{\partial R_{fnc}}{\partial x_1} & \cdots & \frac{\partial R_{fnc}}{\partial x_{nc}} \\ \frac{\partial R_x}{\partial y_1} & \frac{\partial R_x}{\partial y_2} & \frac{\partial R_x}{\partial x_1} & \cdots & \frac{\partial R_x}{\partial x_{nc}} \\ \frac{\partial R_y}{\partial y_1} & \frac{\partial R_y}{\partial y_2} & \frac{\partial R_y}{\partial x_1} & \cdots & \frac{\partial R_y}{\partial x_{nc}} \end{bmatrix} \end{bmatrix} = \begin{bmatrix} R_{m1} \\ R_{m2} \\ \vdots \\ R_{mnc} \\ R_{mw} \\ R_{f1} \\ R_{f2} \\ \vdots \\ R_{fnc} \\ R_x \\ R_y \end{bmatrix}. \qquad (5.8)$$

5.3.1 Phase Equilibrium Calculations in the Natural Variable Formulation

The number of hydrocarbon phases in each gridblock may vary from one Newton iteration to the next for general reservoir simulation problems. For the two-phase gridblocks the equations expressing equality of fugacity of each component in co-existing phases (Eqs. (5.3)) are part of the global Jacobian matrix. If a gridblock remains two-phase in all of the iterations over a timestep, the equilibrium constraints will be satisfied as part of the global Newton iterations. Therefore, for the two-phase gridblocks explicit flash calculations are not necessary as the flash calculations are embedded in the Jacobian

matrix. A two-phase gridblock should always be monitored for possible disappearance of a hydrocarbon phase. If either S_o or S_g becomes negative after updating the saturation solution of the two-phase gridblocks, the corresponding phase saturation is set to zero before initializing the next Newton iteration. In addition, the composition of the other hydrocarbon phase is set to the overall composition of the gridblock and the gridblock is marked as a single-hydrocarbon-phase gridblock (Cao, 2002).

For single-phase gridblocks, the equality of fugacity equations are not part of the governing equations. However, a single-phase gridblock must be tested for possible appearance of the second hydrocarbon phase in the Newton iterations. In GPAS, after updating the phase composition, pressure, and saturation in the single-phase gridblocks, a phase stability test is performed for the updated single-phase composition and pressure. If the stability test indicates existence of a two-phase mixture, a flash calculation is performed to obtain the composition and molar fraction of the existing phases. These phase compositions are used for initializing the next Newton iteration. The corresponding phase saturations for initializing the next Newton iteration are obtained from

$$S_o = (1 - S_w) \frac{\frac{l}{\xi_o}}{\frac{l}{\xi_o} + \frac{1-l}{\xi_g}}, \tag{5.9}$$

$$S_g = 1 - S_o - S_w. \tag{5.10}$$

where S_o, S_g, and S_w are oil saturation, gas saturation, and water saturation, respectively, l is molar fraction of the liquid phase, and ξ_o and ξ_g are molar density of the liquid and gas phases, respectively.

A rigorous flash calculation is not strictly required at this stage because this is only an intermediate solution. Negative flash calculation (Whitson and Michelsen, 1989) is another method that may be applied to test if a single-phase gridblock remains single-phase after an update of variables during Newton iterations. If the liquid phase molar fraction (l) is between 0 and 1, the gridblock switches from single phase to two phases. The next Newton iteration is initialized using Eqs. (5.9) and (5.10) and the resulting phase compositions. In another treatment of phase reappearance, the saturation pressure of the gridblock is calculated and compared to the gridblock's pressure. If the pressure in the gridblock is larger than the saturation pressure, the gridblock remains single phase (Cao, 2002; Schmall, 2013).

In order to ensure consistent phase labeling throughout the simulation, we always apply the phase labeling algorithm after a single-phase gridblock has been tested for stability regardless of appearance of a second hydrocarbon phase. Correct identification of the phase state of a gridblock is important as it will affect the choice of relative permeability function and the values of other physical properties for a phase. Phase identification in compositional reservoir simulation is one of the long-standing challenges, which is still an area of active research (Yuan and Pope, 2012). An algorithm similar to that proposed by Gosset *et al.* (1986) is used to decide whether a single-phase mixture is an oil phase or a gas phase in GPAS. Another method for identifying the state of single-phase fluids in GPAS is to use a reference mass density based on the specific fluid model at hand. For two-phase gridblocks the oil phase is defined as the phase with the larger mole fraction of the heaviest component. Of course, a mass density criterion is another method to decide which phase is the oil phase. However, in multi-contact-miscible (MCM) CO_2 floods the mass density criterion is less reliable because the mass

density of the CO_2-rich liquid phase may become greater than that of the oil phase (Perschke, 1988).

The flowchart given in Figure 5-2 schematically illustrates the variables' update after each Newton iteration for single-phase and two-phase gridblocks. The dashed blue box indicates where the phase equilibrium calculations are explicitly performed in the natural variable formulation.

5.4 IMPLEMENTATION OF TSB PHASE EQUILIBRIUM CALCULATIONS IN GPAS

As mentioned in Section 5.3, in the natural variable formulation the equality of fugacity equations for the two-phase gridblocks are part of the global Jacobian matrix. Thus, it is not possible to replace these calculations for the two-phase gridblocks by TSB methods without re-structuring the entire formulation. Application of the TSB methods for the single-phase gridblocks however is rather straightforward. In a Newton iteration, the conventional stability analysis and possible flash calculations that are performed for single-phase gridblocks after variables' update can be replaced with TSB phase equilibrium calculations. Thus, instead of the original phase equilibrium calculations algorithm in Figure 5-2, we apply the tie-line-based phase equilibrium calculation algorithms employed in Chapters 3 and 4 of this dissertation.

The conventional phase equilibrium calculations in GPAS include phase stability tests and subsequent flash calculations if the stability test indicates an unstable single phase. The initial estimates from the previous two-phase flash results in the same gridblock are not used by default. This is because for the gridblocks that were two phases in the previous timestep, phase equilibrium calculations in the current timestep's iterations are performed only if the gridblock is single-phase in an earlier iteration. We implemented the method, which uses initial estimates from the previous timestep for

speeding up the phase equilibrium calculations in GPAS, even though successful application of this method will require problems with numerous phase transitions during the simulation.

The other heuristic technique that we employed in UTCOMP (Chapters 3 and 4) is to avoid stability analysis and flash calculations for gridblocks that were surrounded by single-phase neighbors in the previous timestep. To apply this heuristic technique for speeding up the phase equilibrium calculations in the natural variable formulation in GPAS, we used a similar approach as in the UTCOMP simulator. We note that the previous timestep's solution must be used to apply the heuristic techniques in fully implicit reservoir simulators not the previous Newton iterations' solution as the latter is not a true solution to the governing equations.

We implemented the compositional space adaptive tabulation (CSAT), a TSB phase equilibrium calculations method, in the natural variable formulation in GPAS. The details of implementation of CSAT in GPAS are the same as in UTCOMP. We also implemented MMC1, one of the multiple-mixing-cell (MMC) based methods introduced in Chapter 4, in GPAS. The summary of the phase equilibrium calculation methods implemented in GPAS are as follows:

- GPAS1: This method involves the conventional phase stability analysis followed by two-phase flash calculations if necessary for the single-phase gridblocks.
- GPAS2: In this method two heuristic techniques are implemented in GPAS to improve the computational performance of conventional phase equilibrium calculations. First, stability analysis is avoided for single-phase gridblocks that were surrounded by single-phase neighbors in the previous timestep. Second, the gridblock's flash results from the previous timestep are used to avoid stability

analysis and approximate flash results in the Newton iterations of the current timestep.

- CSAT: The CSAT framework is used to skip stability analysis and generate initial estimates for flash calculations or possibly approximate the flash results if a distance tolerance is satisfied.
- MMC1: The CSAT framework is applied only with the pre-computed tie-line tables form the MMC simulations. Adaptive tabulation is not performed. If a matching tie-line is not found for an overall composition, regular phase stability analysis and flash calculations will be performed.

5.5 COMPARISON OF THE VARIOUS PHASE EQUILIBRIUM CALCULATION METHODS IN THE NATURAL VARIABLE FORMULATION IN GPAS

In this section, we perform several simulation case studies to compare the performance of the various methods of phase equilibrium calculations in the natural variable formulation as a fully implicit formulation. We perform the simulations using the automatic timestep selection option in GPAS. This timestep selection method controls the timestep size through restricting the relative changes in pressure, phase saturations, and number of moles of components per unit pore volume for all gridblocks. The maximum allowed relative changes in all of the timestep-control variables are set to 50%. When one of the variables that control the timestep size has a very small value in a gridblock e.g. saturation values smaller than 0.01, the relative change in that variable of the gridblock is excluded from the timestep selection algorithm.

Four different simulations are performed using the various phase equilibrium calculation methods explained in Section 5.4 for each simulation case study. All simulation results using different phase equilibrium calculation methods agree well. The

oil production rates of different simulations are compared under the description of each individual simulation case. The Peng-Robinson (PR) EOS (Peng and Robinson, 1976) was used as the fluid model in all of the simulations. The simulation cases considered are two-phase miscible gas injection into oil reservoirs and a depletion drive for an oil reservoir. The initial water saturation was 0.17, which is below the residual water saturation of 0.3. Capillary pressure was assumed to be zero. Corey's model (Corey, 1986) was used for the oil and gas relative permeabilities with the parameters given in Table 5-2.

The simulations were performed on dedicated CPU nodes in the Lonestar clusters of the Texas Advanced Computing Center (TACC). Because of the high memory demand of the simulations with GPAS, the measured total computational time of each simulation varies by 1%. In our table search, we used the partial sorting strategy that was explained in Chapter 3.

For the simulations using the natural variable formulation in GPAS, the contribution of phase stability analysis and subsequent flash calculations in single-phase gridblocks to the total computational time is less than 5%. In a similar formulation, the reported contribution of these calculations to the total computational time is 20% to 40% (Voskov and Tchelepi, 2008). This difference is because of the inefficiencies in the Jacobian matrix construction in our code. Breakdown of the total computational time in our simulations shows that construction and update of the Jacobian matrix contribute to more than 40% of the total computational time. Approximately 45% of the total computational time is spent in the linear solver, which is generally expected. Nevertheless, it is possible that the linear solver time in our code is also excessive and tuning the solver parameters may reduce the total computational time significantly. In

addition, the IPARS framework, which drives the EOS compositional model, may slow down the computations for small scale single processor simulations, which are the case for the simulations performed here. Because of the small contribution of the phase equilibrium calculations to the total computational time in our simulations, we focus our analysis on the phase equilibrium computational time rather than the total computational time.

In the fully implicit formulation in GPAS if the Newton iterations do not converge to the solution within a pre-specified maximum number of iterations, the timestep is discarded and the Newton step is restarted with a smaller timestep. This is computationally expensive as all of the Newton iterations with the larger timestep are discarded. Furthermore, for the MCM displacements that we have examined in this dissertation it is often the case that one gridblock repeatedly switches from single-phase state to two-phase and back to single-phase during consecutive Newton iterations. This will prevent convergence of the Newton iterations to a solution even though the residuals vector in the rest of the gridblocks often satisfies the convergence criteria. To circumvent this convergence issue, we only perform a stability test of the single-phase gridblocks up to a pre-specified number of Newton iterations (MAXNEWT2P), which might be less than the maximum number of Newton iterations (MAXNEWT). We performed our simulations with various combinations of the MAXNEWT2P and MAXNEWT values. Despite different convergence behavior, the simulation results are the same for various reasonable values of these two parameters. The tie-line detection tolerance for all of the simulations performed with CSAT and MMC1 are 0.01 unless otherwise stated under the discussion for each individual case.

5.5.1 Case 1

Case 1 is similar to the first simulation case study in Chapter 4. It is a high pressure N_2 injection in a quarter of a five-spot pattern. Initial composition of the reservoir fluid is 1.3% CO_2, 1.9% N_2, 16% C_1, 8.7% C_2, 5.9% C_3, 9.7% C_{4-6}, 4.7% C_{7+1}, 11.5% C_{7+2}, and 40.3% C_{7+3}. Injected fluid is 90% N_2 and 10% C_1. The initial reservoir pressure is 10,450 psia. The producer operates at constant bottomhole pressure of 10,350 psia. The injector operates at a constant injection rate of 5 MMscf/day. The reservoir model is three-dimensional with 20x20x6 gridblocks. The reservoir is homogenous with uniform permeability of 50 md and porosity of 0.2. The reservoir temperature is 120°F and the total simulation time is 600 days. The component properties used in the EOS model are given in Table 3-2. The summary of computational efficiency results for this case is given in Table 5-3. The simulations with different phase equilibrium calculation methods lead to nearly identical oil production rates as shown in Figure 5-3. A maximum timestep size of five days was specified because of the MCM nature of this displacement. We report the improvements in the phase equilibrium computational time using the tie-line-based methods compared to the conventional phase equilibrium calculations method as the base case. For the simulations performed for this case study, we used values of 20 and 8 for the MAXNEWT and MAXNEWT2P parameters, respectively. We further note that because of the automated timestep selection algorithm, various simulations may experience a different number of timesteps and Newton iterations.

The computational time of the phase equilibrium calculations in the GPAS1 simulation is 39.92 *sec*. Only 1,627,466 stability analyses and 6,548 phase-split calculations are performed. Using the Heuristic techniques in GPAS2 improves the computational time of the phase equilibrium calculations by 61.6%. 1,419,487 stability

analyses were skipped using the heuristic technique where stability analysis is skipped for single-phase gridblocks that were surrounded by single-phase neighbors in the previous timestep. The heuristic technique where the flash results of the previous timestep are used to skip stability analysis was successfully used only 18 times.

The simulation with CSAT improves the phase equilibrium computational time by 76.1%. CSAT skips almost all of the stability analyses (1,599,438). Only 14,448 stability analyses are actually performed due to proximity of the overall composition of interest to the phase boundary based on the interpolated tie line. CSAT was also successfully used to generate the initial estimate for most of the phase-split calculations performed. Only 27 subcritical tie-line tables and two critical tie-line tables were generated by CSAT. 15 tie-line tables contribute to 10,000 hits or more. The maximum number of hits experienced by one subcritical tie-line table is 38,571, which belongs to a tie-line table that is close to the oil tie line. Almost all of the critical tie-line hits occur for the critical oil tie line (1,250,879). The simulation of a similar problem in the UTCOMP simulator with CSAT produced 43 subcritical tie-line tables and two critical tie lines.

The simulation with MMC1 improves the phase equilibrium computational time by 78.2%. Similar to CSAT, almost all of the stability analyses are skipped and approximations are made for most of the phase-split calculations. Only 14,080 stability analyses are actually performed. Adaptive tie-line tabulation is not performed in the simulation with MMC1 and only the MMC tie lines are used in the interpolation. 120 tie-line tables from 20 contacts of three MMC simulations with mixing ratios of 0.2, 0.5, and 0.8 were used as the initial set of tie-line tables in the simulation with MMC1.

Simulations with other values of MAXNEWT and MAXNEWT2P result in similar improvements in the phase equilibrium calculations time using different methods.

5.5.2 Case 2

Case 2 is injection of 90% CO_2, 1% N_2, and 9% C_1 into an oil reservoir with the same initial composition as Case 1. The reservoir model is a quarter of a five-spot pattern. The initial reservoir pressure is 4,300 psia and the reservoir temperature is 120°F. The producer operates at a constant bottomhole pressure of 4,200 psia. The injector operates at a constant injection rate of 3.5 MMscf/day. The reservoir model is 20x20x6 gridblocks with a uniform porosity of 0.2 and a heterogeneous permeability field shown in Figure 5-4. The gridblock sizes in *x*-, *y*-, and *z*-directions are 25, 25 and 12.5 ft, respectively. The permeability field was populated using a Dykstra-Parsons coefficient of 0.8 and dimensionless correlation lengths of 0.25 in all directions. The total simulation time is 450 days. The component properties used in the EOS model are the same as in Case 1.

The summary of the computational efficiency results for this case is given in Table 5-4. The oil production rates for simulations with various phase equilibrium calculation methods agree well (Figure 5-5). A maximum timestep size of five days was used in the simulations. The simulations reported here were performed using values of 25 and 15 for the MAXNEWT and MAXNEWT2P parameters, respectively. We repeated the simulations for various values of these two parameters and the simulation results as well as the computational efficiency results are very similar.

The phase equilibrium calculations only take 40.46 *sec* in the GPAS1 simulation with the conventional phase equilibrium calculations algorithm. 3,679,179 stability analyses and 3,182 phase-split calculations were performed in the GPAS1 simulation. Using the heuristic techniques in the GPAS2 simulation reduces the phase equilibrium computational time by 46.6%. Only 835,004 stability analyses and 3,168 phase-split

calculations were performed in the simulation using the heuristic techniques. Similar to Case 1, almost all of the stability analyses that were skipped in the GPAS2 simulation are due to skipping stability analysis for single-phase gridblocks that were surrounded by single-phase neighbors in the previous timestep. This shows that very simple heuristic techniques can be successfully applied to reduce the computational time of the phase equilibrium calculations in the fully implicit reservoir simulators despite the generally larger timestep sizes.

The simulation with CSAT reduces the computational time of the phase equilibrium calculations by 64.0% compared to the simulation with GPAS1. Similar to Case 1, CSAT skips almost all of the stability analyses and approximations are made for a significant fraction of the phase-split calculations. Only 32,576 stability analyses and 1,048 phase-split calculations were performed using CSAT. CSAT generated 50 tie-line tables adaptively. The simulation of a similar problem with CSAT in the UTCOMP simulator produced 50 subcritical tie-line tables using the same distance tolerance of 0.01. The number of generated tie-line tables in the CSAT simulations with UTCOMP and GPAS are the same even though in UTCOMP the CSAT's interpolation and adaptive tabulation is applied for the entire compositional route of the gas injection problem while in GPAS it is mostly applied to the single-phase portion of the compositional route. The oil and gas tie lines contribute to 61.1% and 2.2% of the total tie-line table hits, respectively.

The simulation with MMC1 reduces the computational time of the phase equilibrium calculations by 54.0%. The tie lines from five contacts of MMC simulations with 11 different mixing ratios were used (122 tie-line tables). Only 119,163 stability analyses and 1,403 phase-split calculations were actually performed. The oil and gas tie

lines contribute to 62.7% and 4.3% of the total tie-line hits, respectively. Almost 99% of the total tie-line hits are due to 30 tie-line tables and 74 tie-line tables are never used.

5.5.3 Case 3

The reservoir model in Case 3 is a quarter of a five-spot pattern. This case is similar to Case 3 in Chapter 4. Initial composition of the reservoir fluid is 0.77% CO_2, 20.25% C_1, 11.8% C_{2-3}, 14.84% C_{4-6}, 28.63% C_{7-14}, 14.9% C_{15-24}, 2.946% C_{25-28}, 1.961% C_{29-32}, 1.305% C_{33-36}, 0.869% C_{37-40}, 0.5781% C_{41-44}, and 1.1505% C_{45+}. Injected fluid is 10% CO_2, 65% C_1, 20.0% C_{2-3}, and 5% C_{4-6}. Initial reservoir pressure is 3,400 psia and the initial reservoir temperature is 260°F. The producer operates at a constant bottomhole pressure of 3,300 psia and the injector operates at a constant injection rate of 1 MMscf/day. The grid model including the permeability and porosity fields of the reservoir is the same as in Case 2. The total simulation time is 600 days. The maximum allowed timestep size is 10 days. The computational efficiencies for this case are summarized in Table 5-5. The comparison of oil production rates for simulations with different phase equilibrium calculation methods are given in Figure 5-6. The simulations using different phase equilibrium calculation methods result in the same oil production rates. The mass density criterion was used for phase identification of single-phase fluids in this simulation case study. Values of 25 and 15 were used for the MAXNEWT and MAXNEWT2P parameters, respectively.

The phase equilibrium calculations take 62.1 s*ec* in the GPAS1 simulation using the conventional phase equilibrium calculations method. The number of stability analyses and phase equilibrium calculations actually performed are 3,469,575 and 2,632, respectively. Employing the heuristic techniques in the GPAS2 simulation improves the computational time of phase equilibrium calculations by 59.9%. Only 686,594 stability

analysis and 2,661 phase-split calculations are performed in the simulation with GPAS2 and most of the stability analyses are skipped by the heuristic techniques.

The CSAT simulation improves the computational time of the phase equilibrium calculations by 79.2%. The tie-line detection tolerance was 0.01. Almost all of the stability analyses are skipped in the simulation with CSAT. Only 2,092 stability analyses and 467 phase-split calculations are actually performed. The adaptive tabulation algorithm in CSAT generates 14 tie-line tables. The number of tie-line tables generated for the simulation of a similar case in the UTCOMP simulator is 17. The oil tie line contributes to 72.9 % of the total tie-line hits. The gas tie line contributes to only 3.3% of the total tie-line hits. No critical tie-line table was generated despite the near-miscible nature of this gas injection problem.

The simulation with MMC1 improves the computational time of the phase equilibrium calculations by 76.0%. This shows that performance of the tie-line-based methods that only use the MMC tie lines is very similar to that of the CSAT method with adaptive tabulation in the fully implicit formulations as well as in the IMPEC-type formulations. Only 78,032 stability analyses and 875 phase-split calculations were actually performed. For this simulation, 38 tie-line tables were collected from 20 contacts of the MMC simulation with a mixing ratio of 0.5. The oil and gas tie lines contribute to 72.5% and 3.5% of the total tie-line table hits, respectively. There are 24 tie-line tables that do not experience any hits and contribute only to failed table searches. The simulation with MMC1 uses a search algorithm based on partial sorting.

5.5.4 Case 4

This simulation case study is a first-contact-miscible gas injection problem. The initial reservoir fluid composition and the injected gas composition are the same as the

simulations in Case 3. The initial reservoir pressure is 5,500 psia. The reservoir model is a quarter of a five-spot pattern with 32x32x6 gridblocks. The producer operates at a constant bottomhole pressure of 5,400 psia and the injector operates at a constant injection rate of 1 MMscf/day. The injected gas and initial oil are first-contact-miscible at pressures above 5,200 psia; that is, the injected gas forms a single phase with the initial oil when mixed at any proportions. The heterogeneous permeability field is given in Figure 5-7 ($k_x = k_y = 2\ k_z$). The permeability field was populated using a Dykstra-Parsons' coefficient of 0.9 and dimensionless correlation length of 0.5 in all directions. The mean of natural logarithm of the permeability field is 1.0. The gridblock sizes in *x*-, *y*-, and *z*-directions are 25 ft, 25 ft, and 12.5 ft, respectively and porosity is 0.2. Gosset *et al.*'s (1986) method was used for phase identification of the single-phase gridblocks for the simulations in this case study. Table 5-6 summarizes the computational efficiency results for the simulations performed for this case study. Figure 5-8 shows comparison of the oil production rate for the simulations performed in this case. Values of 20 and 4 were used for the MAXNEWT and MAXNEWT2P parameters, respectively.

The phase equilibrium calculations take 85.26 *sec* in the simulation with GPAS1. The number of stability analyses and phase-split calculations performed are 5,025,792 and 12, respectively. Applying the heuristic techniques in the GPAS2 simulation improves the phase equilibrium computational time by 68.1%. Only 863,094 stability analyses and 7 phase-split calculations were performed. The number of stability analyses skipped is 4,162,698.

The simulation with CSAT improves the computational time of the phase equilibrium calculations by 77.6%. All of the stability analyses were skipped using CSAT. Only four subcritical tie-line tables and four critical tie-line tables were created.

The subcritical tie-line tables did not experience any hits. However, they are necessary since they facilitate tabulation of the critical tie lines. The critical oil tie line contributes to 73.3% of the critical tie-line table hits. The closest tie line to the critical gas tie line contributes to 9.2% of the total critical tie-line table hits.

The MMC method does not directly apply to a first-contact-miscible gas injection process. The critical oil and gas tie lines can be used as the only pre-computed tie-line tables in the MMC1 method. However, such a simulation is very similar to the CSAT simulation because the critical oil and gas tie lines contribute to almost 80% of the total tie-line hits in the CSAT simulation.

5.5.5 Case 5

Case 5 is production under depletion drive from an initially under-saturated oil reservoir. The initial reservoir fluid composition is the same as the simulations in Case 3. The reservoir model is 32x32x6 gridblocks and one producing well is placed in the center of the reservoir. The gridblock sizes in *x*-, *y*-, and *z*-directions are 200 ft, 200 ft, and 12.5 ft, respectively. The uniform permeabilities in *x*-, *y*-, and *z*-directions are 25 md, 25 md, and 5 md, respectively. The initial reservoir pressure is 2,000 psia, which is well above the bubblepoint pressure of 1,100 psia. The producer operates at a constant bottomhole pressure of 1,000 psia, which is slightly below the bubblepoint pressure. The total simulation time is 600 days. The maximum timestep size is 10 days. For this case three simulations were performed using the phase equilibrium calculation methods in GPAS1, GPAS2, and CSAT. Figure 5-9 compares the oil production rates for the simulations with different phase equilibrium calculation options. The computational efficiency results for the simulations in this case study are summarized in Table 5-7. The values of the MAXNEWT and MAXNEWT2P parameters are 20.

The phase equilibrium calculations only take 24.9 *sec* in the GPAS1 simulation with the conventional phase equilibrium calculations method. The number of stability analyses and phase-split calculations actually performed are 987,667 and 1,989, respectively. The heuristic techniques in the GPAS2 simulation improved the computational time of the phase equilibrium calculations by 84.9%. Only 28,116 stability analyses and 1,205 phase-split calculations were actually performed. Almost all of the stability analyses were skipped because of the technique that skips stability analysis for single-phase gridblocks surrounded by single-phase neighbors in the previous timestep.

The CSAT simulation improves the computational time of the phase equilibrium calculations by 81.0% compared to the conventional phase equilibrium calculations algorithm. Only 37,815 stability analyses and 458 phase-split calculations are actually performed. Only one tie-line table was generated during adaptive tabulation, which is the initial oil tie line. The initial oil tie line was successfully used to skip 948,321 stability analyses.

The MMC method does not apply to a depletion drive reservoir without any injected gas. However, since we always place the oil tie line as the first tie-line table in the pre-computed MMC1 tie lines, the MMC1 simulation will be essentially the same as the CSAT simulation for this case.

5.6 SUMMARY AND CONCLUSIONS

We implemented the CSAT method for speeding up the phase equilibrium calculations for the natural variable formulation in GPAS. We also implemented two other methods to improve the speed of phase equilibrium calculations in GPAS. One of the methods applies two heuristic techniques to skip stability analysis based on phase equilibrium information in the previous timestep. The other method uses the CSAT

framework with prior tie-line tables from the MMC simulations but without adaptive tabulation (MMC1 method in Chapter 4). Several simulation case studies were performed to compare the computational efficiency of various phase equilibrium calculation methods compared to the conventional phase equilibrium calculations algorithm.

The results show that using very simple heuristic techniques significantly improves the computational time of the phase equilibrium calculations in the GPAS simulator. For the cases studied, significant improvements of 61.6%, 46.6%, 59.9%, 68.1%, and 84.9% in the phase equilibrium computational time were obtained. The improvements in the computational time result almost entirely from the technique where stability analysis is skipped for single-phase gridblocks that were surrounded by single-phase neighbors in the previous timestep.

The results also show that the CSAT method significantly improves the computational time of the phase equilibrium calculations. For the cases studied, improvements of 76.1%, 64.0%, 79.2%, 77.6%, and 81.0% in the computational time of the phase equilibrium calculations were observed, which are generally larger than when using the heuristic methods. The results also show that the number of tie-line tables generated in the CSAT simulations of similar cases with the natural variable formulation in GPAS and the UTCOMP simulator are comparable.

The MMC1 method results in comparable improvements in the computational time of the phase equilibrium calculations compared to the CSAT method. For the MCM displacement cases studied, significant improvements of 78.2%, 54%, and 76.0% in the phase equilibrium computational time were observed.

Table 5-1: Primary variables in the natural variable formulation in the presence of different hydrocarbon phases.

	Primary variables	Secondary variables
oil and gas present	$S_o, S_g, y_3, y_4, \ldots, y_{nc}, P$	$y_1, y_2, x_1, x_2, \ldots, x_{nc}$
only oil present	$x_1, x_2, \ldots, x_{nc-1}, S_o, P$	-
only gas present	$y_1, y_2, \ldots, y_{nc-1}, S_g, P$	-

Table 5-2: Corey's relative permeability parameters of the oil and gas phases for the simulation case studies in GPAS.

$k_{rg}^{\ 0} = 0.9$	$k_{ro}^{\ 0} = 0.9$
$S_{gr} = 0.0$	$S_{or} = 0.1$
$e_{gas} = 2.0$	$e_{oil} = 2.0$

Table 5-3: Computational efficiency results for simulations in Case 1.

	GPAS1	GPAS2	CSAT	MMC1
CPU time (*sec*)	1,679	1633	1665	1603
Phase equil. time (*sec*)	39.92	15.32	9.54	8.72
No. of SA performed	1,627,466	207,961	14,448	14,080
No. of phase split performed	6,548	6,548	6,351	243
Number of steps	237	237	237	237
Number of Newton iterations	2,296	2,296	2,233	2,240
Improvement in computational time (%)	-	61.6	76.1	78.2

Table 5-4: Computational efficiency results for simulations in Case 2.

	GPAS1	GPAS2	CSAT	MMC1
CPU time (*sec*)	1,731	1,691	1,751	1,710
Phase equil. time (*sec*)	40.46	21.59	14.57	18.63
No. of SA performed	3,679,179	835,004	32,576	119,163
No. of phase split performed	3,182	3,158	1,048	1,403
Number of steps	234	237	230	232
Number of Newton iterations	2,608	2,602	2,696	2,625
Improvement in computational time (%)	-	46.6	64.0	54.0

Table 5-5: Computational efficiency results for simulations in Case 3.

	GPAS1	GPAS2	CSAT	MMC1
CPU time (*sec*)	2,464	2,373	2,087	2,220
Phase equil. time (*sec*)	62.11	24.90	12.88	14.90
No. of SA performed	3,469,575	686,594	2,092	78,032
No. of phase split performed	2,632	2,661	467	875
Number of steps	197	196	195	192
Number of Newton iterations	2,038	1,990	1,756	1,869
Improvement in computational time (%)	-	59.9	79.2	76.0

Table 5-6: Computational efficiency results for simulations in Case 4.

	GPAS1	GPAS2	CSAT
CPU time (*sec*)	10,633	10,529	10,535
Phase equil. time (*sec*)	85.26	27.19	19.12
No. of SA performed	5,025,792	863,094	0
No. of phase split performed	12	7	1
Number of steps	166	166	166
Number of Newton iterations	1,451	1,451	1,451
Improvement in computational time (%)	-	68.11	77.57

Table 5-7: Computational efficiency results for simulations in Case 5.

	GPAS1	GPAS2	CSAT
CPU time (*sec*)	558	588	537
Phase equil. time (*sec*)	24.95	3.76	4.72
No. of SA performed	987,667	28,116	37,815
No. of phase split performed	1,989	1,205	458
Number of steps	66	66	66
Number of Newton iterations	165	170	165
Improvement in computational time (%)	-	84.9	81.0

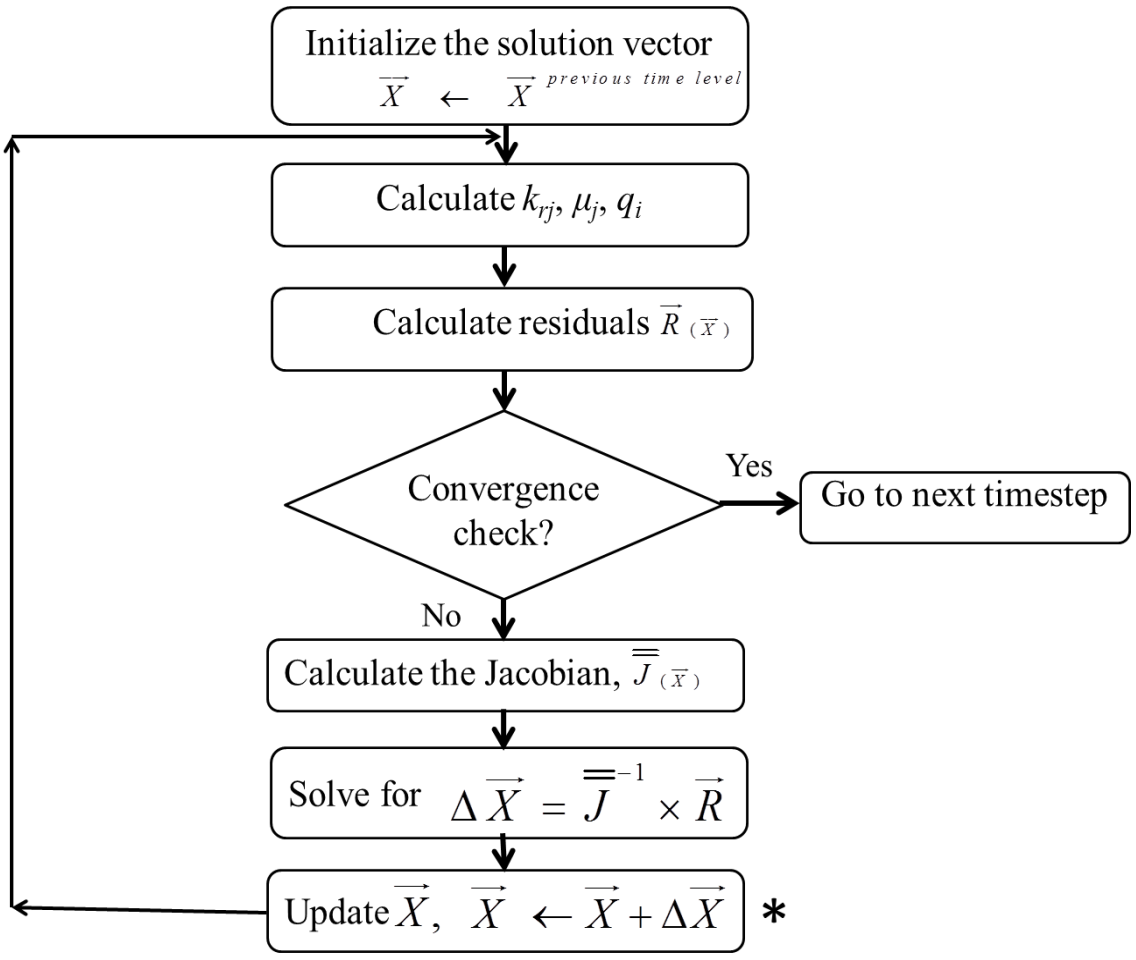

Figure 5-1: Overall computational procedure during one timestep for the natural variable formulation.

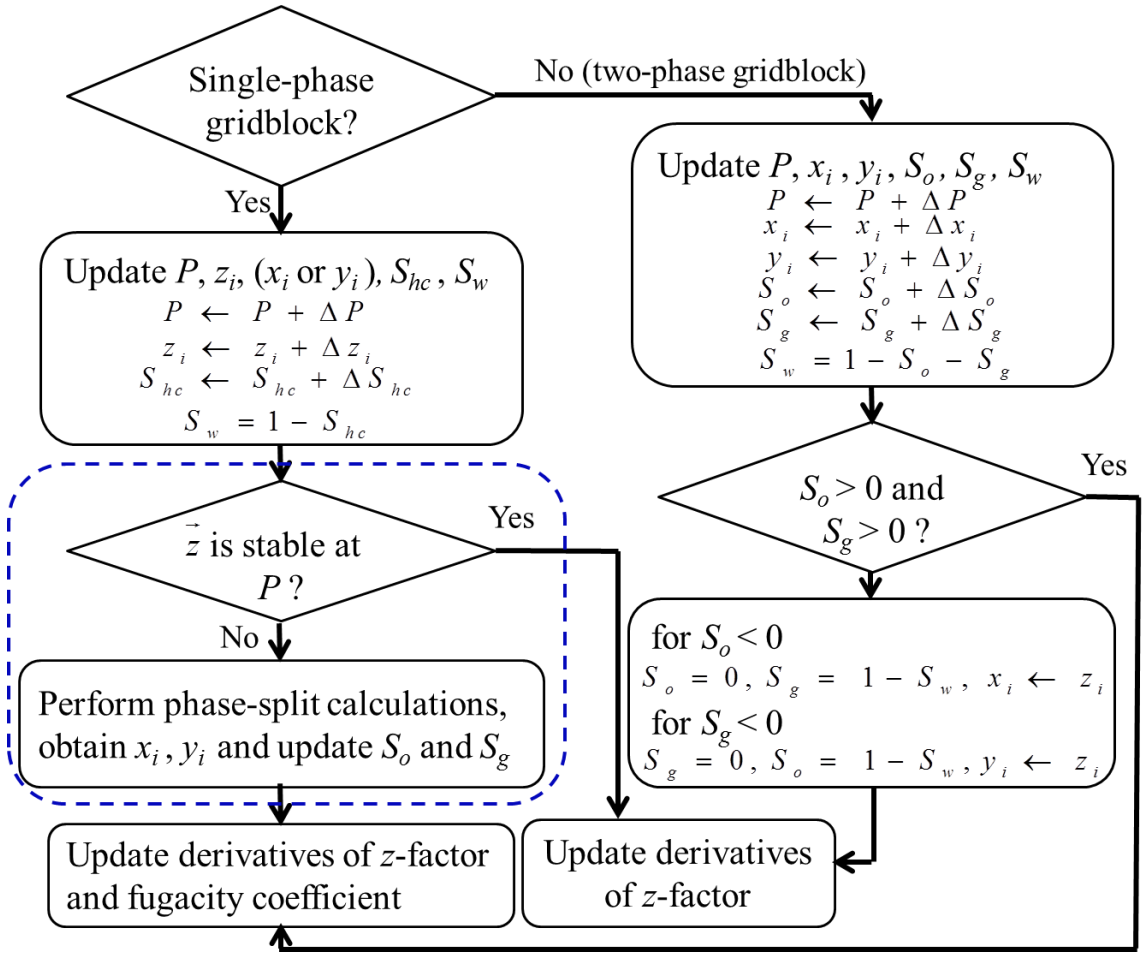

Figure 5-2: Variable update for single-phase and two-phase gridblocks after a Newton iteration.

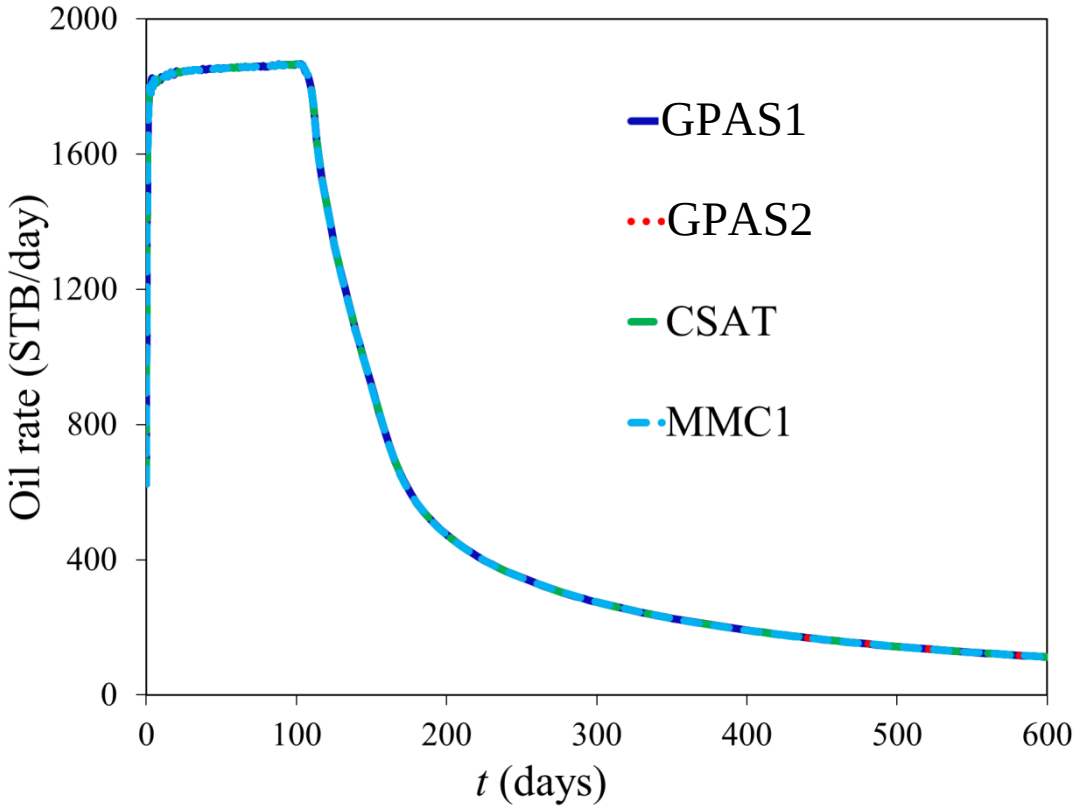

Figure 5-3: Comparison of oil production rate for simulations in Case 1.

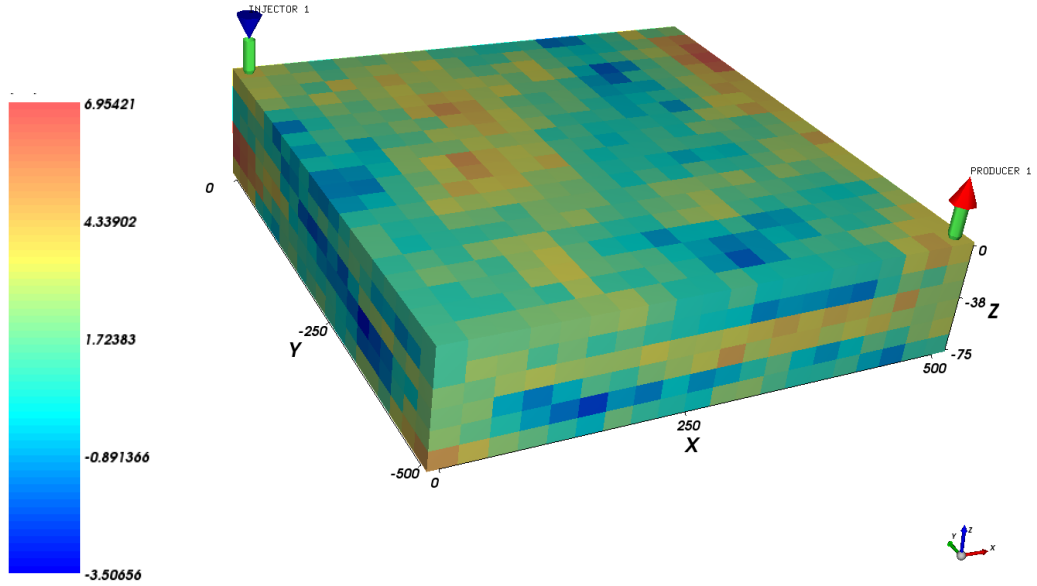

Figure 5-4: Map of *log*(*k*) for the simulations performed in Case 2.

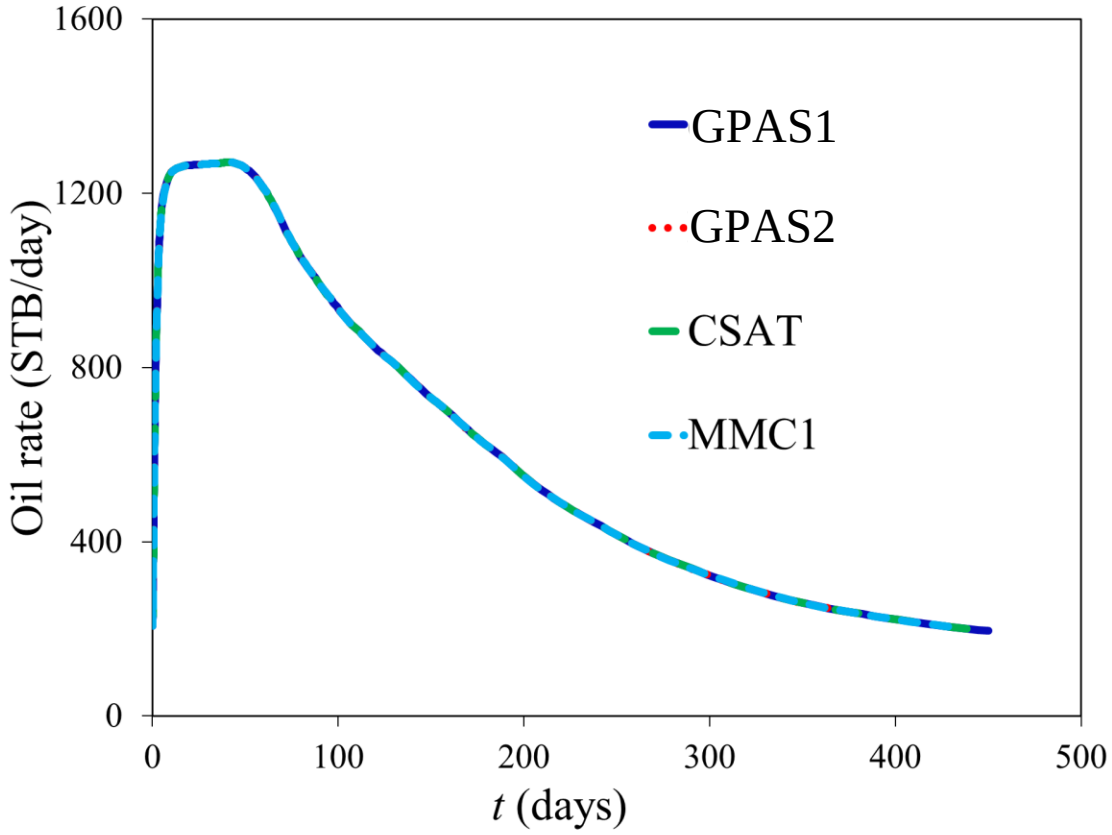

Figure 5-5: Comparison of oil production rates for simulations in Case 2.

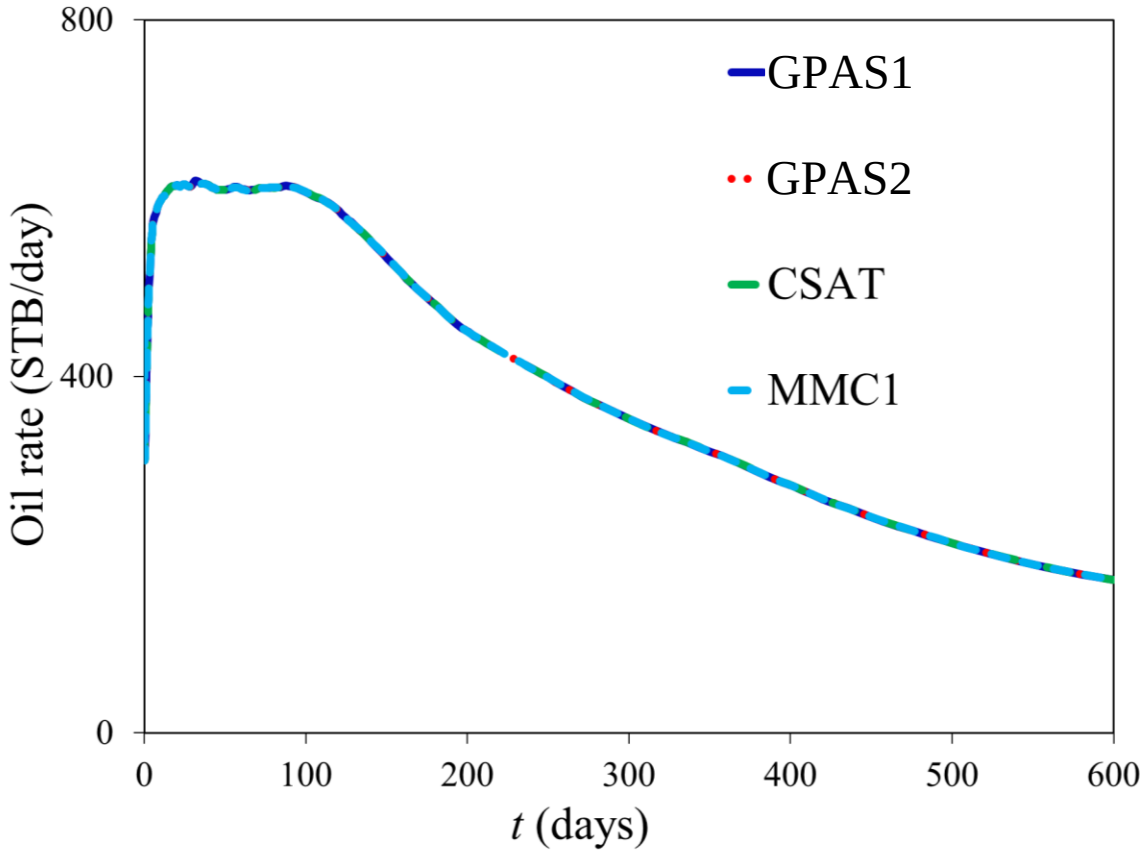

Figure 5-6: Comparison of oil production rates for simulations in Case 3.

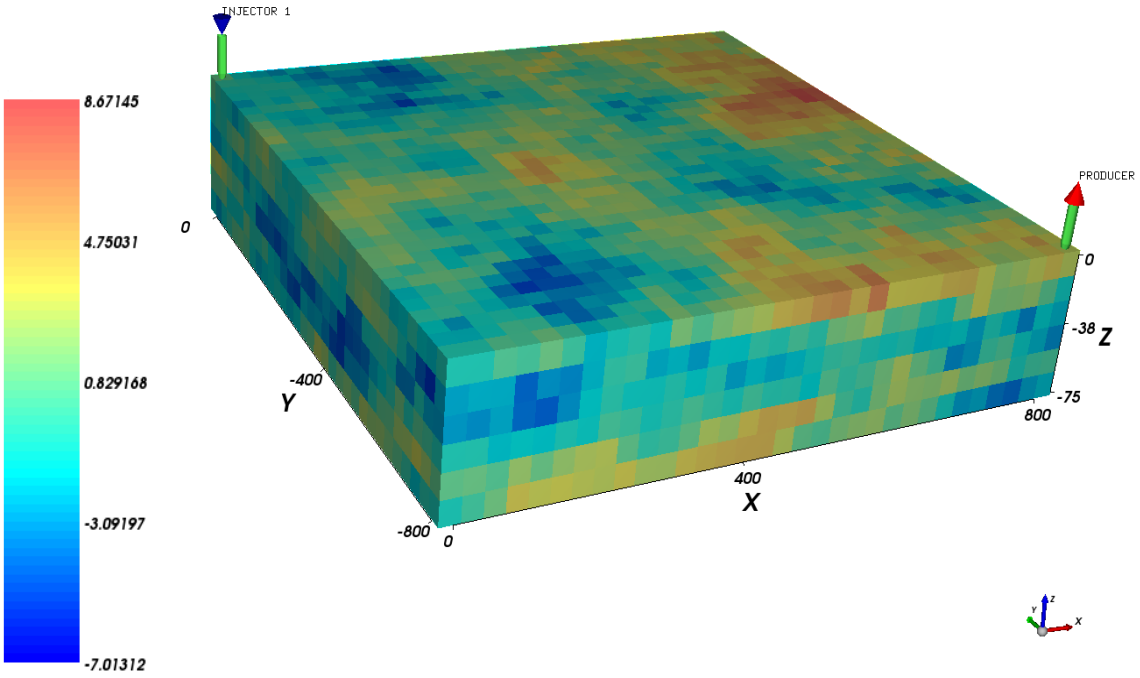

Figure 5-7: Map of *log*(*k*) for the simulations performed in Case 4.

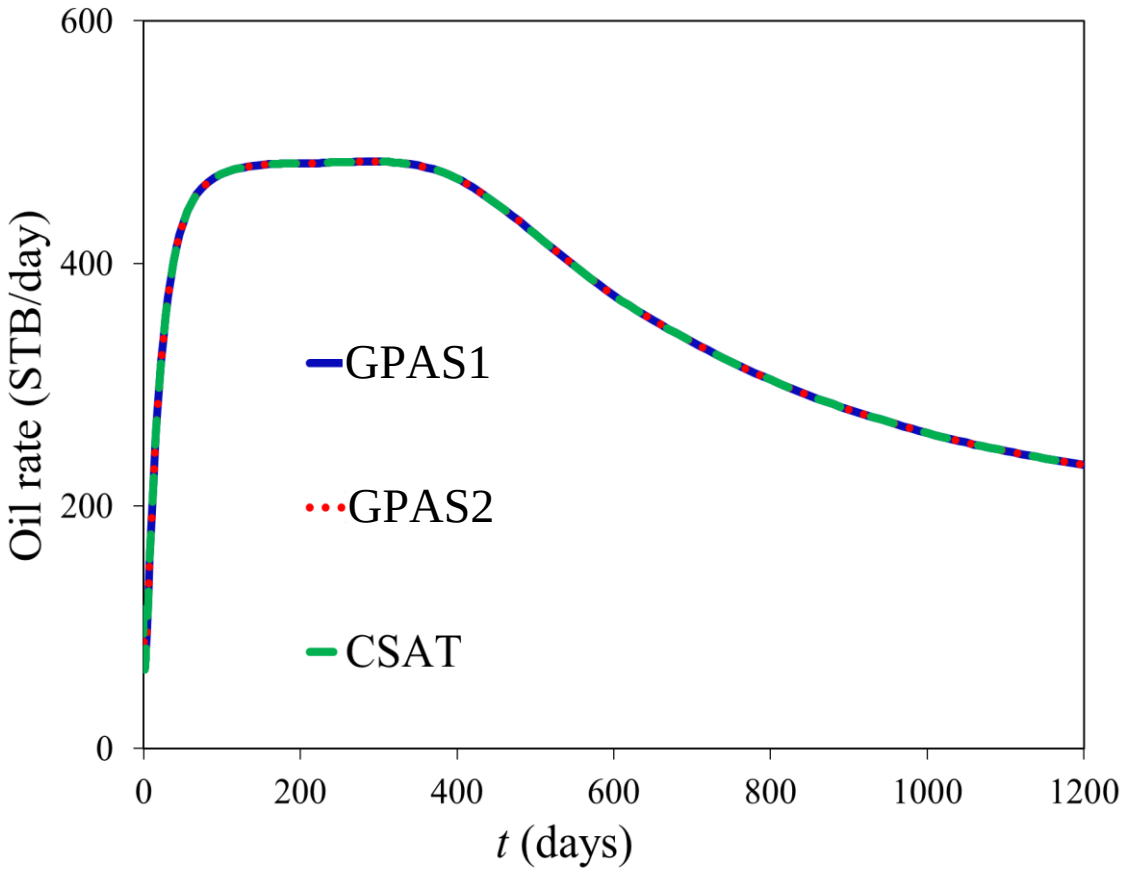

Figure 5-8: Comparison of oil production rates for simulations in Case 4.

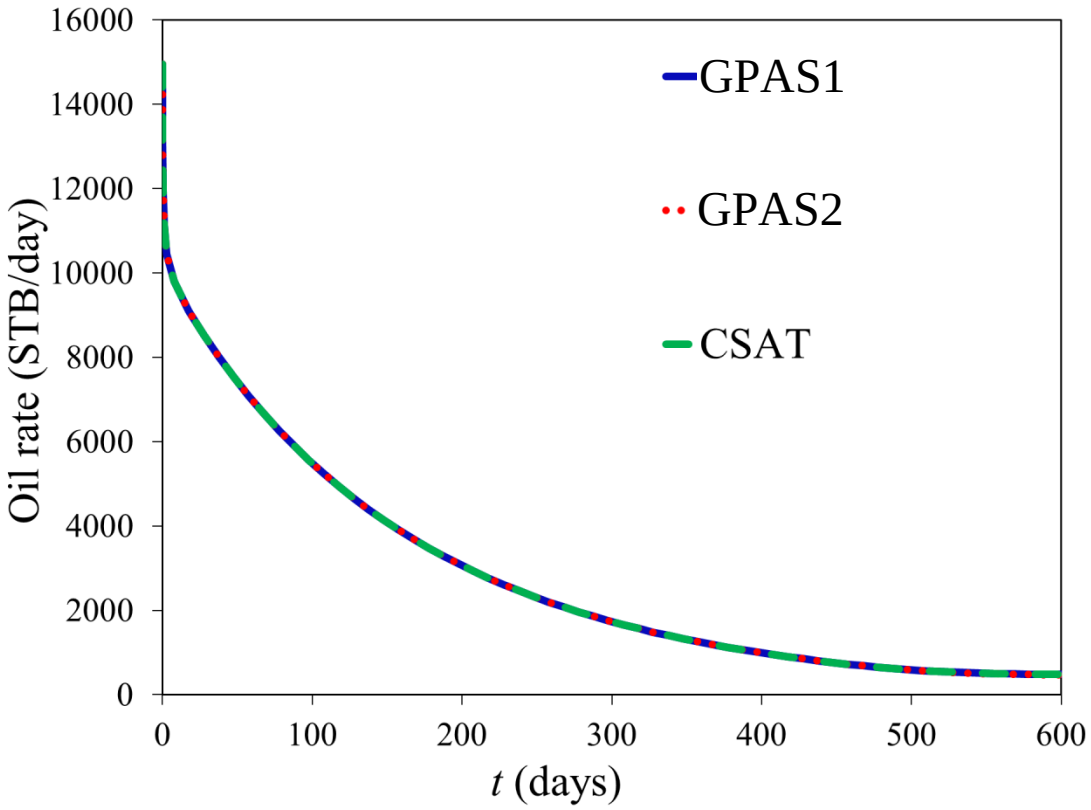

Figure 5-9: Comparison of oil production rates for simulations in Case 5.

Chapter 6: Implementation of the Effect of Capillary Pressure on Phase Behavior in UTCOMP

The goal of this chapter is to investigate the effect of capillary pressure on phase behavior in compositional reservoir simulation. We first present a theoretical study of the capillary equilibrium problem using Gibbs free energy (GFE) and demonstrate that there is a maximum capillary pressure (P_{cmax}) where gas/oil capillary equilibrium is possible. Next, we derive the necessary equations to obtain this maximum capillary pressure. Furthermore, we discuss the phase stability concept as related to the capillary equilibrium problem and suggest several heuristic methods, which can be used to improve the computational speed in the compositional simulators that account for the effect of capillary pressure on phase behavior. Next, we describe our implementation of the effect of capillary pressure on phase behavior in the UTCOMP simulator and demonstrate the capillary condensation problem using simple compositional simulations for a binary fluid. We then perform three simulation case studies to investigate how and to what extent capillary pressure influences the production behavior in actual tight oil and shale gas reservoirs.

6.1 Equilibrium Criteria and Stability Concepts in Presence of Curved Interfaces

In this section we briefly review the equilibrium criteria in the presence of curved interfaces and discuss the geometrical interpretation of capillary equilibrium. We also discuss the stability concept for the capillary equilibrium problem.

The equilibrium criteria for two phases with a curved interface were derived in Chapter 2 using an approach similar to that of Tester and Modell (1997) and Firoozabadi

(1999). The phase equilibrium criteria for an isothermal system when a curved interface separates the two phases α and β are given in Eqs. (6.1) and (6.2),

$$\mu_i^{\alpha}(P^{\alpha},\vec{x}^{\alpha}) = \mu_i^{\beta}(P^{\beta},\vec{x}^{\beta}), \qquad i = 1,2,...,n_c, \tag{6.1}$$

$$P^{\beta} - P^{\alpha} = \sigma \frac{da}{dV^{\beta}}, \tag{6.2}$$

where μ_i is the chemical potential of component i and is evaluated at the corresponding phase's pressure (P) and composition ($\vec{x}$), and the superscripts α and β denote the phase's identity. The area of the interface is denoted by a, V^{β} is volume of phase β, σ is interfacial tension (IFT), and n_c is the number of components. For the general case where the phases α and β are separated by a curved interface with curvature radii of r_1 and r_2, Eq. (6.2) simplifies to the Laplace equation given by

$$P^{\beta} - P^{\alpha} = \sigma\left(\frac{1}{r_1} + \frac{1}{r_2}\right). \tag{6.3}$$

Capillary pressure is usually expressed as a function of phase saturations in compositional simulation. The geometry of the pore space determines the dependency of capillary pressure on saturation. The Leverett *J*-function (Leverett, 1941) approach is often used to describe the saturation dependency of the capillary pressure curves. From Eq. (6.2), the pressure difference between the two equilibrium phases is related to the derivative of the interfacial area with respect to volume of one of the phases. Thus, for the general problem of capillary equilibrium in porous media, the capillary pressure model must consistently relate saturation of a reference phase to the curvature of the interface in the pore space.

6.1.1 Geometrical Interpretation of Capillary Equilibrium

The tangent hyperplane to the molar GFE ($\underline{G}$) hypersurface of a hypothetical single phase mixture at the constant temperature *T*, pressure *P* and at the overall composition $\vec{z}$ is given by (see Chapter 2 for the derivation)

$$T(\vec{x}) = \sum_{i=1}^{n_c} x_i \mu_i(T, P, \vec{z}), \tag{6.4}$$

where $T(\vec{x})$ denotes the tangent hyperplane and $\vec{x}$ is any composition vector. If Eqs. (6.1), which are necessary conditions for capillary equilibrium, are satisfied for the composition vector $\vec{x}^{\alpha}$ at P^{α} and the composition vector $\vec{x}^{\beta}$ at P^{β} then the tangent hyperplane at $\vec{x}^{\alpha}$ to the molar GFE hypersurface at P^{α} is identical with the tangent hyperplane at $\vec{x}^{\beta}$ to the molar GFE hypersurface at P^{β}. Thus, the equilibrium compositions of the two phases in capillary equilibrium correspond to a common tangent hyperplane to the molar GFE hypersurfaces at the corresponding phase's pressure. Furthermore, if a common tangent hyperplane to the molar GFE hypersurfaces at P^{α} and P^{β} exists, then Eqs. (6.1) are satisfied at the points of tangency. If $T^{\alpha}(\vec{x})$ and $T^{\beta}(\vec{x})$ denote the tangent hyperplanes to the molar GFE hypersurfaces at pressure values of P^{α} and P^{β} and composition vectors of $\vec{x}^{\alpha}$ and $\vec{x}^{\beta}$, respectively, then the common tangent hyperplane implies that

$$\begin{aligned} T^{\alpha}(\vec{x}) - T^{\beta}(\vec{x}) &= \sum_{i=1}^{n_c} x_i \mu_i^{\alpha}(T, P^{\alpha}, \vec{x}^{\alpha}) - \sum_{i=1}^{n_c} x_i \mu_i^{\beta}(T, P^{\beta}, \vec{x}^{\beta}) \\ &= \sum_{i=1}^{n_c} x_i [\mu_i^{\alpha}(T, P^{\alpha}, \vec{x}^{\alpha}) - \mu_i^{\beta}(T, P^{\beta}, \vec{x}^{\beta})] = 0. \end{aligned} \tag{6.5}$$

Only n_c - 1 of the phase's mole fractions are independent variables, thus by use of x_1, x_2,…, $x_{nc\text{-}1}$ as the independent variables the last equality of Eq. (6.5) can be simplified to

$$\mu_{n_c}^{\alpha}(T,P^{\alpha},\vec{x}^{\alpha})-\mu_{n_c}^{\beta}(T,P^{\beta},\vec{x}^{\beta})$$
$$+\sum_{i=1}^{n_c-1}x_i[\mu_i^{\alpha}(T,P^{\alpha},\vec{x}^{\alpha})-\mu_{n_c}^{\alpha}(T,P^{\alpha},\vec{x}^{\alpha})-\mu_i^{\beta}(T,P^{\beta},\vec{x}^{\beta})+\mu_{n_c}^{\beta}(T,P^{\beta},\vec{x}^{\beta})]=0. \quad (6.6)$$

In order for Eq. (6.6) to be satisfied for any arbitrary composition vector $\vec{x}$, the coefficients of the independent variables and the constant term must be zero, which results in the condition of chemical potential equality of each component in the phases α and β i.e. Eqs. (6.1). Thus, in the capillary equilibrium problem, Eqs. (6.1) are satisfied if and only if the tangent hyperplane to the molar GFE hypersurface at P^{α} and $\vec{x}^{\alpha}$ is identical with the tangent hyperplane to the molar GFE hypersurface at P^{β} and $\vec{x}^{\beta}$. The formulae for calculation of molar GFE of a mixture are given in Appendix B.

6.1.2 Stability Concept for Capillary Equilibrium

Michelsen (1982a) developed the phase stability concept and criteria in the absence of curved interfaces i.e. when pressure is uniform throughout the system. In the absence of a curved interface the phase stability problem is simpler and is stated as "is the overall composition vector $\vec{z}$ stable at pressure P and temperature T with respect to phase split?" Michelsen (1982a) showed that the necessary and sufficient condition for stability of mixture $\vec{z}$ at T and P is that the tangent plane distance (TPD) is non-negative throughout the composition space i.e. the tangent hyperplane to the molar GFE (or GFE) hypersurface at $\vec{z}$ does not lie above the molar GFE (or GFE) hypersurface at any point. Any composition vector $\vec{x}$ that violates the TPD criterion guarantees existence of a phase split of lower total molar GFE (or GFE) even though $\vec{x}$ is not necessarily related to any of the equilibrium compositions.

In the presence of a curved interface the stability concepts and criteria are not well-defined. There are several complexities. First, the phase stability concept depends on

the statement of the capillary equilibrium problem. Specifying the overall composition and pressure of one of the phases as the independent variables is a natural way of posing the capillary equilibrium problem. For most of the currently available reservoir simulators this choice of the independent variables is intuitive and also the only practical choice. We used the overall composition and pressure of one of the phases as the independent variables in the UTCOMP simulator. Thus, we restrict our approach to the phase stability problem to this set of independent variables.

The phase stability problem is tied to the identity of the phases and whether the phase under study is of larger or smaller pressure. In other words, the stability problem depends on whether the overall composition $\vec{z}$ belongs to the gas-like or liquid-like branch of the molar GFE hypersurface. We use a binary mixture of C_1-C_6 at 130°F to illustrate the problem. Figure 6-1 shows the molar GFE curve of the hypothetical single-phase mixture of C_1-C_6 at 130°F with respect to the overall mole fraction of C_1 denoted by x_1 at two pressure values of 174 psia and 493 psia. There are two possible equilibrium states where one of the equilibrium phases is at 174 psia and the other equilibrium phase is at 493 psia. These two equilibrium states are specified by the common tangent lines shown in Figure 6-1. The red tangent line corresponds to an equilibrium state where the gas phase is at the larger pressure (oil-wet medium) whereas the blue tangent line corresponds to the equilibrium state where the gas phase is at the smaller pressure (gas-wet medium). For any overall composition x_1, where $x_A < x_1 < y_A$ at 493 psia, a two-phase solution with a smaller molar GFE value exists where the gas phase is at the 493 psia and the liquid phase at 174 psia. However, the stability concept is of physical significance only for the gas-like compositions i.e. one can state that a gas-like overall composition $x_1 = y_A - \varepsilon$ (ε is a small positive number) at 493 psia is unstable with respect to appearance

of a liquid phase at the smaller pressure of 174 psia. Whereas, it is not physically meaningful to state that a liquid-like overall composition $x_1 = x_A + \varepsilon$ at 493 psia is unstable with respect to appearance of a gas phase at the same pressure and a different liquid phase of lower pressure (174 psia). Instead, one must discuss stability of the liquid-like overall composition with respect to appearance of a gas-like phase at a larger or smaller pressure depending on wettability. We note that the above-mentioned stability concept is not the best statement of the problem from a physical point of view even though it can be easily applied in compositional simulation. A more physically sound statement of the stability concept in presence of curved interfaces is "whether a given set of mole numbers at a given total volume will stay single-phase or split into two phases in presence of a curved interface?".

The second complexity in the stability concept for capillary equilibrium is the dependence of capillary pressure on phase saturations. The pressure of the second phase depends on the phase saturations, which are a function of the solution of the capillary equilibrium problem. Furthermore, the solution to the capillary equilibrium problem between two pressures may not in general satisfy a particular dependency of capillary pressure on saturation. That is why development of a practical and simple stability criterion similar to the TPD is not straightforward for the capillary equilibrium problem.

The third complexity results from the physical limits of capillary equilibrium (Shapiro and Stenby, 2001). Figure 6-2 shows the molar GFE curves of the hypothetical single-phase mixtures of C_1-C_6 at four different pressure values at 130°F versus x_1. The common tangent lines corresponding to the equilibrium states where the equilibrium liquid phase is at 174 psia and the equilibrium gas phase is at 493 psia and 1,052 psia are also plotted in Figure 6-2. The corresponding equilibrium compositions are given in

Table 6-1. In Figure 6-2, a common tangent line where the equilibrium liquid phase is at 174 psia and the equilibrium gas phase is at 2,000 psia is not possible. Figure 6-3 shows the chemical potentials of C_1 and C_6 in the hypothetical single-phase binary mixture at three different pressure values of 174 psia, 1,052 psia, and 2,000 psia. The green rectangle marks the equilibrium compositions and chemical potentials of an equilibrium state where the equilibrium liquid phase is at 174 psia and the equilibrium gas phase is at 1,052 psia. The upper and lower horizontal sides of the rectangle correspond to the values of chemical potential of C_1 and C_6 respectively at capillary equilibrium. The left and right vertical sides correspond to the mole fraction of C_1 in the equilibrium liquid and gas phases, respectively. Figure 6-3 shows that such a rectangle is not possible when the equilibrium liquid phase is at 174 psia and the equilibrium gas phase is at 2,000 psia. Thus, a solution to Eqs. (6.1) does not exist for a liquid phase at 174 psia and a gas phase at 2,000 psia. In fact, the pressure value of 1,097 psia is the maximum gas-phase pressure where capillary equilibrium is possible with an equilibrium liquid phase at 174 psia for this binary mixture.

Figure 6-4 shows the molar GFE of the hypothetical single-phase mixture of C_1-C_6 at 130°F at pressure values of 174, 2,000, 3,049, and 4,007 psia. Three possible tangent lines that violate the extended TPD criterion of Eq. (6.7) are also given in Figure 6-4 among infinitely many such possible tangent lines. The TPD criterion in Eq. (6.7) is an extension of the traditional TPD criterion to equilibrium in the presence of curved interfaces. According to this extended criterion, the TPD < 0 implies existence of a solution to the capillary equilibrium problem. It is obvious that the extended TPD criterion is not valid in the general form given in Eq. (6.7). However, it seems plausible to state that if the extended TPD for a given overall composition and particular base and

second phase pressure is always positive then a solution to the corresponding capillary equilibrium problem does not exist.

$$\mathrm{TPD} = \sum_{i=1}^{n_c} x_i \left(\mu_i(\vec{x}, P^{second\ phase}) - \mu_i(\vec{Z}, P^{base\ \mathrm{phase}}) \right). \tag{6.7}$$

6.2 FORMULATION OF THE CAPILLARY EQUILIBRIUM LIMITS

Shapiro and Stenby (2001) analyzed the capillary equilibrium problem in the space of intensive variables T, P, μ_1,……., μ_{nc}. These authors proved that 1) for any phase, capillary equilibrium is possible only between the true equilibrium point and the spinodal point. Therefore, the boundary for capillary equilibrium coincides with the spinodal boundary. 2) The phase of lower pressure is always a metastable phase and the phase of larger pressure is always a stable phase at their respective pressures.

The capillary equilibrium limit explains why we were not able to find a solution to the capillary equilibrium problem for the liquid phase pressure of 174 psia and gas phase pressure of 2,000 psia in Figure 6-2. We formulate the conclusions made by Shapiro and Stenby (2001) in compositional space for easier application in a compositional reservoir simulation context.

6.2.1 Formulation and Calculation of the Capillary Equilibrium Limit for Binary Mixtures

For a binary fluid the degree of freedom in presence of capillary equilibrium is three, thus one can specify the pressure of the two phases and temperature to determine the intensive properties at equilibrium. Alternatively, the spinodal condition can be used as an additional constraint in order to find the capillary equilibrium limit for a specified gas- (or oil-) phase pressure and temperature. For a binary fluid the notion of a capillary

equilibrium limit can be stated as "given pressure P^g, what is the maximum value of capillary pressure (P_{cmax}) for which equilibrium is possible for a gas phase at P^g with a liquid phase at $P^o = P^g - P_{cmax}$?" This statement of the problem corresponds to an oil-wet porous medium. Eqs. (6.8) and (6.9) can be solved to find the P_{cmax} , x_1^{sp}, and y_1,

$$\mu_i^g(y_1, P^g) = \mu_i^l(x_1, P^o), \qquad i = 1, 2, \tag{6.8}$$

$$\left(\frac{\partial \mu_1}{\partial x_1}\right)_{T,P^o} = 0, \tag{6.9}$$

where the value of x_1 obtained from solving Eqs. (6.8) and (6.9) (denoted by x_1^{sp}) is the spinodal composition of the liquid phase at the minimum P^o where capillary equilibrium is possible, and y_1 is the mole fraction of component 1 in the gas phase at P^g that is in equilibrium with the liquid phase of composition x_1^{sp}.

It is important to specify whether P^o is larger or smaller than P^g i.e. whether the rock is oil wet or gas wet. For a gas-wet rock, the equilibrium gas phase is in metastable state and the sought variables become the limiting oil pressure P^o, the spinodal composition of the gas phase y_1^{sp}, and the corresponding equilibrium composition of the liquid phase x_1. In this case, the spinodal condition of the gas phase given in Eq. (6.10) must be used instead of Eq. (6.9).

$$\left(\frac{\partial \mu_1}{\partial y_1}\right)_{T,P^g} = 0. \tag{6.10}$$

The P_{cmax} problem for a given oil-phase pressure P^o for an oil-wet rock can be posed as "given the oil-phase pressure P^o, what is the maximum value of capillary pressure (P_{cmax}) for which capillary equilibrium is possible for an oil phase at P^o with a gas phase at $P^g = P^o + P_{cmax}$?" This problem can be solved in a similar manner based on

the principle that the limit of capillary equilibrium coincides with the spinodal boundary of the phase at lower pressure.

We performed the P_{cmax} calculations for a binary mixture of C_1-C_6 at 300°F for a given P^g. Figure 6-5 shows P_{cmax} i.e. the maximum possible pressure difference between the oil and gas phases where capillary equilibrium is possible versus P^g for an oil-wet and a gas-wet medium. Figure 6-6 shows the corresponding equilibrium and spinodal compositions for the same binary mixture versus the pressure in the gas phase. The solid lines are the true equilibrium lines and are calculated at equal liquid and gas phase pressure. The dashed red line is the actual gas phase's spinodal boundary at P^g which is in capillary equilibrium with the stable liquid represented by the dotted blue line. The entire possible gas-phase equilibrium compositions where the gas phase is metastable are in the region marked with "metastable gas". The dashed blue line represents the composition of the spinodal liquid at P^o ($P^o=P^g-P_c$) which is in capillary equilibrium with the stable gas phase at P^g, represented by the dotted red line. The liquid-phase compositions in the "metastable liquid" region are in equilibrium with the gas-phase compositions in the "stable gas" region at P^g. We reiterate that the dotted and dashed blue lines in Figure 6-6 were calculated at P^o in equilibrium with P^g.

The practical significance of Figure 6-5 and Figure 6-6 is that if capillary equilibrium is applied in a compositional reservoir simulator there will be a theoretical limit on the gas/oil capillary pressure values that can occur during the simulation. For instance, in the compositional simulation of a depletion process with a binary mixture of C_1-C_6 as the initial reservoir fluid at 300°F, if the pressure everywhere in the reservoir is greater than 1,500 psia throughout the simulation, then the maximum possible capillary pressure value between the oil and gas phases is approximately 70 psia. Thus, the

simulator will not be able to find a two-phase solution for larger capillary pressure values and forces the corresponding overall compositions to be single phase. This is a true physical limit assuming applicability of bulk-phase thermodynamics that further emphasizes the importance of using a consistent capillary pressure model in the compositional simulator.

In order to study saturation of the phases in capillary equilibrium, we performed capillary equilibrium calculations at P^g values of 1,500, 1,600, and 1,900 psia for several overall compositions (z_1) for the binary mixture of C_1-C_6 at 300°F. For each value of P^g and z_1, the entire range of oil-phase pressures which resulted in capillary equilibrium with physical values of oil and gas saturations was calculated. Figure 6-7 shows the pressure difference at capillary equilibrium versus the oil saturation (S_o) for the entire range of physical saturations at several P^g and z_1 values. Figure 6-7 shows that for a given P^g and z_1, not only is there a limit on the capillary pressure value where capillary equilibrium is possible but also the entire capillary equilibrium window corresponds to a limited range of physical oil saturation values. If the saturation-dependent capillary pressure model in the compositional simulator does not intersect the curve corresponding to a particular P^g and z_1 in Figure 6-7, then a two-phase solution to the capillary equilibrium problem cannot be found and z_1 is assumed single-phase at P^g.

6.2.2 Formulation of the Capillary Equilibrium Limit for Multicomponent Mixtures

As mentioned in Chapter 2, when one approaches the spinodal boundary from the stable region the spinodal condition is given only by Eq. (6.11). For a general n_c-component system on the stable branch of the phase surface corresponding to a single phase, n_c+1 intensive variables can be specified independently. Thus, for an n_c-

component system at a given pressure and temperature there are n_c-2 degrees of freedom for specifying a unique spinodal point and the composition of the spinodal boundary is given by $x_{nc\text{-}1} = f(x_1, \ldots, x_{nc\text{-}2})$. In general the spinodal boundary is an n_c-2 hypersurface on each stable branch of the phase surface at a given temperature and pressure.

In a general n_c-component system, for a given gas-phase pressure P^g and temperature T, finding the maximum capillary pressure where capillary equilibrium is possible (P_{cmax}) requires determining the $2n_c$ -1 unknowns of equilibrium oil composition $\vec{x} = (x_1, x_2, \ldots, x_{nc\text{-}1})$, equilibrium gas composition $\vec{y} = (y_1, y_2, \ldots, y_{nc\text{-}1})$ and the corresponding oil-phase pressure, P^o. The available equations are Eqs. (6.1) (n_c equations) and the spinodal condition of the oil phase at P^o. Thus, n_c-2 of the above variables must be specified in order to obtain a determinate system of equations. However, this statement of the P_{cmax} problem is not directly applicable to the compositional simulation in practice.

For a given overall composition vector $\vec{z} = (z_1, z_2, \ldots, z_{nc\text{-}1})$ and P^g where $P^o < P^g$, P_{cmax} can be obtained by solving the following set of equations,

$$\begin{vmatrix} \left(\frac{\partial^2 \underline{G}}{\partial x_1^2}\right)_{T,P^o,x_2,\ldots x_{n_c-1}} & \left(\frac{\partial^2 \underline{G}}{\partial x_1 \partial x_2}\right)_{T,P^o,x_3,\ldots x_{n_c-1}} & \ldots\ldots & \left(\frac{\partial^2 \underline{G}}{\partial x_1 \partial x_{n_c-1}}\right)_{T,P^o,x_2,\ldots x_{n_c-2}} \\ \left(\frac{\partial^2 \underline{G}}{\partial x_1 \partial x_2}\right)_{T,P^o,x_3,\ldots x_{n_c-1}} & \left(\frac{\partial^2 \underline{G}}{\partial x_2^2}\right)_{T,P^o,x_1,\ldots x_{n_c-1}} & \ldots\ldots & \left(\frac{\partial^2 \underline{G}}{\partial x_2 \partial x_{n_c-1}}\right)_{T,P^o,x_1,\ldots x_{n_c-2}} \\ \vdots & \vdots & \vdots & \vdots \\ \left(\frac{\partial^2 \underline{G}}{\partial x_1 \partial x_{n_c-1}}\right)_{T,P^o,x_2,\ldots x_{n_c-2}} & \left(\frac{\partial^2 \underline{G}}{\partial x_2 \partial x_{n_c-1}}\right)_{T,P^o,x_1,\ldots x_{n_c-2}} & \ldots\ldots & \left(\frac{\partial^2 \underline{G}}{\partial x_{n_c-1}^2}\right)_{T,P^o,x_2,\ldots x_{n_c-2}} \end{vmatrix} = 0 \ , \quad (6.11)$$

$$\mu_i^g(\vec{y}, P^g) = \mu_i^l(\vec{x}, P^o), \qquad i = 1, 2, \ldots, n_c, \quad (6.12)$$

$$z_i = x_i l + y_i (1 - l), \qquad i = 1, 2, \ldots, n_c - 1, \quad (6.13)$$

where $\underline{G}$ is the molar GFE and the unknown variables are equilibrium oil-phase composition $\vec{x} = (x_1, x_2, \ldots, x_{nc-1})$, equilibrium gas-phase composition $\vec{y} = (y_1, y_2, \ldots, y_{nc-1})$, the limiting oil-phase pressure P^o, and the oil-phase molar fraction (l). A similar set of equations may be written for the case where P^o is larger than the P^g. Analogous equations apply when the P^o is specified and the limiting capillary pressure value for a gas phase of larger or smaller pressure in equilibrium with the liquid phase is required. We use Eqs. (6.11) through (6.13) to find the P_{cmax} for the multicomponent mixtures that we study in the simulation case studies.

One can use Eqs. (6.11) through (6.13) and develop a parameterization framework that tabulates the tie lines for the entire range of capillary equilibrium. For a given overall composition, one can calculate the capillary equilibrium tie lines for several discrete values of gas-phase pressure and for the entire range of capillary pressure where capillary equilibrium is possible (for a particular wetting state of the medium). A set of two-

dimensional tables can be computed and a search algorithm can be developed where a matching tie line can be found for a given overall composition and gas phase pressure.

6.2.3 Heuristic Techniques for Capillary Equilibrium Calculations in Compositional Simulation

Even though development of a simple and practical stability analysis method for the capillary equilibrium problem seems unlikely, it is possible to use some heuristic methods that result from the theory of capillary equilibrium to improve the computational performance of the capillary equilibrium calculations. For instance in Figure 6-6, for pressure values greater than the critical pressure of 2,112 psia at temperature of 300°F (P > 2112 psia) equilibrium is impossible and thus capillary equilibrium is also impossible. In other words, for the binary mixture of C_1-C_6 for a given overall composition and gas-phase or liquid-phase pressure, capillary equilibrium is impossible if there is no tie line through the overall composition at zero capillary pressure. It seems reasonable to extend this observation to a general n_c-components mixture. Thus, it appears that "a necessary condition for capillary equilibrium for a given overall composition $\vec{z}$ and gas-phase pressure P^g is that a tie line through $\vec{z}$ exists at zero capillary pressure." Consequently, a supercritical overall composition cannot be in capillary equilibrium if the phase behavior can be described only by the bulk-phase thermodynamics. Thus, one can parameterize the critical tie-line surface using the supercritical state criterion (SSC) and rule out a significant portion of the compositional space from capillary equilibrium calculations. We have not observed any example that violates this heuristic method in the capillary equilibrium calculations that we have performed.

Another heuristic technique is possible for the capillary equilibrium problem where a liquid-like overall composition $\vec{z}$ and the liquid phase pressure P^o are given for a

liquid-wet rock. If it is known that $\vec{z}$ is close to the liquid branch of the phase surface, then in order for capillary equilibrium to be possible, $\vec{z}$ must be (globally) unstable at P^o at zero capillary pressure. If the given liquid-like $\vec{z}$ is stable at P^o then the tangent hyperplane to the molar GFE hypersurface at $\vec{z}$ and P^o lies below the entire GFE hypersurface at any pressure equal to or larger than P^o; thus, capillary equilibrium will be impossible.

6.3 Alternative Formulation of the Capillary Equilibrium Problem

Thus far we have discussed the capillary equilibrium problem where the overall composition $\vec{z}$ and the gas-phase or liquid-phase pressure (P^g or P^o) are given. This statement of the capillary equilibrium problem is similar to what we encounter in the UTCOMP simulator where pressure of one of the phases and $\vec{z}$ is given in a gridblock. Shapiro and Stenby (2001) also discuss a second type of capillary equilibrium problem where the gas-phase's pressure and composition are given and the liquid phase's pressure and composition are the unknowns.

Another type of the capillary equilibrium calculations that (to the best of our knowledge) has not been discussed in the literature is solving the capillary equilibrium problem for a given temperature T, total volume V^t, and total number of moles of each component $\vec{n}$. This statement of the capillary equilibrium problem, hereafter called *VT* capillary equilibrium, is more amenable to experimental study especially for the cases where the desired overall composition $\vec{z}$ in the pressure range of interest is locally unstable. Here, the pressure of both of the equilibrium phases can change depending on geometry of the pore space as the mole numbers of one or more components vary at constant total volume. The capillary equilibrium calculations in this case are very similar to the *VT* flash problem (Mikyška and Firoozabadi, 2011 and 2012) and require minimum

alteration of the traditional *VT* flash algorithm at zero capillary pressure. This is because in the *VT* flash calculations the pressure of a phase is a dependent variable and the value of pressure difference of the equilibrium phases is one of the constraint equations. Eqs. (6.14) to (6.17) must be solved for the *VT* capillary equilibrium problem

$$\mu_i^g(V^g, T, \vec{n}^g) = \mu_i^l(V^l, T, \vec{n}^l), \qquad i = 1, 2, ..., n_c, \tag{6.14}$$

$$P^g(V^g, T, \vec{n}^g) - P^l(V^l, T, \vec{n}^l) = P_c, \tag{6.15}$$

$$V^g + V^l = V^t, \tag{6.16}$$

$$n_i^o + n_i^g = n_i^t, \qquad i = 1, 2, ..., n_c, \tag{6.17}$$

where V denotes volume, n denotes mole number, the superscripts g, l, and t refer to gas phase, liquid phase, and the total system, respectively, and subscript i is the component index.

Eqs. (6.14) through (6.17) are similar to those used in the traditional *VT* flash calculations (Mikyška and Firoozabadi, 2011) except for introduction of the capillary pressure in Eq. (6.15). Mikyška and Firoozabadi (2011) presented a new volume function and solution method that can be applied to the capillary equilibrium problem with few modifications.

We implemented the *VT* capillary equilibrium calculations and performed several P_{cmax} calculations for a real gas condensate fluid (Figure 6-19). As expected, the *VT* capillary equilibrium calculations are also bounded by the same P_{cmax} values as the capillary equilibrium calculations where pressure of one of the equilibrium phases and the overall composition are specified.

The P_{cmax} concept implies a discontinuity in the transition from two-phase to single-phase states in the capillary equilibrium calculations. A possible explanation for

this discontinuity is that the P_{cmax} values in our calculations correspond to extremely small pore sizes where bulk-phase thermodynamics and equation-of-state (EOS) description of the fluid is not valid anymore.

6.4 IMPLEMENTATION OF THE EFFECT OF CAPILLARY PRESSURE ON PHASE BEHAVIOR IN THE UTCOMP SIMULATOR

This section describes our implementation of the effect of capillary pressure on phase behavior in the UTCOMP simulator. The overall computational procedure in the UTCOMP simulator is given in Chang (1990). The original UTCOMP considers the effect of capillary pressure on fluid transport through an explicitly-treated contribution to flow potential of each phase; however, only a single overall pressure value is used for the phase equilibrium calculations and phase property calculations. In two-hydrocarbon-phase gridblocks the reference pressure is the pressure of the oil phase (P_2), while the pressures of the other phases are expressed as $P_j = P_2 + P_{c2j}$, where P_{c2j} is capillary pressure between the second phase and phase j. In the single hydrocarbon-phase gridblocks the reference pressure is the pressure of the single hydrocarbon phase. Under such assumptions of independency of phase behavior and capillary pressure and using a single reference pressure in each gridblock the derivation of the pressure equation is straightforward as given in Chang (1990).

The derivation of the pressure equation when the effect of capillary pressure on phase behavior is accounted for is similar to the original derivation with no capillary pressure. However, several terms of the pressure equation require special attention in this case. In our implementation the independent variables in each gridblock are the total component mole numbers N_w, N_1, …., N_{nc} (N_w is the total number of moles of water, the number subscripts represent the hydrocarbon components, and n_c is the number of

hydrocarbon components) and the oil-phase pressure (P^o) or the gas-phase pressure (P^g) in the two-phase gridblocks. The user must specify which phase pressure is the reference pressure in the two-phase gridblocks before the start of the simulation. The derivatives of the total fluid volume with respect to the pressure in the reference phase and the component mole numbers are different from the case without capillary pressure effects on phase behavior. The fluid volume derivatives are much more complicated when the capillary pressure effects on phase behavior are included because the derivatives of the capillary pressure also enter the calculations.

The pore volume is considered a function of the pressure of the reference phase in our implementation of the capillary pressure effect on phase behavior. For simulation of tight oil and shale gas reservoirs the reference phases are the oil and gas phases, respectively.

For each timestep in UTCOMP the pressure equation is first solved to obtain the pressure of the reference phase in each gridblock in the next timestep. If a gridblock has two hydrocarbon phases in the previous timestep the solution of the pressure equation in that gridblock is the pressure of the reference phase in the next timestep. If the gridblock has only a single hydrocarbon phase the solution of the pressure equation for that gridblock is the pressure of the phase that existed in the previous timestep. After solving the pressure equation the components' mass conservation equations are used to explicitly calculate the overall mole fraction of each component in each gridblock. The phase equilibrium calculations are then performed with the known overall composition and pressure of the reference phase. In the original UTCOMP formulation, phase tracking, saturation calculations, and capillary pressure calculations are performed in separate subroutines after performing the phase equilibrium calculations. However, in our

implementation all of these calculations must be performed simultaneously because the phase equilibrium depends on capillary pressure, which in turn depends on identity and saturation of the phases. The phase properties such as viscosity and molar density are calculated at the corresponding phase's pressure. Figure 6-8 shows the overall computational procedure in the UTCOMP simulator after implementation of the capillary pressure effect on phase behavior. The entire blocks in Figure 6-8 must be consistent in terms of using a particular pressure for a phase.

In the subsections that follow we discuss several implementation details and numerical challenges related to our implementation of the capillary pressure effect on phase behavior in the UTCOMP simulator.

6.4.1 Fluid Volume Derivatives

Calculation of the fluid volume derivatives is the most complicated part of the original UTCOMP formulation. These derivatives become even more complicated when the dependency of phase equilibrium on capillary pressure is included in the simulator. We use a numerical derivative scheme for calculation of total fluid volume derivatives in two-hydrocarbon-phase gridblocks. Analytical derivatives are used for single-hydrocarbon-phase gridblocks. The computation of the numerical derivatives is very fast because the unperturbed solution to the capillary equilibrium problem in each gridblock is available from the phase equilibrium calculations subroutine and the perturbed solutions can be found in very few successive substitution (SS) or Newton iterations using the unperturbed solution's results as the initial guess.

6.4.2 Calculation of Water Saturation

The saturation of each phase in each gridblock must be calculated from

$$S_j = \frac{\frac{n_j}{\xi_j}}{\sum_{k=1}^{n_p} \frac{n_k}{\xi_k}}, \qquad j = 1 \text{ (water)},\ 2 \text{ (oil)},\ 3 \text{ (gas)}, \tag{6.18}$$

where ξ is molar density, n is number of moles, the subscript j denotes phase j, and n_p is the number of phases. In general, the molar density of water is a function of the water phase pressure. Water phase pressure depends on oil/water capillary pressure (P_{cwo}) which is in general a function of one hydrocarbon phase saturation in addition to water saturation. This will substantially add to the computational intensity of the phase equilibrium calculations in the presence of water. Thus, in our implementation we neglect the effect of water/hydrocarbon capillary pressure on molar density of the water phase and calculate the saturation of the water phase by

$$S_w = \frac{n_w}{V_p \xi_w}, \tag{6.19}$$

where V_p is the pore volume, and ξ_w and n_w are the molar density and number of moles of water, respectively. The water saturation value is then used in the calculation of gas/oil capillary pressure in the phase equilibrium calculations. In any iteration of the phase equilibrium calculations, the saturations of the hydrocarbon phases are calculated from

$$S_j = (1 - S_w) \frac{\frac{l_j}{\xi_j}}{\frac{l_2}{\xi_2} + \frac{l_3}{\xi_3}}, \qquad j = 2 \text{ (oil)}, 3 \text{ (gas)}, \tag{6.20}$$

where l_j and ξ_j are molar fraction and molar density of hydrocarbon phase j, respectively.

6.4.3 Phase Equilibrium Calculations

A rigorous stability analysis method does not exist when the effect of capillary pressure on the phase behavior is included in the compositional model. Therefore, we directly perform the flash calculations using the initial estimate from the previous timestep. If a solution to the capillary equilibrium problem is not found, the mixture is assumed single phase. A phase tracking algorithm is used to determine the identity of the hydrocarbon phase in single-hydrocarbon-phase gridblocks. Because the reference phase may change during the simulation and from one simulation problem to the next, the phase equilibrium calculations must be able to perform the capillary equilibrium calculations for any specified reference phase pressure and overall composition.

For a given overall composition $\vec{z}$ and reference phase pressure, the $2n_c + 2$ system of equations given in Eqs. (6.21) through (6.24) can be solved for the $2n_c + 2$ unknowns of P^g (or P^o), oil and gas phase compositions ($\vec{x}$ and $\vec{y}$) and the molar fraction of the oil phase (l),

$$f_i^o(\vec{x}, P^o) = f_i^g(\vec{y}, P^g), \qquad i = 1, 2, ..., n_c, \tag{6.21}$$

$$P^g - P^o = P_c(S_o, S_g, \vec{x}, \vec{y}), \tag{6.22}$$

$$z_i = x_i l + y_i(1-l), \qquad i = 1, 2, ..., n_c - 1, \tag{6.23}$$

$$\sum_{i=1}^{n_c} x_i = \sum_{i=1}^{n_c} y_i = 1, \tag{6.24}$$

where f is fugacity, z denotes overall composition, x and y denote composition of the oil and gas phases, S is saturation, the subscripts/superscripts o and g denote respectively the oil and gas phases, and the subscript i is the component index. We use SS method followed by Newton iterations to solve this system of equations. The Li and Johns' constant-K flash was used to solve the Rachford-Rice (RR) equation (Rachford and Rice,

1952). Either the gas phase or oil phase pressures can be used as the base phase pressure in the above system of equations. The functional dependency of the capillary pressure function in Eq. (6.22) is the most general form possible.

6.4.4 Treatment of Phase Appearance and Disappearance

The natural choice of the reference phase pressure for compositional simulation of shale gas and tight oil reservoirs are gas-phase pressure and oil-phase pressure, respectively. With this choice of the reference phases, it is unlikely that the reference phase disappears in a gridblock for compositional simulation of a depletion process in shale gas and tight oil reservoirs. Furthermore, the reference phase will be the phase that exists in single-hydrocarbon-phase gridblocks. Thus, no special treatment is required when a second phase appears. On the other hand, it is possible to have the reference phase (the oil phase) disappear in compositional simulation of gas injection in tight oil reservoirs. In this case one can use the oil phase as the reference phase with a minor special treatment for the timesteps where the reference phase disappears in a gridblock.

We exemplify the special treatments required for compositional simulation with the effects of capillary pressure on phase behavior in UTCOMP by modeling the depletion process of an initially single-phase gas condensate reservoir using the oil pressure as the reference pressure in the two-phase gridblocks. In this case, when the second hydrocarbon phase (oil or condensate) appears in a single-phase (gas) gridblock, the oil-phase pressure will be used as the reference phase pressure in calculation of volume derivatives for the pressure matrix of the next timestep. Therefore, the entire reference-pressure dependent terms required for setting up the pressure matrix of the next timestep including the pore volume and its derivative must be adjusted for the oil-phase pressure.

Furthermore, in the same example, when a hydrocarbon phase disappears in a previously two-hydrocarbon-phase gridblock the treatment depends on identity of the remaining single phase. In this case, the failed capillary equilibrium calculations were performed for the gridblock's overall composition at the oil-phase pressure that resulted from solving the pressure matrix on the premise that an oil phase exists in the next timestep. If the phase tracking algorithm identifies the remaining single phase i.e. the overall composition as the oil phase (the assumed reference phase in two-hydrocarbon-phase gridblocks) then no special treatment is required (the pressure will be temporally continuous in transition from two-phase to single-phase). However, if the stable overall composition is identified as the gas phase then using the oil-phase (reference-phase) pressure for the remaining gas phase results in a temporal discontinuity in pressure and physical properties. Thus, in order to ensure continuity of the remaining gas-phase's pressure and physical properties, we use the gridblock's oil-phase pressure plus the gas/oil capillary pressure of the previous timestep as the gas-phase pressure of the current timestep.

In order to test the above mentioned treatment of phase appearance and disappearance we compared the simulation results of a gas condensate reservoir using the oil-phase pressure as the reference pressure with simulation results of the same reservoir using the gas-phase pressure as the reference pressure. The results of the two simulations were identical.

6.4.5 The Well Calculations

If the flowing bottomhole pressure is specified as the well condition then the corresponding molar flow rate is treated implicitly in the pressure matrix in UTCOMP. It is possible that the pressure of one of the phases, e.g. an immobile oil-phase's pressure,

become smaller than the specified flowing bottomhole pressure during the simulation. This situation acts as influx of fluid into the well gridblock and results in larger pressure values in the well gridblock for the solution of the pressure matrix. However, UTCOMP does not allow a producing well to introduce fluid into the gridblock in the case of a negative drawdown. This leads to a volume error in the well gridblock if left untreated. Thus, we include the contribution of a particular phase to molar flow rate of fluid components in the producer only if the phase's pressure in the well gridblock in the previous timestep is larger than the specified flowing bottomhole pressure.

6.4.6 The Capillary Pressure Model

We used the original gas/oil capillary pressure model in the UTCOMP simulator, given in Eq. (6.25), for the simulations of binary fluids in the next section,

$$P_{cgo} = -C_{pc}\sigma\sqrt{\frac{\phi}{k}}\left(\frac{\bar{S}_g}{\bar{S}_g + \bar{S}_o}\right)^{E_{pc}}, \tag{6.25}$$

where $\bar{S}_o$ and $\bar{S}_g$ are the normalized saturation of oil and gas phases respectively, σ is IFT, k is permeability, ϕ is porosity, and C_{pc} and E_{pc} are constants obtained from matching experimental data of capillary pressure. Eq. (6.25) is based on the dimensionless scaling using the Leverett *J*-function (Leverett, 1941).

For simulations with the real reservoir fluids we used the capillary pressure model adopted from Skjaeveland *et al.* (2000) and Helland and Skjaeveland (2004). The gas/oil and gas/water capillary pressure curves in this model are given in Eqs. (6.26) and (6.27), respectively. We note that the functional form of this capillary pressure model is very flexible in modeling different displacement processes for media of different wettability.

$$P_{cgo} = c_g \left(1 - S_g\right)^{-a_g} + c_o \left(1 - S_o\right)^{-a_o}, \tag{6.26}$$

$$P_{cgw} = c_{g2} \left(1 - S_g\right)^{-a_{g2}} + c_w \left(1 - S_w\right)^{-a_w}. \tag{6.27}$$

In Eqs. (6.26) and (6.27), S_g and S_o are the gas and oil saturations, c_g, c_o, a_g, a_o, c_{g2}, c_w, a_{g2}, and a_w are constants of the capillary pressure model that can be matched to the experimental data for a particular displacement process. We apply the gas/oil capillary pressure model in Eq. (6.26) for unit IFT and use the normalized gas/oil capillary pressure curve as the input to the simulator.

6.5 SIMULATION STUDY WITH BINARY FLUIDS

We perform several simulations with the binary fluid system of C_1-C_6 at 300°F to demonstrate the significance of the P_{cmax} concept in compositional reservoir simulation and the possibility of capillary condensation when the effect of capillary pressure on the phase behavior is considered in the simulations. This binary fluid system was selected for the initial study because the limited degrees of freedom allow for a consistency check of the details of the capillary equilibrium calculations. A linear one-dimensional reservoir model with one producer and one injector both operating at constant bottomhole pressure is used for the simulations with the binary fluid. The parameters of the linear reservoir are given in Table 6-2. The gas/oil IFT was calculated by use of the Macleod and Sugden correlation (Pedersen *et al.*, 2014). The injector and producer are at the opposite ends of the reservoir in a line-drive pattern. The injector is used to maintain the reservoir pressure by injecting the initial reservoir fluid.

6.5.1 Demonstration of Capillary Condensation for a Single-Phase Gas Mixture

For this simulation, the initial composition of the reservoir fluid is 79% C_1 and 21% C_6. The initial fluid composition was selected so that the reservoir fluid remains

single-phase for the entire pressure range of the simulation (1,500 psia to 2,600 psia) without including the capillary pressure (P_c) effects on phase behavior. Hereafter, we use the term "with P_c and CE" (with capillary pressure and capillary equilibrium) to refer to the simulations where the effect of capillary pressure on phase behavior is included in the simulation. Furthermore, we use the term "with P_c without CE" (with capillary pressure and without capillary equilibrium) to refer to the simulations where the effect of capillary pressure is considered only on fluid transport but not on phase equilibrium and phase properties.

Figure 6-9 compares the pressure profiles of the oil and gas phases for the simulation with P_c and CE with the pressure profile of the simulation without P_c at 100 days. The dimensionless distance (x_D) is calculated from the injector. The steady-state saturation profiles are achieved after almost 70 days for both cases. The entire reservoir remains single-phase in the simulation without P_c throughout the simulation. Figure 6-10 shows the profiles of gas saturation (S_{gas}), gas relative permeability (k_{rg}), overall mole fraction of C_1 (z_1), and gas/oil capillary pressure (P_c) at steady-state for the simulation with P_c and CE. Capillary condensation occurs near the producer and significantly decreases the gas relative permeability. The overall mole fraction of C_1 in the region with two-phases is within the range that capillary equilibrium is possible (cf. Figure 6-6). For the simulation without P_c, the overall mole fraction of C_1 remains at its initial value everywhere in the reservoir. The capillary pressure values throughout the simulation and at steady-state are smaller than the P_{cmax} values in Figure 6-5 in the pressure range of interest.

Figure 6-11 compares the gas production rate and cumulative gas production for the simulation with P_c and CE with the simulation without P_c. The gas production rate is

smaller when the effect of capillary pressure on phase behavior is considered in the simulation. The capillary condensation phenomenon decreases the steady-state gas production rate by 4.67% compared to the simulation without P_c. Figure 6-12 compares the oil production rate and cumulative oil production for the simulation with P_c and CE with the simulation without P_c. The oil production rate at steady-state is smaller in the simulation with P_c and CE.

6.5.2 Effect of Capillary Pressure on Production Behavior of a Gas Condensate Reservoir with a Binary Fluid

We performed several simulations with an initial fluid composition of 70% C_1 and 30% C_6 to demonstrate the influence of capillary pressure on production behavior in a gas condensate reservoir with a simple binary fluid. The other reservoir parameters are given in Table 6-2. The reservoir fluid is single-phase gas at the initial reservoir pressure (2,500 psia) with a dewpoint pressure of 2,090 psia at the reservoir temperature of 300°F. Thus, condensate will form close to the producer in the reservoir even without considering the capillary pressure effects on phase behavior.

We verified the steady-state gas saturation profile for the simulation without capillary pressure with the theory of two-phase steady-state flow (Chopra and Carter, 1986). According to this theory, the ratio of gas to oil relative permeability at steady-state (k_{rg}/k_{ro}) is equal to the PVT ratio of the constant composition expansion (CCE) test ($V_g\mu_g/V_o\mu_o$) as given by

$$\frac{k_{rg}}{k_{ro}} = \frac{V_g \mu_g}{V_o \mu_o} \quad \text{or} \quad \frac{k_{rg}\mu_o}{k_{ro}\mu_g} = \frac{V_g}{V_o}, \tag{6.28}$$

where V_g and V_o are the volumes of gas and oil obtained from the CCE experiment respectively, μ_g and μ_o are the gas and oil viscosities respectively, and k_{rg} and k_{ro} are the

gas and oil relative permeabilities, respectively. At a given pressure, knowledge of the PVT properties is sufficient to determine the relative permeability ratio at steady state. Figure 6-13 compares the ratio of gas to oil volume (V_g/V_o) versus pressure from the CCE calculations (performed using UTCOMP) with the ratio of two-phase-gridblocks' gas to oil mobility ($k_{rg}\mu_o/k_{ro}\mu_g$) versus pressure at steady-state conditions. The steady-state profile from the simulation without capillary pressure is in excellent agreement with the prediction of the analytical theory of two-phase flow. Figure 6-14 compares the steady-state gas and oil relative permeability profiles of the simulation without P_c, the simulation with P_c and CE, and the simulation with P_c without CE. In the two-phase region near the wellbore (the condensate drop-out region), the gas relative permeability is smaller in the simulation with P_c and CE compared to the other two simulations.

Figure 6-15 shows the oil and gas pressure profiles of the simulations with P_c and CE, and with P_c without CE and the pressure profile of the simulation without P_c at steady state. The first appearance of two phases in the linear model is close to the pressure value of 2,090 psia (the dewpoint pressure at 300°F). Figure 6-16 shows the gas saturation profiles of the simulations with P_c and CE, the simulation with P_c without CE, and the simulation without P_c at steady-state. The gas saturation in the two-phase region near the wellbore is smaller when the effect of capillary pressure on phase behavior is considered in the simulation. Figure 6-17 compares the capillary pressure profiles of the steady-state simulations with P_c and CE, and with P_c without CE at 5 days and 100 days. Figure 6-17 shows that capillary pressure values as high as 350 psia are possible during the simulation when the effect of capillary pressure on phase behavior is not included in the compositional simulation (the simulation with P_c without CE). However, for the current thermodynamic model the gas/oil capillary pressure values remain smaller than

50 psia throughout the simulation when the effect of capillary pressure on phase behavior is considered in the simulation.

Figure 6-18 compares the gas production rate for the simulation with P_c and CE, the simulation with P_c without CE, and the simulation without P_c. The steady-state gas production rate is larger (2.8%) when capillary pressure is not included in the simulation model (the simulation without P_c). The steady-state gas production rate is only slightly smaller in the simulation with P_c and CE compared to the simulation with P_c without CE.

We performed another set of simulations where the injector and producer operate at bottomhole pressure values of 2,100 psia and 1,000 psia, respectively. The rest of the reservoir parameters are given in Table 6-2. Under these operating conditions, capillary equilibrium was possible for capillary pressure values as large as 210 psia during the simulation, which is consistent with the P_{cmax} values in Figure 6-5. For this case, the steady-state gas production rate in the simulation with P_C and CE is 8.2% smaller than in the simulation without P_c. This shows that larger P_{cmax} values result in more significant impact of capillary pressure on production behavior.

6.6 SIMULATIONS WITH REAL RESERVOIR FLUIDS

We perform three simulation case studies with real reservoir fluids to investigate the effect of capillary pressure on production behavior from gas condensate and tight oil reservoirs. We perform two sets of simulations for the first and second case studies and one set of simulations for the third case study. In the first and second case studies we perform one-dimensional simulations using the same linear model, as for the binary fluids. For this set of simulations we report the steady-state gas production rates. We also perform unsteady-state areal two-dimensional simulations of depletion process in gas condensate or tight oil reservoir for each case study. All the simulations were performed

using the Peng-Robinson (PR) EOS (Peng and Robinson, 1976). The capillary pressure model used in the simulations is adopted from Helland and Skjaeveland (2004). The gas/oil IFT was calculated by use of the Macleod and Sugden correlation (Pedersen *et al.*, 2014).

6.6.1 Case 1

The first simulation case study is a gas condensate reservoir. The component properties used for EOS modeling and the initial reservoir fluid composition are given in Table 6-3. The reservoir temperature is 130°F, which is larger than the critical temperature of -60°F and smaller than the cricondentherm of 340°F. The upper dewpoint pressure at the reservoir temperature is 3,093 psia. The minimal critical pressure of the initial composition at 130°F is 4,470.70 psia. The initial reservoir pressure is 3,500 psia.

The maximum capillary pressure (P_{cmax}) where capillary equilibrium is possible for the initial fluid composition for an oil-wet system versus pressure of the equilibrium gas phase is given in Figure 6-19. The P_{cmax} values in Figure 6-19 are not limited to physical phase molar fractions. Figure 6-19 shows the limiting maximum capillary pressure where Eqs. (6.1) are satisfied and the resulting tie line extends through the overall composition of interest. This corresponds to a tangent hyperplane to the molar GFE hypersurface where the line connecting the points of tangency extends through the overall composition of interest (more precisely the projection of the tangent line on the hyperplane $\underline{G} = 0$ extends through the overall composition of interest). Thus, Figure 6-19 only shows the maximum capillary pressure values where one necessary condition for capillary equilibrium is satisfied i.e. equality of components' chemical potentials in equilibrium phases. The other necessary conditions for capillary equilibrium are that i) the phase saturations (or molar fractions) are in the physical range ii) the capillary

pressure dependence on saturation is satisfied iii) and of course, the GFE of the two-phase fluid is smaller than the single phase. The latter condition is usually satisfied for the current problem statement because the second phase is at a lower pressure.

To further illustrate the significance of P_{cmax}, Figure 6-20 shows the resulting gas-phase molar fractions versus capillary pressure for three different gas-phase pressure values of 2,500, 3,100, and 3,500 psia. At 2,500 psia, the initial reservoir fluid splits into two hydrocarbon phases at zero capillary pressure. The capillary equilibrium calculations of the initial reservoir fluid at the gas-phase pressure of 2,500 psia lead to physical values of gas phase molar fraction for the entire possible range of capillary pressure values in Figure 6-19. This is always the case for gas-like overall compositions which are two-phase at zero capillary pressure. On the other hand, at 3,100 psia and 3,500 psia the initial reservoir fluid is single-phase at zero capillary pressure. At a specified gas-phase pressure of 3,100 psia, for capillary pressure values smaller than three psia, a solution to the equality of chemical potentials exist however a physical solution does not exist because the gas-phase molar fractions is greater than one. For capillary pressure values greater than three psia and smaller than 75.8 psia (the P_{cmax} value from Figure 6-19) a physical solution to the capillary equilibrium problem exists. At a gas-phase pressure of 3,500 psia a physical solution to the capillary equilibrium problem does not exist even though the gas-phase pressure is smaller than the minimal critical pressure. In fact, the gas-phase pressure value of 3,212.5 psia is the maximum pressure where a physical solution to the capillary equilibrium problem for the initial fluid composition is possible. The corresponding equilibrium state is characterized by the fact that the tangent hyperplane at the initial composition to the GFE hypersurface at the gas-phase pressure is the same as

the tangent hyperplane to the GFE hypersurface at the oil-phase pressure at the spinodal point.

6.6.1.1 Linear Model Simulations

The IFT-normalized gas/oil capillary pressure curve and the gas/water capillary pressure curve used in the simulations of Case 1 are given in Figure 6-21 and Figure 6-22, respectively. The condensate buildup is modeled using an imbibition-type capillary pressure curve because the oil saturation increases as the condensate drops out during depletion and the oil phase is the wetting phase with respect to the gas phase. The water phase is at the residual saturation of 0.3 for the simulations of Case 1. Table 6-4 gives the parameters of the capillary pressure curves in Figure 6-21 and Figure 6-22, the parameters of the Corey-type relative permeabilities and the other model parameters.

Figure 6-23 shows an excellent agreement between the V_g/V_o from the CCE simulation (performed with UTCOMP) and the gas to oil mobility ratio at steady-state from the UTCOMP simulation without P_c. The two-phase steady-state flow theory of Chopra and Carter (1986) does not apply in the presence of capillary pressure; however, it is straightforward to show that for one-dimensional flow with capillary forces Eqs. (6.29) must hold everywhere in the reservoir at steady-state flow,

$$zf_i = \frac{x_i\lambda_o\nabla P^o + y_i\lambda_g\nabla P^g}{\lambda_o\nabla P^o + \lambda_g\nabla P^g} = zi_i, \qquad i = 1,...,n_c, \tag{6.29}$$

where zf_i and zi_i are the flowing mole fraction and the injection mole fraction of component i, respectively, λ is mobility, P is pressure, x_i and y_i are mole fraction of component i in the oil and gas phases, respectively, and the subscripts (or superscripts) o and g represent the oil and gas phases, respectively. We calculated the profiles of the

flowing mole fraction of C_1 and C_4-C_6 at steady-state from Eq. (6.29) and compared them with zi_i for the linear model (Figure 6-24). The results show good agreement between the flowing mole fractions and the injection fluid compositions.

Figure 6-25 compares the gas production rate for the simulation with P_c and CE and the simulation without P_c. The simulation with P_c without CE was not successfully completed because of the very large capillary pressure values. The steady-state gas production rate decreases by 5.42% when the effect of capillary pressure on the phase behavior is included in the model. Figure 6-26 shows the oil and gas relative permeability profiles for the simulation with P_c and CE and the simulation without P_c in the linear model at steady state. The relative permeability profiles at steady-state flow are very similar except in in the vicinity of the producer. Figure 6-27 shows the profiles of oil and gas viscosities at steady-state for the simulation without P_c and the simulation with P_c and CE. Figure 6-28 shows the capillary pressure profiles for the simulation with P_c and CE at 1, 10, 100, and 1000 days. At early time the capillary pressure values as high as 600 psia occur in the simulation where the oil saturation is small. However, at steady state the maximum capillary pressure is slightly more than 100 psia because the oil saturation builds up near the producer and consequently capillary pressure decreases.

6.6.1.2 Unsteady-State Areal Model Simulations

The number of gridblocks in the two-dimensional areal model is 20×20. The gridblock sizes in *x*- and *y*-directions are 25 ft. The permeabilities in *x*- and *y*-directions are 1 md. The other reservoir parameters are the same as those in Table 6-4. There is only one producer at one corner of the reservoir without any injector.

Figure 6-29 through Figure 6-32 compare the gas production rate, cumulative gas production, oil production rate, and cumulative oil production for the simulation with P_c

and CE, the simulation with P_c without CE, and the simulation without P_c in the areal model. The gas production rate and cumulative gas production of the simulation without P_c and the simulation with P_c and CE are very close initially. The gas production rate and cumulative gas production of the simulation with P_c and CE at 360 days are respectively 12.6% and 0.09% smaller than in the simulation without P_c. The gas production rate and the cumulative gas production of the simulation with P_c without CE at 360 days are respectively 40.2% and 31.5% larger than in the simulation without P_c. The simulation with P_c and CE results in smaller oil recovery rate and cumulative oil production than the other two simulations. The simulation with P_c without CE is not a thermodynamically consistent simulation especially considering the large capillary pressure values that we are using in the simulation model. In this simulation with the original UTCOMP, the oil-phase pressure is used as the reference phase in the two-hydrocarbon-phase gridblocks; thus, the calculations of fluid properties and phase equilibrium are performed at the oil-phase pressure. This will result in significant difference in the gas saturation and gas properties in the well gridblock where the value of capillary pressure is very large (~800 psia) at the early time i.e. the phase equilibrium calculations are performed at a pressure that is smaller than the gas phase pressure by the value of capillary pressure.

Figure 6-33 shows the total hydrocarbon moles produced in both oil and gas phases for the simulation with P_c and CE and the simulation without P_c. The number of hydrocarbon moles initially in place is 385,280. In the simulation with P_c and CE the total hydrocarbon moles produced at 360 days is 0.13% smaller than in the simulation without P_c. The recoveries of the individual hydrocarbon components are different in the simulation with P_c and CE compared to the simulation without P_c. Figure 6-34 through Figure 6-37 compare the recoveries of C_1, C_3, $C_{4\text{-}6}$, and $C_{7\text{-}80}$ versus time for the

simulation with P_c and CE and the simulation without P_c. The recovery of C_1 at 360 days in the simulation with P_c and CE is 0.41% larger than in the simulation without P_c. The recoveries of C_2, C_3, $C_{4\text{-}6}$, and $C_{7\text{-}80}$ at 360 days in the simulation with P_c and CE are respectively 0.58%, 2.01%, 5.93%, and 15.97% smaller than in the simulation without P_c. Figure 6-38 through Figure 6-41 show the effluent mole fraction of C_1, C_3, $C_{4\text{-}6}$, and $C_{7\text{-}80}$ versus time for the simulation with P_c and CE and the simulation without P_c. In the simulation with P_c and CE the recoveries and the effluent mole fractions of the intermediate and heavy components are smaller throughout the simulation than in the simulation without P_c. This is because the saturation of the condensed liquid, which is richer in the intermediate and heavy components than the gas phase, is larger in the reservoir when the effect of capillary pressure on phase behavior is considered in the simulation. Figure 6-42 through Figure 6-44 show the oil saturation in the well gridblock, in the middle gridblock and in the gridblock at the end of the reservoir versus time in the simulation with P_c and CE and the simulation without P_c. The increased condensation in the middle and at the end of the reservoir is shown in Figure 6-43 and Figure 6-44. The oil phase first appears in the well gridblock at a pressure of 3,156.02 psia after 0.0012 days in the simulation with P_c and CE. In the simulation without P_c, oil first appears in the well gridblock after 0.0015 days at a pressure of 3,093 psia.

Figure 6-45 compares the oil saturation profile of the simulation without P_c (*a*), the simulation with P_c and CE (*b*), and the simulation with P_c without CE (*c*) at 360 days for the areal model. In the simulation with P_c and CE, the oil saturation near the producer is slightly smaller than in the simulation without P_c. In the region away from the producer, the oil saturation in the simulation with P_c and CE is larger than in the simulation without P_c because of considering the capillary pressure effect on phase

behavior. However, the differences in oil saturation are small, approximately 0.010 in the middle of the reservoir and 0.0097 at the end of the reservoir. The differences in oil saturation throughout the simulation are not sufficiently large to significantly change the gas production behavior even though the production behaviors of the individual hydrocarbon components are affected by the capillary pressure. Figure 6-46 compares the profiles of gas relative permeability of the simulations without P_c (*a*), with P_c and CE (*b*), and with P_c without CE (*c*) at 360 days for the areal model.

Figure 6-47 shows the capillary pressure profiles of the simulation with P_c and CE at 5 days and 360 days. The values of average reservoir pressure at 5 and 360 days are 3,065 and 1,066 psia, respectively. At 5 days the IFT value at the well gridblock and in the middle of the reservoir are 1.63 and 0.19 dynes/cm, respectively. Even though the oil saturation in the middle of the reservoir is smaller than in the well gridblock, the effect of IFT difference on capillary pressure dominates the effect of saturation difference. Thus, capillary pressure is larger near the well compared to the middle of the reservoir at 5 days. At 360 days the IFT values at the well gridblock and in the middle of the reservoir are 5.06 and 4.0 dynes/cm, respectively. The capillary pressure in the middle of the reservoir is larger than in the well gridblock at 360 days because of the smaller oil saturation. The oil saturation is below the residual saturation value of 0.3 everywhere in the reservoir at 360 days.

6.6.2 Case 2

In the second simulation case study we use the reservoir fluid from Hatter's Pond (Rai, 2003) gas condensate reservoir. The component properties used for EOS modeling and the initial reservoir fluid composition are given in Table 6-5. The critical temperature of the reservoir fluid is 308.17°F. We used the reservoir temperature of 450°F. The upper

dewpoint pressure at the reservoir temperature is 3,168.26 psia. The minimal critical pressure of the initial composition at 460°F is 3,800 psia. The initial reservoir pressure is 3,500 psia.

The maximum capillary pressure where capillary equilibrium is possible for the initial fluid composition for an oil-wet system versus pressure of the equilibrium gas phase is given in Figure 6-48. The capillary pressure and relative permeability model parameters are the same as those used in Case 1 (Table 6-4).

6.6.2.1 Linear Model Simulations

Figure 6-49 shows an excellent agreement between the V_g/V_o from the CCE simulation (performed with UTCOMP) and the gas to oil mobility ratio at steady-state from the UTCOMP simulation without capillary pressure.

Figure 6-50 compares the gas production rate for the simulation without P_c, the simulation with P_c without CE, and the simulation with P_c and CE. The steady-state gas production rate of the simulation without P_c is very similar to the simulation with P_c without CE. The steady-state gas production rate in the simulation with P_c and CE is only 3.75% smaller than the simulation without P_c. Figure 6-51 shows the oil and gas relative permeability profiles for the simulation with P_c and CE, the simulation without P_c, and the simulation with P_c without CE in the linear model at steady state. The relative permeability profiles at steady-state flow are very similar except in in the vicinity of the producer. Figure 6-52 shows the profile of oil and gas viscosities at steady-state for the simulation without P_c, the simulation with P_c and CE, and the simulation with P_c without CE. Figure 6-53 shows the capillary pressure profiles for the simulation with P_c and CE and the simulation with P_c without CE at 1 and 1,000 days. In the simulation with P_c and CE the capillary pressure value does not exceed 220 psia at the early time whereas in the

simulation with P_c without CE the capillary pressure is greater than 900 psia near the producer. At steady-state condition the capillary pressure profiles are very similar.

6.6.2.2 Unsteady-State Areal Model Simulations

In this section, the permeabilities in the *x*- and *y*-directions in the areal reservoir model are 10 *md*. The other parameters of the areal reservoir model are the same as those used in Case 1. Figure 6-54 through Figure 6-57 compare the gas production rate, cumulative gas production, oil production rate, and cumulative oil production for the simulation with P_c and CE, the simulation with P_c without CE, and the simulation without P_c in the areal model. The gas production rate in the simulation with P_c and CE is initially larger than in the simulation without P_c (between 5 and 45 days), and at later time (greater than 45 days) becomes smaller than in the simulation without P_c. The gas production rate at 70 days in the simulation with P_c and CE is 13.5% smaller than in the simulation without P_c. The gas production rate at 70 days in the simulation with P_c without CE is 2.23 times the gas production rate in the simulation without P_c. However, the simulation with P_c without CE is not thermodynamically consistent. The cumulative gas production of the simulation with P_c and CE and the simulation with P_c without CE are respectively 0.42% and 36.1% larger than the simulation without P_c at 70 days. The oil production rate and cumulative oil production in the simulation with P_c and CE at 70 days are 28.5% and 9.62% smaller than in the simulation without P_c, respectively. In the simulation with P_c without CE, the oil production rate is 3.11 times the oil production rate in the simulation without P_c. The cumulative oil production in the simulation with P_c without CE is 32.9% larger than in the simulation without P_c.

Figure 6-58 shows the total hydrocarbon moles produced in both oil and gas phases for the simulation with P_c and CE and the simulation without P_c. Initially, there

are 203,564 hydrocarbon moles in the reservoir. The total hydrocarbon moles produced in the simulation with P_c and CE at 70 days is 0.44% smaller than in the simulation without P_c. The recoveries of the individual components vary significantly in the simulation with P_c and CE compared to the simulation without P_c even though the produced total hydrocarbon moles are very close. Figure 6-59 through Figure 6-62 compare the recoveries of C_1, $C_{4\text{-}6}$, C_{7p1}, and C_{7p2} versus time for the simulation with P_c and CE and the simulation without P_c. The recovery of C_1 at 70 days in the simulation with P_c and CE is 0.72% larger than in the simulation without P_c. The recoveries of $C_{4\text{-}6}$, C_{7p1}, C_{7p2}, and C_{7p3} at 70 days in the simulation with P_c and CE are respectively 1.94%, 3.82%, 10.85%, and 13.73% smaller than in the simulation without P_c. Figure 6-63 through Figure 6-66 show the effluent mole fraction of C_1, $C_{4\text{-}6}$, C_{7p1}, and C_{7p2} versus time for the simulation with P_c and CE and the simulation without P_c. The recoveries and the effluent mole fractions of the intermediate and heavy components are smaller in the simulation with P_c and CE compared to the simulation without P_c for the entire simulation time. This is because of the increased liquid drop-out in the reservoir that results from considering the effect of capillary pressure on phase behavior. The condensed liquid in the reservoir is richer in the intermediate and heavy components than the initial gas thus the produced gas is leaner. This explains why in the simulation with P_c and CE the oil production rate is smaller and the gas production rate is initially larger than in the simulation without P_c.

Figure 6-67 through Figure 6-69 show the oil saturation in the well gridblock, in the middle gridblock and in the gridblock at the end of the reservoir versus time in the simulation with P_c and CE and the simulation without P_c. The increased condensation in the middle and at the end of the reservoir is shown in Figure 6-68 and Figure 6-69. Noteworthy, the dewpoint pressure is approximately 3,194.8 psia and is reached after

0.00012 days in the well gridblock in the simulation with P_c and CE. In the simulation without P_c, oil first appears in the well gridblock at a pressure of 3,149.2 psia after 0.00014 days.

Figure 6-70 compares the oil saturation profiles of the simulation without P_c (*a*), the simulation with P_c and CE (*b*), and the simulation with P_c without CE (*c*) at 70 days for the areal model. The oil saturation near the producer is smaller in the simulation with P_c and CE than in the simulation without P_c. However, in the regions away from the producer, the oil saturation in the simulation with P_c and CE is larger than in the simulation without P_c because of increased condensation resulting from considering the capillary pressure effect on phase behavior. Figure 6-71 compares the profiles of gas relative permeability of the simulation without P_c (*a*), the simulation with P_c and CE (*b*) and the simulation with P_c without CE (*c*) at 70 days for the areal model. The gas relative permeability profiles of different simulations are consistent with the oil saturation profiles.

Figure 6-72 shows the gas/oil capillary pressure profiles of the simulation with P_c and CE at 10 days and 70 days. The average reservoir pressure at 10 and 70 days are 2,249 and 1,060 psia, respectively. At 10 days the IFT value at the well gridblock and in the middle of the reservoir are 2.30 and 0.40 dynes/cm, respectively. The gas/oil capillary pressure is larger in the well gridblock compared to the middle of the reservoir at 10 days. At 70 days the IFT values at the well gridblock and in the middle of the reservoir are 3.78 and 2.94 dynes/cm, respectively. The capillary pressure in the middle of the reservoir is larger than in the well gridblock at 70 days because of the smaller oil saturation.

6.6.3 Case 3

In this case, we demonstrate application of the UTCOMP simulator in modeling the capillary pressure effects on phase behavior and the bubblepoint suppression in tight oil reservoirs. We use the fluid and the reservoir parameters of the Bakken tight oil reservoir reported by Nojabaei *et al.* (2013 and 2014) to investigate the effect of capillary pressure on phase behavior in tight oil reservoirs. The gas/oil capillary pressure curve normalized by IFT is given in Figure 6-73. The gas/water capillary pressure curve is given in Figure 6-74. Similar to the simulations of Nojabaei *et al.* (2014), the relative permeability curves were adopted from Shoaib and Hoffman (2009). The capillary pressure model parameters, the Corey-type relative permeability model parameters, and the other reservoir parameters are given in Table 6-6.

The component properties used for EOS modeling and the initial reservoir fluid composition are given in Table 6-7. The reservoir temperature is 240°F. The bubblepoint pressure at the reservoir temperature is 2,863 psia. The minimal critical pressure of the initial composition at 240°F is 4,031 psia. The initial reservoir pressure is 4,200 psia.

The maximum capillary pressure where capillary equilibrium is possible for the initial fluid composition (P_{cmax}) for an oil-wet system ($P^o < P^g$) versus pressure of the equilibrium oil phase is given in Figure 6-75. Figure 6-75 also shows the physical limit on the P_{cmax} values calculated from Eqs. (6.11) through (6.13). For oil-phase pressure values smaller than approximately 130 psia this physical limit is related to the condition that the GFE of the two-phase system must be smaller than the stable single phase. For example, for oil pressure of 110 psia the P_{cmax} value is 1,131 psia. However, for capillary pressure values larger than 728 psia the GFE of the two-phase capillary equilibrium solution is greater than the stable single-phase's GFE. For oil-phase pressure values

greater than 1,855 psia the physical limit on P_{cmax} is related to the physical saturation values. For example, at oil-phase pressure value of 2,800 psia the value of P_{cmax} is 162.84 psia while for capillary pressure values greater than 20.8 psia a solution to the capillary equilibrium problem with physical saturation values does not exist. The physical limit on the P_{cmax} imposed by physical saturation values tends to zero at the true bubblepoint pressure (calculated at zero capillary pressure). In fact, for the problem statement of "given a liquid-like overall composition and oil-phase pressure", capillary equilibrium with physical phase saturations is possible only for pressure values smaller than the true bubblepoint pressure. We note that the initial composition is metastable between the pressure values of 1,855 psia and 2,863 psia. From the geometry of the GFE hypersurfaces one may expect that when the initial liquid-like overall composition is metastable at the given liquid-phase pressure, the physical saturation limit on capillary pressure is reached before the spinodal limit i.e the P_{cmax} limit. The capillary pressure value where the P_{cmax} limit and the physical saturation limit become equal (P_c = 409.5 psia at P^o = 1,855 psia) is the maximum possible bubblepoint suppression (409.5 psia) for the given overall composition at the temperature of interest (240°F). This maximum possible bubblepoint suppression corresponds to the oil-phase pressure where the initial composition is at the spinodal limit (1,855 psia).

It is not always possible to design a capillary equilibrium experiment where the only possible outcomes are either stable single-phase oil at a given pressure (P^o) or two phases in capillary equilibrium where the oil phase is at P^o. This is why using *VT* capillary equilibrium calculations may be more physical for compositional simulation including the capillary pressure effects on phase behavior.

6.6.3.1 Unsteady-State Areal Model Simulations for Case 3

Figure 6-76 through Figure 6-79 compare the oil production rate, cumulative oil production, gas production rate, and cumulative gas production for the simulation with P_c and CE, the simulation with P_c without CE, and the simulation without P_c in the areal model. The production behaviors of the simulation with P_c without CE and the simulation without P_c are very similar. The cumulative oil and gas productions in the simulation with P_c without CE are respectively 0.08% and 0.09% larger than in the simulation without P_c. This is because the oil phase pressure is used as the reference pressure in the UTCOMP simulation with P_c without CE. The oil and gas production rates in the simulation with P_c and CE remain larger than in the simulation without P_c because of the favorable capillary pressure effects on phase behavior of the oil phase. The oil and gas production rates at 200 days in the simulation with P_c and CE are respectively 5.77% and 5.79% larger than in the simulation without P_c. The cumulative oil and gas productions at 200 days in the simulation with P_c and CE are respectively 6.87% and 6.93% larger than in the simulation without P_c. Figure 6-80 shows the gas saturation in the well gridblock versus pressure of the oil phase in the well gridblock for different simulations. The bubblepoint pressure is reduced from 2,863 psia in the simulation without P_c to 2,788.9 psia in the simulation with P_c and CE because of the capillary pressure effect on phase behavior. The gas phase appears in the simulation without P_c and the simulation with P_c and CE in the well gridblock at 0.00277 and 0.00301 days, respectively. Our simulation results for the Bakken tight oil are in reasonable quantitative agreement with those reported by Nojabaei *et al.* (2014) obtained by use of an extended black-oil formulation.

Figure 6-81 compares the gas saturation profiles of the simulation without P_c (*a*), the simulation with P_c and CE (*b*), and the simulation with P_c without CE (*c*) at 200 days

for the areal model. Throughout the simulation and at 200 days the gas saturation near the producer is smaller in the simulation with P_c and CE than in the simulation without P_c because of the effect of capillary pressure on phase behavior. However, far from the producer the gas saturation is larger in the simulation P_c and CE than in the simulation without P_c. This is because in the simulation with P_c and CE the average reservoir pressure at 200 days is 131 psia smaller than in the simulation without P_c. The relative permeability profiles at 200 days are consistent with the gas saturation profiles. The profiles of oil viscosity in different simulations at 200 days are given in Figure 6-82. The oil viscosity in the simulation with P_c and CE at 200 days in the entire reservoir is smaller than in the simulation without P_c.

Figure 6-83 shows the capillary pressure profiles in the simulation with P_c and CE at 20 days and 200 days. The value of capillary pressure near the producer is larger than in the middle of the reservoir for the entire simulation time. At 20 days the IFT values in the well gridblock and in the middle of the reservoir are 7.14 and 2.81 dynes/cm, respectively. At 200 days the IFT values in the well gridblock and in the middle of the reservoir are 19.4 and 5.80 dynes/cm, respectively. Thus, larger IFT and gas saturation values in the well gridblock results in larger capillary pressure values compared to the middle of the reservoir.

6.7 SUMMARY AND CONCLUSIONS

We presented a GFE analysis of the capillary equilibrium problem and discussed the phase stability analysis concepts in the presence of capillary equilibrium. We showed that the TPD criterion cannot be used in its general form to make a conclusion on a phase's stability in the presence of capillary pressure. We demonstrated that there is a limiting maximum capillary pressure (P_{cmax}) where gas/oil capillary equilibrium is

possible. We formulated the capillary equilibrium limits in a context that is applicable to most current compositional reservoir simulators. Next, the theory was used to calculate the P_{cmax} for several fluid models. Several heuristic methods were discussed for improving the computational time of the capillary equilibrium calculations in compositional reservoir simulators that use pressure of one of the phases and the overall composition of the gridblock as the independent variables.

An alternative formulation of the capillary equilibrium problem where the total number of moles of each component, total volume, and temperature are used as the independent variables (*VT* capillary equilibrium calculations) was presented. The *VT* formulation results in the same P_{cmax} values as the traditional formulation of the capillary equilibrium problem.

The effect of capillary pressure on phase behavior was implemented in the UTCOMP simulator. We demonstrated the problem of capillary condensation for a simple binary mixture in a compositional reservoir simulation context. We also performed steady-state linear and unsteady-state areal model simulations for two real gas condensate fluids to investigate the effect of capillary pressure on production behavior. The results show that the steady-state gas production rate in the linear model decreases as the effect of capillary pressure on phase behavior is included in the model (the simulation with P_c and CE). This is because of the increased liquid condensation near the producer in the presence of capillary pressure. The gas production rate in the unsteady-state areal model simulations is initially larger in the simulations with P_c and CE compared to the simulations without capillary pressure (the simulations without P_c). However, as the reservoir becomes more depleted, the gas production rate in the simulations with P_c and CE becomes smaller than the gas production rate in the simulations without P_c. The total

number of hydrocarbon moles produced is very similar in the simulations with P_c and CE and the simulations without P_c. However, the recoveries and the effluent mole fractions of the intermediate and heavy components are smaller in the simulations with P_c and CE than in the simulations without P_c. This is because some of the intermediate and heavy components are trapped in the reservoir due to the increased liquid condensation when the effect of capillary pressure on phase behavior is included in the simulation. In the unsteady-state areal model simulations, the oil production rate in the simulations with P_c and CE is smaller compared to the simulations without P_c. In general, using even very high capillary pressure values the gas production behavior was not very sensitive to the capillary pressure effects on phase behavior in the gas condensate reservoirs under unsteady-state conditions for the cases studied. We note that we performed our simulations in simple reservoir models with a uniform effective permeability. The gas production behavior might show more sensitivity to accounting for the effect of capillary pressure on phase behavior in highly heterogeneous reservoir models.

We also performed unsteady-state areal model simulations for the Bakken tight oil reservoir and demonstrated the bubblepoint suppression that results from the effect of capillary pressure on phase behavior. The results of the simulations in our simple reservoir model show that when the effect of capillary pressure on the phase behavior is included in the simulation the oil production rate is increased by almost 6% compared to the simulation without P_c. This is because of the smaller gas saturation and oil viscosity that result from considering the effect of capillary pressure on phase behavior in the simulation with P_c and CE.

Table 6-1: Equilibrium compositions for the capillary equilibrium of the binary mixture of C_1-C_6 at 130°F where the liquid phase is at the smaller pressure.

Liquid		Gas	
P (psia)	x_1	P (psia)	x_1
174.4	0.169	493.7	0.971
174.4	0.429	1052.9	0.981
174.4	0.485	1097.2	0.982

Table 6-2: Parameters of the linear reservoir model for the simulations with binary fluid.

Number of gridblocks	100	S_{or}	0.3
Gridblock size (ft)	25	S_{gr}	0.1
Porosity	0.03	k_{ro}^{0}	0.6
Permeability (md)	100	k_{rg}^{0}	0.6
Formation compressibility	0	n_o	2
Water compressibility	0	n_g	3
Initial water saturation	0	Initial reservoir pressure (psia)	2600
Temperature (°F)	300	Injector's pressure (psia)	2600
C_{pc}	16,125	Producer's pressure (psia)	1500
E_{pc}	1.1		

Table 6-3: Component properties used in EOS modeling and the initial fluid composition for simulations in Case 1.

	P_c (psia)	T_c (R)	V_c (ft^3/lbmol)	*MW*	ω	Parachor	BIP with N_2	Initial fluid (z_i)
N_2	492.32	227.16	1.44	28.01	0.04	41	0	0.0040
C_1	667.19	343.08	1.59	16.04	0.008	77	0.03	0.7376
C_2	708.35	549.72	2.38	30.07	0.098	108	0.04	0.1515
C_3	615.76	665.64	3.26	44.10	0.152	150.3	0.09	0.0548
C_{4-6}	501.82	817.09	4.78	66.99	0.229	219.16	0.1	0.0428
C_{7-80}	404.14	1322.28	9.25	116.8	0.37	335.85	0.1	0.0093

Table 6-4: The reservoir model parameters used in the simulations in Case 1.

No. of gridblocks (linear model)	100	S_{wr}	0.3
Gridblock size (ft)	25	S_{or}	0.3
Porosity	0.03	S_{gr}	0.25
Permeability (md)	100	e_w	3
Formation compressibility	1E-6	e_g	2
Temperature (°F)	130	e_o	2
Initial water saturation	0.3	k_{rw}^0	0.1
C_g	20.0	k_{ro}^0	0.5
C_o	-10.9	k_{rg}^0	0.6
a_g	2.0	a_w	-3.0
a_o	2.0	C_w	2000
C_{g2}	300	a_{g2}	0
Initial reservoir pressure (psia)	3500	Injector's pressure (psia)	3500
Producer's pressure (psia)	1000		

Table 6-5: Component properties used in EOS modeling and the initial fluid composition for simulations in Case 2.

	P_c (psia)	T_c (R)	V_c (ft^3/lbmol)	MW	ω	Parachor	BIP with N_2	Initial fluid (z_i)
N_2	492.45	227.16	1.43	28.02	0.04	80.05	0	0.0283
CO_2	1070.16	547.56	1.50	44.01	0.225	125.74	0	0.0613
C_1	667.38	343.08	1.59	16.04	0.008	45.82	-0.05	0.4625
C_{2-3}	661.79	608.24	2.82	35.82	0.1253	102.34	-0.05	0.1624
C_{4-6}	508.47	831.10	4.91	69.2	0.2348	197.71	-0.05	0.1439
C_{7p1}	292.46	915.88	7.14	109.33	0.3319	312.37	-0.05	0.1007
C_{7p2}	211.98	1465.90	13.44	210.23	0.5931	600.65	-0.05	0.0394
C_{7p3}	124.66	1974.41	23.18	424.84	1.0344	1213.82	-0.05	0.0015

Table 6-6: The reservoir model parameters used in the simulations in Case 3.

Gridblocks in x and y direction	20×20	S_{wr}	0.2
Gridblock size (ft)	50	S_{or}	0.3
Porosity	0.044	S_{gr}	0.3
Permeability (md)	10	e_w	3
Formation compressibility	1E-6	e_g	2
Temperature (°F)	240	e_o	3
Initial water saturation	0.2	k_{rw}^0	0.3
C_g	4.0	k_{ro}^0	1.0
C_o	5.0	k_{rg}^0	0.5
a_g	1.5	a_w	-5.0
a_o	0.0	C_w	2000
C_{g2}	500	a_{g2}	0
Initial reservoir pressure (psia)	4200	Producer's pressure (psia)	100

Table 6-7: Component properties used in EOS modeling and the initial fluid composition for simulations in Case 3.

	P_c (psia)	T_c (R)	V_c (ft^3/lbmol)	MW	ω	Parachor	BIP with C_1	Initial fluid (z_i)
C_1	655.02	335.34	1.58	16.53	0.0102	74.8	0	0.3674
C_2	721.99	549.97	2.34	30.43	0.1028	107.7	0.005	0.1488
C_3	615.76	665.97	3.25	44.09	0.152	151.9	0.0035	0.0933
C_4	546.46	759.21	4.11	58.12	0.1894	189.6	0.0035	0.0575
C_{5-6}	461.29	875.48	5.39	78.29	0.2684	250.2	0.0037	0.0641
C_{7-12}	363.34	1053.25	8.81	120.56	0.4291	350.2	0.0033	0.1585
C_{13-21}	249.61	1332.09	15.19	220.72	0.7203	590	0.0033	0.0733
C_{22-80}	190.12	1844.49	36	443.52	1.0159	1216.8	0.0033	0.0370

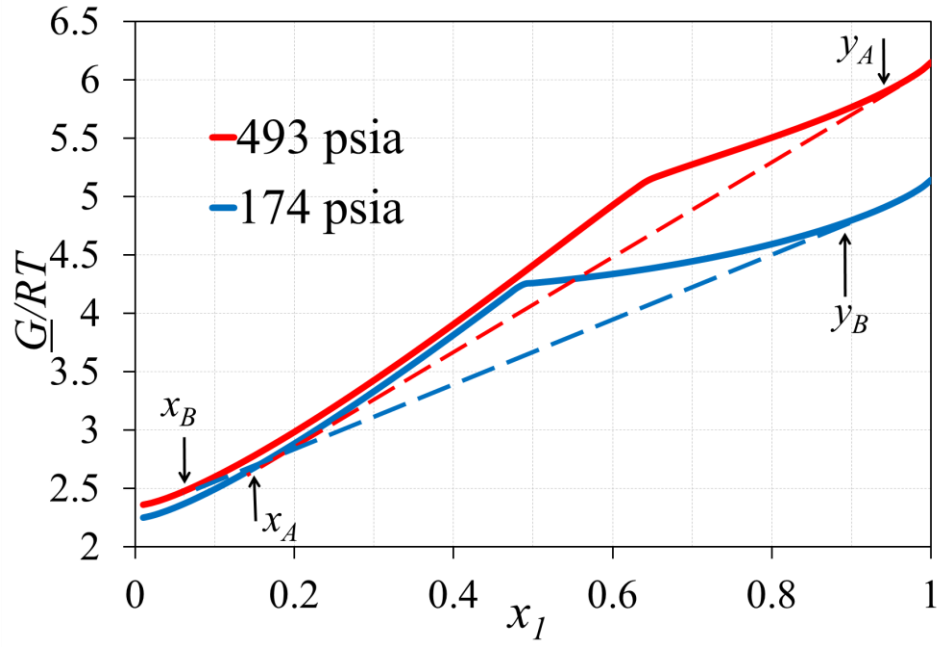

Figure 6-1: Dimensionless molar GFE of the hypothetical single-phase mixture of C_1-C_6 at 130°F at pressure values of 174 psia and 493 psia.

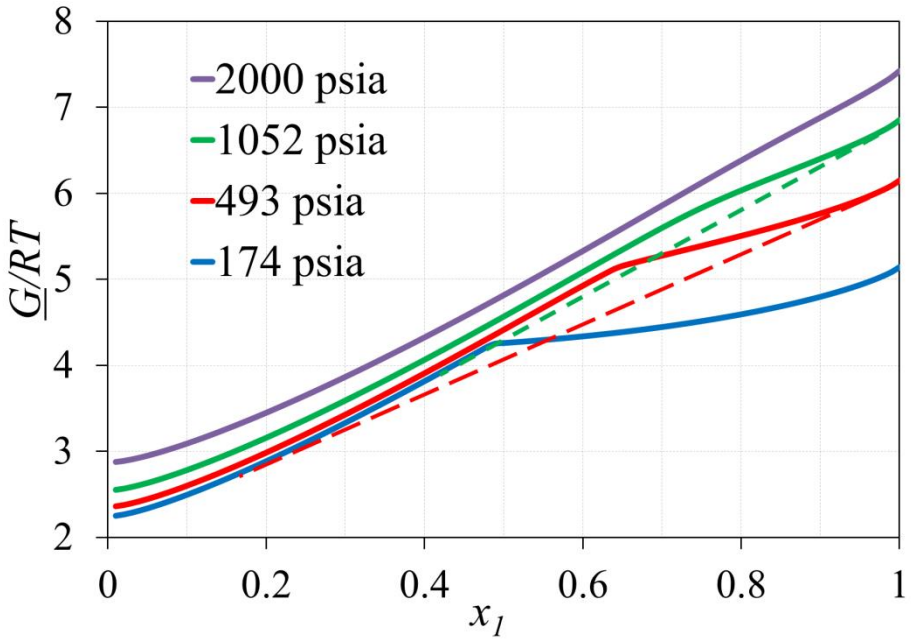

Figure 6-2: Dimensionless molar GFE of the hypothetical single-phase mixture of C_1-C_6 at 130°F at pressure values of 174, 493, 1052, and 2000 psia.

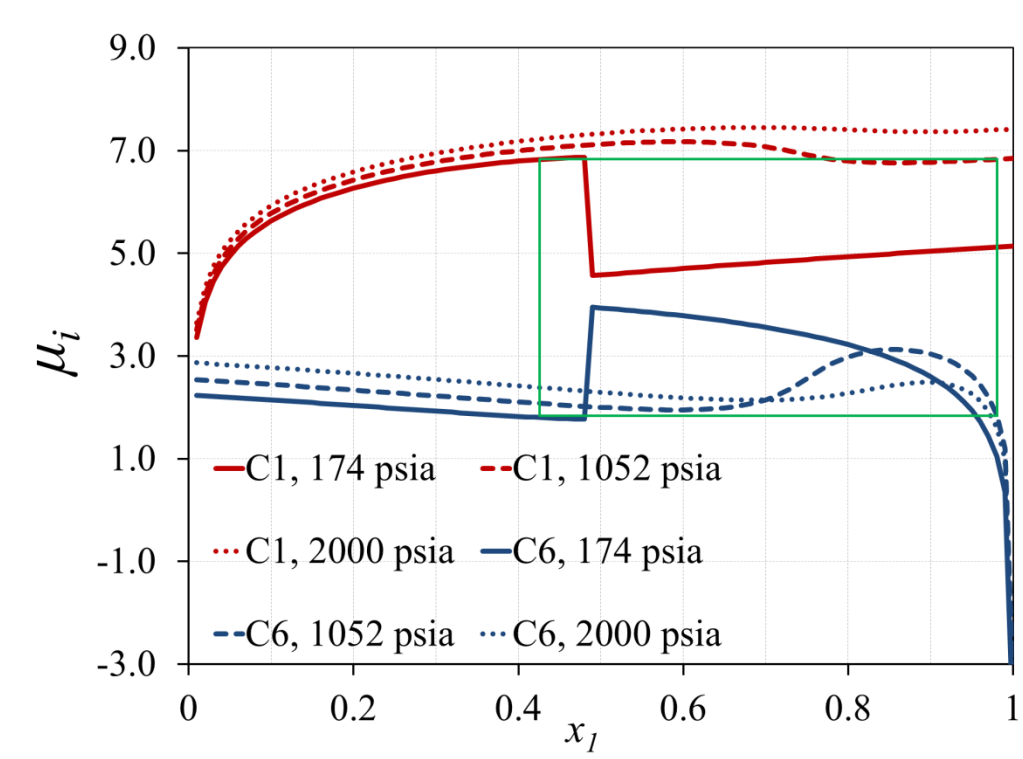

Figure 6-3: The chemical potentials of C_1 and C_6 in the hypothetical single-phase binary mixture at pressure values of 174, 1052, and 2000 psia at 130°F. The green rectangle marks the equilibrium compositions and chemical potentials when the equilibrium liquid phase is at 174 psia and the equilibrium gas phase is at 1,052 psia.

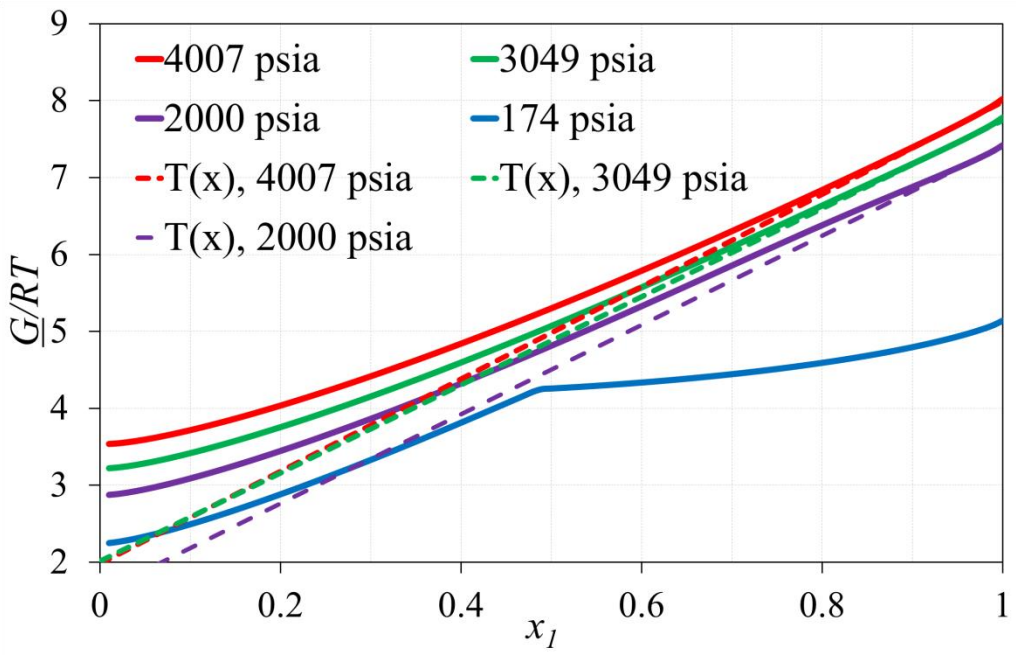

Figure 6-4: Dimensionless molar GFE of the hypothetical single-phase mixture of C_1-C_6 at 130°F at pressure values of 174, 2000, 3049, and 4007 psia. Three tangents lines that violate the extended TPD criteria of capillary equilibrium are also given.

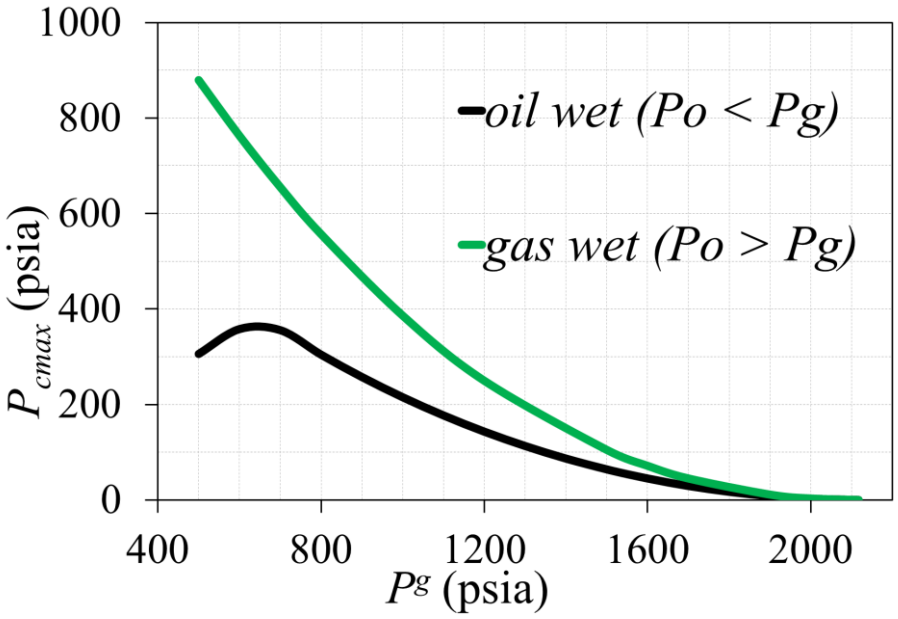

Figure 6-5: P_{cmax} versus P^g for the binary mixture of C_1-C_6 at 300°F.

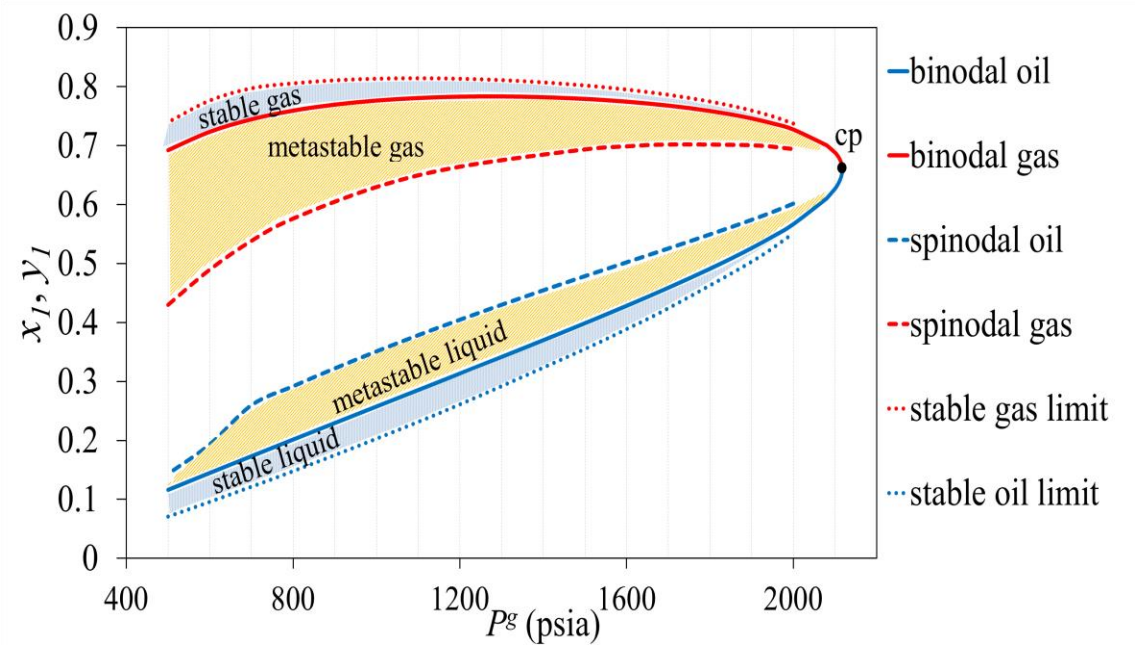

Figure 6-6: The equilibrium and spinodal compositions versus P^g for the binary mixture of C_1-C_6 at 300°F.

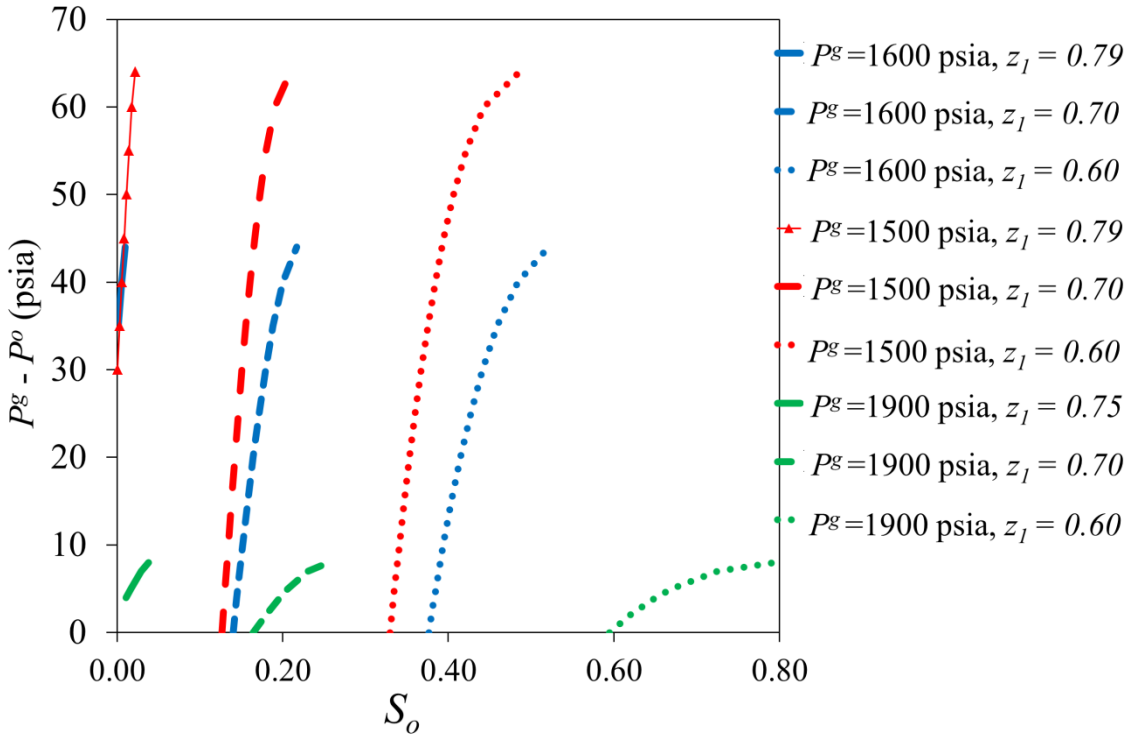

Figure 6-7: The physical saturation range for the entire possible capillary equilibrium range for several P^g and z_1 for the binary mixture of C_1-C_6 at 300°F.

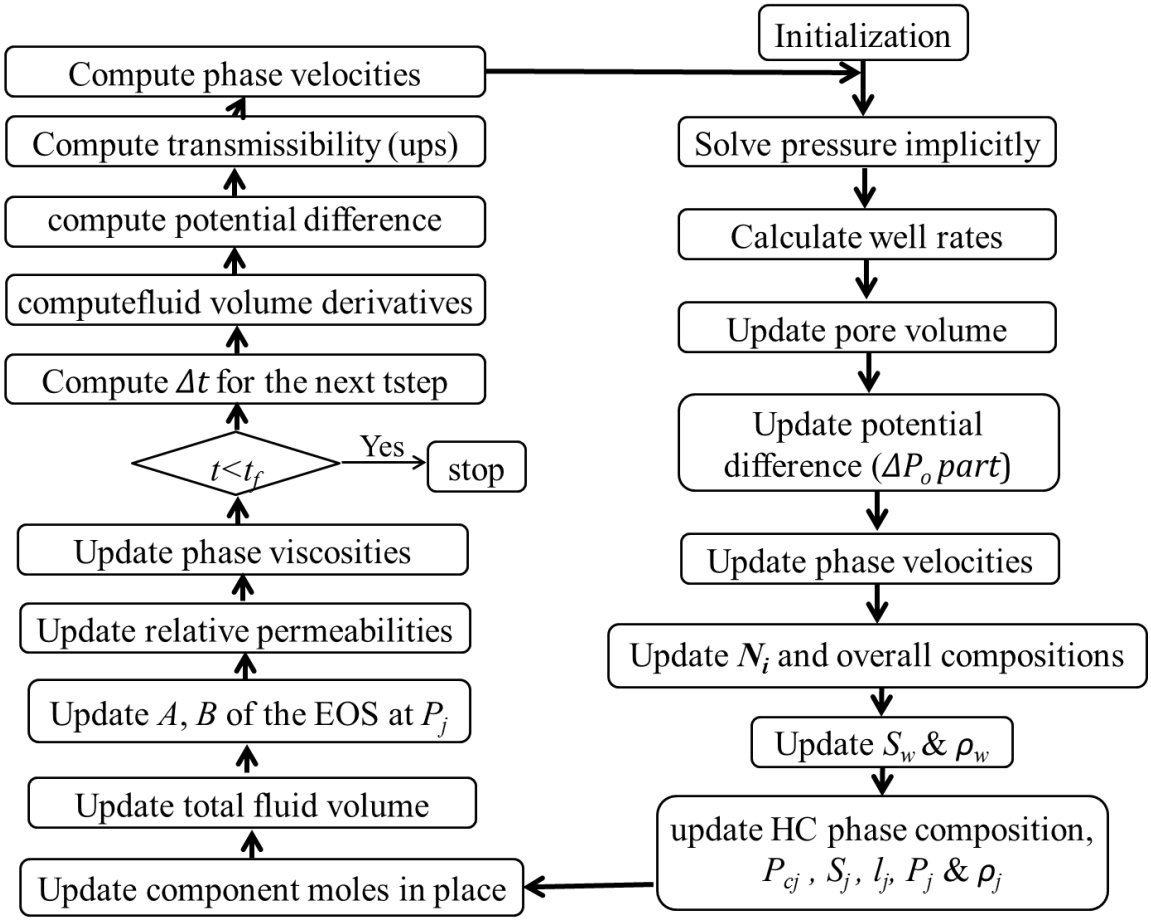

Figure 6-8: The overall computational procedure in the UTCOMP simulator after implementation of the effect of capillary pressure on phase behavior.

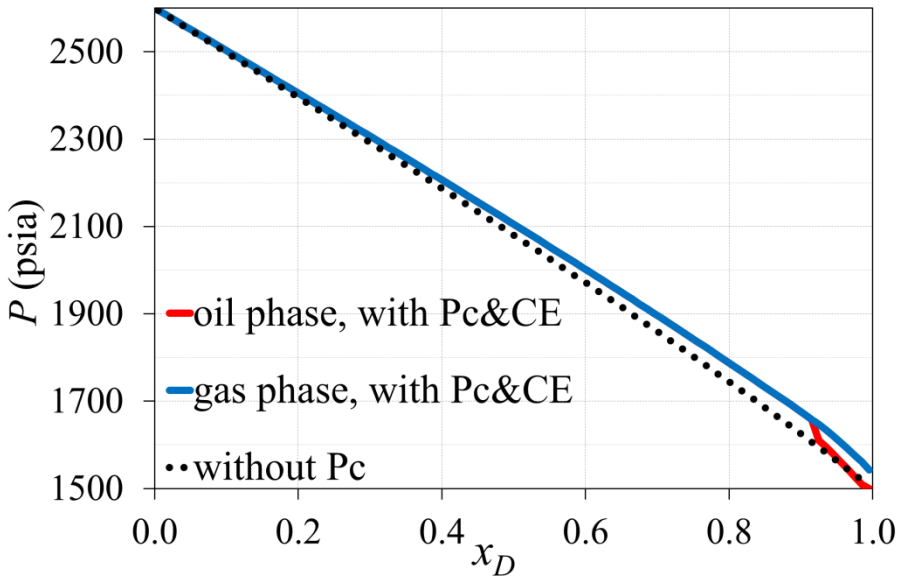

Figure 6-9: Pressure profiles of oil and gas phases for the simulation with P_c and CE at steady-state (100 days) and the pressure profile for the simulation without P_c at steady-state (100 days).

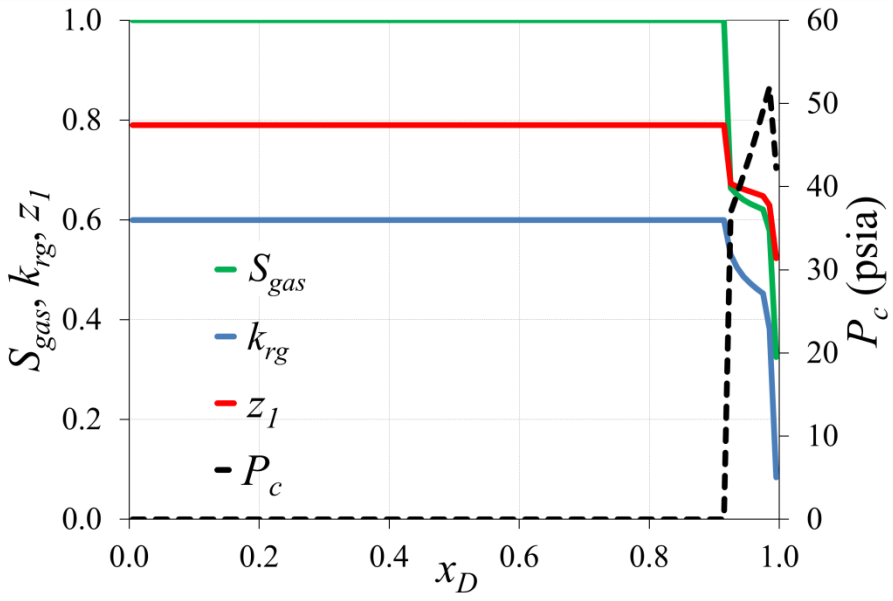

Figure 6-10: Profiles of gas saturation, gas relative permeability, overall mole fraction of C_1, and capillary pressure at steady state (100 days) for the simulation with the capillary pressure effect on phase behavior for the binary fluid C_1-C_6 at 300°F.

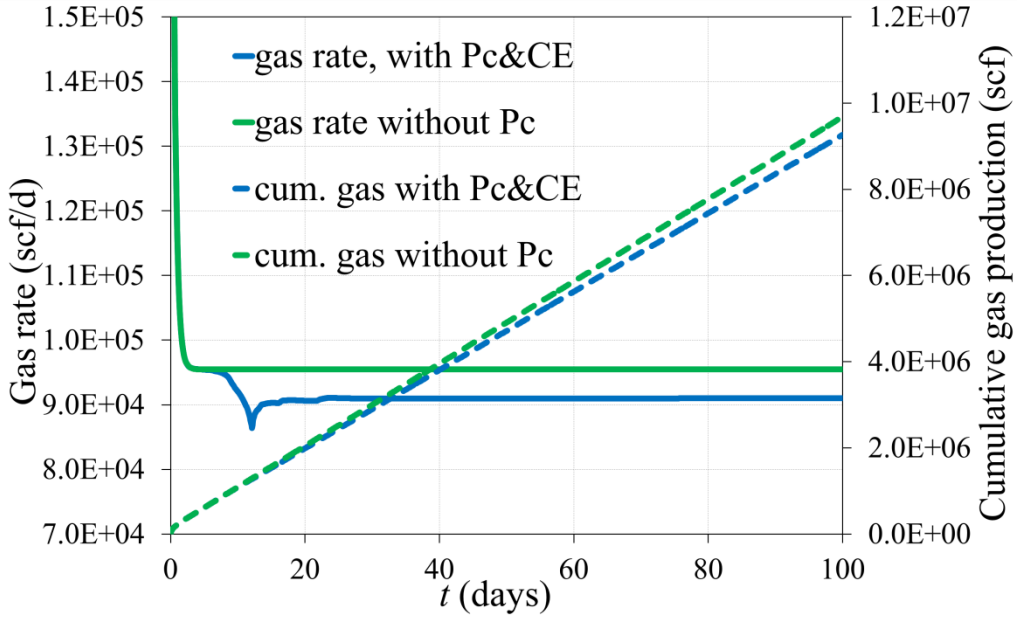

Figure 6-11: Gas production rate and cumulative gas production for the simulation with P_c and *CE* and the simulation without P_c.

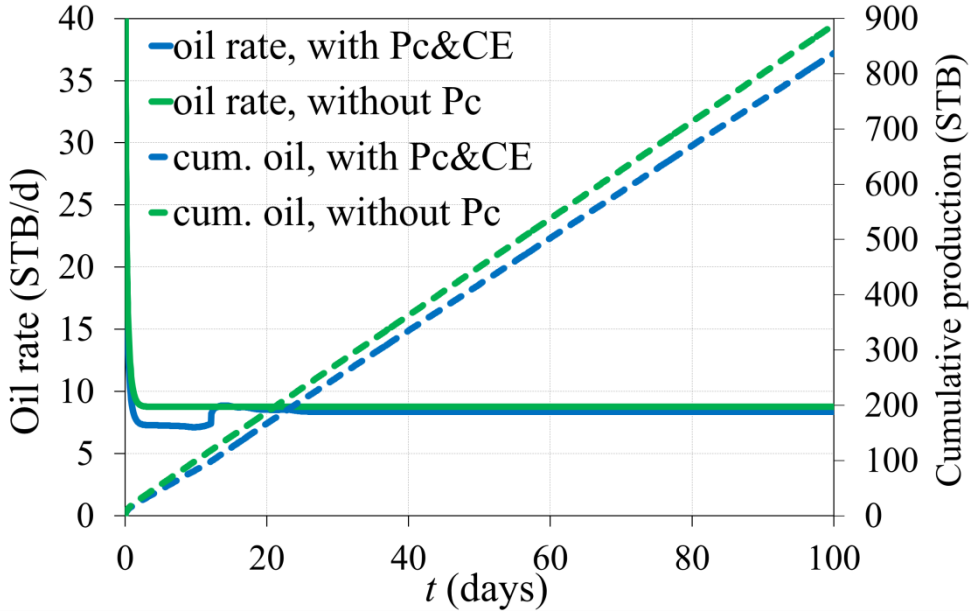

Figure 6-12: Oil production rate and cumulative oil production for the simulation with P_c and CE and the simulation without P_c.

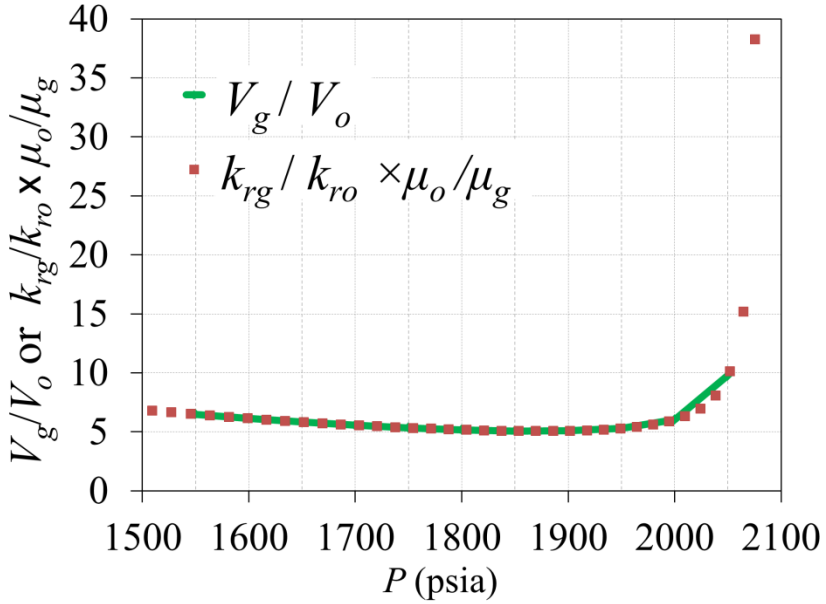

Figure 6-13: Ratio of gas to oil volume (V_g/ V_o) versus pressure from a CCE calculation and the ratio of two-phase-gridblocks' gas to oil mobility versus pressure at steady-state conditions (from the UTCOMP simulation without P_c).

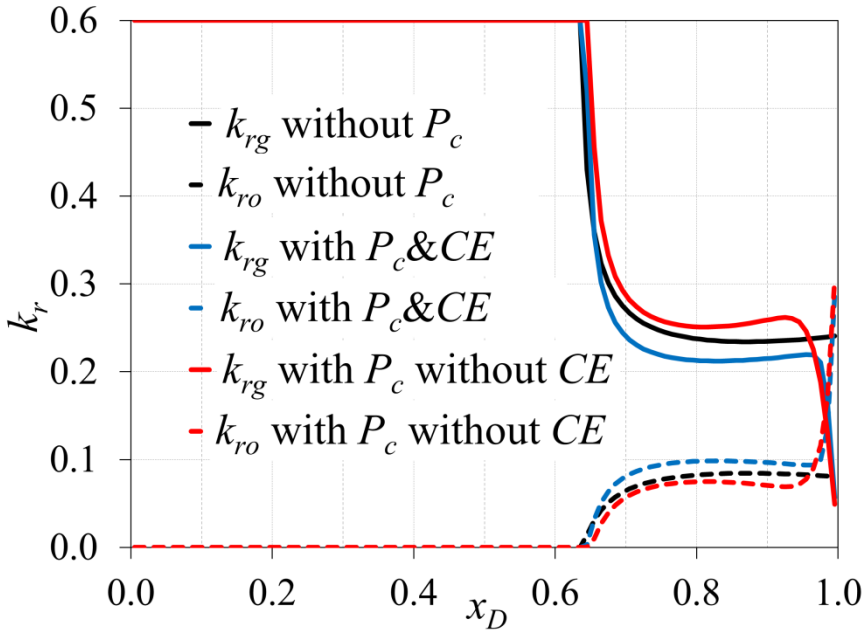

Figure 6-14: The gas and oil relative permeability profiles of the simulation without P_c, simulation with P_c and CE, and simulation with P_c without *CE* at steady-state.

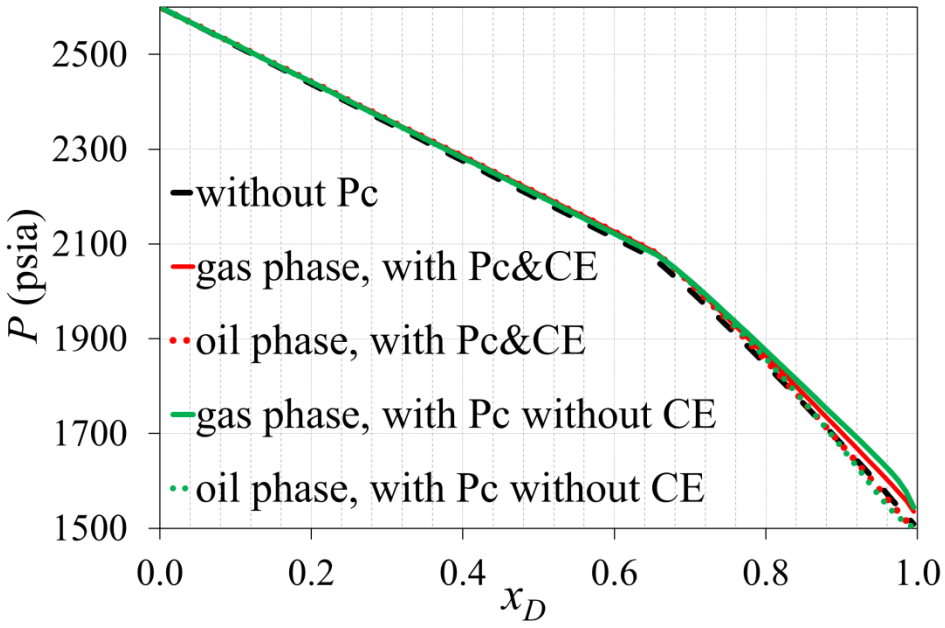

Figure 6-15: The oil and gas pressure profiles of the simulation with P_c and CE, and the simulation with P_c without CE, and the pressure profile of the simulation without P_c at steady state.

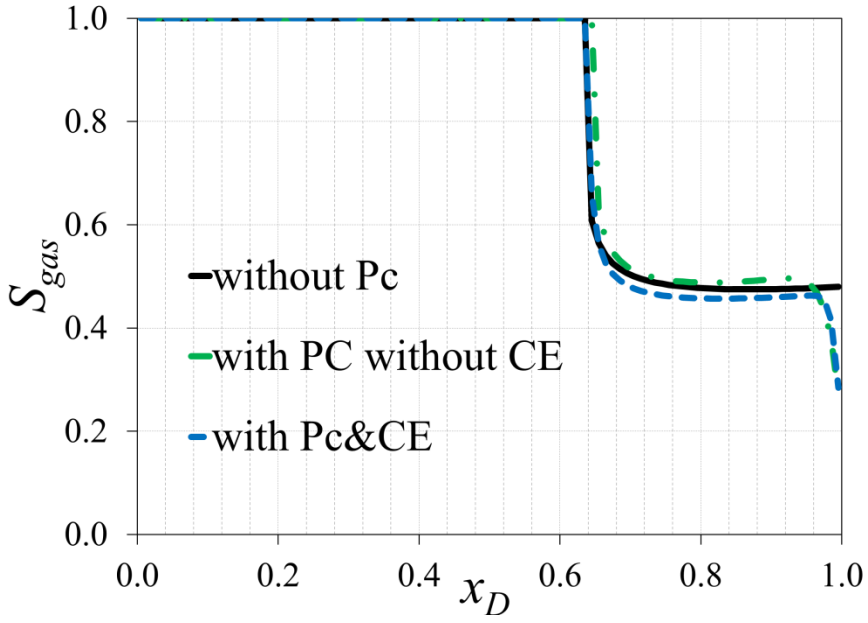

Figure 6-16: The gas saturation profile of the simulation with P_c and CE, simulation with P_c without CE, and simulation without P_c at steady-state.

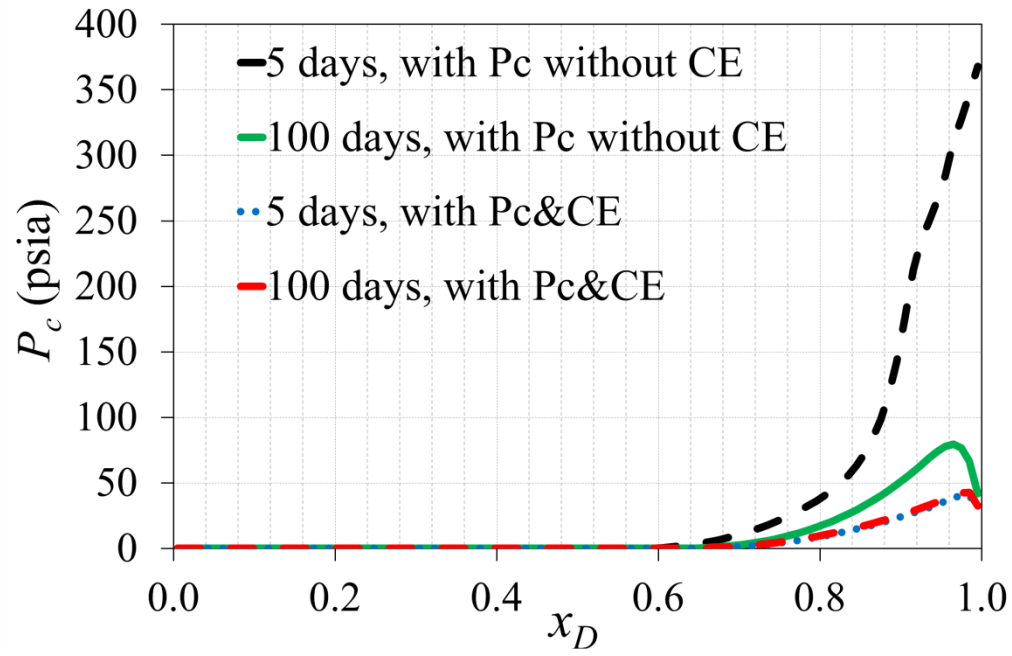

Figure 6-17: The capillary pressure profile of the simulations with P_c and CE and with P_c without CE at 5 days and 100 days (linear steady-state simulations).

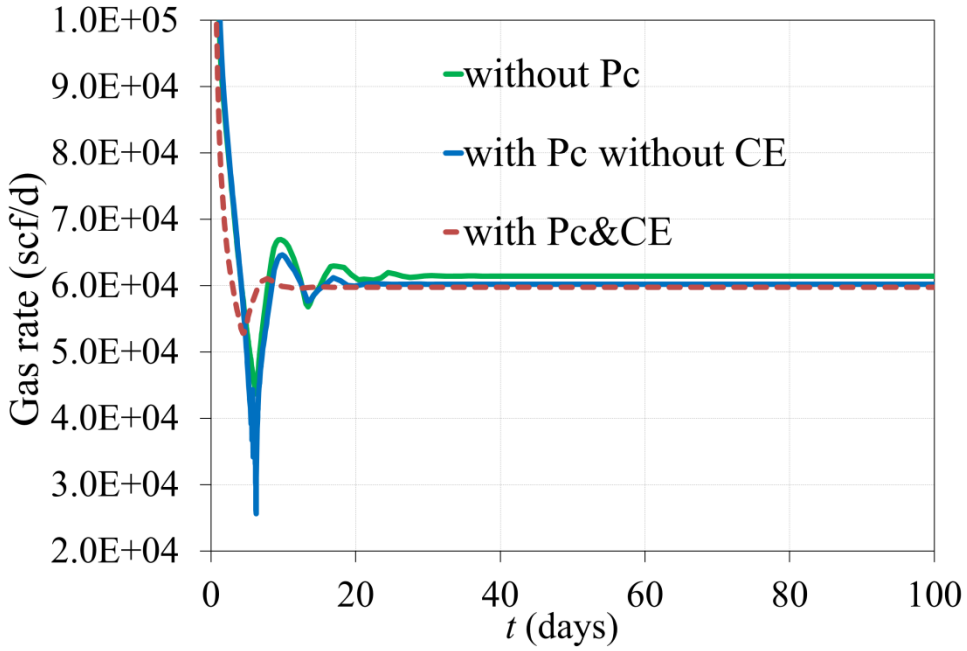

Figure 6-18: Gas production rate for the simulation with P_c and CE, the simulation with P_c without CE, and the simulation without P_c.

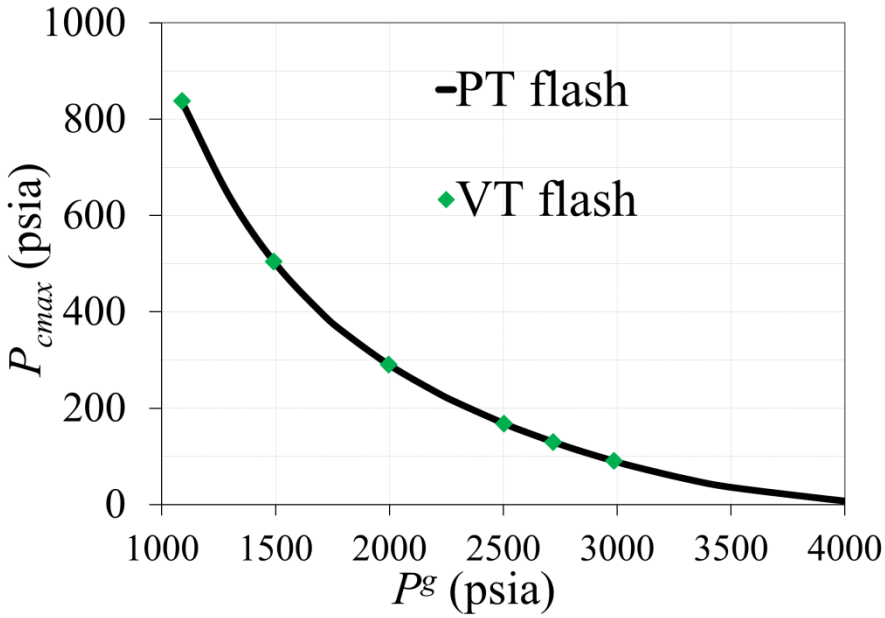

Figure 6-19: P_{cmax} for the initial reservoir fluid composition in Case 1 for an oil-wet system by use of *PT* and *VT* capillary equilibrium calculations.

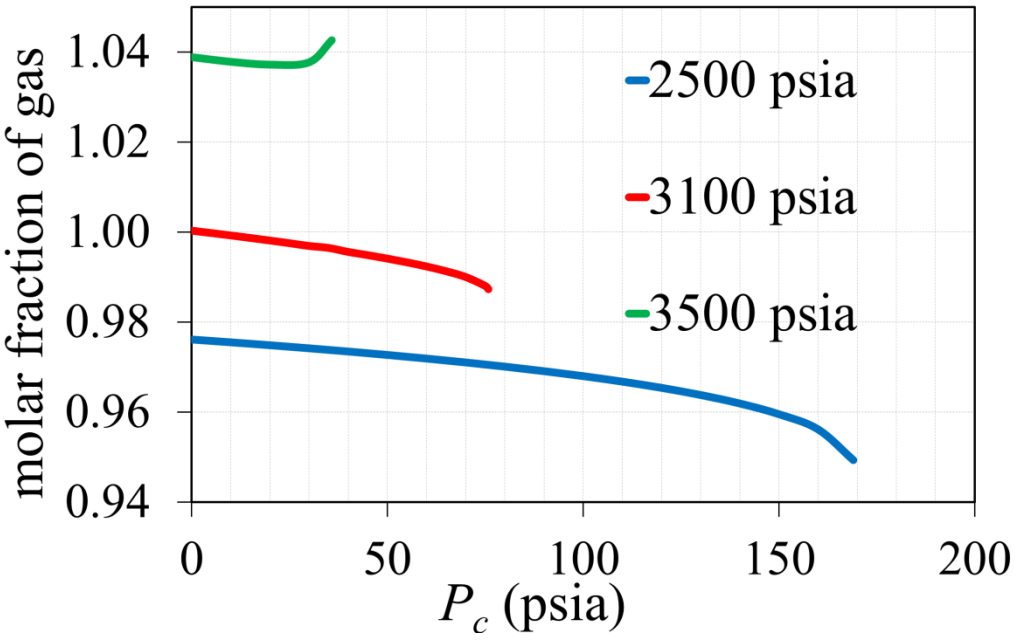

Figure 6-20: The molar fraction of gas phase versus capillary pressure for three different gas phase pressure values of 2500, 3100, and 3500 psia resulting from phase equilibrium calculations including capillary pressure effects.

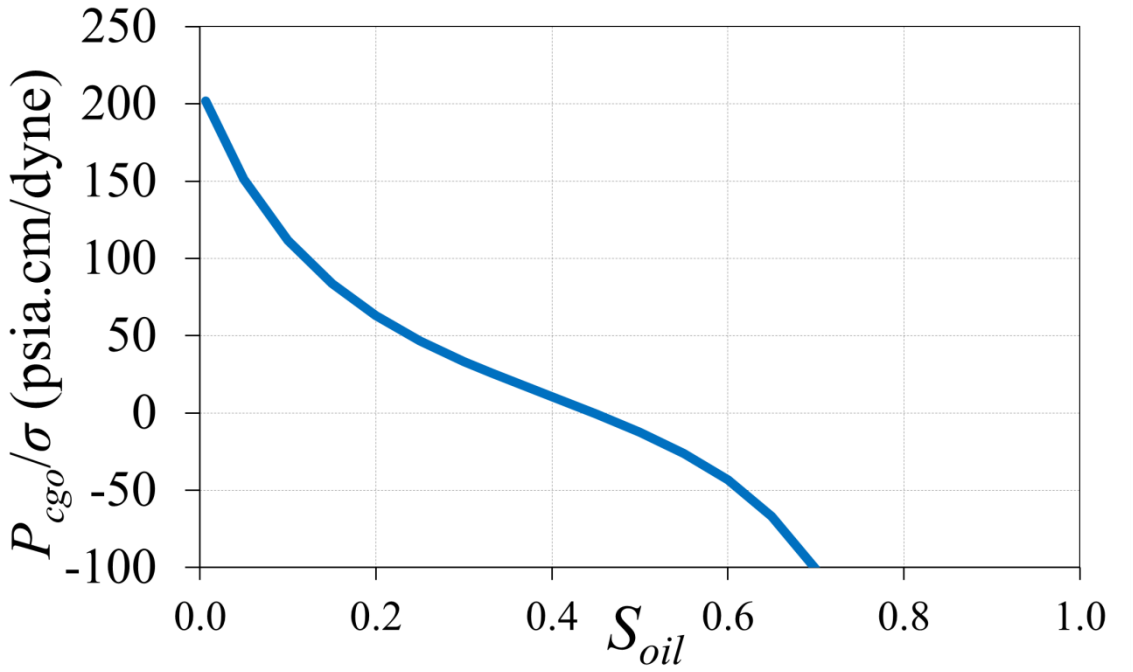

Figure 6-21: The gas/oil capillary pressure curve normalized by IFT for the simulations of Case 1.

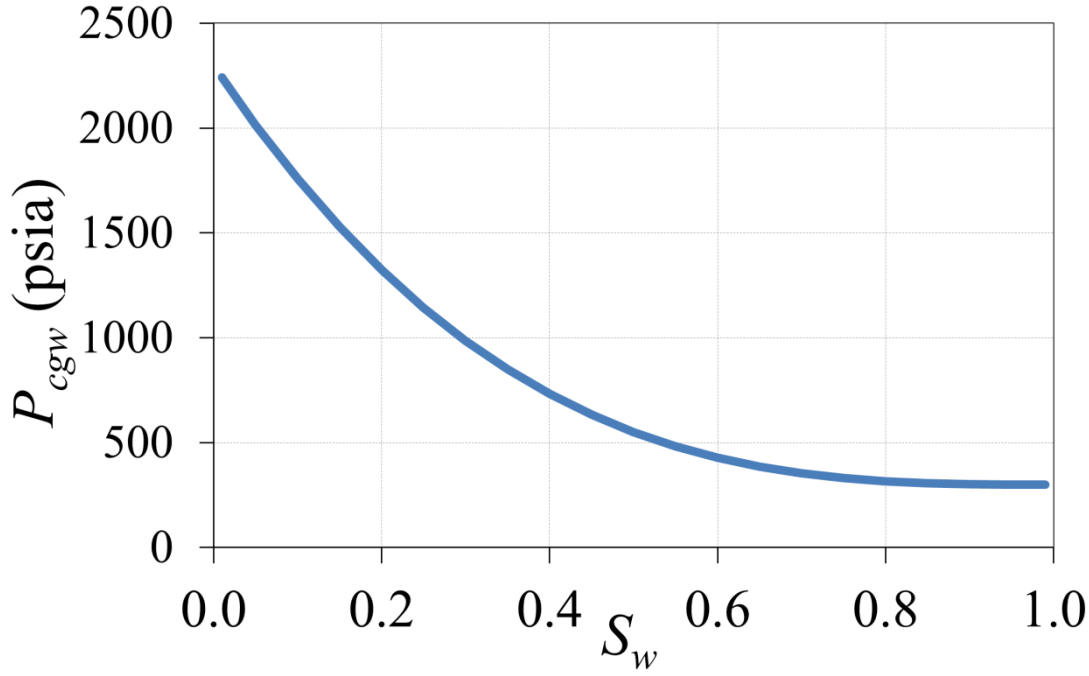

Figure 6-22: The gas/water capillary pressure curve for the simulations of Case 1.

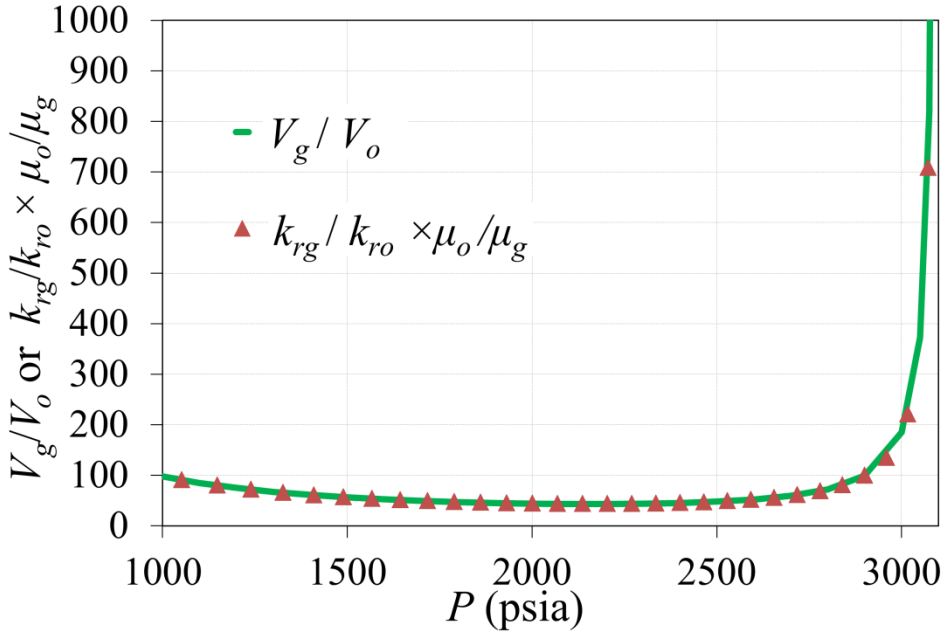

Figure 6-23: Ratio of gas to oil volume (V_g/V_o) versus pressure from a CCE calculation and the ratio of two-phase-gridblocks' gas to oil mobility versus pressure at steady-state conditions (from the UTCOMP simulation without P_c effects of Case 1).

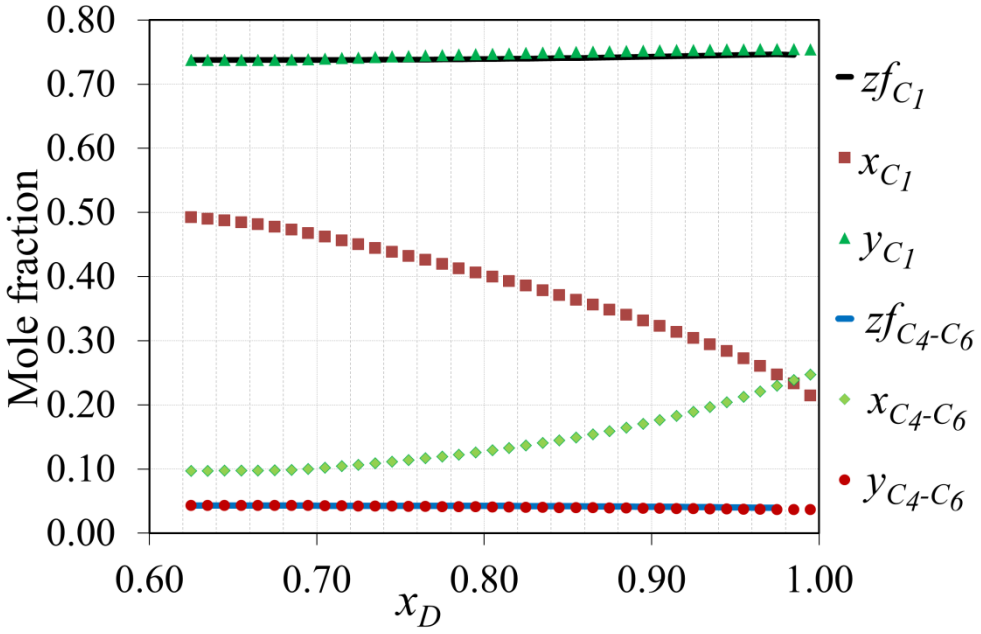

Figure 6-24: Profile of mole fraction of C_1 and C_4-C_6 in the flowing stream, the oil phase, and the gas phase at steady state for the simulations of linear model in Case 1.

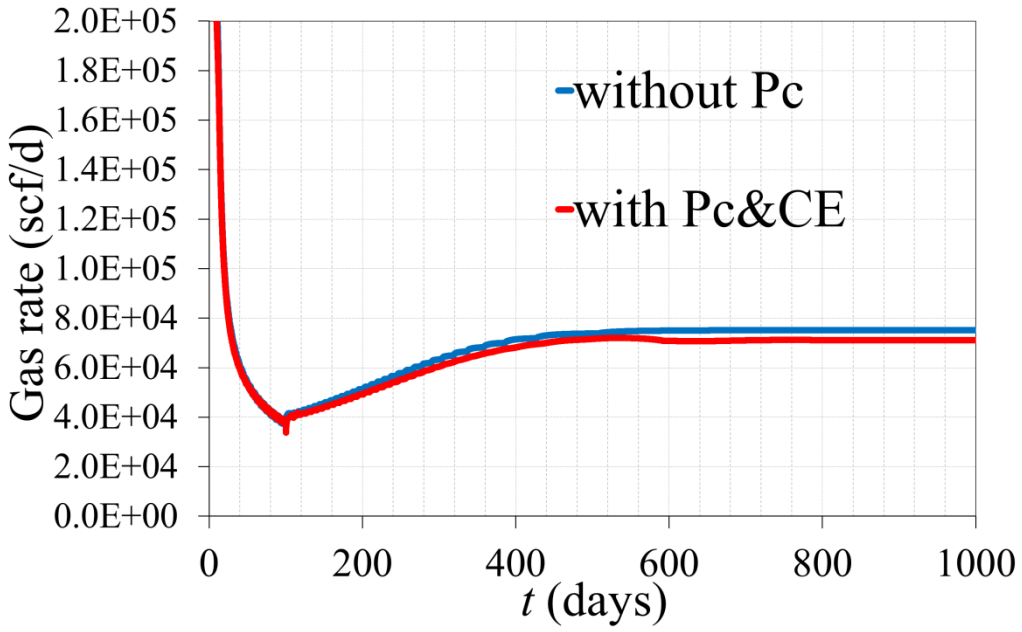

Figure 6-25: Gas production rate for the simulation with P_c and CE, and the simulation without P_c in the linear model (Case 1).

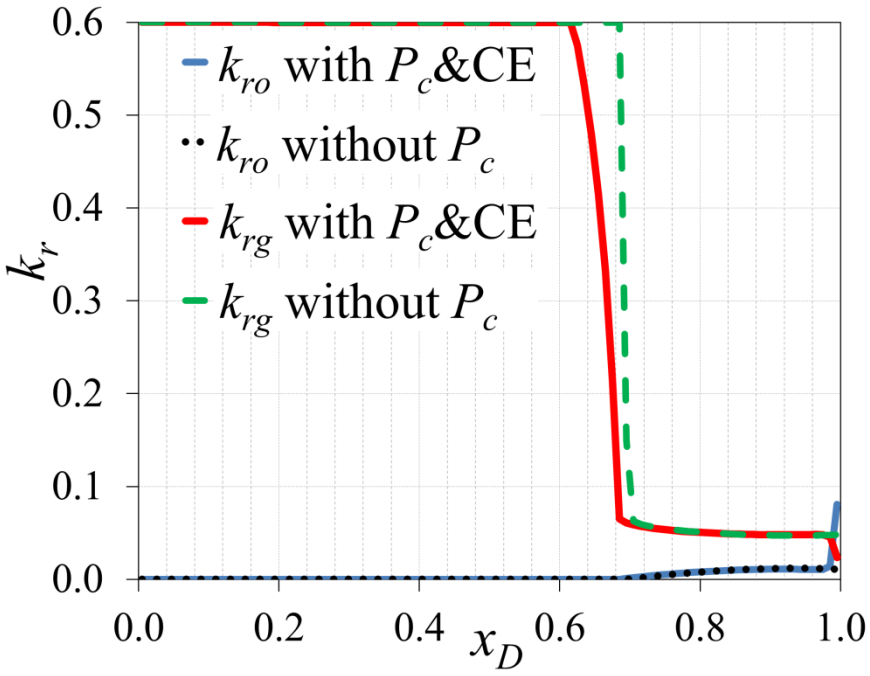

Figure 6-26: Steady-state relative permeability profiles for the simulation with P_c and CE, and the simulation without P_c (Case 1).

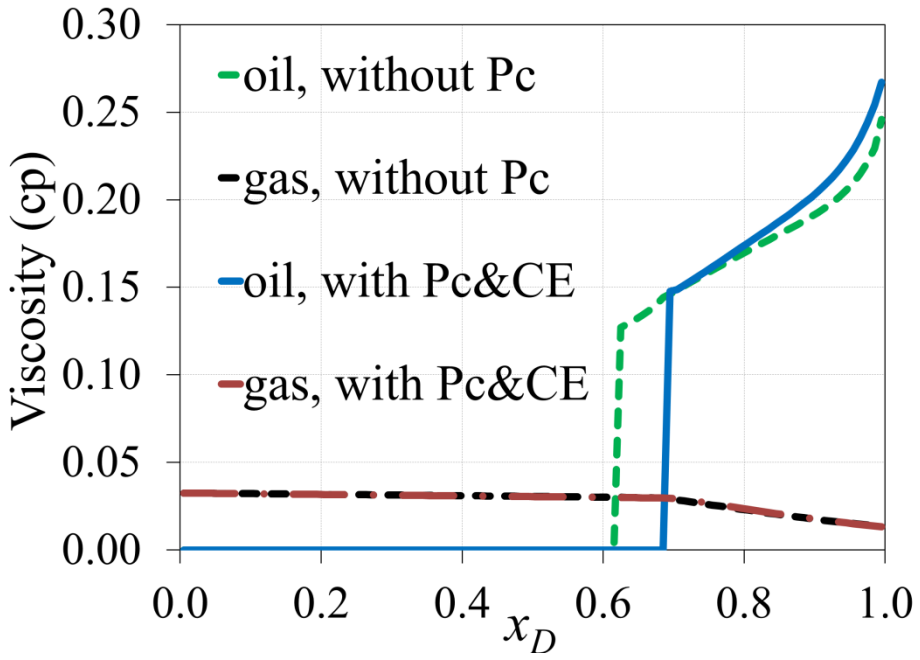

Figure 6-27: Profiles of oil and gas viscosity at steady-state for the simulation with P_c and CE, and the simulation without P_c (Case 1).

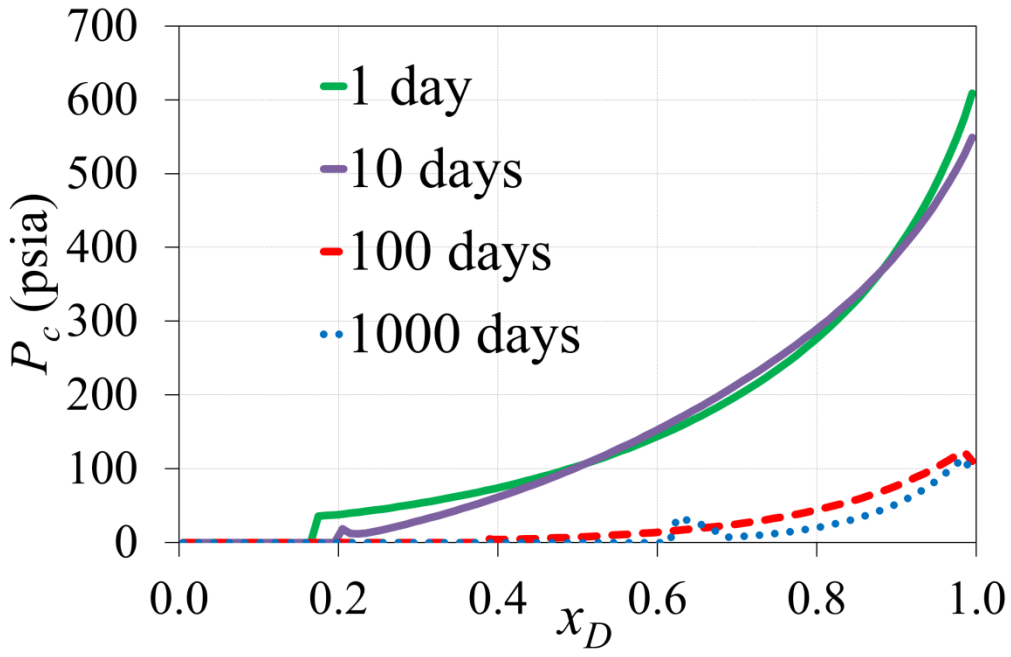

Figure 6-28: Capillary pressure profile for the simulation with P_c and CE in the linear model at 1, 10, 100 and 1000 days (Case 1).

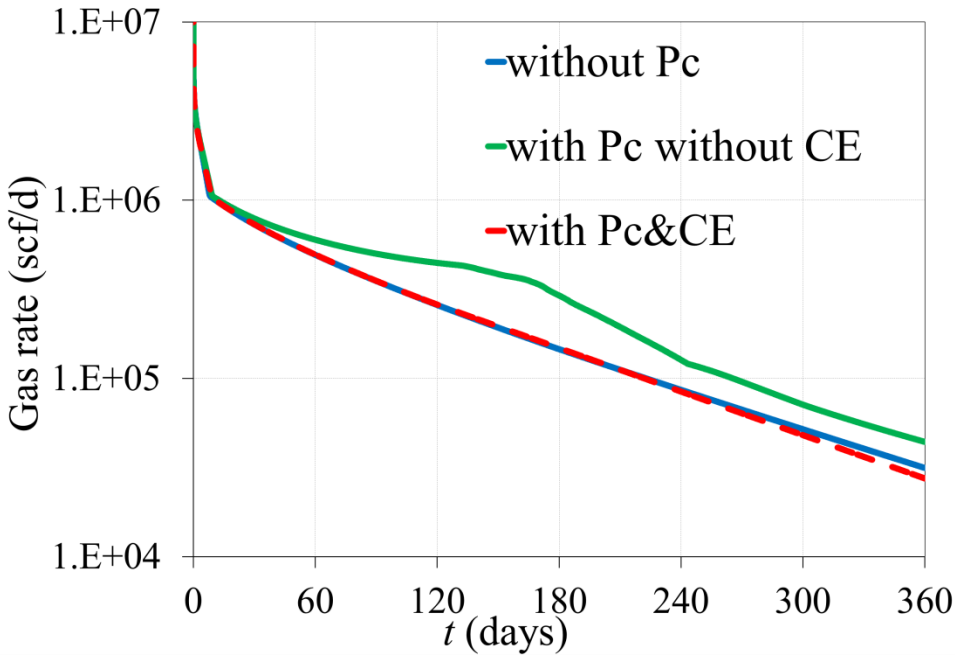

Figure 6-29: Gas production rate for the simulation with P_c and CE, the simulation with P_c without CE, and the simulation without P_c in the areal model (Case 1).

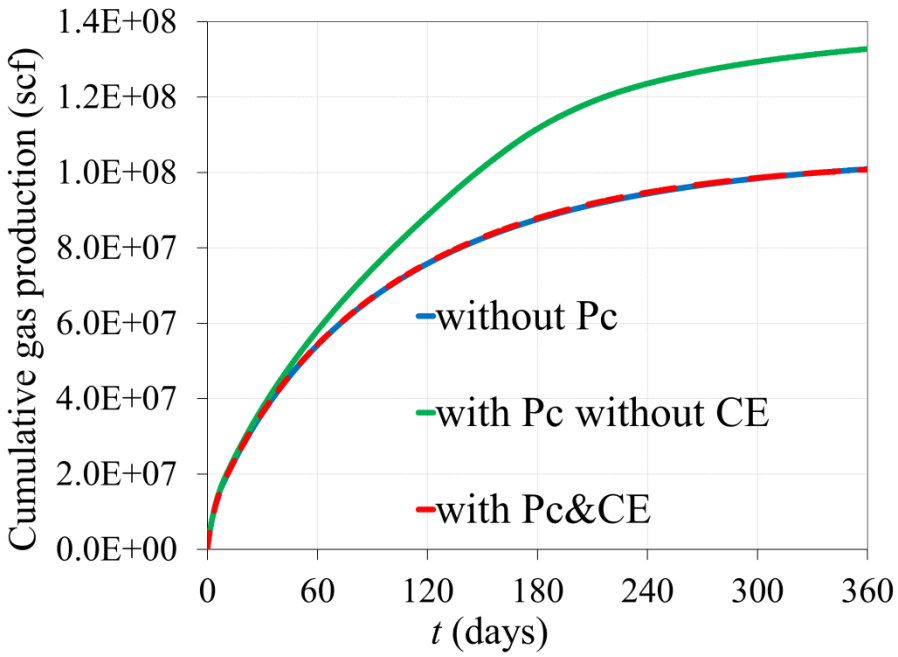

Figure 6-30: Cumulative gas production for the simulation with P_c and CE, the simulation with P_c without CE, and the simulation without P_c in the areal model (Case 1).

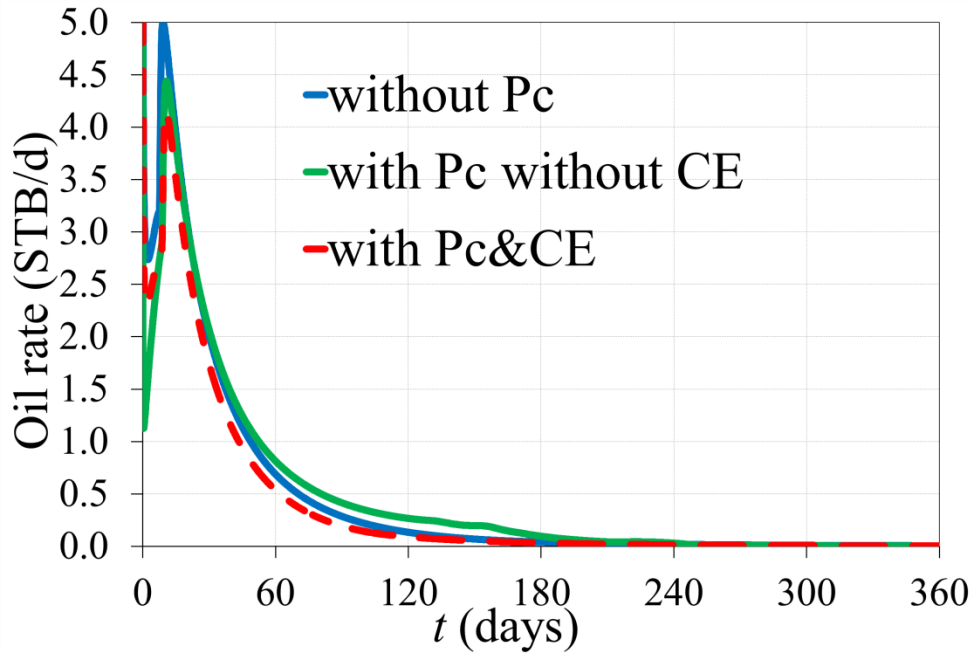

Figure 6-31: Oil production rate for the simulation with P_c and CE, the simulation with P_c without CE, and the simulation without P_c in the areal model (Case 1).

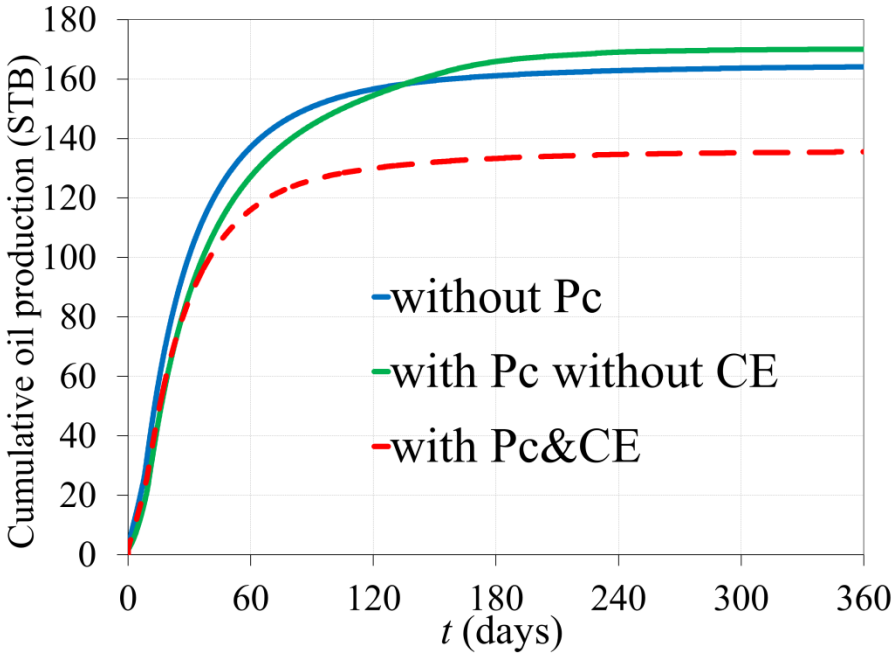

Figure 6-32: Cumulative oil production for the simulation with P_c and CE, the simulation with P_c without CE, and the simulation without P_c in the areal model (Case 1).

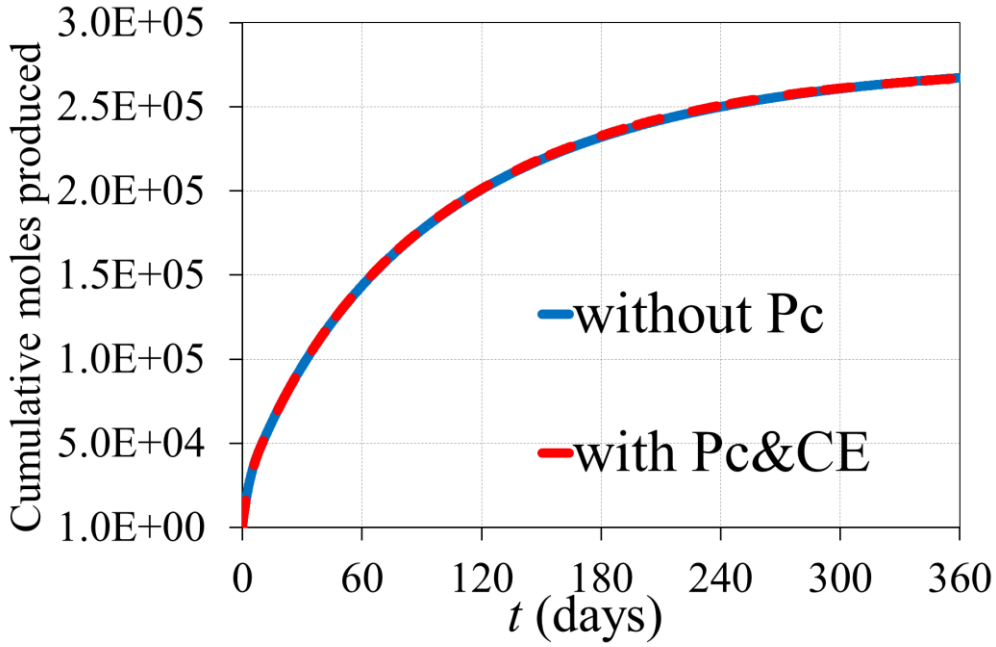

Figure 6-33: Cumulative hydrocarbon moles produced in oil and gas phases in the simulation with P_c and CE and the simulation without P_c in the areal model (Case 1).

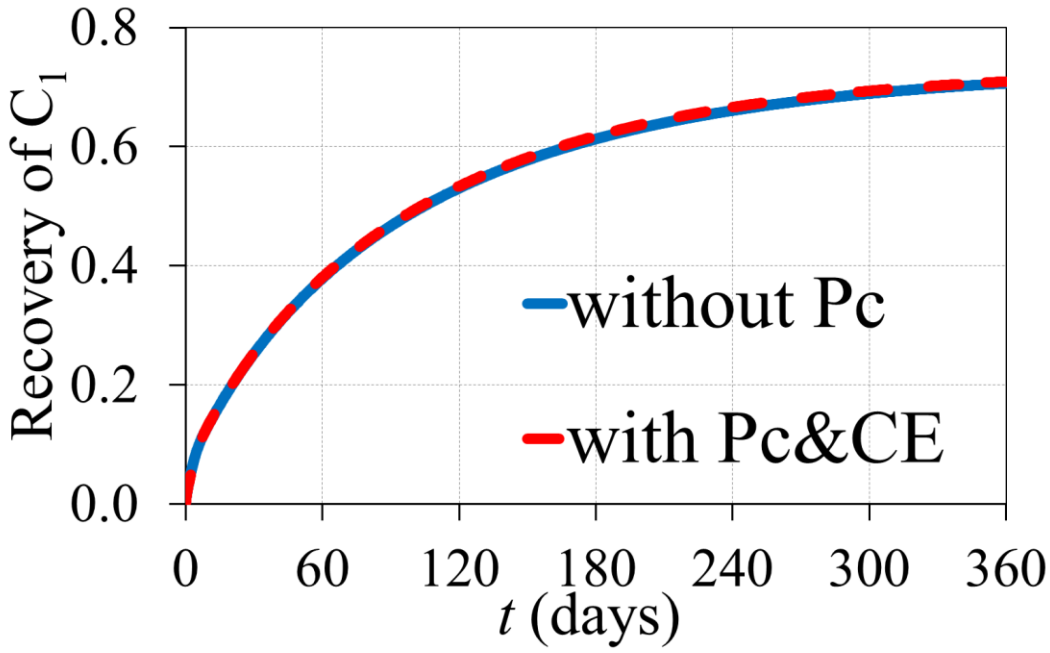

Figure 6-34: Recovery of C_1 versus time in the simulation with P_c and CE and the simulation without P_c in the areal model (Case 1).

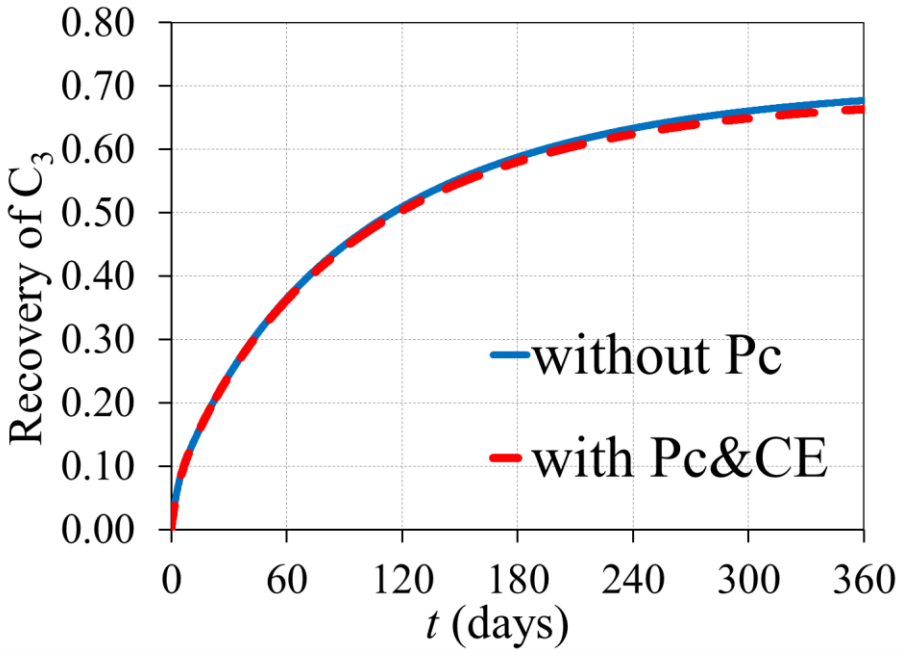

Figure 6-35: Recovery of C_3 versus time in the simulation with P_c and CE and the simulation without P_c in the areal model (Case 1).

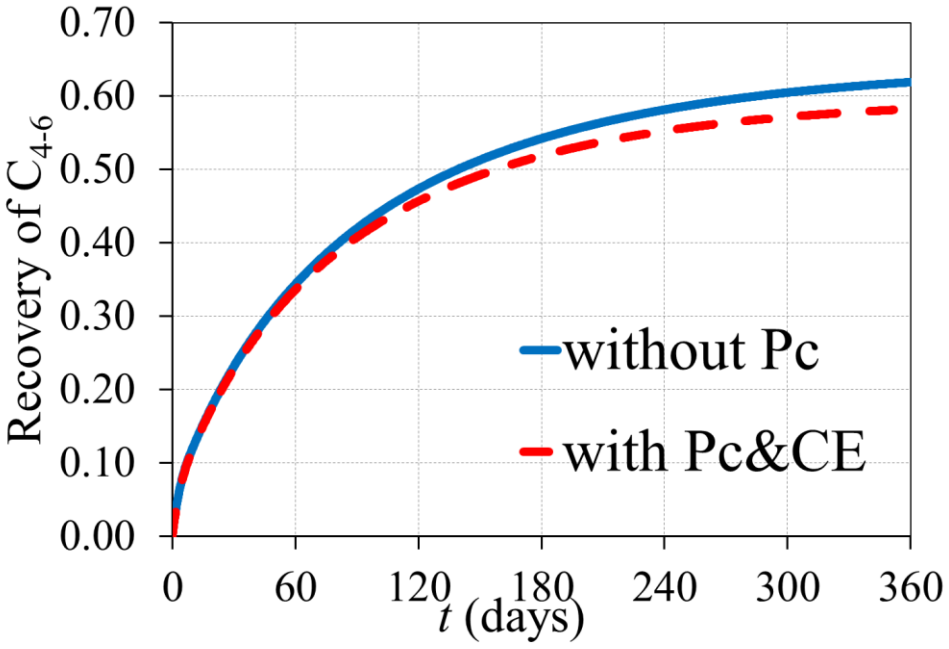

Figure 6-36: Recovery of C_{4-6} versus time in the simulation with P_c and CE and the simulation without P_c in the areal model (Case 1).

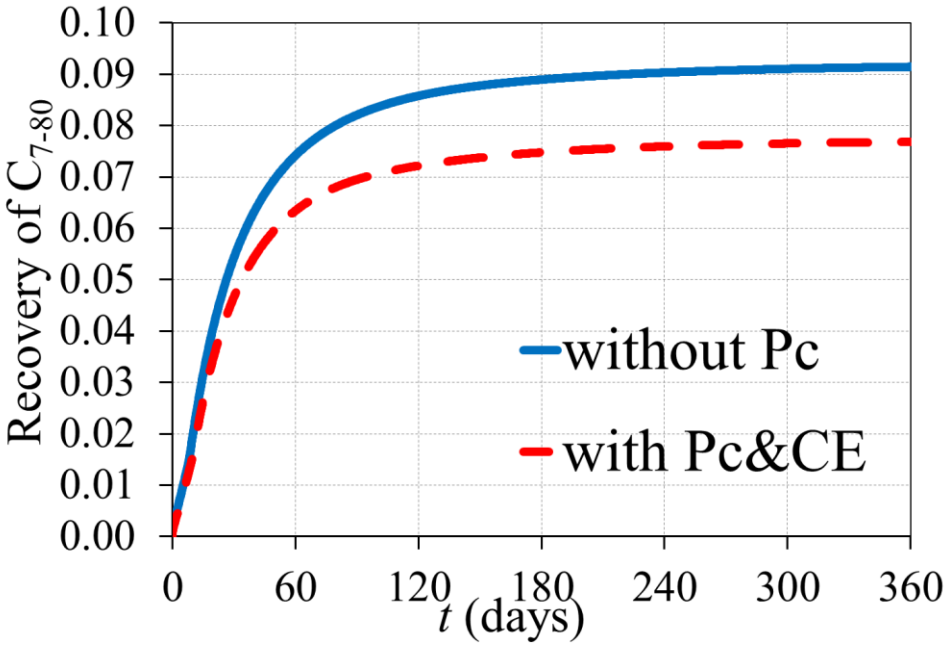

Figure 6-37: Recovery of $C_{7\text{-}80}$ versus time in the simulation with P_c and CE and the simulation without P_c in the areal model (Case 1).

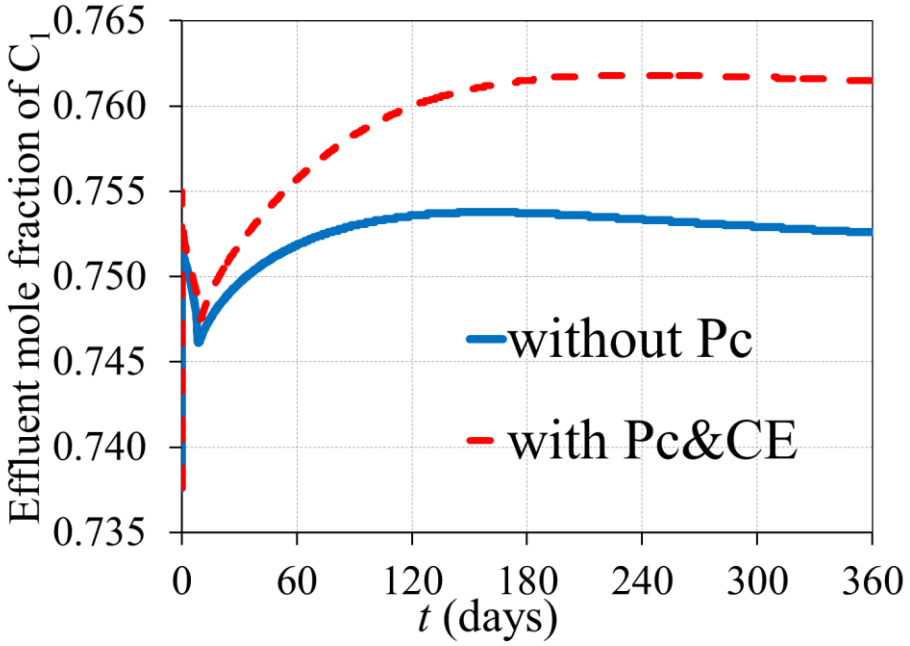

Figure 6-38: Effluent mole fraction of C_1 versus time in the simulation with P_c and CE and the simulation without P_c in the areal model (Case 1).

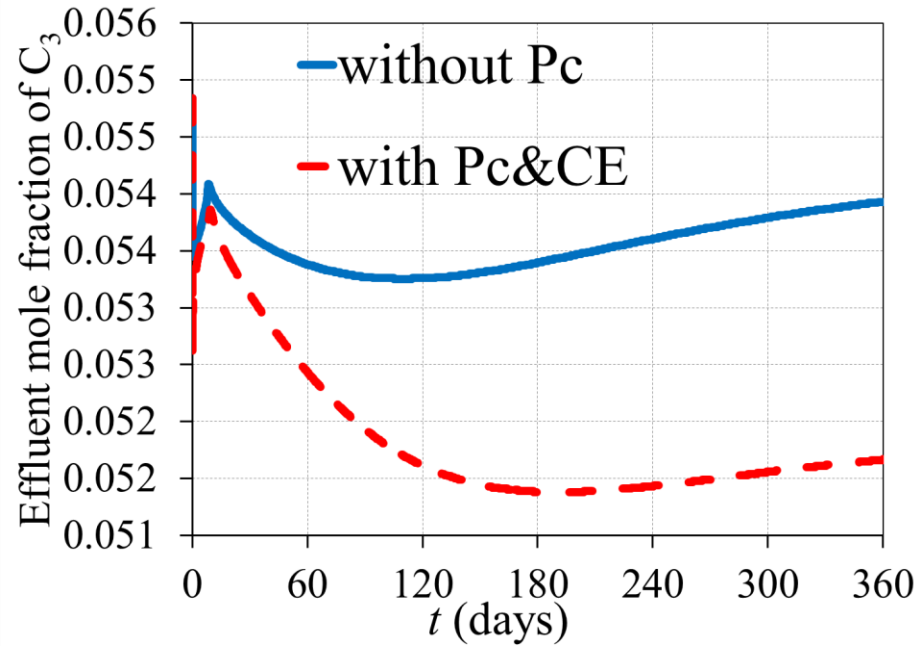

Figure 6-39: Effluent mole fraction of C_3 versus time in the simulation with P_c and CE and the simulation without P_c in the areal model (Case 1).

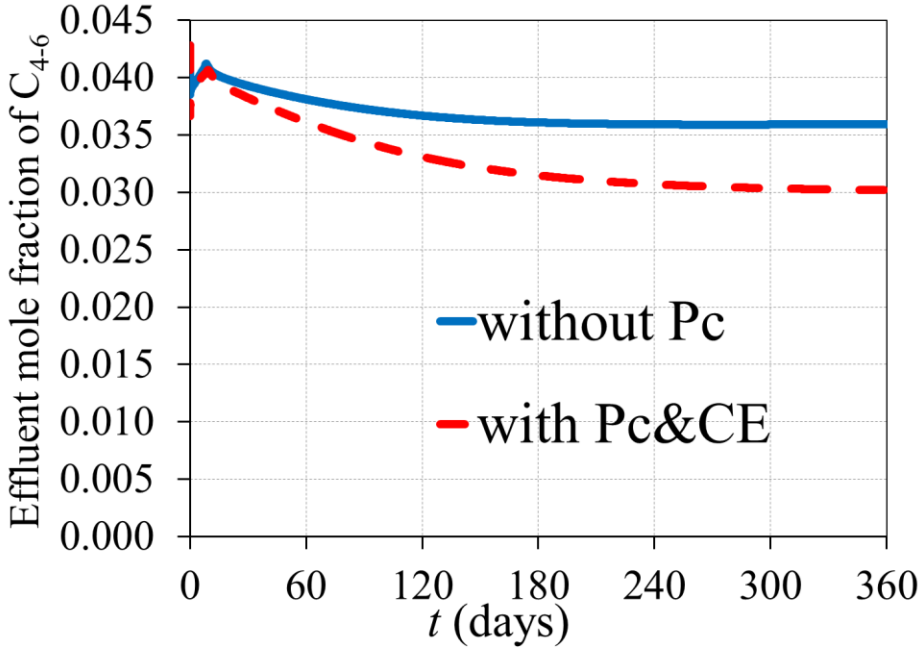

Figure 6-40: Effluent mole fraction of C_{4-6} versus time in the simulation with P_c and CE and the simulation without P_c in the areal model (Case 1).

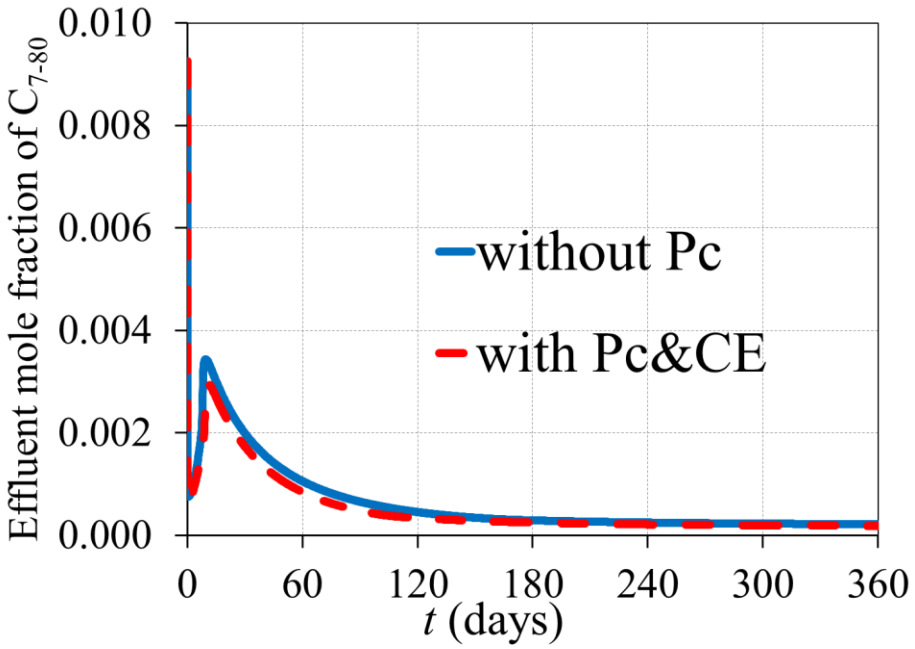

Figure 6-41: Effluent mole fraction of C_{7-80} versus time in the simulation with P_c and CE and the simulation without P_c in the areal model (Case 1).

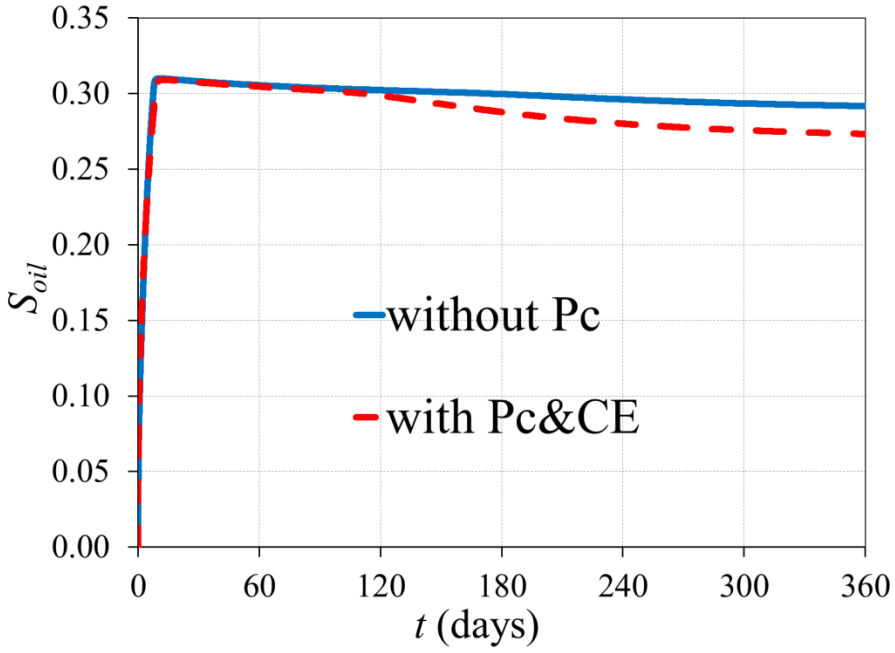

Figure 6-42: Oil saturation versus time in the well gridblock in the simulation with P_c and CE and in the simulation without P_c in the areal model (Case 1).

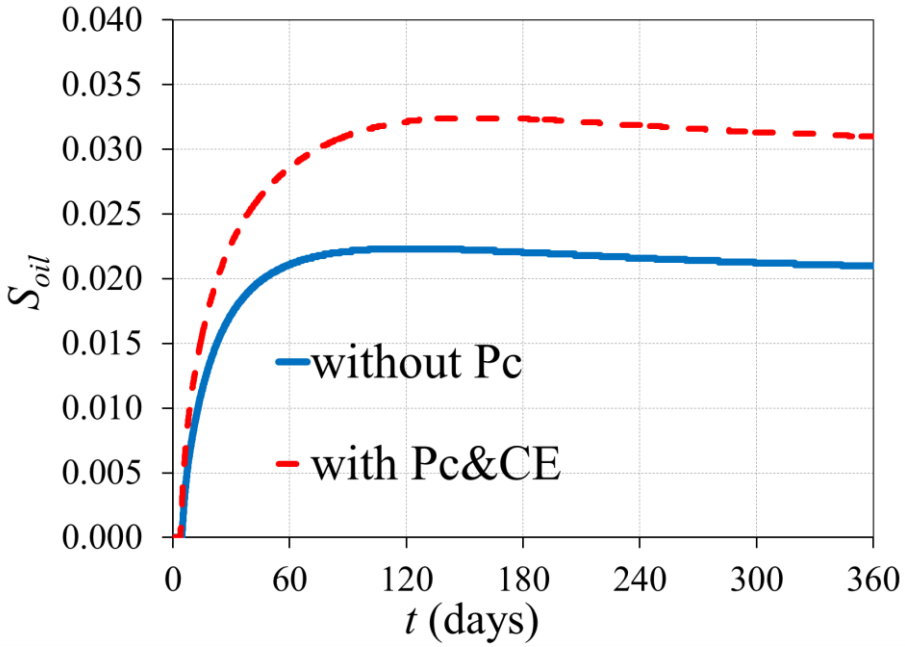

Figure 6-43: Oil saturation versus time in the middle of the reservoir in the simulation with P_c and CE and in the simulation without P_c in the areal model (Case 1).

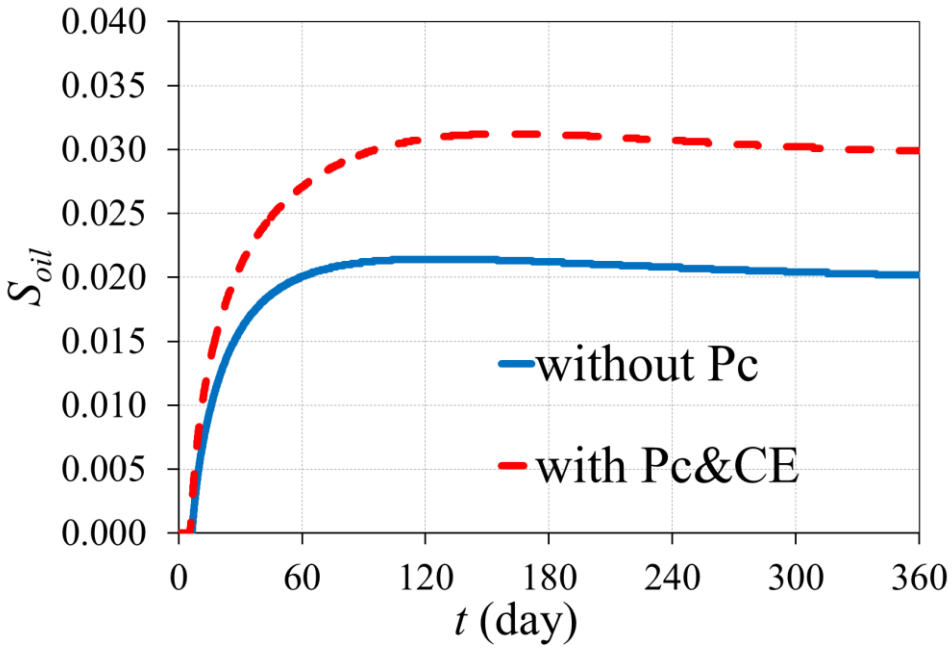

Figure 6-44: Oil saturation versus time in the gridblock at the end of the reservoir in the simulation with P_c and CE and in the simulation without P_c in the areal model (Case 1).

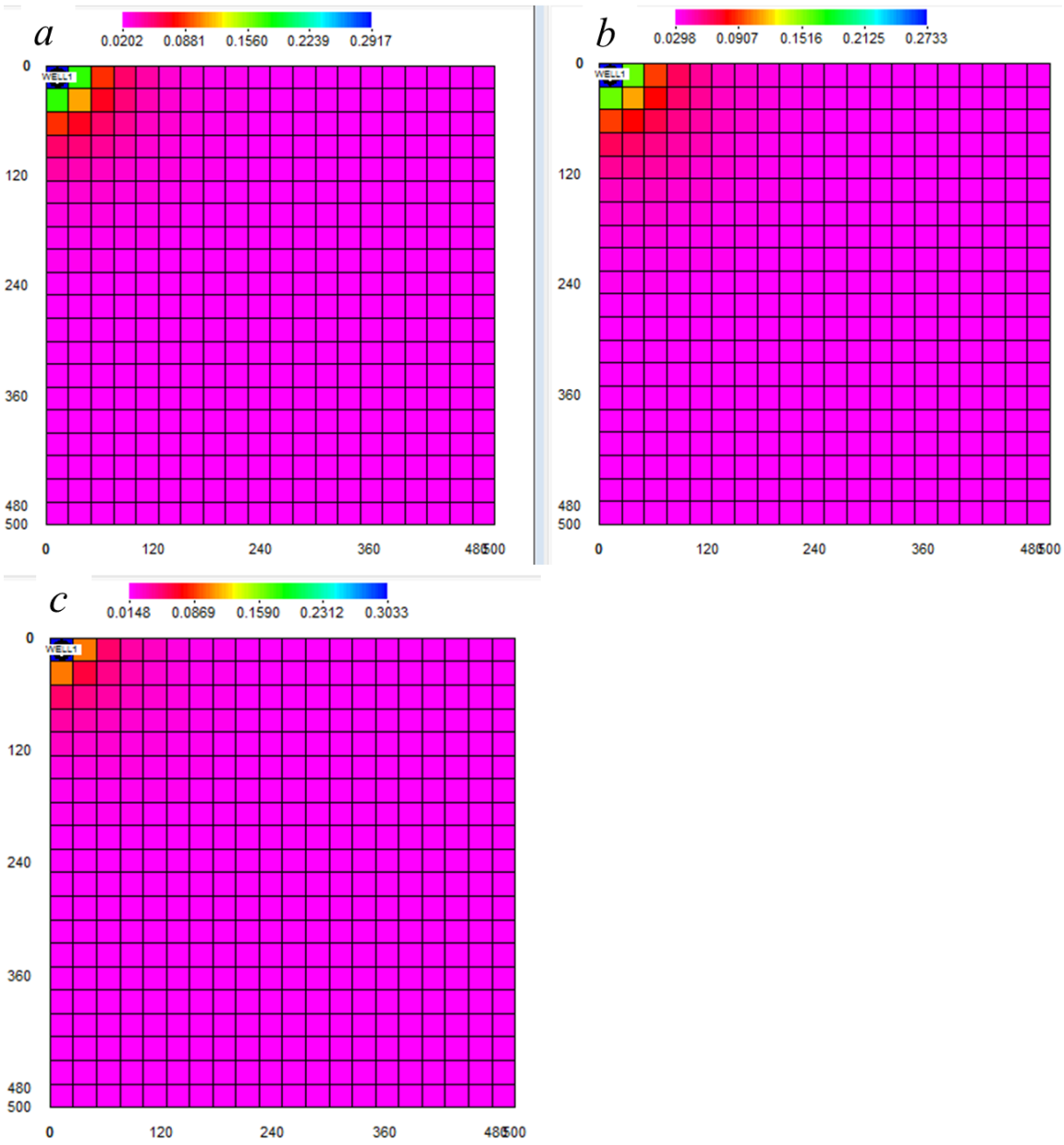

Figure 6-45: Oil saturation profile of the simulation without P_c (*a*), the simulation with P_c and CE (*b*), and the simulation with P_c without CE (*c*) at 360 days for the areal model (Case 1). The producer is in the gridblock at the upper-left corner of the model.

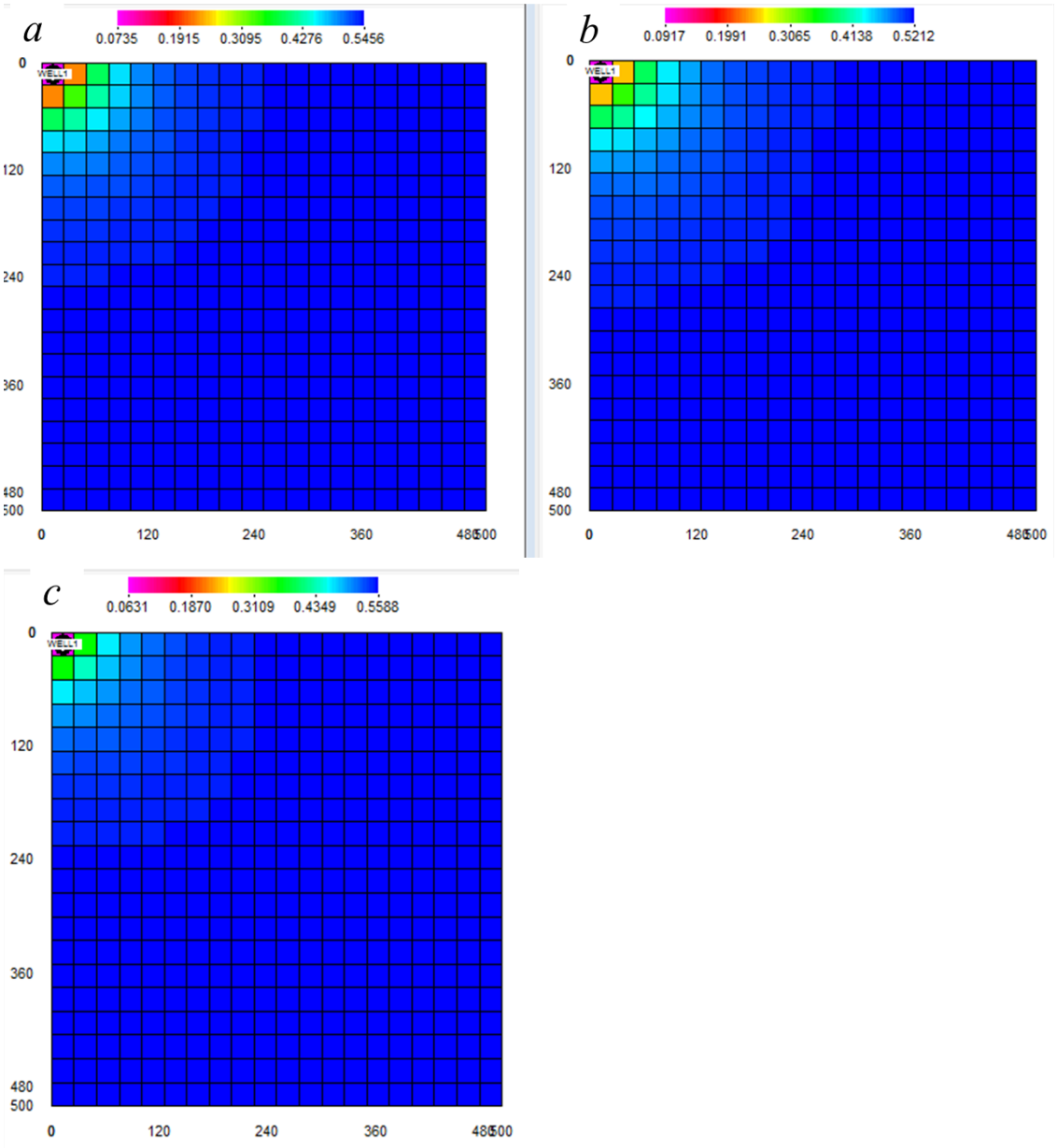

Figure 6-46: Profiles of gas relative permeability of the simulation without P_c (*a*), the simulation with P_c and CE (*b*), and the simulation with P_c without CE (*c*) at 360 days for the areal model (Case 1). The producer is in the gridblock at the upper-left corner of the model.

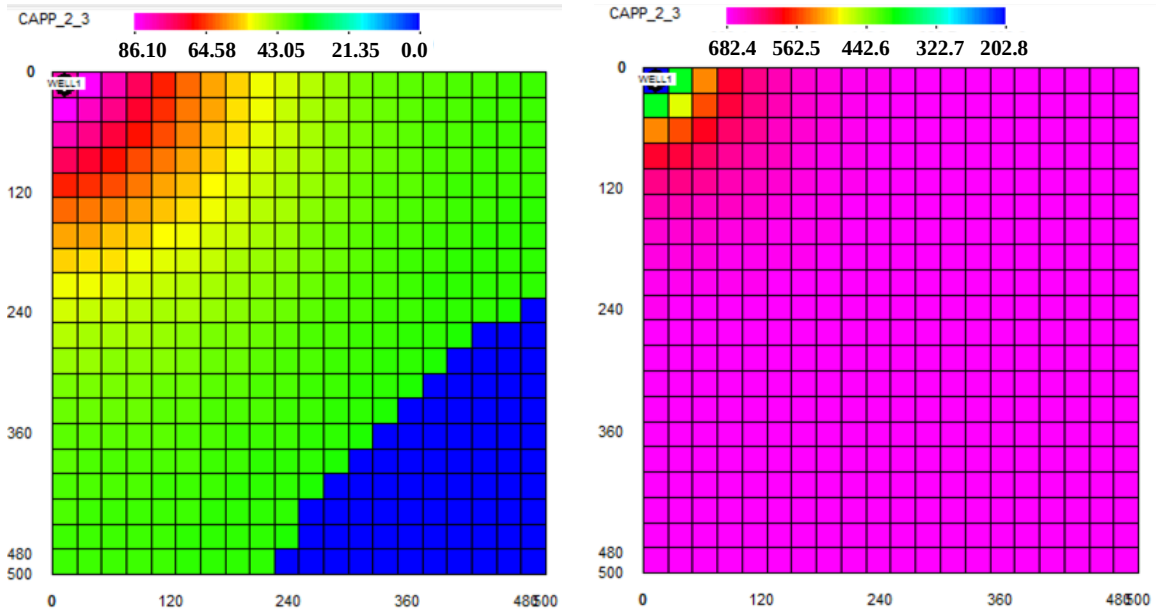

Figure 6-47: Capillary pressure profile of the simulation with P_c and CE at 5 days (left) and 360 days (right) for the areal model (Case 1). The producer is in the gridblock at the upper-left corner of the model.

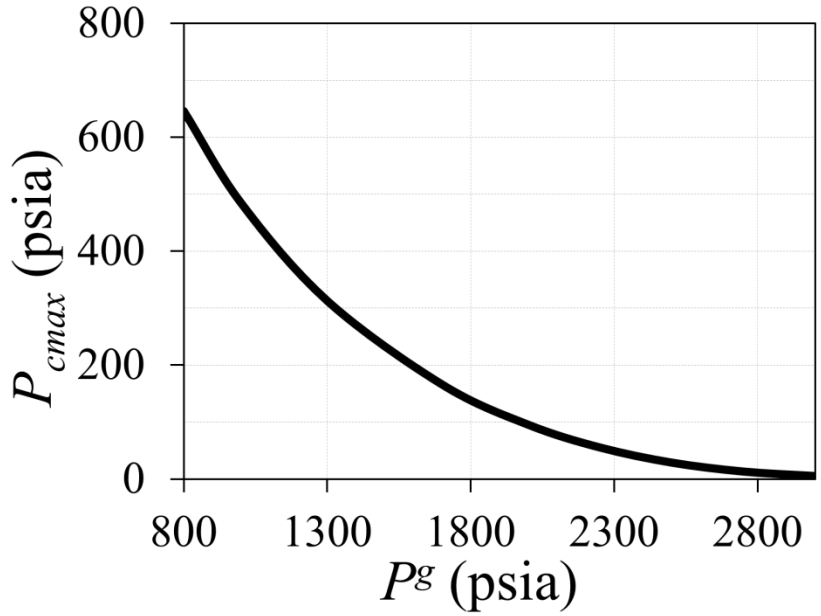

Figure 6-48: P_{cmax} versus gas-phase's pressure for the Hatter's Pond initial fluid at 450°F.

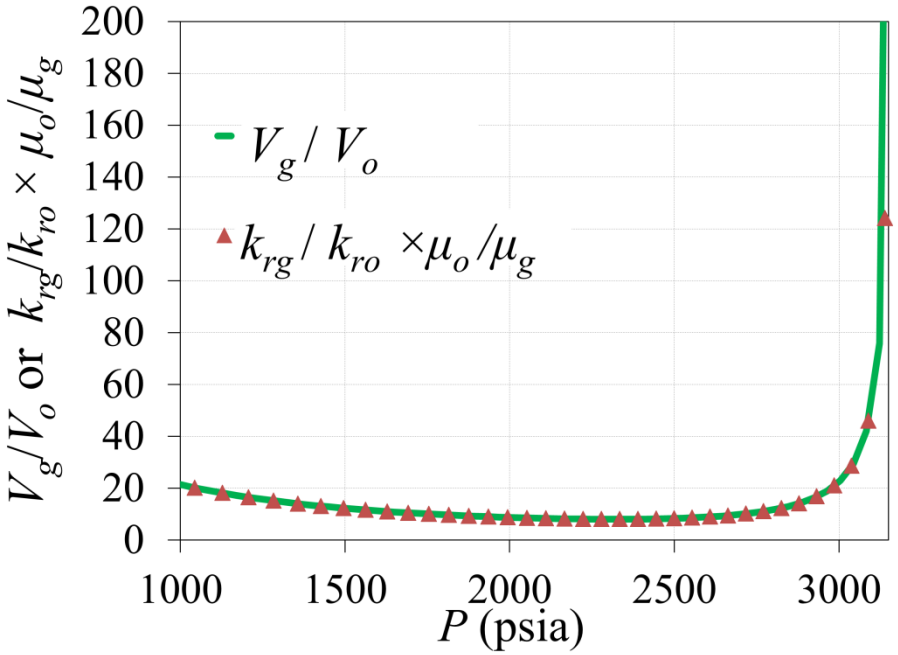

Figure 6-49: Ratio of gas to oil volume (V_g/V_o) versus pressure from a CCE calculation and the ratio of two-phase-gridblocks' gas to oil mobility versus pressure at steady-state conditions for the linear model in Case 2 (from the UTCOMP simulation without P_c effects).

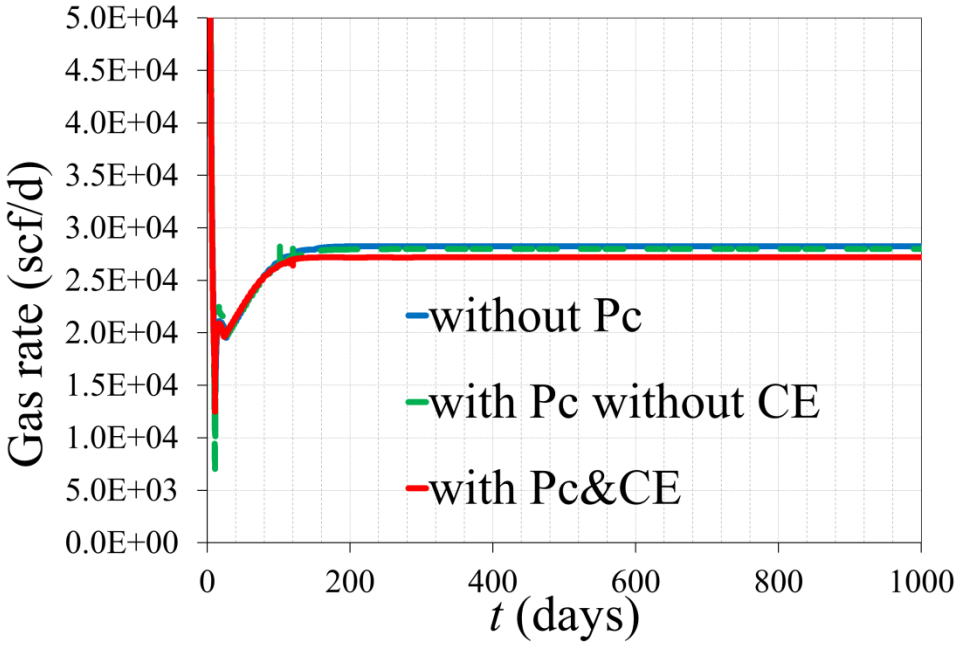

Figure 6-50: Gas production rate for the simulation with P_c and CE, the simulation with P_c without CE, and the simulation without P_c in the linear model (Case 2).

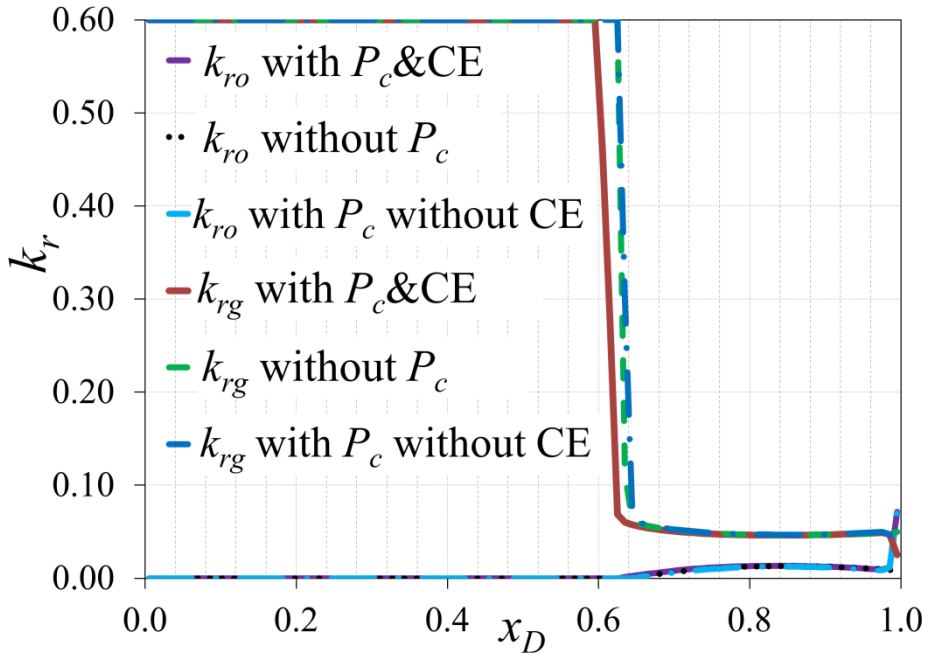

Figure 6-51: Steady-state relative permeability profile for the simulation with P_c and CE, the simulation without P_c, and the simulation with P_c without CE for Case 2.

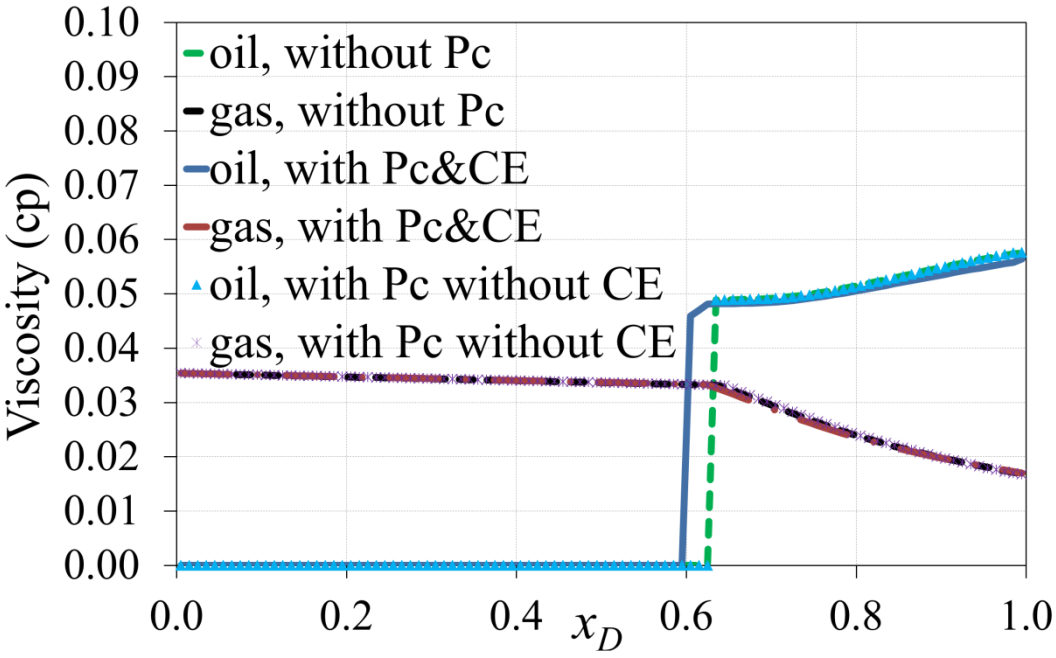

Figure 6-52: Steady-state oil and gas viscosity profile for the simulation with P_c and CE, the simulation without P_c, and the simulation with P_c without CE for Case 2.

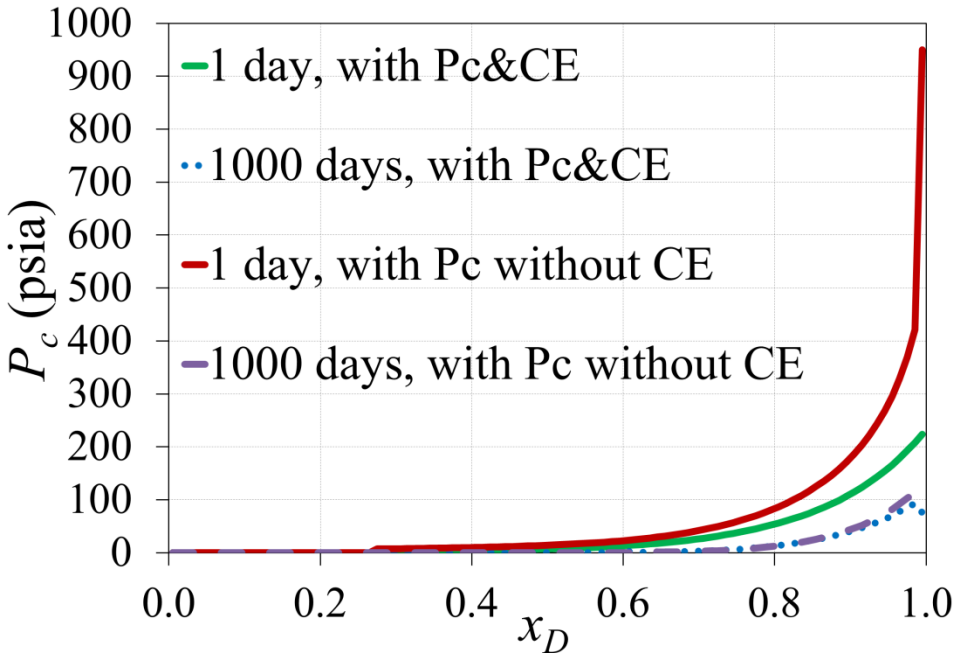

Figure 6-53: Capillary pressure profile for the simulation with P_c and CE and the simulation with P_c without CE at 1 and 1000 days in the linear model (Case 2).

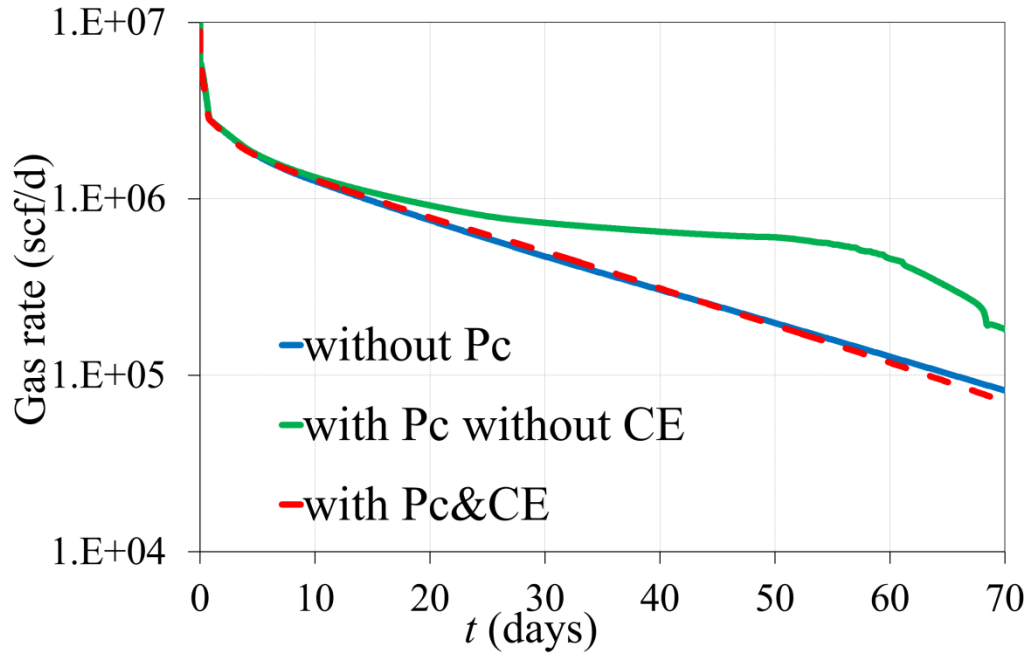

Figure 6-54: Gas production rate for the simulation with P_c and CE, the simulation with P_c without CE, and the simulation without P_c in the areal model (Case 2).

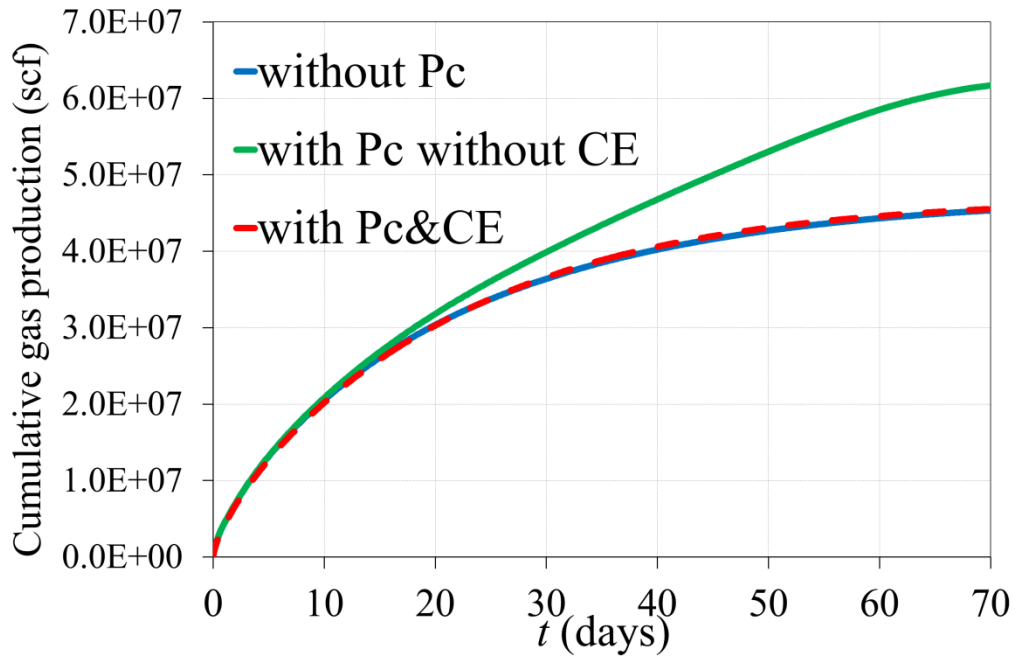

Figure 6-55: Cumulative gas production for the simulation with P_c and CE, the simulation with P_c without CE, and the simulation without P_c in the areal model (Case 2).

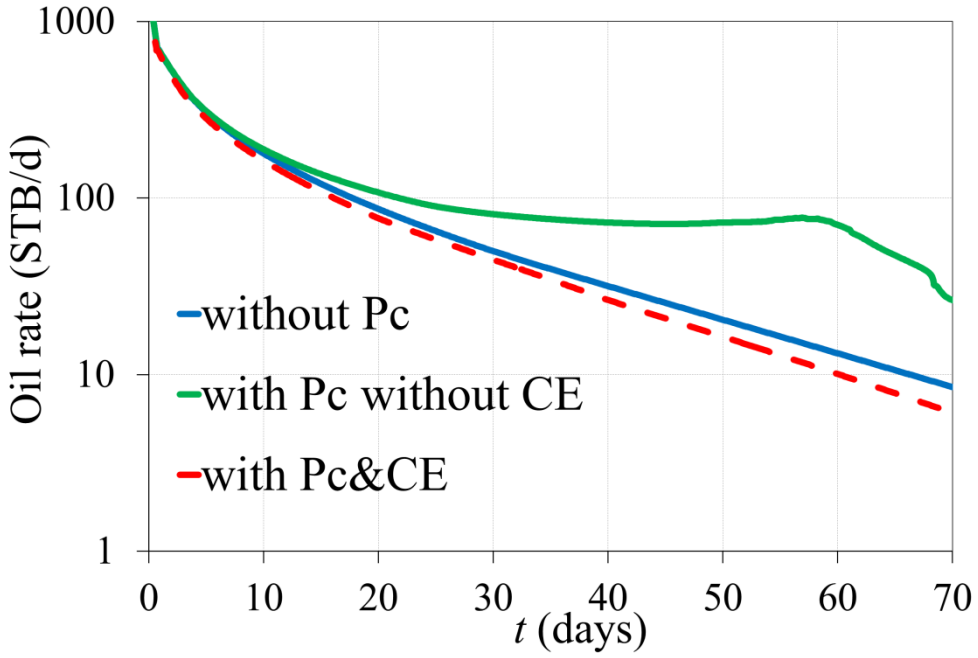

Figure 6-56: Oil production rate for the simulation with P_c and CE, the simulation with P_c without CE, and the simulation without P_c in the areal model (Case 2).

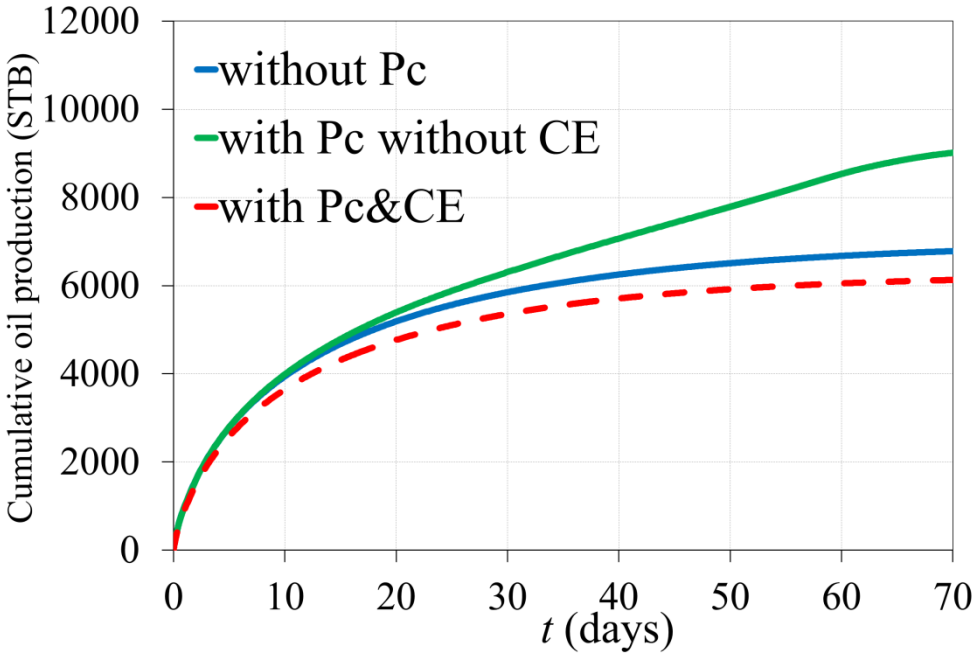

Figure 6-57: Cumulative oil production for the simulation with P_c and CE, the simulation with P_c without CE, and the simulation without P_c in the areal model (Case 2).

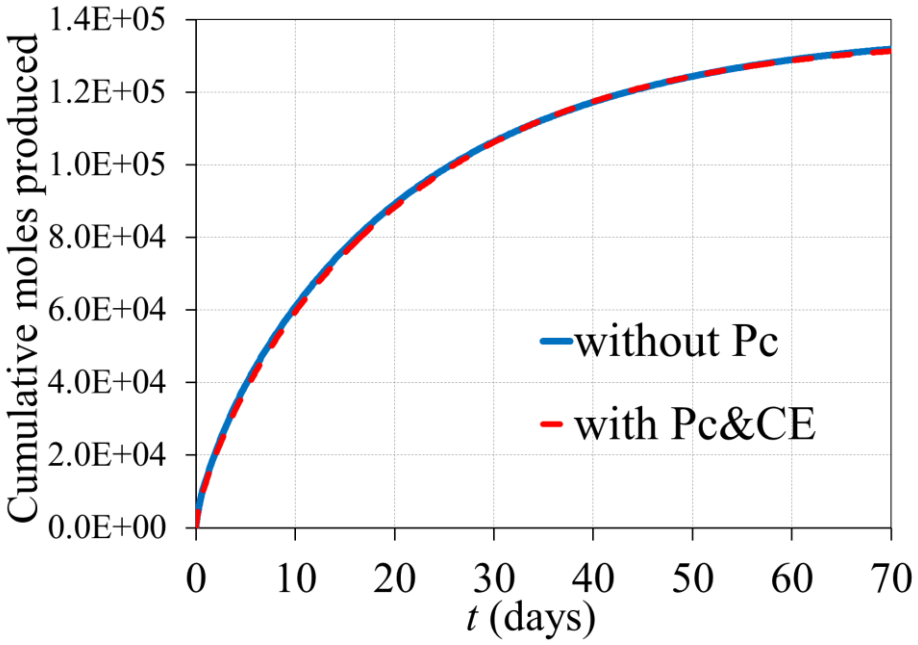

Figure 6-58: Cumulative hydrocarbon moles produced in oil and gas phases in the simulation with P_c and CE and the simulation without P_c in the areal model (Case 2).

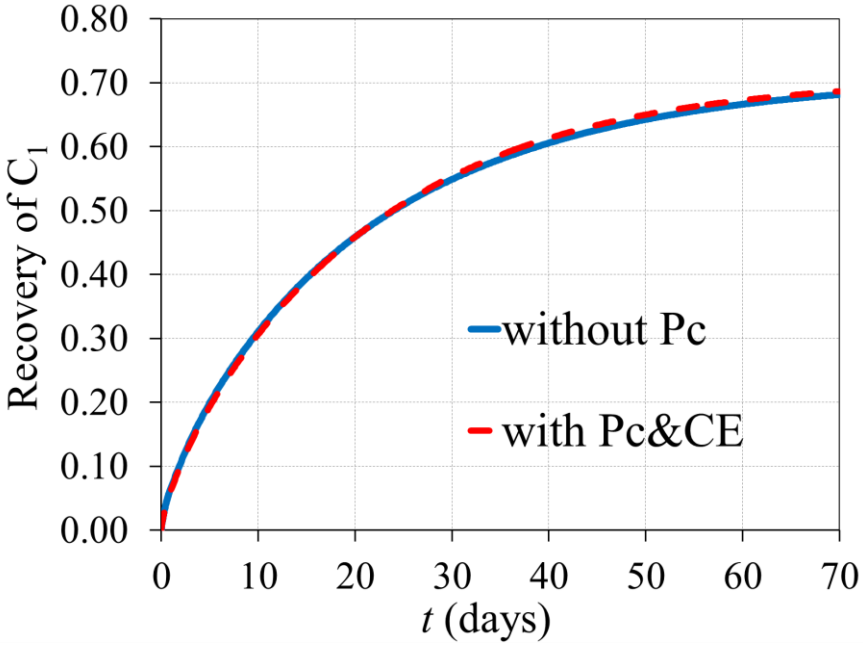

Figure 6-59. Recovery of C_1 versus time in the simulation with P_c and CE and the simulation without P_c in the areal model (Case 2).

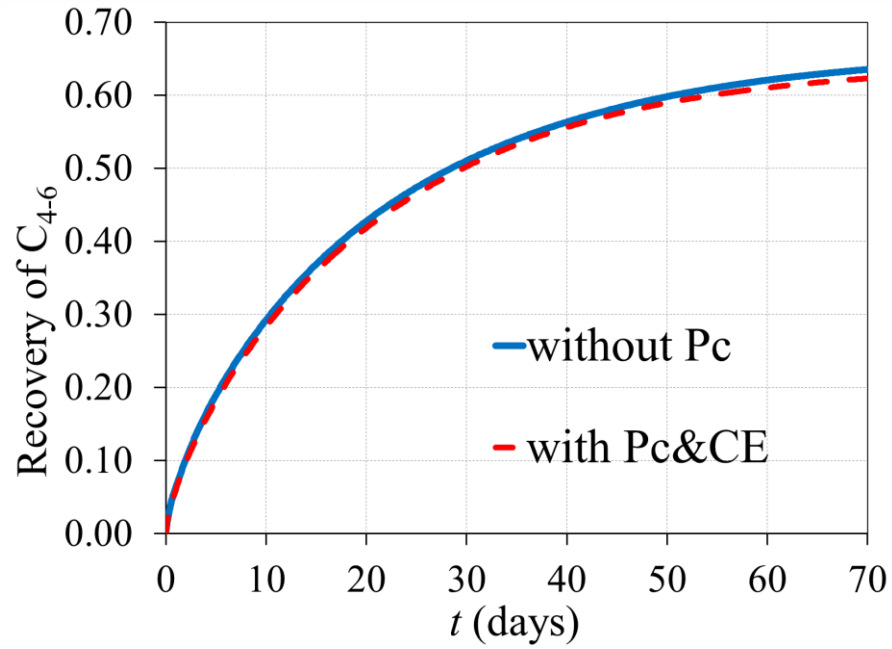

Figure 6-60: Recovery of $C_{4\text{-}6}$ versus time in the simulation with P_c and CE and the simulation without P_c in the areal model (Case 2).

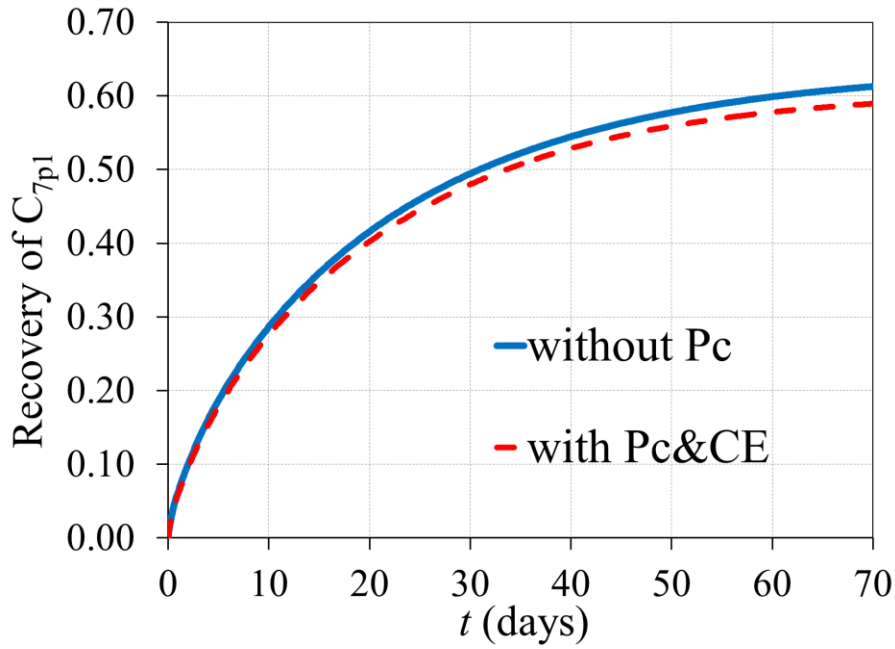

Figure 6-61: Recovery of C_{7p1} versus time in the simulation with P_c and CE and the simulation without P_c in the areal model (Case 2).

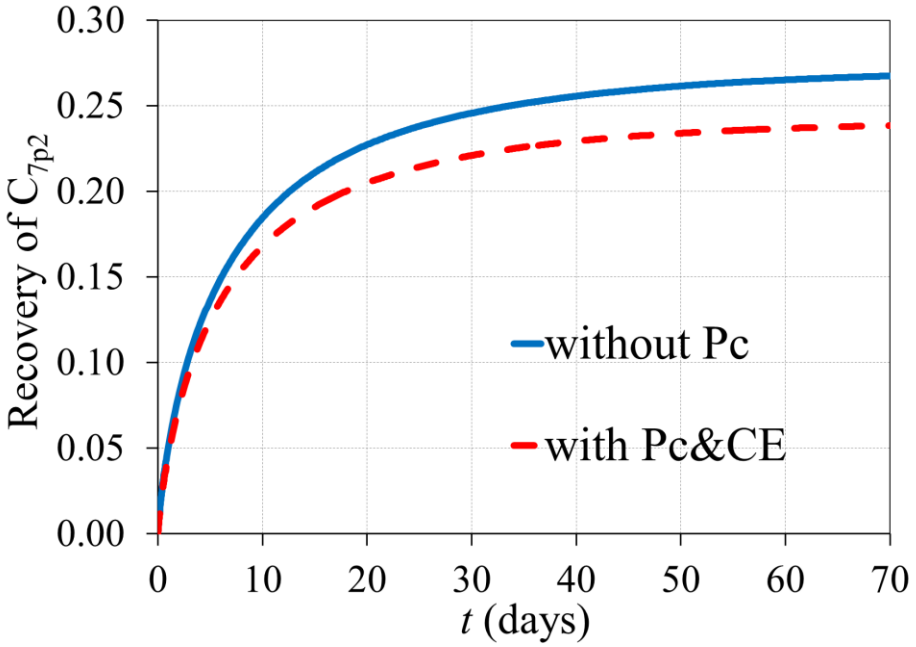

Figure 6-62: Recovery of C_{7p2} versus time in the simulation with P_c and CE and the simulation without P_c in the areal model (Case 2).

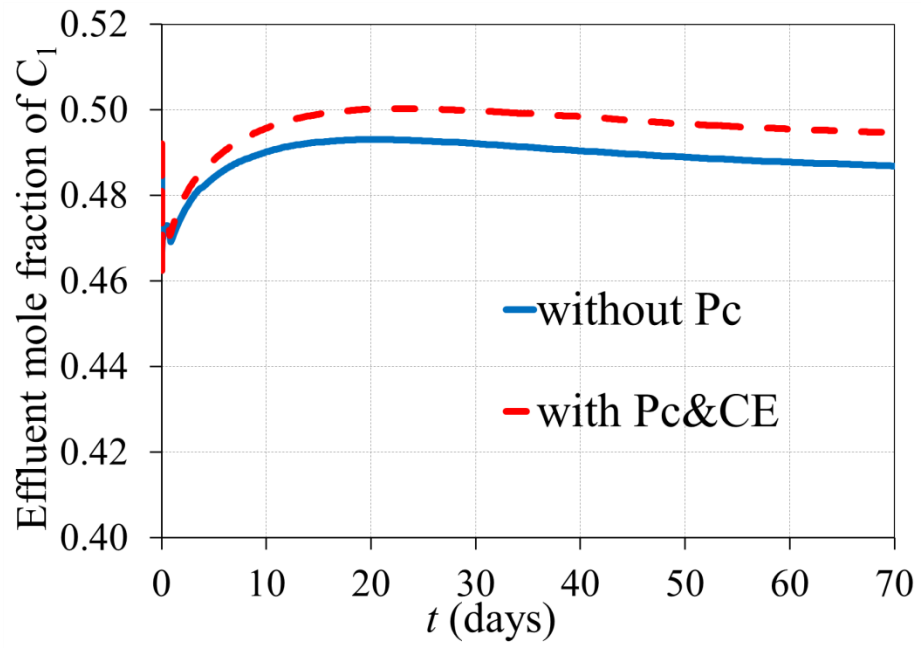

Figure 6-63: Effluent mole fraction of C_1 versus time in the simulation with P_c and CE and the simulation without P_c in the areal model (Case 2).

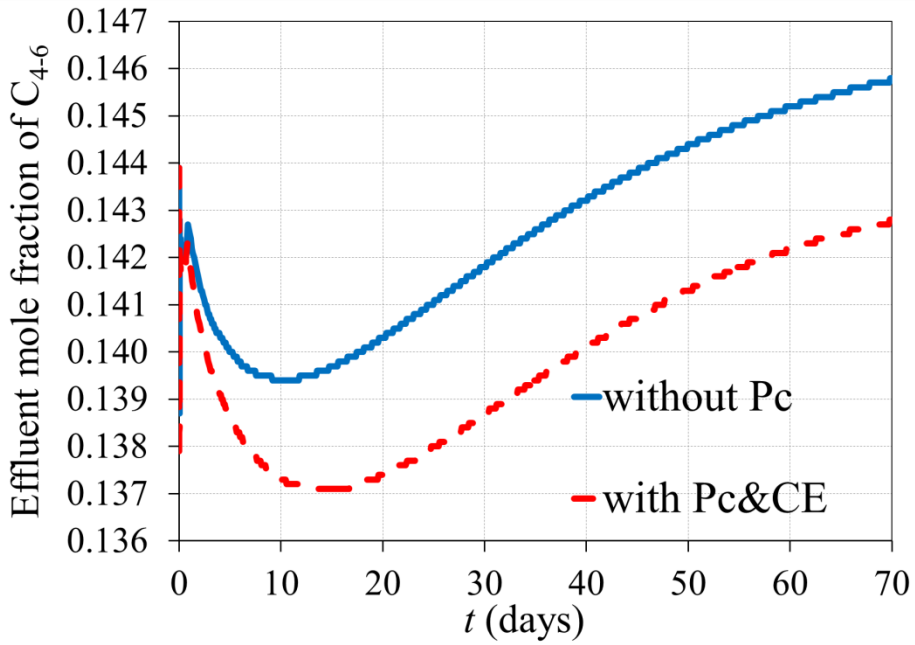

Figure 6-64: Effluent mole fraction of C_{4-6} versus time in the simulation with P_c and CE and the simulation without P_c in the areal model (Case 2).

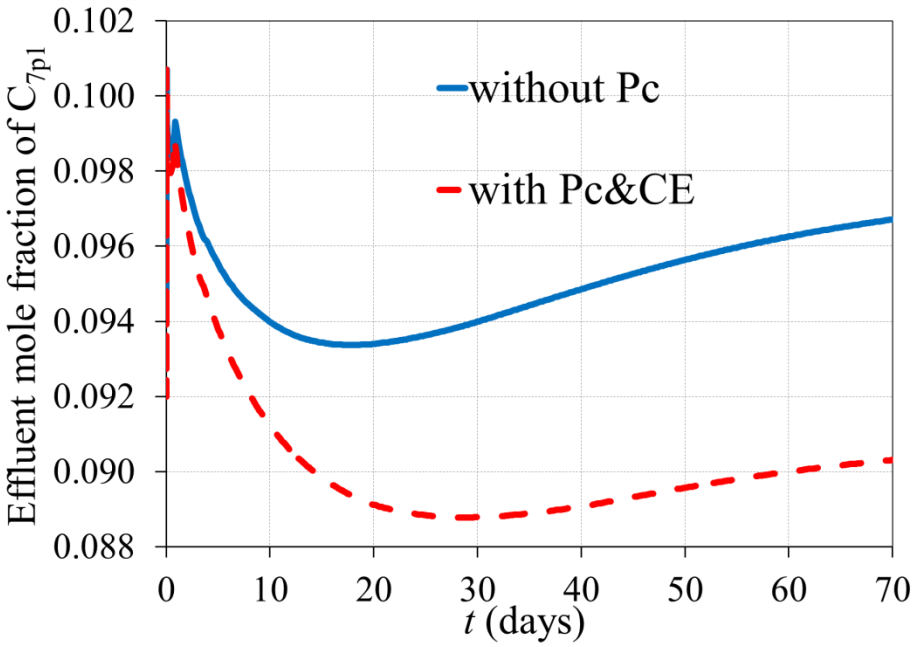

Figure 6-65: Effluent mole fraction of C_{7p1} versus time in the simulation with P_c and CE and the simulation without P_c in the areal model (Case 2).

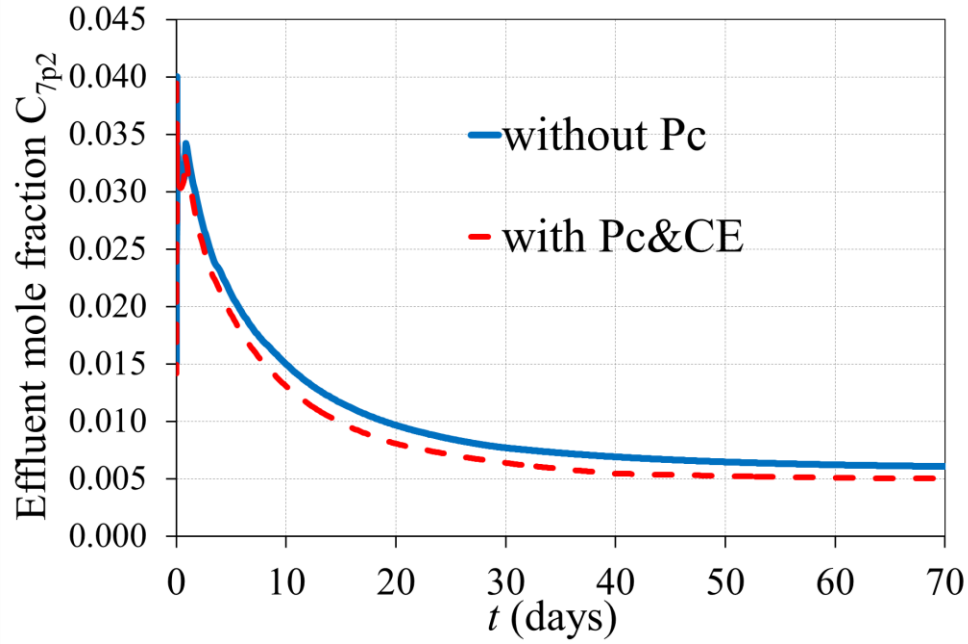

Figure 6-66: Effluent mole fraction of C_{7p2} versus time in the simulation with P_c and CE and the simulation without P_c in the areal model (Case 2).

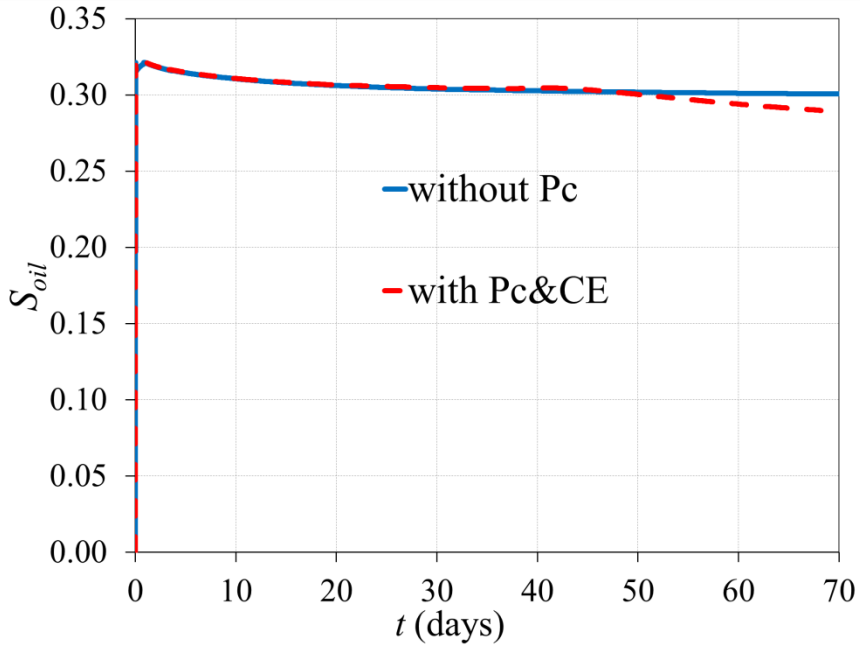

Figure 6-67: Oil saturation in the well gridblock in the simulation with P_c and CE and the simulation without P_c in the areal model (Case 2).

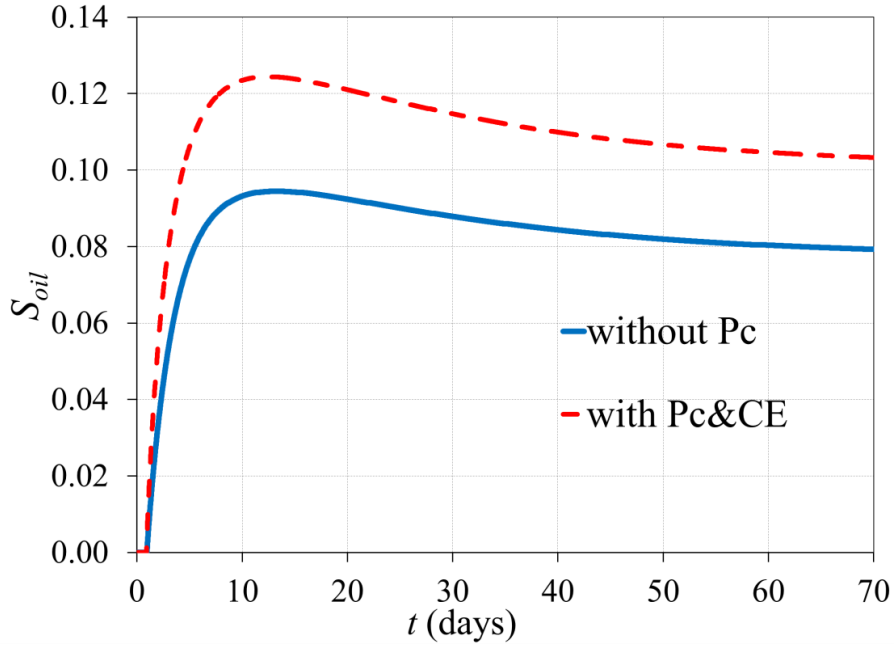

Figure 6-68: Oil saturation in the gridblock in the middle of the reservoir in the simulation with P_c and CE and the simulation without P_c in the areal model (Case 2).

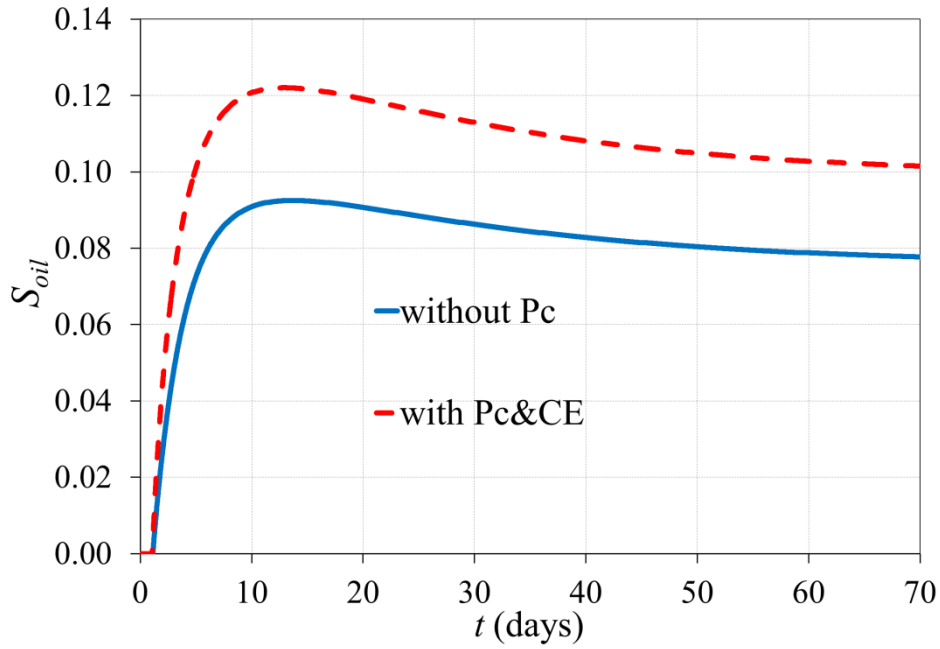

Figure 6-69: Oil saturation in the gridblock at the end of the reservoir in the simulation with P_c and CE and the simulation without P_c in the areal model (Case 2).

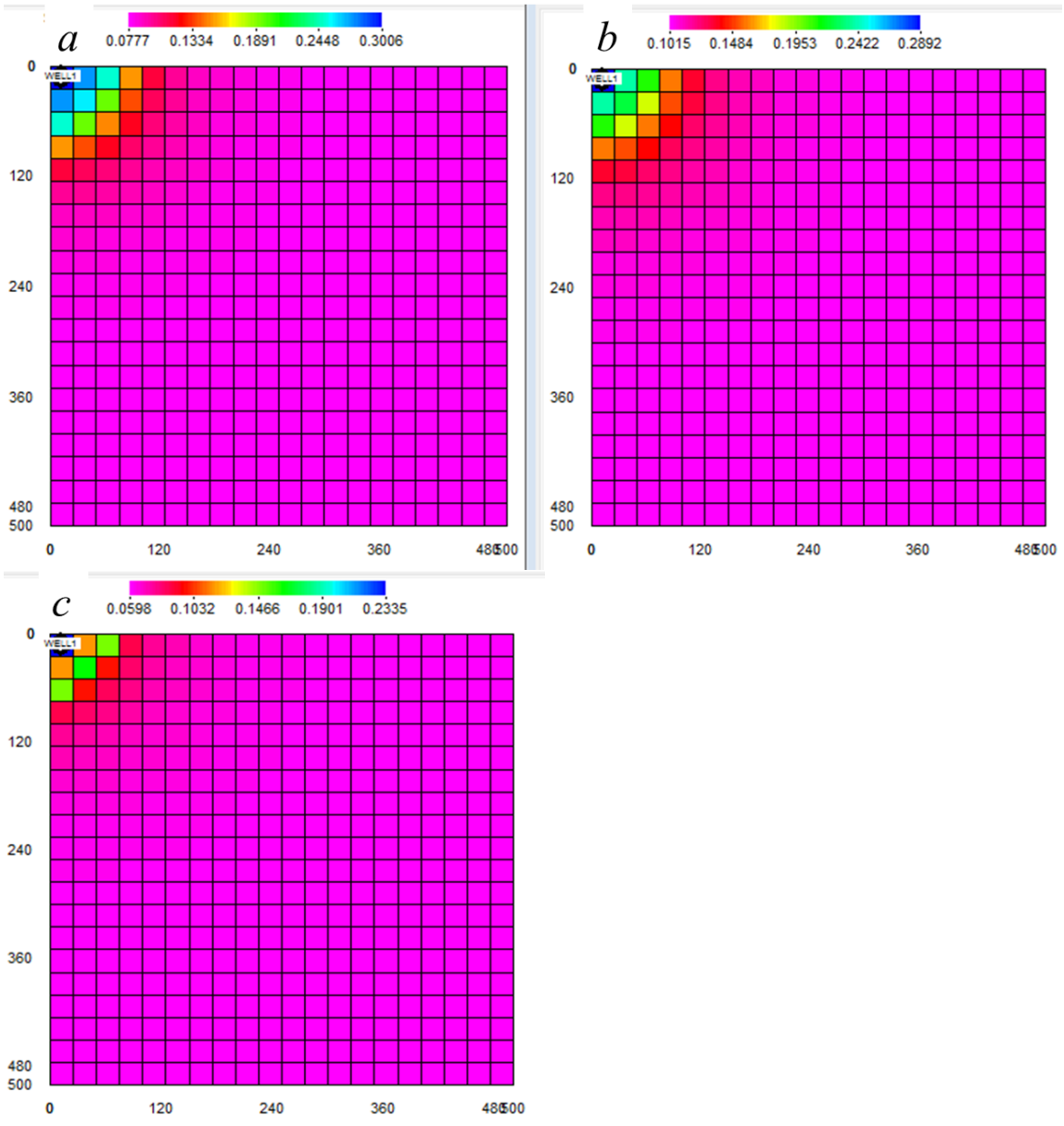

Figure 6-70: Oil saturation profile of the simulation without P_c (*a*), the simulation with P_c and CE (*b*), and the simulation with P_c without CE (*c*) at 70 days for the areal model (Case 2). The producer is in the gridblock at the upper-left corner of the model.

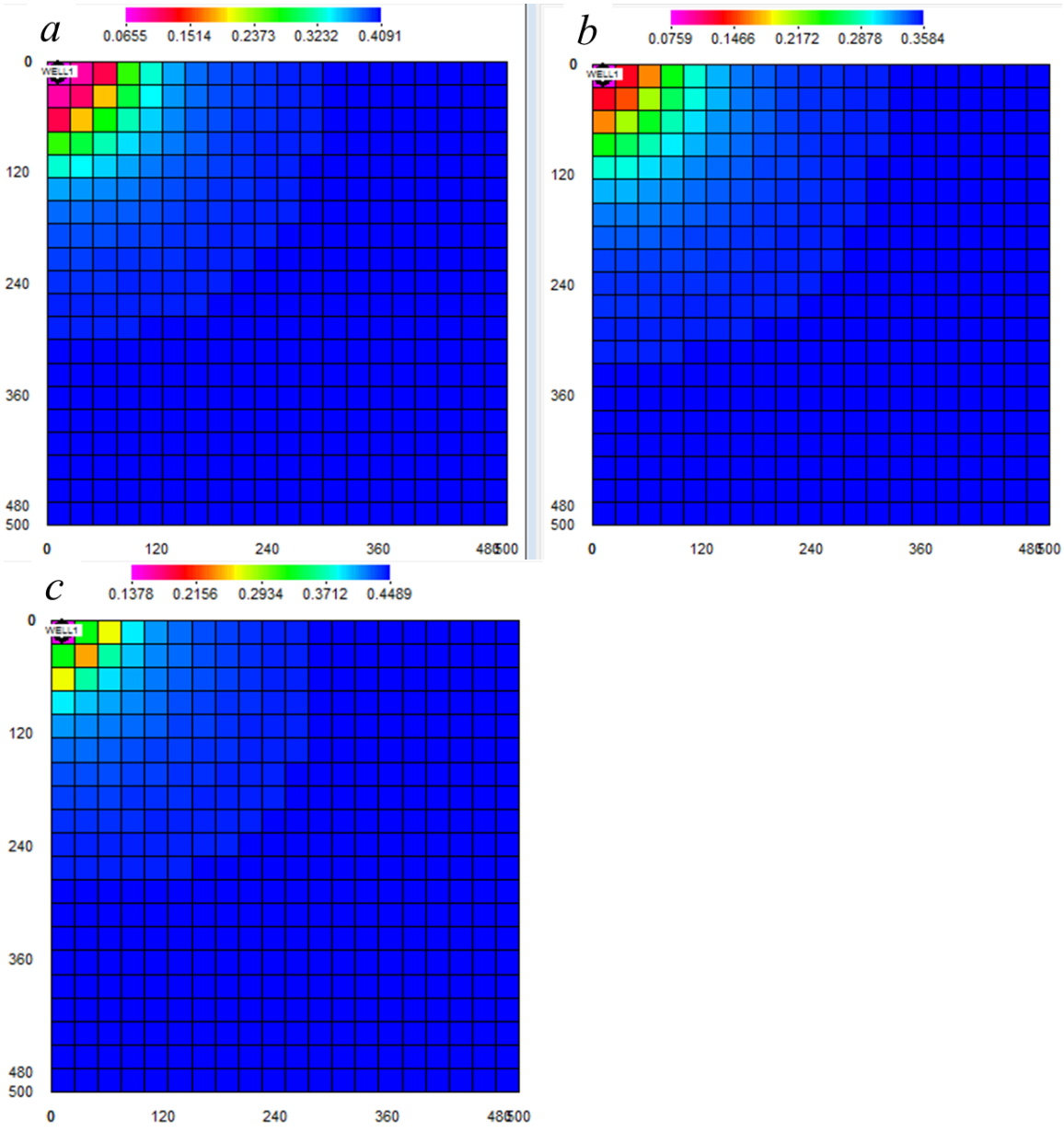

Figure 6-71: Gas relative permeability profile of the simulation without P_c (*a*), the simulation with P_c and CE (*b*), and the simulation with P_c without CE (*c*) at 70 days for the areal model (Case 2). The producer is in the gridblock at the upper-left corner of the model.

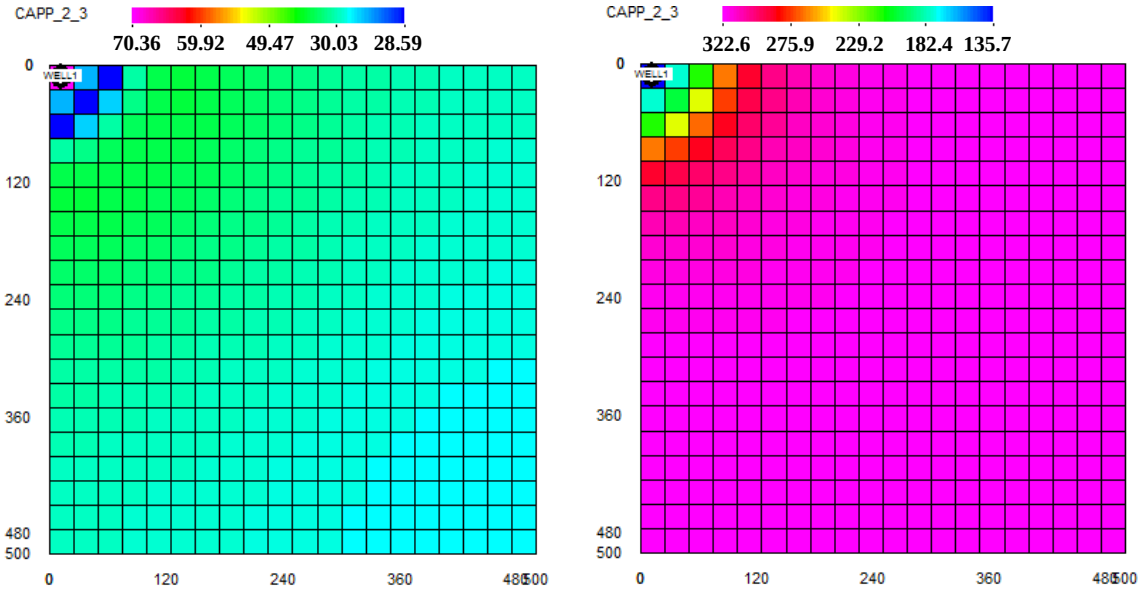

Figure 6-72: Gas/oil capillary pressure profile of the simulation with P_c and CE at 10 days (left) and 70 days (right) for the areal model (Case 2). The producer is in the gridblock at the upper-left corner of the model.

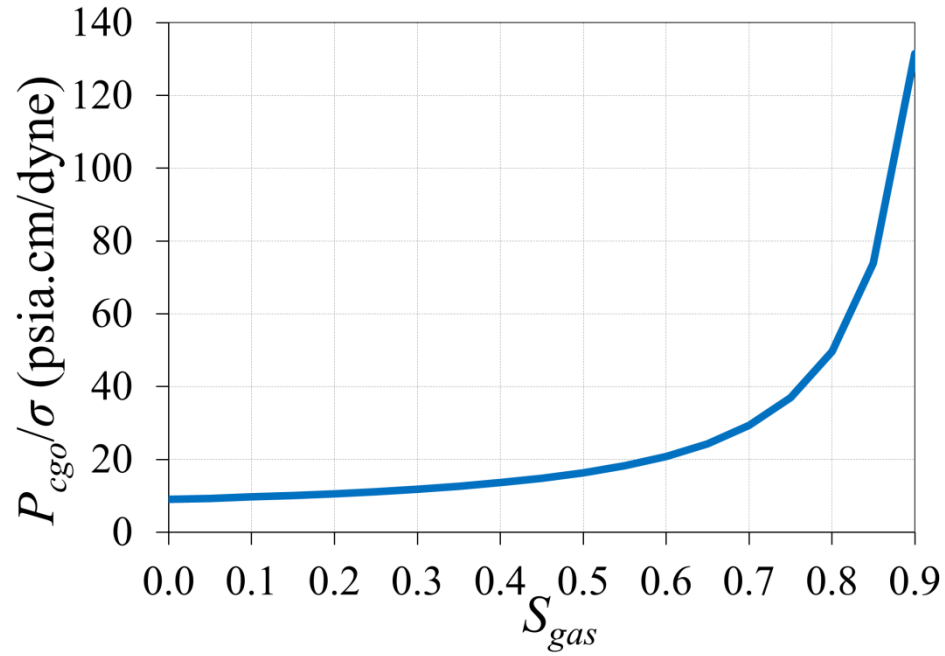

Figure 6-73: The gas/oil capillary pressure curve normalized by IFT for the simulations of Case 3.

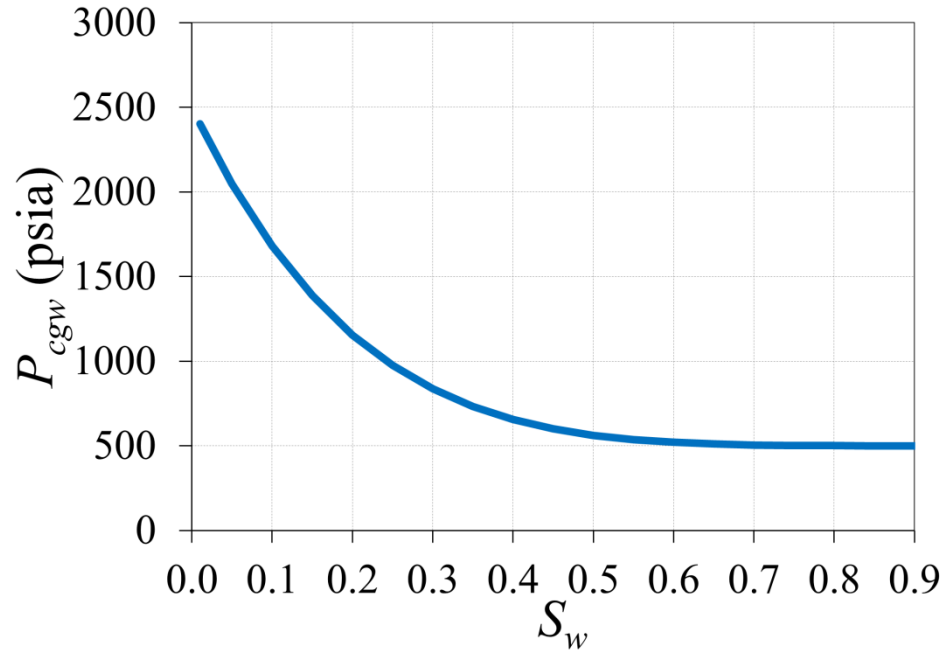

Figure 6-74: The gas/water capillary pressure curve for the simulations of Case 3.

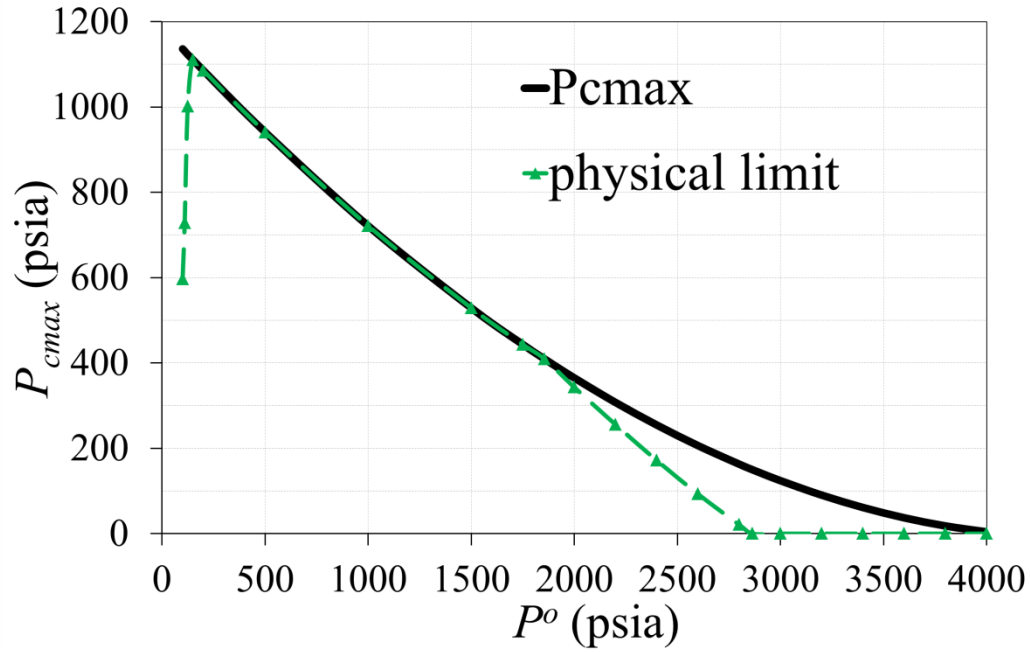

Figure 6-75: Maximum capillary pressure where capillary equilibrium is possible for Bakken oil reservoir fluid at 240°F.

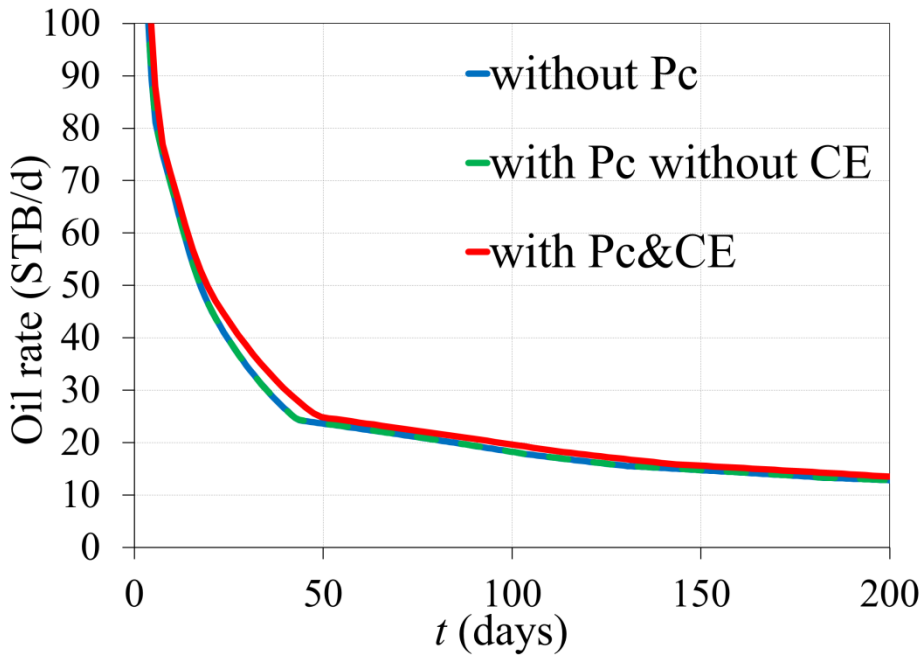

Figure 6-76: Oil production rate for the simulation with P_c and CE, the simulation with P_c without CE, and the simulation without P_c in the areal model (Case 3).

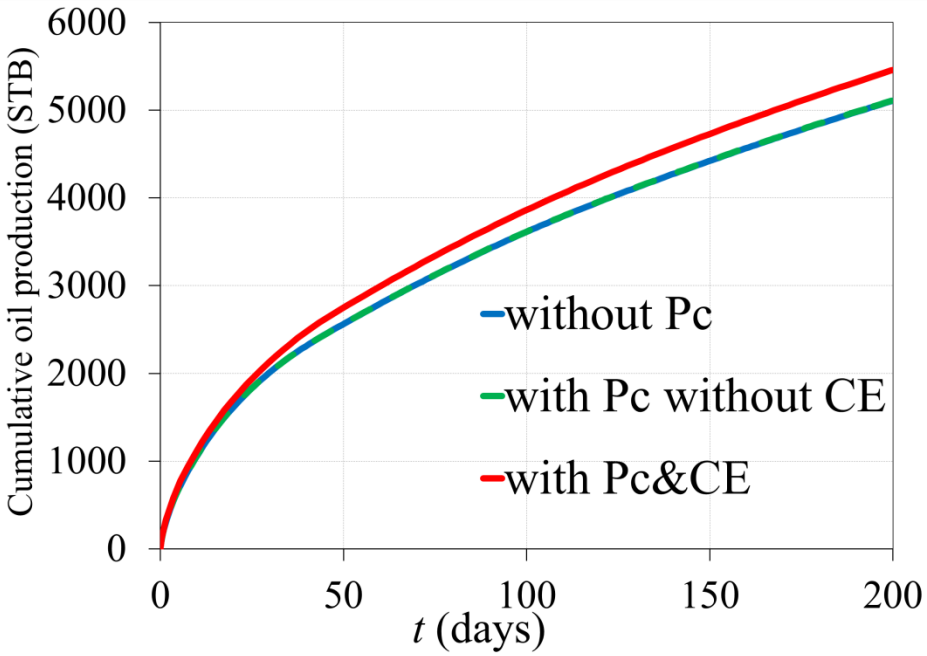

Figure 6-77: Cumulative oil production for the simulation with P_c and CE, the simulation with P_c without CE, and the simulation without P_c in the areal model (Case 3).

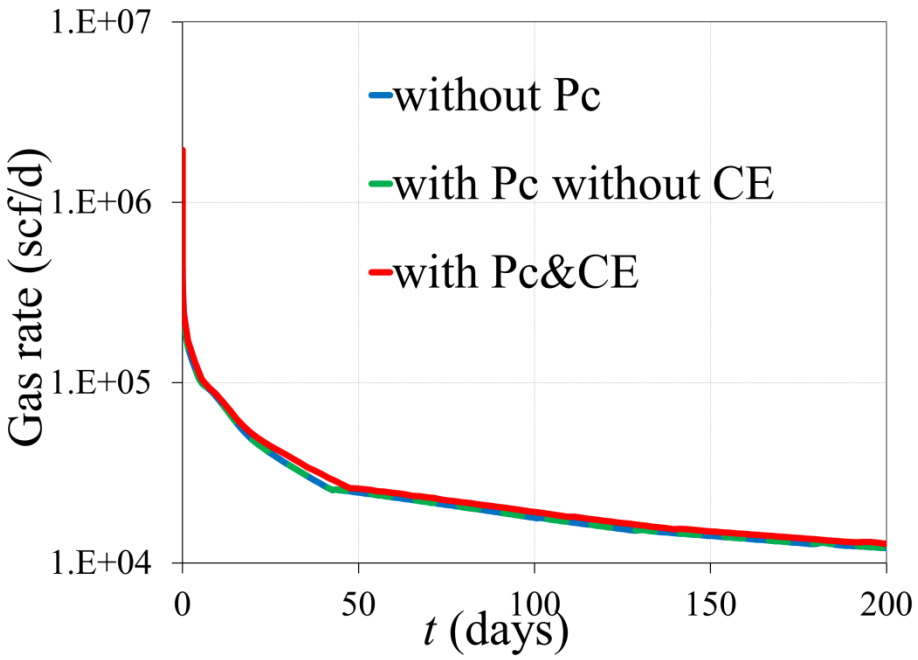

Figure 6-78: Gas production rate for the simulation with P_c and CE, the simulation with P_c without CE, and the simulation without P_c in the areal model (Case 3).

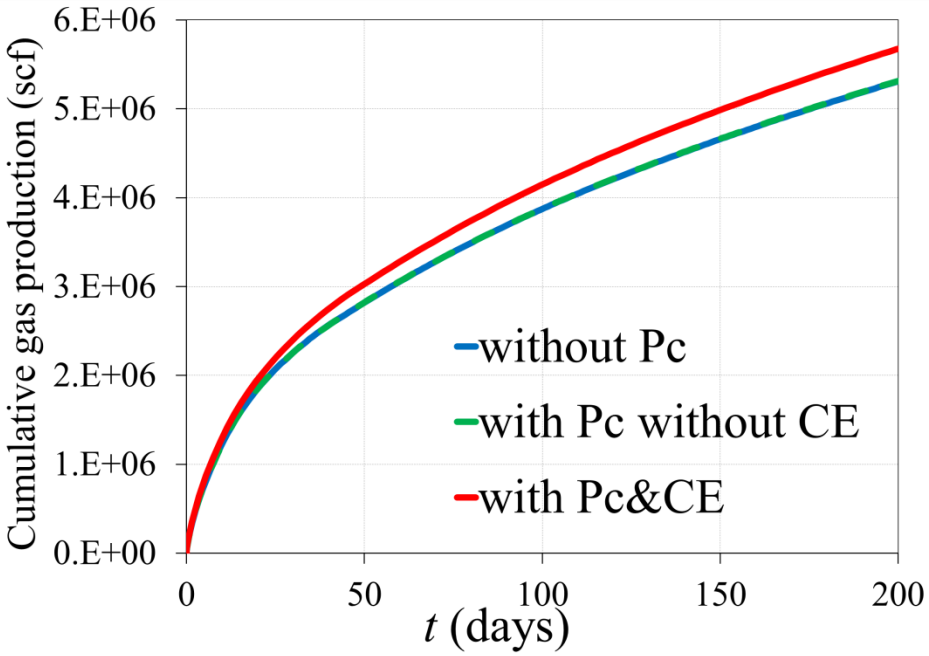

Figure 6-79: Cumulative gas production for the simulation with P_c and CE, the simulation with P_c without CE, and the simulation without P_c in the areal model (Case 3).

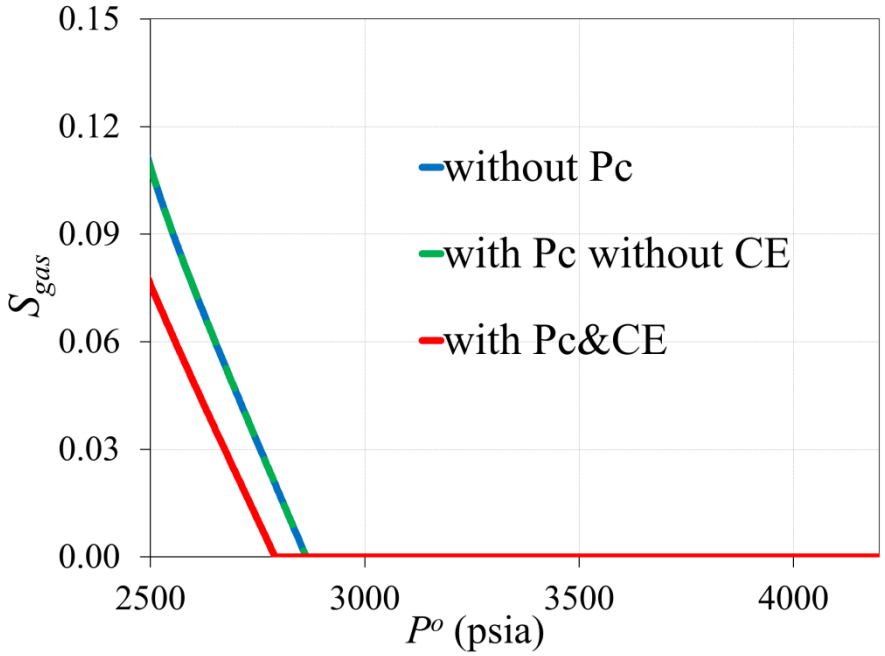

Figure 6-80: The gas saturation in the well gridblock versus the pressure in the oil phase in the well gridblock (Case 3).

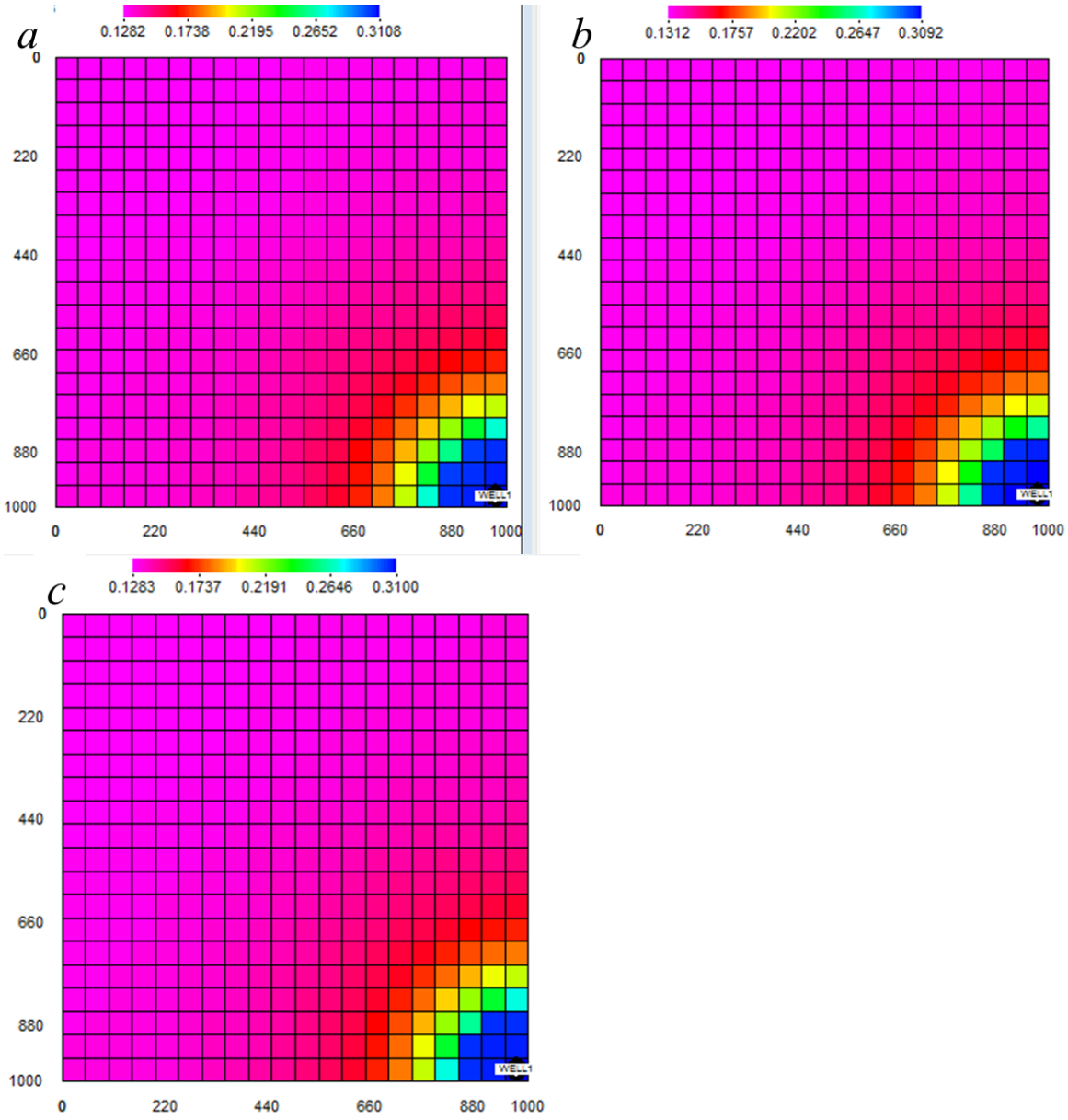

Figure 6-81: Gas saturation profile of the simulation without P_c (*a*), the simulation with P_c and CE (*b*), and the simulation with P_c without CE (*c*) at 200 days for the areal model (Case 3). The producer is in the gridblock at the lower-right corner of the model.

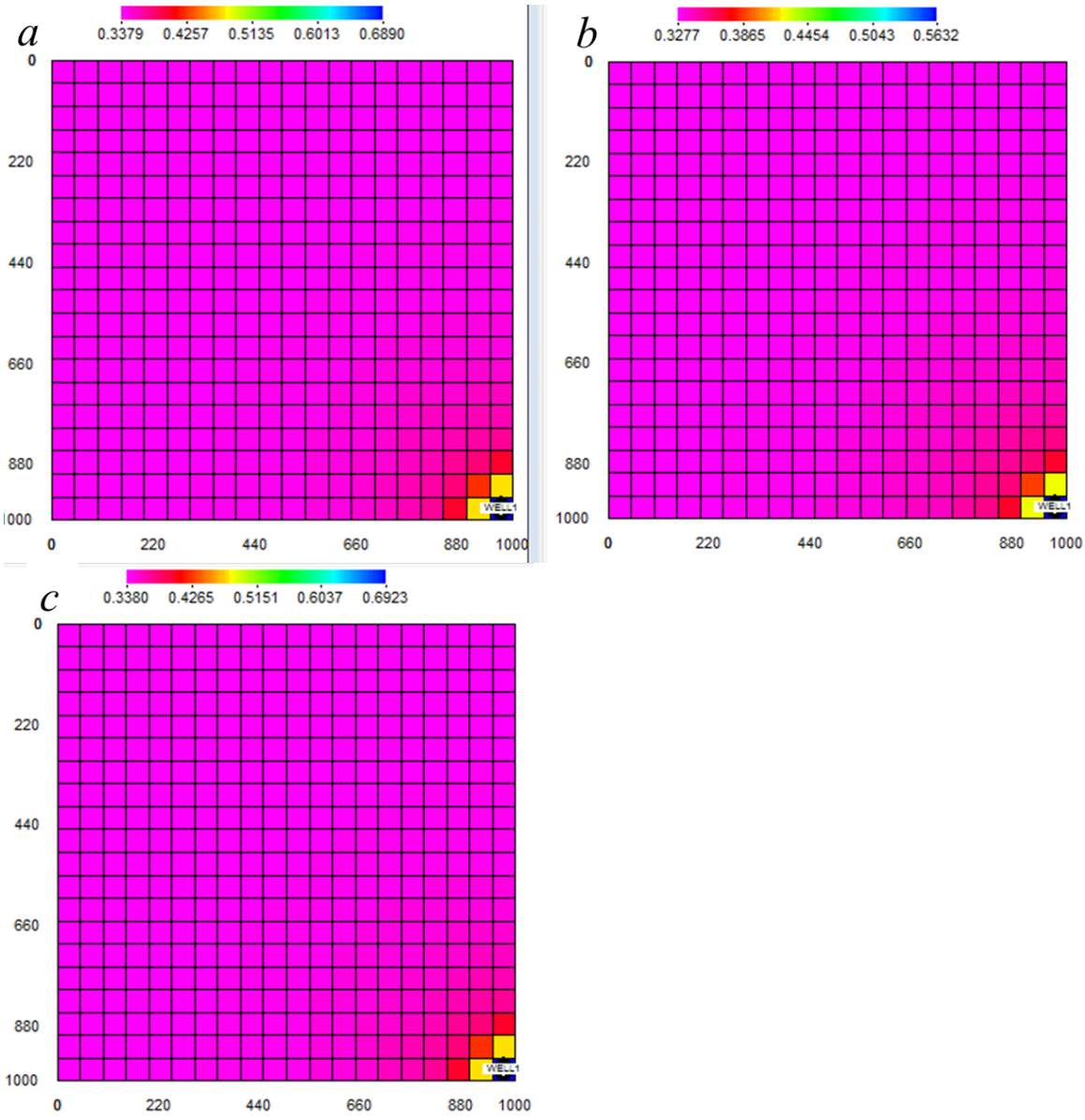

Figure 6-82: Oil viscosity profile of the simulation without P_c (*a*), the simulation with P_c and CE (*b*), and the simulation with P_c without CE (*c*) at 200 days for the areal model (Case 3). The producer is in the gridblock at the lower-right corner of the model.

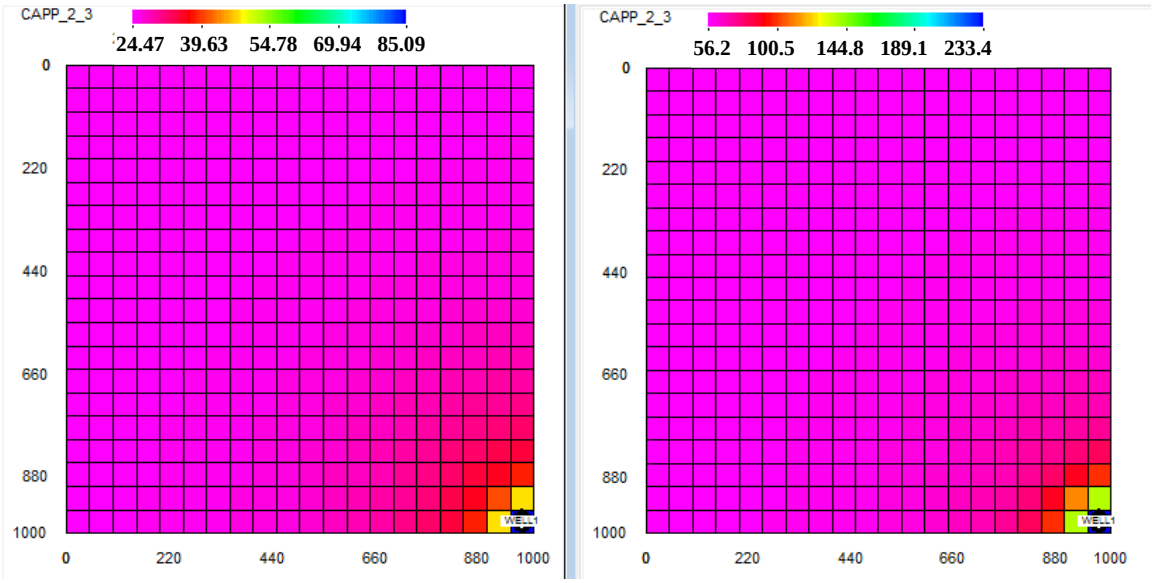

Figure 6-83: The capillary pressure profile in the simulation with P_c and CE at 20 days (left) and 200 days (right) for Case 3. The producer is in the gridblock at the lower-right corner of the model.

Chapter 7: Conclusions and Recommendations for Future Research

This chapter presents the summary and conclusions of this dissertation and provides several recommendations for future research.

7.1 SUMMARY AND CONCLUSIONS

In Chapter 3 we implemented the compositional space adaptive tabulation (CSAT), a tie-simplex-based (TSB) phase behavior modeling method, in UTCOMP. We compared the computational performance of CSAT in skipping stability analysis and generating initial estimates for flash calculations against the standard phase behavior modeling methods in UTCOMP. CSAT substantially reduces the number of stability analysis performed in all of the simulation cases that we studied. The improvement in the computational time using CSAT is less than 30% for most cases when compared to original UTCOMP where only initial estimates from the flash calculation results from previous timesteps are used (with only HM1). This is because the contribution of stability analysis to the total computational time is small when flash results from the previous timestep are used to avoid stability analysis. Furthermore, the timesteps of an IMPEC-type simulator are small and thus the previous timestep provides good initial estimates for performing flash calculations in the next timestep. Thus, using CSAT to generate initial estimates for flash calculations is not advantageous in UTCOMP.

When another option is activated in UTCOMP where stability analysis is skipped for the gridblocks that were single-phase and surrounded by single-phase neighbors in the previous timestep, the computational advantages of CSAT become smaller. Thus, there is little advantage to use CSAT in an IMPEC-type simulator over other simpler schemes

that use the phase equilibrium and phase-state information from the previous timestep to avoid stability analysis for the type of simulation cases that we have performed.

Performance of CSAT in the UTCOMP simulator depends on the values of several parameters such as the tie-line detection tolerance (ε). In all of our cases the simulations were successful with $\varepsilon = 0.01$ and DMIN = 0.01. We found that using smaller values for these parameters improves accuracy, but may lead to an unacceptably large table-search time. Performance of CSAT also depends on the specific gas injection problem being considered. Under ideal conditions where a significant portion of the gridblocks is in the single-phase region, CSAT leads to good computational gains.

In Chapter 4, we demonstrated using several numerical examples that only a small number of tie lines of the multiple-mixing-cell (MMC) method provide good coverage of the entire compositional route of three-dimensional compositional simulations. The MMC tie lines were shown to bound the entire three-dimensional compositional simulation tie lines for a four-component system. The MMC tie lines were used as prior tie-line tables in three tie-line-based *K*-value simulation methods in order to improve speed and robustness of compositional simulation. The CSAT method was also extended to an adaptive *K*-value simulation method using interpolated tie lines to approximate the results of flash calculations in addition to skipping stability analysis.

Several simulation case studies were performed to compare the computational efficiency of the three MMC-based methods, the CSAT method (adaptive *K*-value simulation), and a method based on pure heuristic techniques against the original UTCOMP formulation. The computational efficiency results show that the MMC-based methods and the CSAT method can improve the total computational time by up to 50% with acceptable accuracy for the cases studied. Two of the MMC-based methods use an

interpolation and tabulation framework similar to CSAT, but with only the MMC tie lines without adaptive tabulation, and perform comparable to CSAT in terms of computational efficiency and accuracy. The improvements in the computational time are between 40% and 50% using these two MMC-based methods. The MMC approach is advantageous over adaptive tie-line tabulation in terms of robustness because the MMC approach uses prior contacts as initial guesses of *K*-values for successive contacts in generating the tie-line tables. Furthermore, negative flash calculations are avoided during the simulation in the MMC-based methods.

The results also show that using very simple heuristic techniques improves the computation time by almost 30% for the cases that we studied with the same level of accuracy as the more complicated techniques. We also demonstrated that at the limit of infinite number of contacts the MMC tie lines produce the same tie-line ruled surfaces that the method-of-characteristics (MOC) solution traverses.

In Chapter 5, we implemented several tie-line-based methods namely the CSAT and MMC-based methods along with the heuristics methods for speeding up the phase equilibrium calculations in the natural variable formulation in GPAS, a fully implicit reservoir simulator. We performed several simulation case studies to compare the computational efficiency of various phase equilibrium calculation methods with the conventional phase equilibrium calculations algorithm. The computational time of the phase equilibrium calculations comprises a small portion of the total computational time in GPAS for the cases that we studied.

The results show that the CSAT method improves the computational time of the phase equilibrium calculations by up to 78.3% in the multi-contact-miscible (MCM) cases studied. Comparably, the MMC-based method improves the computational time of

the phase equilibrium calculations by up to 78.2% for the same accuracy in the MCM cases studied. Furthermore, the very simple heuristic techniques improve the computational time of the phase equilibrium calculations by up to 61.6% for the same cases in the GPAS simulator. The improvements in the computational time using the heuristic methods result almost entirely from the technique where stability analysis is skipped for single-phase gridblocks that were surrounded by single-phase neighbors in the previous timestep.

In Chapter 6, we presented a Gibbs free energy (GFE) analysis for two phases in capillary equilibrium (CE). We analyzed the phase stability concepts where the effect of capillary pressure on phase behavior is included. We showed that there is a limiting maximum capillary pressure (P_{cmax}) where gas/oil capillary equilibrium is possible and presented the equations required to calculate the P_{cmax} using the limit of local stability in a context that is applicable to most current compositional reservoir simulators. We discussed several heuristic methods for improving the computational time of the capillary equilibrium calculations in compositional reservoir simulators that use pressure of one phase and overall composition of the gridblock as the independent variables. Furthermore, we suggested the *VT* capillary equilibrium as an alternative formulation of the capillary equilibrium problem that is more amenable to experimental study. The P_{cmax} values obtained from the *VT* capillary equilibrium calculations and the traditional capillary equilibrium calculations are the same.

We implemented the effect of capillary pressure on phase behavior in the UTCOMP simulator. The capillary condensation problem was demonstrated for a simple binary mixture in a compositional reservoir simulation context. In order to investigate the effect of capillary pressure on production behavior, steady-state linear and unsteady-state

areal model simulations were performed for two real gas condensate fluids. The steady-state gas production rate is slightly smaller when the effect of capillary pressure on phase behavior is included in the linear model (the simulation with P_c and CE) because of the increased liquid condensation near the producer with capillary pressure. In the unsteady-state areal model simulations the gas production rate is initially larger in the simulation with P_c and CE compared to the simulation without capillary pressure (without P_c). At late time, the gas production rate in the simulation with P_c and CE becomes smaller than the gas production rate in the simulation without P_c because of larger depletion. On the other hand, the oil production rate in the simulation with P_c and CE is smaller throughout the simulation compared to the simulation without P_c. The recoveries and the effluent mole fractions of the intermediate and heavy components are smaller in the simulation with P_c and CE than in the simulation without P_c because capillary pressure increases the saturation of the condensed liquid in the reservoir. The gas production behavior is not very sensitive to the capillary pressure in the gas condensate reservoirs under unsteady-state conditions for the cases studied.

Unsteady-state areal model simulations were performed for the Bakken tight oil reservoir to demonstrate the bubblepoint suppression that results from the effect of capillary pressure on phase behavior. The oil production rate is increased by almost 6% when the effect of capillary pressure on phase behavior is included in the simulation because of the smaller gas saturation and oil viscosity in the reservoir in the simulation with P_c and CE. This value is in reasonable agreement with the results from Nojabaei *et al.* (2014).

7.2 RECOMMENDATIONS FOR FUTURE RESEARCH

In this section we discuss several recommendations for future research on the topics addressed in this dissertation.

7.2.1 Application of CSAT and MMC-Based Methods to More Complex EOSs

More complex EOSs such as the perturbed-chain statistical associating fluid theory (PC-SAFT) EOS (Gross and Sadowski, 2001) are computationally more expensive than the PR EOS (Peng and Robinson, 1976). Application of the CSAT method or the MMC-based methods with the PC-SAFT EOS will most probably lead to more computational gains than with the PR EOS especially in a general purpose compositional reservoir simulator.

7.2.2 Application of the MMC-Based Simulation Methods to Three-Phase Compositional Simulation Problems

The MMC-based *K*-value simulation methods that we developed in this dissertation for two-phase equilibrium calculations can be extended to three-phase equilibrium in compositional simulation. The MMC-based methods are even more attractive in three-phase equilibrium calculations because good initial estimates of the *K* values are required in three-phase equilibrium problems. Furthermore, the robustness problems are often more severe in three-phase compositional simulation. Development and application of a technique for more accurate extrapolation/interpolation of *K* values from the MMC tie lines may significantly improve the speed and robustness of three-phase equilibrium calculations in compositional simulators.

7.2.3 Further Theoretical Investigation of the MMC Tie Lines and the Simulation Tie Lines

We demonstrated that the MMC tie lines bound the simulation tie lines in the tie-line space for a four-component displacement. We also showed that the MMC tie lines are very close to the simulation tie lines for any number of components. Further theoretical investigation is required to prove that the MMC tie lines bound the compositional simulation tie lines for a compositional simulation with any number of components. More advanced interpolation techniques based on the MMC tie lines can be developed if the bounding property of the MMC tie lines is shown to be universal.

7.2.4 Development of an EOS-Free Compositional Simulation Formulation Based on the MMC Tie Lines

The MMC tie lines may be used to develop an EOS-free compositional simulation framework where the equilibrium phase compositions and physical properties are interpolated from the values for the corresponding MMC tie lines similar to Zaydullin *et al.*'s formulation (2013). This is particularly appealing if one can show that the MMC tie lines bound the compositional simulation tie lines because the MMC tie lines and the compositional simulation tie lines occupy the same space in the tie-line space.

7.2.5 Experimental Investigation of the Transition from Two Phases to Single Phase in the Capillary Equilibrium Problem

The capillary equilibrium limit that was discussed in Chapter 6, particularly the P_{cmax} concept implies a discontinuity in the transition from two-phase equilibrium to single-phase assuming validity of the bulk-phase thermodynamics at high capillary pressures. However, we intuitively expect the phase transition as a physical phenomenon to be continuous. It would be interesting to experimentally observe the variation in phase states at the limit of capillary equilibrium and upon perturbation of the independent

variables of the system in a transparent single-pore model of desired geometry. It is likely the case that the P_{cmax} values correspond to very small pore sizes where the bulk-phase thermodynamics is not applicable anymore.

7.2.6 Further Numerical Investigation of the Transition from Two Phases to Single Phase in the Capillary Equilibrium Problem

We suggest further numerical investigation of the transition from two phases to single phase at the limit of capillary equilibrium in a single-pore model using a consistent capillary pressure-saturation model and various capillary equilibrium formulations.

7.2.7 Integrating the Capillary Equilibrium Problem and the Phase Behavior in Nanopores and Implementing the Resulting Model in UTCOMP

For very small pore sizes the assumption of bulk-phase thermodynamics does not apply. On the other hand, the pore sizes in shale gas and tight oil reservoirs vary over wide ranges that correspond to applicability of the bulk-phase thermodynamics and applicability of other phase behavior models such as the density function theories. A thorough investigation of the transition from the bulk-phase thermodynamics to the phase behavior of fluids under confinement is required. The appropriate combination of the phase behavior models over the entire range of the pore sizes must be implemented in a general purpose compositional reservoir simulator such as UTCOMP in order to obtain reliable performance predictions in shale gas and tight oil reservoirs.

7.2.8 Further Investigation of the Effect of Capillary Equilibrium on Production Performance in Highly Heterogeneous Reservoir Models

The simulation case studies that we performed for investigation of the effect of capillary equilibrium on production performance in tight oil and shale gas reservoirs used simple reservoir models with a single effective permeability value for the entire reservoir.

Real shale gas reservoirs are characterized by heterogeneity in permeability and other rock properties at different scales because of natural fractures, hydraulic fractures, layering, presence of organic matter, and so forth. Further numerical simulation studies in more complex reservoir models that include heterogeneity of the physical properties of the rock are required in order to obtain a thorough understanding of the effect of capillary equilibrium on production behavior in shale gas and tight oil reservoirs.

Furthermore, we suggest a thorough numerical simulation study of the effect of water/oil capillary pressure on fluid properties of the oil phase and production performance of the tight oil reservoirs. The water/oil capillary pressure can be very large which may significantly affect the fluid properties of the oil phase.

Appendix A: Legendre Transforms

Legendre transforms allow for describing a function in terms of its derivatives. For example, a function $y = f(x)$ can be transformed into $y^{(1)} = g(dy/dx)$ where the independent variable is dy/dx by use of the Legendre transform. If y is a continuously differentiable function of $x_1, x_2, \ldots, x_{nc+2}$ then dy is given by

$$dy = \sum_{i=1}^{n_c+2} \left(\frac{\partial y}{\partial x_i}\right)_{x_{j\neq i}} dx_i = \sum_{i=1}^{n_c+2} C_i dx_i, \tag{A.1}$$

If w is defined as

$$w = y - \sum_{i=1}^{n_c+2} C_i x_i, \tag{A.2}$$

then dw is given by

$$dw = dy - d\sum_{i=1}^{n_c+2} C_i x_i = -\sum_{i=1}^{n_c+2} x_i dC_i, \tag{A.3}$$

thus, w is now a function of $C_1, C_2, \ldots, C_{nc+2}$ i.e.

$$w = w\left(\left(\frac{\partial y}{\partial x_1}\right)_{x_{j\neq 1}}, \left(\frac{\partial y}{\partial x_2}\right)_{x_{j\neq 2}}, \ldots\ldots, \left(\frac{\partial y}{\partial x_{n_c+2}}\right)_{x_{j\neq n_c+2}} \right), \tag{A.4}$$

w is called the total Legendre transform of y. One can obtain the first and second Legendre transforms of y by transforming only the first and second independent variables into their derivative variables (Firoozabadi, 1999).

If the total internal energy (U) as a function of total entropy S, total volume V, and mole numbers $n_1, n_2, \ldots, n_{nc}$ is used as the basis function $y^{(0)}$, then the first, second, and (m-2)-th order Legendre transforms are derived as follows

$$y^{(0)} = U(S, V, n_1, n_2, ..., n_{n_c}), \tag{A.5}$$

$$dy^{(0)} = dU = TdS - PdV + \sum_{i=1}^{n_c} \mu_i dn_i, \tag{A.6}$$

$$y^{(1)} = U - \frac{\partial U}{\partial S} S = U - TS, \tag{A.7}$$

$$\begin{aligned} dy^{(1)} &= TdS - PdV + \sum_{i=1}^{n_c} \mu_i dn_i - TdS - SdT \\ &= -SdT - PdV + \sum_{i=1}^{n_c} \mu_i dn_i, \end{aligned} \tag{A.8}$$

$$y^{(2)} = U - \frac{\partial U}{\partial S} S - \frac{\partial U}{\partial V} V = U - TS + PV, \tag{A.9}$$

$$\begin{aligned} dy^{(2)} &= TdS - PdV + \sum_{i=1}^{n_c} \mu_i dn_i - TdS - SdT + PdV + VdP \\ &= -SdT + VdP + \sum_{i=1}^{n_c} \mu_i dn_i, \end{aligned} \tag{A.10}$$

$$y^{(m-2)} = U - TS + PV - \mu_1 n_1 - \mu_2 n_2 ... - \mu_{m-2} n_{m-2}, \tag{A.11}$$

$$dy^{(m-2)} = SdT + VdP - n_1 d\mu_1 - n_2 d\mu_2 ... - n_{m-2} d\mu_{m-2} + \mu_{m-1} dn_{m-1} + \mu_m dn_m, \tag{A.12}$$

where $m = n_c + 2$, μ_i is chemical potential of component i, T is temperature, and P is pressure. From the above equations the Gibbs free energy (GFE), denoted by G, is equal to $y^{(2)}$ and the Helmholtz free energy, denoted by A, is equal to $y^{(1)}$. The last variable in the ordering is always a constraint in the stability theory (Tester and Modell, 1997).

One can use the variable set of S, V, n_1, n_2, ..., n_{nc-1}, n (where n is the total number of moles) as the set of independent variables and obtain the same stability criterion as in Eq. (2.60). By use of this set of independent variables, the determinant η_2 and the other lower-order Legendre transforms can be converted into the mole fraction form as follows

$$\eta_2 = \frac{1}{n^{n_c-1}} \begin{vmatrix} \left(\frac{\partial^2 \underline{G}}{\partial z_1^2}\right)_{T,P,z_2,\ldots z_{n_c-1}} & \left(\frac{\partial^2 \underline{G}}{\partial z_1 \partial z_2}\right)_{T,P,z_3,\ldots z_{n_c-1}} & \ldots\ldots & \left(\frac{\partial^2 \underline{G}}{\partial z_1 \partial z_{n_c-1}}\right)_{T,P,z_2,\ldots z_{n_c-2}} \\ \left(\frac{\partial^2 \underline{G}}{\partial z_1 \partial z_2}\right)_{T,P,z_3,\ldots z_{n_c-1}} & \left(\frac{\partial^2 \underline{G}}{\partial z_2^2}\right)_{T,P,z_1,\ldots z_{n_c-1}} & \ldots\ldots & \left(\frac{\partial^2 \underline{G}}{\partial z_2 \partial z_{n_c-1}}\right)_{T,P,z_1,\ldots z_{n_c-2}} \\ \vdots & \vdots & \vdots & \vdots \\ \left(\frac{\partial^2 \underline{G}}{\partial z_1 \partial z_{n_c-1}}\right)_{T,P,z_2,\ldots z_{n_c-2}} & \left(\frac{\partial^2 \underline{G}}{\partial z_2 \partial z_{n_c-1}}\right)_{T,P,z_1,\ldots z_{n_c-2}} & \ldots\ldots & \left(\frac{\partial^2 \underline{G}}{\partial z_{n_c-1}^2}\right)_{T,P,z_1,\ldots z_{n_c-2}} \end{vmatrix}, \quad \text{(A.13)}$$

where $\underline{G}$ is the molar GFE and z_i is overall mole fraction of component *i*. The derivatives in Eq. (A.13) are constrained mole fraction derivatives equivalent to derivatives at constant *n* (total number of moles) where z_{nc} varies to keep the total number of moles constant. Firoozabadi (1999) showed that in an analogous manner Eq. (2.62) in terms of mole fraction derivatives is given by

$$\left(\frac{\partial \mu_{m-1}}{\partial z_{m-1}}\right)_{T,P,\mu_1,\mu_2,\ldots,\mu_{m-2}} > 0. \quad \text{(A.14)}$$

Appendix B: Calculation of Gibbs Free Energy (GFE) and Helmholtz Free Energy

In order to calculate the value of molar GFE ($\underline{G}$), specification of a reference state is necessary. To specify a reference state for a real fluid we need to specify pressure, temperature and also the state of aggregation at the reference point from ideal gas, real gas, liquid or solid. Furthermore, we must specify the molar entropy at the reference point e.g. $\underline{S}_R = 0$, and either but not both of molar enthalpy or molar internal energy i.e. $\underline{H}_R = 0$ or $\underline{U}_R = 0$. A typical choice of the reference state is the ideal gas state of a pure component at $T_R = 273$ K and $P_R = 14.7$ psia (Elliott and Lira, 1999).

The molar GFE of a real mixture may be written in terms of components' fugacity coefficients and the molar GFE of the mixture in ideal gas state ($\underline{G}^{ig}$) as (Elliott and Lira, 1999)

$$\underline{G}(T,P,\vec{x}) = \underline{G}^{ig}(T,P,\vec{x}) + RT\sum_{i=1}^{n_c} x_i ln\phi_i(T,P,\vec{x}), \tag{B.1}$$

where T is temperature, P is pressure, $\vec{x}$ is the composition vector, R is the universal gas constant, i is the component index, ϕ_i is fugacity coefficient of component i in the real mixture, and n_c is the number of components. $\underline{G}^{ig}$ is the molar GFE of an ideal gas mixture at the same temperature, pressure, and composition as the real mixture. Molar enthalpy of the ideal gas mixture $\underline{H}^{ig}$, molar entropy of the ideal gas mixture $\underline{S}^{ig}$, and $\underline{G}^{ig}$ are given by

$$\underline{H}^{ig}(T,P,\vec{x}) = \sum_{i=1}^{n_c} x_i \underline{H}_i^{ig}(T,P), \tag{B.2}$$

$$\underline{S}^{ig}(T,P,\vec{x}) = \sum_{i=1}^{n_c} x_i \underline{S}_i^{ig}(T,P) - R\sum_{i=1}^{n_c} x_i lnx_i, \tag{B.3}$$

$$\underline{G}^{ig}(T,P,\vec{x}) = \sum_{i=1}^{n_c} x_i \underline{G}_i^{ig}(T,P) + RT\sum_{i=1}^{n_c} x_i lnx_i, \tag{B.4}$$

where $\underline{H}^{ig}_{i(T,P)}$, $\underline{S}^{ig}_{i(T,P)}$, and $\underline{G}^{ig}_{i(T,P)}$ are molar enthalpy, molar entropy, and molar GFE of the ideal gas component at *T* and *P*. Substituting Eq. (B.4) into Eq. (B.1) results in

$$\begin{aligned}\underline{G}(T,P,\vec{x}) = \sum_{i=1}^{n_c} x_i \underline{G}_i^{ig}(T,P) + RT\sum_{i=1}^{n_c} x_i ln x_i \\ + RT\sum_{i=1}^{n_c} x_i ln\phi_i(T,P,\vec{x}),\end{aligned} \tag{B.5}$$

The $\underline{G}^{ig}_{i(T,P)}$ can be obtained from

$$\underline{H}_i^{ig}(T) = \underline{H}_i^{ig}(T_R) + \int_{T_R}^{T} C_p dT, \tag{B.6}$$

$$\underline{S}_i^{ig}(T,P) = \underline{S}_i^{ig}(T_R,P_R) + \int_{T_R}^{T} \frac{C_p}{T} dT - Rln\frac{P}{P_R}, \tag{B.7}$$

$$\underline{G}_i^{ig}(T,P) = \underline{H}_i^{ig}(T,P) - T\underline{S}_i^{ig}(T,P), \tag{B.8}$$

where C_p is the isobaric heat capacity of ideal gas. Enthalpy of the ideal gas is independent of pressure. Substituting Eqs. (B.6) through (B.8) into Eq. (B.5) results in

$$\begin{aligned}\underline{G}(T,P,\vec{x}) = \sum_{i=1}^{n_c} x_i (\underline{H}_i^{ig}(T_R) + \int_{T_R}^{T} C_p dT) \\ - T\sum_{i=1}^{n_c} x_i (\underline{S}_i^{ig}(T_R,P_R) + \int_{T_R}^{T} \frac{C_p}{T} dT - Rln\frac{P}{P_R}) \\ + RT\sum_{i=1}^{n_c} x_i ln x_i + RT\sum_{i=1}^{n_c} x_i ln\phi_i(T,P,\vec{x}),\end{aligned} \tag{B.9}$$

The ϕ_i in Eq. (B.9) is evaluated from an equation of state (EOS) e.g. the Peng-Robinson (PR) EOS (Peng and Robinson, 1976). The expressions of fugacity coefficient using the PR EOS are given in Chang (1990). For isothermal applications one can set $T_R = T$, $\underline{H}^{ig}_{i(T_R)} = 0$, and $\underline{S}^{ig}_{i(T_R,P_R)} = 0$ to simplify Eq. (B.9) to

$$\begin{aligned}\underline{G}(T,P,\vec{x}) &= \sum_{i=1}^{n_c} x_i(\underline{H}_i^{ig}(T_R) - T\underline{S}_i^{ig}(T_R,P_R)) \\ &\quad - RTlnP_R + RT\sum_{i=1}^{n_c} x_i ln[\phi_i(T,P,\vec{x})x_iP] \\ &= -RTlnP_R + RT\sum_{i=1}^{n_c} x_i ln[\phi_i(T,P,\vec{x})x_iP].\end{aligned} \tag{B.10}$$

The molar Helmholtz free energy ($\underline{A}$) can be calculated from

$$\underline{A}(T,P,\vec{x}) = \underline{G}(T,P,\vec{x}) - P\underline{V}, \tag{B.11}$$

where $\underline{V}$ is molar volume of the real mixture at T, P, and composition $\vec{x}$. For a given total volume V, temperature T, and vector of mole number of components $\vec{n}$, the PR EOS results in the following expression for the total Helmholtz free energy A (Firoozabadi, 1999)

$$\begin{aligned}A(T,P,\vec{n}) &= -nRTln\frac{V-B}{RT} - \frac{A^*}{2\sqrt{2}}ln\left(\frac{V+(1+\sqrt{2})B}{V+(1-\sqrt{2})B}\right) \\ &\quad + RT\sum_{i=1}^{n_c} n_i \ln n_i + \sum_{i=1}^{n_c} n_i\left(\underline{U}_i^{ig}(T_R,P_R) - T\underline{S}_i^{ig}(T_R,P_R)\right),\end{aligned} \tag{B.12}$$

where A^* and B are the energy and covolume parameters of the mixture and n_i is the number of moles of component i. When $\underline{H}_i^{ig}(T_R)$ is set to zero in Eq. (B.9) then $\underline{U}_i^{ig}(T_R,P_R)$ in Eq. (B.12) is given by

$$\underline{U}_i^{ig}(T_R,P_R) = -P_R\underline{V}_i^{ig} = -RT_R, \tag{B.13}$$

where $\underline{V}_i^{ig}$ is molar volume of component i in ideal gas state. If consistent values are used for the reference states then the Eqs. (B.10) and (B.11) result in the same value of $\underline{A}$ as Eq. (B.12) when normalized by the total number of moles.

Appendix C: Constant-Volume-Depletion (CVD) Simulations for the Gas Condensate Fluids of Cases 1 and 2 in Chapter 6

We performed CVD simulations for the real gas condensate fluids that were used in the simulations of Cases 1 and 2 in Chapter 6. Three CVD simulations were performed for each fluid. One of the CVD simulations was performed at zero capillary pressure and the other two CVD simulations were performed for the pore radii of 1 nm and 5 nm. The traditional CVD experiments or simulations are started at the saturation point with a fixed amount of the reservoir fluid (Pedersen *et al.*, 2014). However, since the dewpoint pressure is different for the simulations with different capillary pressure values, starting the CVD simulations at the saturation point requires using either different initial amounts of the reservoir fluid or different initial volumes for the different CVD simulations. Thus, we begin the CVD simulations at a pressure larger than the dewpoint pressure of the CVD simulation with the smallest pore radius. We successively decrease the gas pressure and remove the excess gas in each step in order to maintain the volume at its initial value (V_d). The liquid volume (V_o), number of gas moles produced (n_g), gas compressibility factor (z factor) and interfacial tension (σ) are calculated in each step. This procedure will lead to the same values of V_o/V_d, n_g/ n_{gi} and intensive properties of the oil and gas phases as the traditional CVD calculations. Furthermore, this CVD simulation is very similar to the actual reservoir simulation problem (a single-cell approximation) where the initial reservoir pressure is above the dewpoint pressure and allows a fair comparison of gas production from different simulations. We start the CVD simulations from the pressure of 3,500 psia using one mole of the initial reservoir fluid and decrease the pressure to 1,000 psia in 100 steps.

The dewpoint pressure of the gas condensate fluid in Case 1 of Chapter 6 at 130°F in the CVD simulation without capillary pressure is 3,093 psia. The dewpoint pressures with the pore radii of 5 nm and 1 nm are 3,114.7 psia and 3176.4 psia, respectively. Figure C-1 through Figure C-5 show the V_o/V_d, cumulative gas produced, gas moles produced in each step, interfacial tension, and *z* factor of the gas phase from the CVD simulation without capillary pressure and the CVD simulations with the pore radii of 1 nm and 5 nm for the gas condensate fluid in Case 1 of Chapter 6. The volume of the condensed liquid (Figure C-1) and *z* factor of the gas phase (Figure C-5) increase as the capillary pressure increases in the CVD simulations. Interfacial tension decreases as the capillary pressure increases in the CVD simulation (Figure C-4). The amount of produced gas is slightly larger at the initial steps of depletion and is smaller at the later steps of depletion in the CVD simulations with the larger capillary pressure values (Figure C-3).

The dewpoint pressure of the gas condensate fluid in Case 2 of Chapter 6 at 450°F is 3,168.3 psia at zero capillary pressure. The dewpoint pressures in the pore radii of 1 nm and 5 nm are 3,190.80 psia and 3,174.44 psia, respectively. Figure C-6 through Figure C-10 show the V_o/V_d, cumulative gas produced, produced gas in each step, interfacial tension, and *z* factor of the gas phase from the CVD simulation without capillary pressure and the CVD simulations with pore radii of 1 nm and 5 nm for the gas condensate fluid in Case 2 of Chapter 6. The effect of capillary pressure on the volume of the condensed liquid, *z* factor of the gas phase, interfacial tension, and produced gas in each step in the CVD simulations of this fluid follow the same trends as those observed in the CVD simulations with the previous fluid.

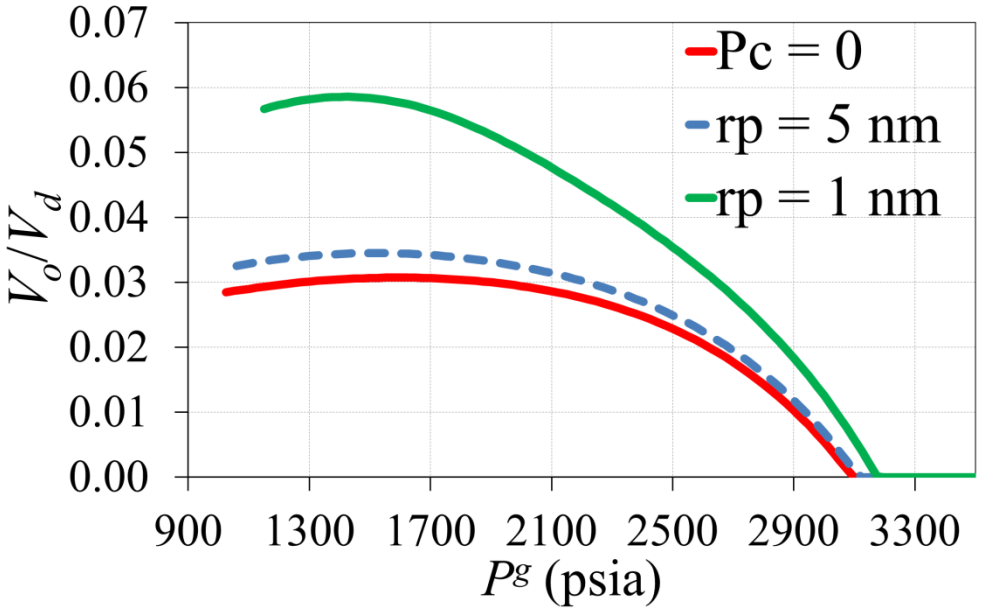

Figure C-1: V_o/V_d from the CVD simulation without capillary pressure and the CVD simulations with pore radii of 1 nm and 5 nm for the gas condensate fluid in Case 1 of Chapter 6.

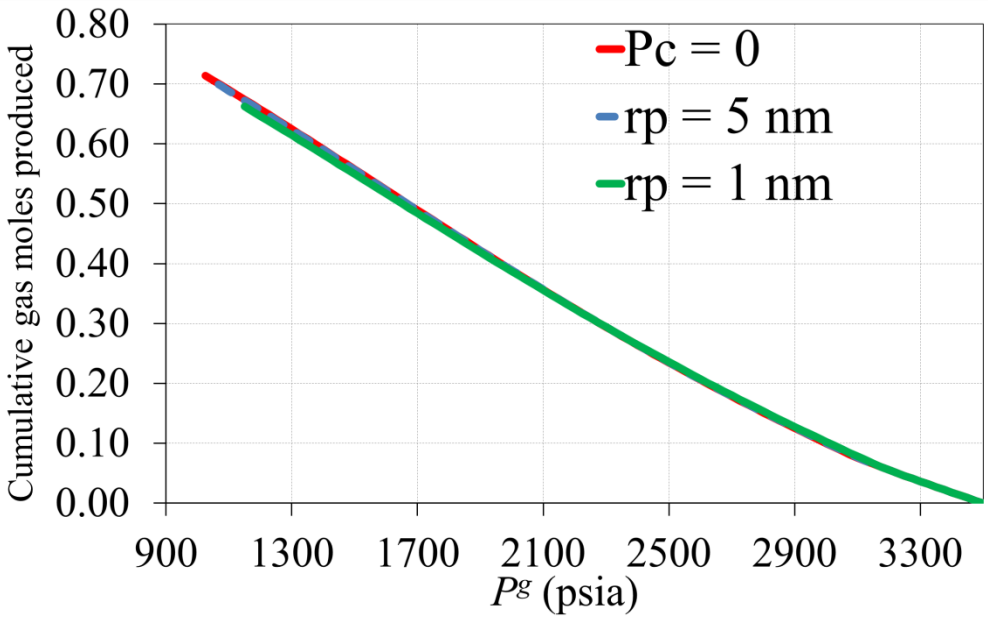

Figure C-2: Cumulative gas produced from the CVD simulation without capillary pressure and the CVD simulations with pore radii of 1 nm and 5 nm for the gas condensate fluid in Case 1 of Chapter 6.

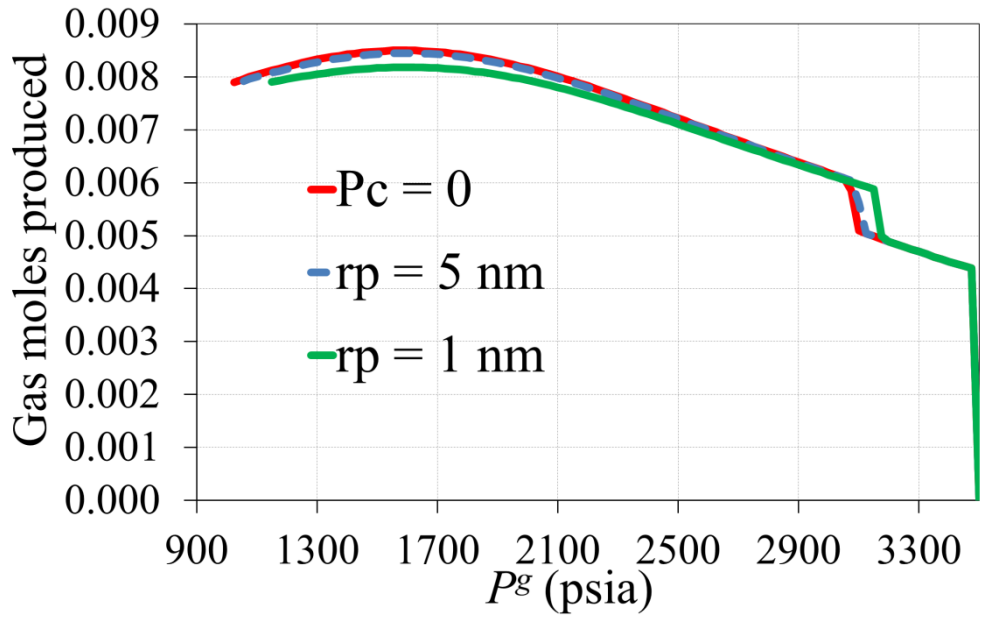

Figure C-3: Produced gas from the CVD simulation without capillary pressure and the CVD simulations with pore radii of 1 nm and 5 nm for the gas condensate fluid in Case 1 of Chapter 6.

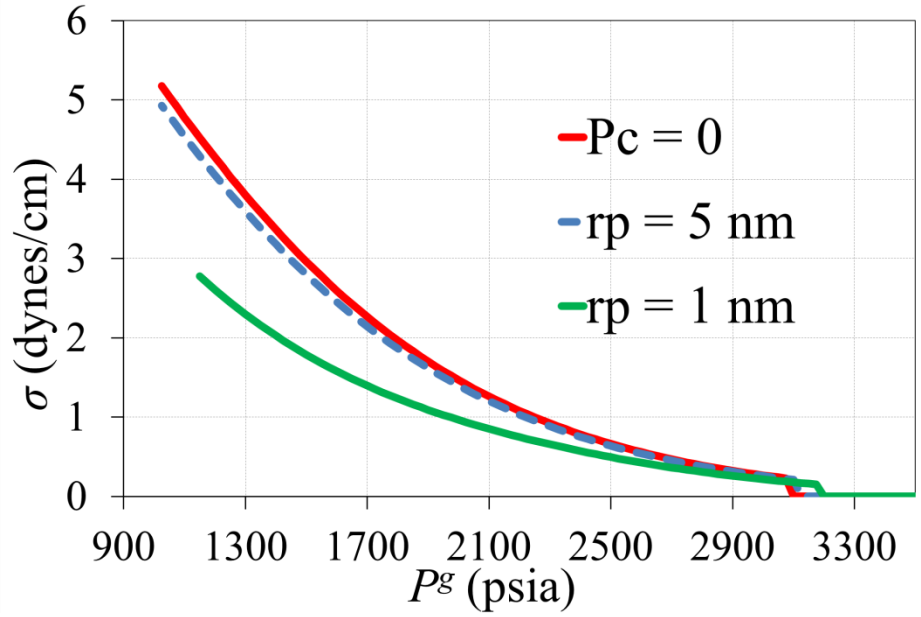

Figure C-4: Gas/oil interfacial tension from the CVD simulation without capillary pressure and the CVD simulations with pore radii of 1 nm and 5 nm for the gas condensate fluid in Case 1 of Chapter 6.

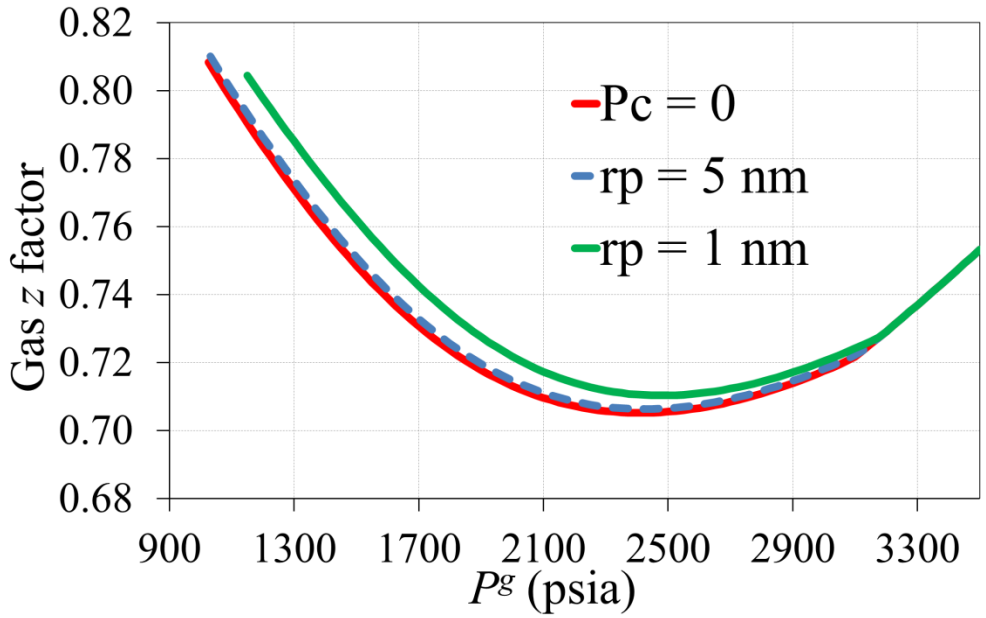

Figure C-5: Gas phase's z factor from the CVD simulation without capillary pressure and the CVD simulations with pore radii of 1 nm and 5 nm for the gas condensate fluid in Case 1 of Chapter 6.

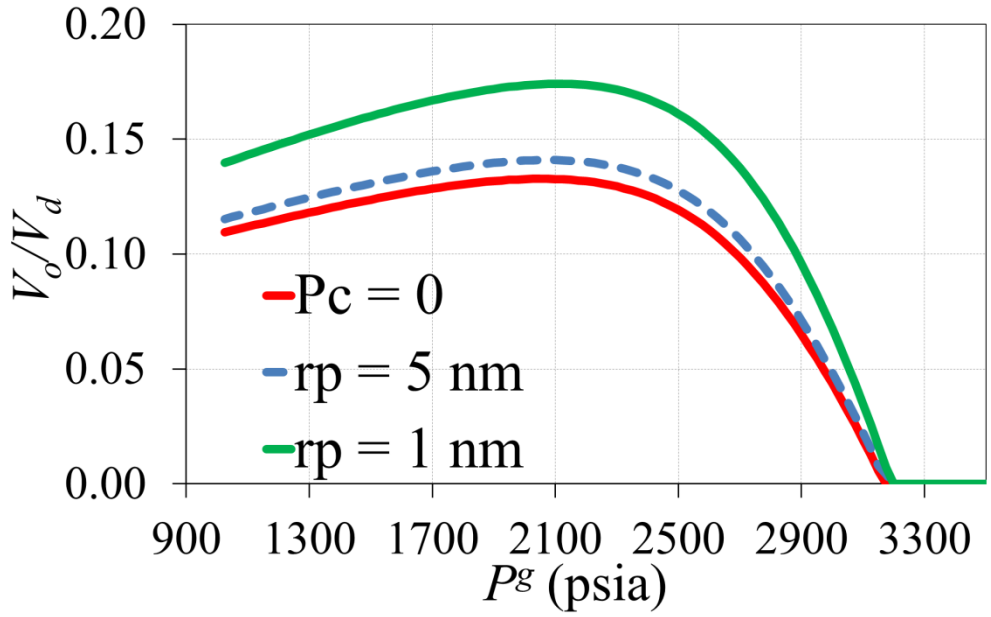

Figure C-6: V_o/V_d from the CVD simulation without capillary pressure and the CVD simulations with pore radii of 1 nm and 5 nm for the gas condensate fluid in Case 2 of Chapter 6.

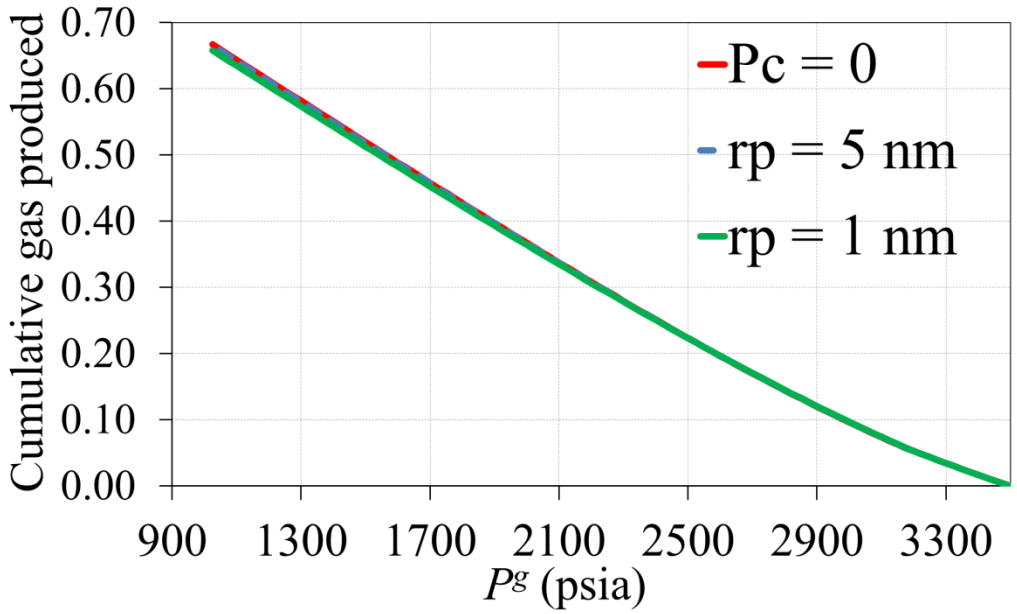

Figure C-7: Cumulative gas produced from the CVD simulation without capillary pressure and the CVD simulations with pore radii of 1 nm and 5 nm for the gas condensate fluid in Case 2 of Chapter 6.

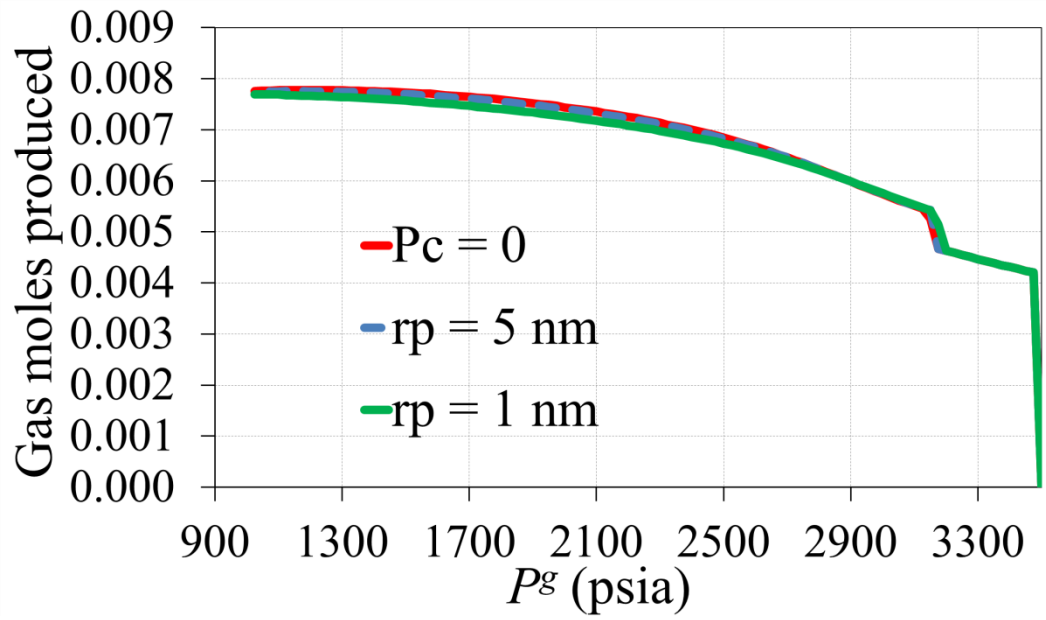

Figure C-8: Produced gas from the CVD simulation without capillary pressure and the CVD simulations with pore radii of 1 nm and 5 nm for the gas condensate fluid in Case 2 of Chapter 6.

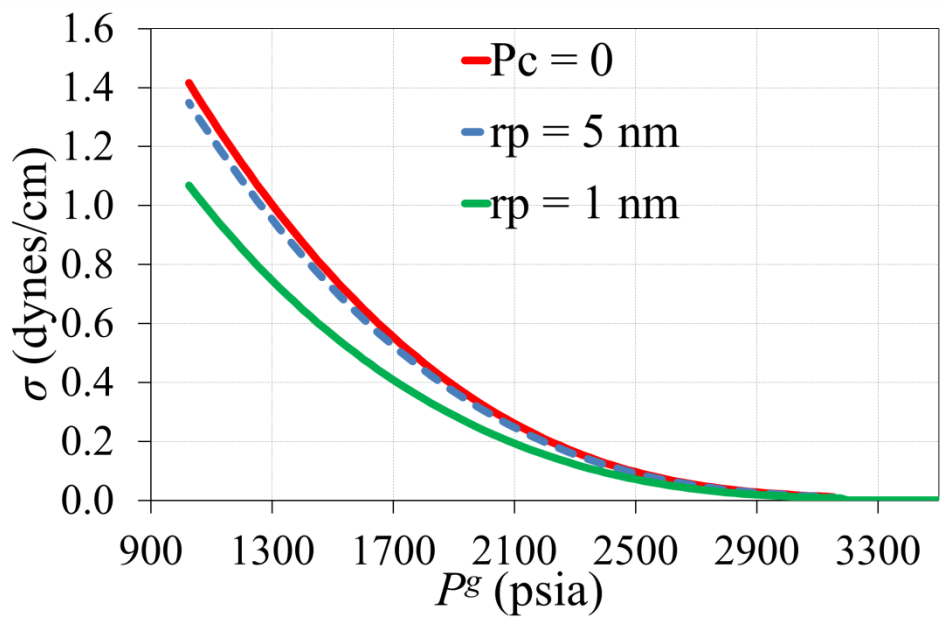

Figure C-9: Gas/oil interfacial tension from the CVD simulation without capillary pressure and the CVD simulations with pore radii of 1 nm and 5 nm for the gas condensate fluid in Case 2 of Chapter 6.

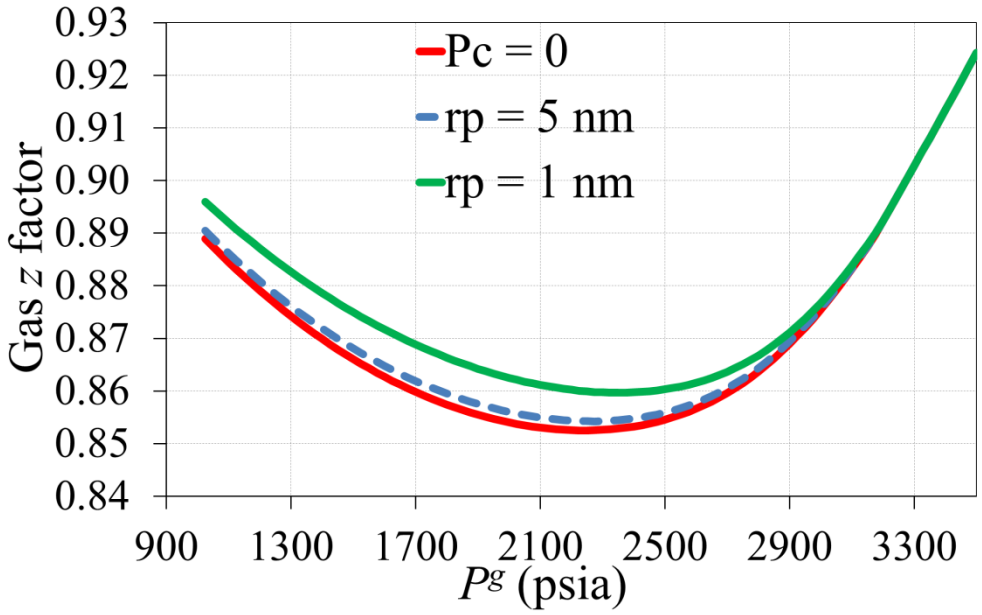

Figure C-10: Gas phase's z factor from the CVD simulation without capillary pressure and the CVD simulations with pore radii of 1 nm and 5 nm for the gas condensate fluid in Case 2 of Chapter 6.

Glossary

Symbols

a	=	Total surface area of an open system
A	=	Helmholtz free energy
$\underline{A}$	=	Molar Helmholtz free energy
A^*	=	Dimensionless attraction term for a cubic equation of state
B	=	Dimensionless covolume parameter for a cubic equation of state
c_f	=	Formation compressibility
C_{pc}	=	Coefficient of the capillary pressure model in UTCOMP
C_p	=	Heat capacity of an isobaric process
D	=	Depth of the gridblock
D_L	=	Longitudinal dispersion coefficient
e_j	=	Exponent of phase j in the Corey relative permeability model
E_{pc}	=	Exponent of the capillary pressure model in UTCOMP
f_{ij}	=	Fugacity of component i in phase j
$\overrightarrow{f_j}$	=	Vector of fugacity of components in phase j
F	=	Number of degrees of freedom
F_i	=	Overall fractional flow of component i
G	=	Gibbs free energy
$\underline{G}$	=	Molar Gibbs free energy
H	=	Enthalpy
H	=	Hessian matrix in Eq. (2.51)
J	=	Jacobian matrix
k	=	Permeability
$\overline{\overline{k}}$	=	Permeability tensor
k_{rj}	=	Relative permeability of phase j
K_i	=	Equilibrium ratio (K value) of component i
$\overline{\overline{K_{ij}}}$	=	Dispersion tensor of component i in phase j
l	=	Molar fraction of the liquid phase

L	=	Length of the linear model
MW	=	Molecular weight
n_c	=	Number of components in the mixture
n_P	=	Number of phases
n_i	=	Number of moles of component *i* in a mixture
n_{ij}	=	Number of moles of component *i* in phase *j*
$\overrightarrow{n_j}$ or $\overrightarrow{n^j}$	=	Vector of number of moles of components in phase *j*
N	=	Total number of moles
N_B	=	Number of gridblocks
N_i	=	Total number of moles of component *i* in the system
Pe	=	Cell Peclet number
P	=	Absolute pressure
P_c	=	Capillary pressure
P_c	=	Critical pressure in the Tables of fluid components' EOS properties and in Eq. (2.71)
$P_{c\max}$	=	Maximum capillary pressure where capillary equilibrium is possible
P_R	=	Reference pressure
P_{vp}	=	Vapor pressure in the absence of capillary pressure
q_i	=	Molar flow rate of component *i*
Q	=	Heat
Q_{rev}	=	Heat exchanged in a reversible process
r	=	Pore radius
R	=	Universal gas constant
$\overrightarrow{R}$	=	The residuals vector
S	=	Entropy
S	=	Saturation in Chapters 3, 5, and 6
$\underline{S}$	=	Molar entropy
$\overline{S_j}$	=	Normalized saturation of phase *j*
S_{jr}	=	Residual saturation of phase *j*

t	=	Time
T	=	Absolute temperature
T_c	=	Critical temperature
T_R	=	Reference temperature
TL	=	Length of tie line
$T(\vec{x})$	=	Tangent hyperplane to the Gibbs free energy hypersurface
U	=	Internal energy
$\underline{U}$	=	Molar internal energy
v	=	Molar fraction of gas phase
v_i	=	Interstitial velocity
V	=	Volume
$\underline{V}$	=	Molar volume
V_b	=	Bulk volume
V_c	=	Critical volume
V_d	=	Initial volume or volume at the dewpoint in the CVD test simulations
V_p	=	Pore volume
$\overline{V_{ti}}$	=	Partial derivative of the total fluid volume with respect to total number of moles of component *i*
$\vec{x}$	=	Composition vector
x_i	=	Mole fraction of component *i*
x_{ij}	=	Mole fraction of component *i* in phase *j*
$\overrightarrow{X}$	=	Vector of independent variables
$\vec{y}$	=	Composition vector
y_i	=	Mole fraction of component *i*
$y^{(m)}$	=	*m*-th order Legendre transform of function *y*
W	=	Work
$\vec{z}$	=	Overall composition vector
zf_i	=	Flowing mole fraction of component *i*
zi_i	=	Injection mole fraction of component *i*
z_i	=	Overall mole fraction of component *i*

Greek letters

α_L	=	Longitudinal dispersivity
γ_j	=	Specific weight of phase *j*
γ_i	=	Tie line parameter corresponding to component *i*
ε	=	Tie-line detection tolerance
τ	=	Dimensionless time in Eq. (3.9)
ϕ	=	Porosity
ϕ_i	=	Fugacity coefficient of component *i*
ϕ_{ij}	=	Fugacity coefficient of component *i* in phase *j*
η_i	=	The local stability criterion determinant corresponding to the *i*–th order Legendre transform of the basis function
θ_i	=	i^{th} reduced parameter
λ_{rj}	=	Relative mobility of phase *j*
λ_j	=	Mobility of phase *j*
σ	=	Interfacial tension
σ_{LJ}	=	Collision diameter
ω	=	Acentric factor
μ_i	=	Chemical potential of component *i*
μ_j	=	Viscosity of phase *j*
ξ_j	=	Molar density of phase *j*
χ	=	Independent variable in Eq. (3.12)
ψ	=	Dimensionless distance in Eq. (3.9)

Superscripts

c	=	Critical property
g	=	Gas

ig	=	Ideal gas
k	=	Index for iteration steps
l	=	Liquid
o	=	Oil
t	=	Total fluid
v	=	Gas

Subscripts

b	=	Bulk
g	=	Gas
gw	=	Gas-water
max	=	Maximum
o	=	Oil
og	=	Oil-gas
p	=	Pore
rev	=	Reversible
t	=	Total fluid
w	=	Water

Abbreviations

ASS	=	Accelerated successive substitution
BIP	=	Binary interaction parameter
CCE	=	Constant composition expansion
CDE	=	Convection-diffusion equation
CE	=	Capillary equilibrium
CFL	=	Courant-Friedrichs-Lewy

CPU	=	Central processing unit
CSAT	=	Compositional space adaptive tabulation
CSP	=	Compositional space parameterization
CVD	=	Constant volume depletion
DMIN	=	Minimum acceptable distance to phase boundary
EOS	=	Equation of state
GFE	=	Gibbs free energy
GPAS	=	Fully implicit "general purpose adaptive simulator" developed at the University of Texas at Austin
HM1	=	Heuristic method 1
HM2	=	Heuristic method 2
IFT	=	Interfacial tension
IMPEC	=	Implicit pressure explicit composition
IPARS	=	Integrated parallel accurate reservoir simulator
MCM	=	Multi-contact miscible
MCP	=	Minimal critical pressure
MMC	=	Multiple mixing cell
MME	=	Minimum miscibility enrichment
MMP	=	Minimum miscibility pressure
MOC	=	Method of characteristics
PC-SAFT	=	Perturbed-chain statistical associating fluid theory
PR	=	Peng-Robinson
RR	=	Rachford-Rice equation
scf/d	=	Standard cubic feet per day
sec	=	Second
SS	=	Successive substitution
SSC	=	Supercritical state criterion
STB/d	=	Stock tank barrel per day
TDBA	=	Tie-line distance based approximation
TPD	=	Tangent plane distance

TSB	=	Tie-simplex based
UTCOMP	=	IMPEC-type compositional reservoir simulator developed at The University of Texas at Austin

References

Abbott, M.M., Smith, J.M., and Van Ness, H.C., 2001. *Introduction to Chemical Engineering Thermodynamics* (pp. 91-100). McGraw-Hill.

Abhvani, A.S., and Beaumont, D.N., 1987. Development of an Efficient Algorithm for the Calculation of Two-Phase Flash Equilibria. SPE Reservoir Engineering, 2(4), 695-702.

Adepoju, O.O., Lake, L.W., and Johns, R.T., 2013. Investigation of Anisotropic Mixing in Miscible Displacements. SPE Reservoir Evaluation and Engineering, 16(1), 85-96.

Adepoju, O.O., 2013. Scale-up of Dispersion for Simulation of Miscible Displacements. PhD Dissertation, The University of Texas at Austin, Austin, Texas.

Ahmadi, K., and Johns, R.T., 2011. Multiple-Mixing-Cell Method for MMP Calculations. SPEJ, 16(4), 733-742, doi:10.2118/116823-PA.

Ahmadi Rahmatabadi, K., 2011. Advances in Calculation of Minimum Miscibility Pressure. PhD Dissertation, The University of Texas at Austin, Austin, Texas.

Al-Rub, F. A.A., and Datta, R., 1998. Theoretical Study of Vapor Pressure of Pure Liquids in Porous Media. Fluid phase equilibria, 147(1), 65-83.

Al-Rub, F. A. A., and Datta, R., 1999. Theoretical Study of Vapor–Liquid Equilibrium Inside Capillary Porous Plates. Fluid phase equilibria, 162(1), 83-96.

Aziz, K., and Wong, T.W., 1988. Considerations in the Development of Multipurpose Reservoir Simulation Models. In proceedings of the 1st and 2nd International Forum on Reservoir Simulation, Alpbach, Austria (pp. 12-16).

Baker, L.E., and Luks, K.D., 1980. Critical Point and Saturation Pressure Calculations for Multipoint Systems. Soc. Pet. Eng. J, 20, 15-24.

Baker, L.E., Pierce, A.C., and Luks, K.D., 1982. Gibbs Energy Analysis of Phase Equilibria. SPEJ 22(5), 731-742.

Balay, S., Gropp, W., MnInnes, L.C., and Smith, B., April 1998. PETSc 2.0 User manual. Argonne National Laboratory, ANL-95/11-Revision 2.0.22.

Bear, J., 1972. *Dynamics of Fluids in Porous Media*. American Elsevier Publishing Company, New York, USA.

Beegle, B.L., Modell, M., and Reid, R.C., 1974. Legendre Transforms and Their Application in Thermodynamics. AIChE Journal, 20(6), 1194-1200.

Belkadi, A., Yan, W., Michelsen, M.L., and Stenby, E.H., 2011. Comparison of Two Methods for Speeding up Flash Calculations in Compositional Simulations, Paper SPE 142132, presented at the SPE Reservoir Simulation Symposium, Woodlands, TX.

Branco, C.M., and Rodriguez, F., 1996. A Semi-Implicit Formulation for Compositional Reservoir Simulation. SPE Advanced Technology Series, 4(01), 171-177.

Brusilovsky, A.I., 1992. Mathematical Simulation of Phase Behavior of Natural Multicomponent Systems at High Pressures With an Equation of State. SPE reservoir engineering, 7, 117-117. doi:10.2118/20180-PA.

Cao, H., 2002. Development of Techniques for General Purpose Simulators. PhD dissertation, Stanford University, Stanford, California.

Chang, Y.B., 1990. Development and Application of an Equation of state Compositional Simulator. PhD dissertation, The University of Texas at Austin, Austin, Texas.

Charlton, S.R., and Parkhurst, D.L. 2011. Modules Based on the Geochemical Model PHREEQC for Use in Scripting and Programming Languages. Computers & Geosciences, 37(10), 1653–1663. doi:10.1016/j.cageo.2011.02.005.

Chopra, A.K., and Carter, R.D., 1986. Proof of the Two-Phase Steady-State Theory for Flow Through Porous Media. SPE Formation Evaluation, 1(6), 603-608.

Clarkson, C.R., Wood, J., Burgis, S., Aquino, S., and Freeman, M., 2012. Nanopore-Structure Analysis and Permeability Predictions for a Tight Gas Siltstone Reservoir By Use of Low-Pressure Adsorption and Mercury-Intrusion Techniques. SPE Reservoir Evaluation and Engineering, 15(06), 648-661.

Coats, K.H., 1980. An Equation of State Compositional Model. SPE J, 20(5), 363-376.

Collins, D.A., Nghiem, L.X., Li, Y.K., and Grabenstetter, J.E., 1992. An Efficient Approach to Adaptive-Implicit Compositional Simulation with an Equation of State. SPE Reservoir Engineering, 7(2), 259-264.

Cook, A.B., Walker, C.J., and Spencer, G.B., 1969. Realistic K Values of C_{7+} Hydrocarbons for Calculating Oil Vaporization During Gas Cycling at High Pressures. Journal of Petroleum Technology, 21(7). doi:10.2118/2276-PA.

Corey, A.T., 1986. *Mathematics of Immiscible Fluids in Porous Media*. Water Resources Publication, Littleton (CO).

Crowe, C.M., and Nishio, M., 1975. Convergence Promotion in the Simulation of Chemical Processes-The General Dominant Eigenvalue Method. AIChE Journal, Vol. 21(3), 528-533.

Devegowda, D., Sapmanee, K., Civan, F., and Sigal, R.F., 2012. Phase Behavior of Gas Condensates in Shales Due to Pore Proximity Effects: Implications for Transport, Reserves and Well Productivity. Society of Petroleum Engineers. doi:10.2118/160099-MS.

DiCarlo, D.A., Akshay, S., and Blunt, M.J., 2000. Three-Phase Relative Permeability of Water-Wet, Oil-Wet, and Mixed-Wet Sandpacks. SPE Journal, 5(01), 82-91.

Dindoruk, B. 1992. Analytical Theory of Multiphase, Multicomponent Displacement in Porous Media. PhD dissertation, Stanford University, Stanford, California.

Dindoruk, B., Orr, F.M., Jr., and Johns, R.T., 1997. Theory of Multicontact Miscible Displacement with Nitrogen. SPEJ, 2(3), 268–279.

Du, L., and Chu, L., 2012. Understanding Anomalous Phase Behavior in Unconventional Oil Reservoirs. Society of Petroleum Engineers. doi:10.2118/161830-MS.

Egwuenu, A.M., Johns, R.T., and Li, Y., 2005. Improved Fluid Characterization For Miscible Gas Floods. Society of Petroleum Engineers. doi:10.2118/94034-MS.

Elliott, J.R., and Lira, C.T. 1999. *Introductory chemical engineering thermodynamics*. Upper Saddle River, NJ: Prentice Hall PTR.

Entov, V.M., Turetskaya, F.D., and Voskov, D.V., 2001. On Approximation of Phase Equilibria of Multicomponent Hydrocarbon Mixtures and Prediction of Oil Displacement by Gas Injection. In 8th European Conference on the Mathematics of Oil Recovery.

Fanchi, J. R., 1983. Multidimensional Numerical Dispersion. SPEJ, 23(1), 143-151.

Fevang, Ø., and Whitson, C.H., 1996. Modeling gas-condensate well deliverability. SPE Reservoir Engineering, 11(04), 221-230.

Firincioglu, T., Ozkan, E., and Ozgen, C., 2012. Thermodynamics of Multiphase Flow in Unconventional Liquids-Rich Reservoirs. Society of Petroleum Engineers. doi:10.2118/159869-MS.

Firoozabadi, A., 1999. *Thermodynamic of Hydrocarbon Reservoirs*. New York: McGraw-Hill.

Fraces, C., Voskov, D.V., and Tchelepi, H.A., 2009. A New Method for Thermodynamic Equilibrium Computation of Systems With an Arbitrary Number of Phases. Society of Petroleum Engineers. doi:10.2118/119060-MS.

Gautam, R., and Seider, W.D., 1979. Computation of Phase and Chemical Equilibrium: Part I. Local and Constrained Minima in Gibbs Free Energy. AIChE Journal, 25(6), 991-999.

Gibbs, J.W., 1878. On the Equilibrium of Heterogeneous Substances. American Journal of Science, (96), 441-458.

Gill, P.E., Murray, W., and Wright, M.H., 1981. *Practical Optimization*. Academic press, London.

Gill, P.E., and Murray, W., 1974. Newton-Type Methods for Unconstrained and Linearly Constrained Optimization. Mathematical Programming, 7(1), 311-350.

Gorucu, S.E., and Johns, R.T., 2014. Comparison of Reduced and Conventional Two-Phase Flash Calculations. Society of Petroleum Engineers. doi:10.2118/163577-PA.

Gosset, R., Heyen, G., and Kalitventzeff, B., 1986. An Efficient Algorithm to Solve Cubic Equations of State. Fluid Phase Equilibria, 25(1), 51-64.

Goudarzi, A., Delshad, M., Mohanty, K.K., and Sepehrnoori, K., 2015. Surfactant Oil Recovery in Fractured Carbonates: Experiments and Modeling of Different Matrix Dimensions. Journal of Petroleum Science and Engineering, 125, 136-145, doi:10.1016/j.petrol.2014.11.008.

Gropp, W., Morgan, T., Smith, B., Arbogast, T., Dawson, C.N., Lake, L.L., McKinney, D.C., Pope, G.A., Sepehrnoori, K., and Wheeler, M.F., 1996 (May). New Generation Framework for Petroleum Reservoir Simulation. First Annual Report, Advanced Technology Initiative, Argonne National Laboratory and The University of Texas at Austin.

Gross, J., and Sadowski, G., 2001. Perturbed-Chain SAFT: An Equation of State Based on a Perturbation Theory for Chain Molecules. Industrial and Engineering Chemical Research, 40 (4), 1244–1260.

Haajizadeh, M., Fayers, F.J., Cockin, A.P., Roffey, M., and Bond, D.J., 1999. On the Importance of Dispersion and Heterogeneity in the Compositional Simulation of Miscible Gas Processes. Society of Petroleum Engineers. doi:10.2118/57264-MS.

Haajizadeh, M., Fayers, F.J., and Cockin, A.P., 2000. Effects of Phase Behavior, Dispersion and Gridding on Sweep Patterns for Nearly Miscible Gas Displacement. Society of Petroleum Engineers. doi:10.2118/62995-MS.

Hamada, Y., Koga, K., and Tanaka, H., 2007. Phase Equilibria and Interfacial Tension of Fluids Confined in Narrow Pores. The Journal of chemical physics, 127(8), 084908.

Han, C., Delshad, M., Sepehrnoori, K., and Pope, G.A., 2005. A Fully Implicit, Parallel, Compositional Chemical Flooding Simulator. Society of Petroleum Engineers. doi:10.2118/97217-MS.

Haugen, K.B., and Beckner, B., 2013. A Critical Comparison of Reduced and Conventional EOS Algorithms. SPE Journal, 18(02), 378-388, doi:10.2118/141399-PA.

Heidemann, R.A., 1975. The Criteria for Thermodynamic Stability. AIChE Journal, 21(4), 824-826.

Heidemann, R.A., and Khalil, A.M., 1980. The Calculation of Critical Points. AIChE Journal, 26(5), 769-779.

Helfferich, F.G., 1981. Theory of Multicomponent, Multiphase Displacement in Porous Media. Soc. Pet. Eng. J, 21(1), 51-62. doi:10.2118/8372-PA.

Helland, J.O., and Skjæveland, S.M., 2004. Three-Phase Capillary Pressure Correlation for Mixed-Wet Reservoirs. Society of Petroleum Engineers. doi:10.2118/92057-MS.

Hendriks, E.M., and Van Bergen, A.R.D., 1992. Application of a Reduction Method to Phase Equilibria Calculations. Fluid Phase Equilibria, 74, 17-34.

Iranshahr, A., Voskov, D.V., and Tchelepi H.A., 2010. Tie-Simplex Parameterization for EOS-Based Thermal Compositional Simulation. SPEJ, 15(2), 545-556.

Iranshahr, A., Voskov, D.V., and Tchelepi, H.A., 2012. Gibbs Energy Analysis: Compositional Tie-Simplex space. Fluid Phase Equilibria, 321, 49-58.

Iranshahr, A., Voskov, D.V., and Tchelepi, H.A., 2013. Tie-Simplex Based Compositional Space Parameterization: Continuity and Generalization to Multiphase Systems. AIChE Journal, 59(5), 1684-1701.

Jaubert, J.N., Wolff, L., Neau, E., and Avaullee, L., 1989. A very Simple Multiple-Mixing-Cell Calculation to Compute the Minimum Miscibility Pressure Whatever the Displacement Mechanism. Industrial and Engineering Chemistry Research, 37(12), pp. 4854-4859. doi: 10.1021/ie980348r.

Javadpour, F., Fisher, D., and Uusworth, M., 2007. Nanoscale Gas Flow in Shale Sediments. Journal of Canadian Petroleum Technology, Vol. 46, No. 10, pp. 55-61.

Javadpour, F., 2009. Nanopores and Apparent Permeability of Gas Flow in Mudrocks (Shales and Siltstone). Journal of Canadian Petroleum Technology, 48(8), 16-21. doi:10.2118/09-08-16-DA.

Jensen, B.H. and Fredenslund, A., 1987. A Simplified Flash Procedure for Multicomponent Mixtures Containing Hydrocarbons and One Non-Hydrocarbon Using Two-Parameter Cubic Equation of State. Ind. Eng. Chem. Res., 26(10), 2129-2134.

Jerauld, G.R., Lin, C.Y., Webb, K.J., and Seccombe, J.C., 2008. Modeling Low-Salinity Waterflooding. SPE Reservoir Evaluation and Engineering, 11(6), 1000. doi:10.2118/102239-PA.

Jessen, K., Stenby, E.H., and Orr, F.M., 2004. Interplay of Phase Behavior and Numerical Dispersion in Finite-Difference Compositional Simulation. SPEJ 9, 193–201.

Johns, R.T., Fayers, F.J., and Orr, F.M., 1994. Effect of Gas Enrichment and Dispersion on Nearly Miscible Displacements in Condensing/Vaporizing Drives. SPE Adv. Tech. Ser. 2, 26–34.

Johns, R.T., and Garmeh, G., 2010. Upscaling of Miscible Floods in Heterogeneous Reservoirs Considering Reservoir Mixing. Society of Petroleum Engineers. doi:10.2118/124000-PA.

Johns, R.T., 1992. Analytical Theory of Multicomponent Gas Drives With Two-Phase Mass Transfer. PhD dissertation, Stanford University, Stanford, California.

Johns, R.T. and Orr, F.M., Jr., 1996. Miscible Gas Displacement of Multicomponent Oils. SPEJ, 1(1), 39–50.

Johns, R.T., Sah, P., and Solano, R., 2002. Effect of Dispersion on Local Displacement Efficiency for Multicomponent Enriched-Gas Floods Above the Minimum Miscibility Enrichment. Society of Petroleum Engineers. doi:10.2118/75806-PA.

Katsube, T.J., 2000. Shale Permeability and Pore-Structure Evolution Characteristics. Geological Survey of Canada, 15, 1-9.

Kenyon, D., and Behie, G.A., 1987. Third SPE Comparative Project: Gas Cycling of Retrograde Condensate Reservoirs. J. Pet. Tech. 39(8), 981-997. SPE-12278-PA. doi: 10.2118/12278-PA.

Khorsandi, S., Ahmadi, K., Johns, R.T., 2014. Analytical Solutions for Gas Displacements with Bifurcating Phase Behavior. Society of Petroleum Engineers. doi:10.2118/166487-PA.

Killough, J.E., and Kossack, C.A., 1987. Fifth Comparative Solution Project: Evaluation of Miscible Flood Simulators. Paper SPE 16000 presented at the SPE Reservoir Simulation Symposium, San Antonio, Texas.

Kianinejad, A., Aminzadeh, B., Chen, X, and Dicarlo, D.A., 2014. Three-Phase Relative Permeabilities as a Function of Flow History. Paper SPE 169083 presented at the Society of Petroleum Engineers Improved Oil Recovery Symposium, Tulsa, Oklahoma, 12-16 April, http://dx.doi.org/10.2118/169083-MS.

Kianinejad, A., Saidian, M., Mavaddat, M., Ghazanfari, M.H., Kharrat, R., and Rashtchian, D., 2015. Worm-like Micelles: A New Approach for Heavy Oil Recovery from Fractured Systems. The Canadian Journal of Chemical Engineering, 93 (5): 951-958, doi: 10.1002/cjce.22166.

Korrani, A.K.N., Jerauld, G.R., and Sepehrnoori, K. 2014. Coupled Geochemical-Based Modeling of Low Salinity Waterflooding. SPE Improved Oil Recovery Symposium, Tulsa, Okla., USA, 12-16 April, http://dx.doi.org/10.2118/169115-MS.

Korrani, A.K.N., 2014. Mechanistic Modeling of Low Salinity Water Injection. PhD Dissertation, The University of Texas at Austin, Austin, Texas.

Kulkarni, M.M., 2005. Multiphase Mechanisms and Fluid Dynamics in Gas Injection Enhance Oil Recovery Processes. PhD Dissertation, Louisiana State University, Baton Rouge, Louisiana.

Lake, L.W., 1989. *Enhanced Oil Recovery*. Prentice Hall Inc.

Lashgari, H.R., Sepehrnoori, K., Delshad, M., and DeRouffignac, E., 2015. Development of a Four-Phase Chemical-Gas Model in an IMPEC Reservoir Simulator. Presented at the SPE Reservoir Simulation Symposium, Houston, 23–25 February. SPE-173250-MS. http://dx.doi.org/10.2118/173250-MS.

Leverett, M.C., 1941. Capillary Behavior in Porous Solids. Society of Petroleum Engineers. doi:10.2118/941152-G.

Li, Y.K., and Nghiem, L.X., 1982. The Development of a General Phase Envelope Construction Algorithm for Reservoir Fluid Studies. Society of Petroleum Engineers. doi:10.2118/11198-MS.

Li, D., 1994. Curvature Effects on the Phase Rule. Fluid phase equilibria, 98, 13-34.

Li, Y., and Johns, R.T., 2006. Rapid Flash Calculations for Compositional Simulation. SPE Reservoir Evaluation and Engineering, 9(5), 521-529.

Li, Y., and Johns, R.T., 2007. A Rapid and Robust Method to Replace Rachford-Rice in Flash Calculations. Society of Petroleum Engineers. doi:10.2118/106080-MS.

Li, L., Khorsandi, S., Johns, R.T., and Ahmadi, K., 2014a. Multiple Mixing Cell Method for Three-Hydrocarbon-Phase Displacements. Society of Petroleum Engineers. doi:10.2118/169150-MS.

Li, Z., Jin, Z., and Firoozabadi, A., 2014b. Phase Behavior and Adsorption of Pure Substances and Mixtures and Characterization in Nanopore Structures by Density Functional Theory. Society of Petroleum Engineers. doi:10.2118/169819-PA.

Ma, Y., and Jamili, A., 2014. Modeling the Effects of Porous Media in Dry Gas and Liquid Rich Shale on Phase Behavior. Society of Petroleum Engineers. doi:10.2118/169128-MS.

Marcondes, F., and Sepehrnoori, K., 2010. An Element-Based Finite-Volume Method Approach for Heterogeneous and Anisotropic Compositional Reservoir Simulation. Journal of Petroleum Science and Engineering, 73(1), 99-106.

Mehra, R.K., Heidemann, R.A., and Aziz, K., 1983. Accelerated Successive Substitution Algorithm. Canadian Journal of Chemical Engineering, 61(4), 590-595.

Metcalfe, R.S., Fussell, D.D., and Shelton, J.L., 1973. A Multicell Equilibrium Separation Model for the Study of Multiple Contact Miscibility in Rich-Gas Drives. SPEJ, 13(3). doi:10.2118/3995-PA.

Michelsen, M.L., 1980. Calculation of Phase Envelopes and Critical Points for Multi-Component Mixtures, Fluid Phase Equilibria, 4, 1-10.

Michelsen, M.L., 1982a. The Isothermal Flash Problem, Part I Stability Analysis. Fluid Phase Equilibria, 9, 1-19.

Michelsen, M.L., 1982b. The Isothermal Flash Problem, Part II Phase-Split Calculations. Fluid Phase Equilibria, 9, 21-40.

Michelsen M.L., 1986. Simplified Flash Calculations for Cubic Equations of State. Ind. Eng. Chem. Process Des. Dev., 25(1), 184-188.

Michelsen, M.L., 1998. Speeding up the Two-Phase PT-Flash, with Applications for Calculation of Miscible Displacement. Fluid Phase Equilibria, 143, 1-12.

Michelsen, M.L., Mollerup, J.M., 2004. *Thermodynamic Models: Fundamentals and Computational Aspects*. Tie-line publications.

Michelsen, M., Yan, W., and Stenby, E.H., 2013. A Comparative Study of Reduced-Variables-Based Flash and Conventional Flash. Society of Petroleum Engineers. doi:10.2118/154477-PA.

Mikyška, J., and Firoozabadi, A., 2011. A New Thermodynamic Function for Phase-Splitting at Constant Temperature, Moles, and Volume. AIChE Journal, 57(7), 1897-1904.

Mikyška, J., and Firoozabadi, A., 2012. Investigation of Mixture Stability at Given Volume, Temperature, and Number of Moles. Fluid Phase Equilibria, 321, 1-9.

Mohebbinia, S., Sepehrnoori, K., and Johns, R.T., 2013. Four-Phase Equilibrium Calculations of Carbon Dioxide/Hydrocarbon/Water Systems with a Reduced Method. SPE Journal, 18(05), 943-951.

Mohebbinia, S., 2013. Advanced Equation of State Modeling for Compositional Simulation of Gas Floods. PhD dissertation. The University of Texas at Austin, Austin, Texas.

Morishige, K., Fujii, H., Uga, M., and Kinukawa, D., 1997. Capillary Critical Point of Argon, Nitrogen, Oxygen, Ethylene, and Carbon Dioxide in MCM-41. Langmuir, 13(13), 3494-3498.

Naraghi, M.E., and Javadpour, F., 2015. A Stochastic Permeability Model for the Shale-Gas Systems. International Journal of Coal Geology, 140, 111-124.

Nghiem, L.X., and Li, Y.K., 1984. Computation of Multiphase Equilibrium Phenomena with an Equation of State. Fluid Phase Equilibria, 17 (1), 77-95.

Nichita, D. V., Gomez, S., and Luna, E., 2002a. Multiphase Equilibria Calculation by Direct Minimization of Gibbs Free Energy with a Global Optimization Method. Computers and Chemical Engineering, 26(12), 1703-1724.

Nichita, D.V., Gomez, S., and Luna, E., 2002b. Phase Stability Analysis with Cubic Equations of State by Using a Global Optimization Method. Fluid Phase Equilibria, 194, 411-437.

Nojabaei, B., Johns, R.T., and Chu, L., 2013. Effect of Capillary Pressure on Phase Behavior in Tight Rocks and Shales. SPE Reservoir Evaluation and Engineering, 16(03), 281-289.

Nojabaei, B., Siripatrachai, N., Johns, R.T., and Ertekin, T., 2014. Effect of Saturation Dependent Capillary Pressure on Production in Tight Rocks and Shales: A Compositionally-Extended Black Oil Formulation. Society of Petroleum Engineers. doi:10.2118/171028-MS.

Okuno, R., 2009. Modeling of Multiphase Behavior for Gas Flooding Simulation. PhD dissertation, The University of Texas at Austin, Austin, Texas.

Okuno, R., Johns, R.T., and Sepehrnoori, K., 2010. Three-Phase Flash in Compositional Simulation Using a Reduced Method. SPEJ, 15(3), 689-703.

Orr, F. M. Jr., 2007. *Theory of Gas Injection Processes*. Copenhagen, Denmark, Tie-line Publications.

Ortiz, V., López-Álvarez, Y.M., and López, G.E., 2005. Phase Diagrams and Capillarity Condensation of Methane Confined in Single- and Multi-Layer Nanotubes. Molecular Physics, 103(19), 2587-2592.

Pan, F., 2009. Development and Application of a Coupled Geomechanics Model for a Parallel Compositional Reservoir Simulator. PhD dissertation, The University of Texas at Austin, Austin, Texas.

Pan, F., Sepehrnoori, K., and Chin, L., 2007. Development of a Coupled Geomechanics Model for a Parallel Compositional Reservoir Simulator. Society of Petroleum Engineers. doi:10.2118/109867-MS.

Parashar, M., Wheeler, J.A., Pope, G., Wang, K., and Wang, P., 1997. A New Generation EOS Compositional Reservoir Simulator: Part II-Framework and Multiprocessing. Society of Petroleum Engineers. doi:10.2118/37977-MS.

Pedersen, K.S., Thomassen, P., and Fredenslund, A., 1985. Thermodynamics of Petroleum Mixtures Containing Heavy Hydrocarbons. 3. Efficient Flash Calculation Procedure Using the SRK Equation of State. Industrial Engineering Chemical Process Design and development, 24(4): 948-954.

Pedersen, K.S., Christensen, P.L., and Shaikh, J.A., 2014. *Phase Behavior of Petroleum Reservoir Fluids*. CRC Press.

Pederson, K.S., Fjellerup, J., Thomassen, P., and Fredenslund, A., 1986. Studies of Gas Injection into Oil Reservoirs by a Cell-to-Cell Simulation Model. Society of Petroleum Engineers. doi:10.2118/15599-MS.

Peng, D.Y., and Robinson D.B., 1976. A New Two-Constant Equation of State. Industrial and Engineering Chemistry Fundamentals, 15(1), 59-64.

Peng, D.Y., and Robinson, D.B., 1977. A Rigorous Method for Predicting the Critical Properties of Multicomponent Systems from an Equation of State. AIChE Journal, 23(2), 137-144.

PennPVT Toolkit. 2010. Gas Flooding Joint Industry Project. EMS Energy Institute, Pennsylvania State University, University Park, Pennsylvania.

Perschke, D.R., 1988. Equation of State Phase Behavior Modeling for Compositional Simulation. PhD dissertation, The University of Texas at Austin, Austin, Texas.

Perschke, D.R., Chang, Y.B., Pope, G.A., and Sepehrnoori, K., 1989. Comparison of Phase Behavior Algorithms for an Equation-of-State Compositional Simulator. Paper SPE, 19443.

Ping, G., Liangtian, S., Shilun, L., and Lei, S., 1996. A Theoretical Study of the Effect of Porous Media on the Dew Point Pressure of a Gas Condensate. Society of Petroleum Engineers. doi:10.2118/35644-MS.

Pope, G.A., Wu, W., Narayanaswamy, G., Delshad, M., Sharma, M.M., and Wang, P., 2000. Modeling Relative Permeability Effects in Gas-Condensate Reservoirs with a New Trapping Model. SPE Reservoir Evaluation and Engineering, 3(02), 171-178.

Qi, Z., Wang, S., Du, Z., Liang, B., Deng, R., and Zhao, W., 2007. A New Approach for Phase Behavior and Well Productivity Studies in the Deep Gas-Condensate Reservoir with Low Permeability. Society of Petroleum Engineers. doi:10.2118/106750-MS.

Rachford, H.H. Jr. and Rice, J.D., 1952. Procedure for Use of Electronic Digital Computers in Calculating Flash Vaporization Hydrocarbon Equilibrium. (Technical Note 136). J. Pet. Tech., 4(10):19; Trans., AIME, 195: 327-328. SPE-952327-G.

Rai, R.R., 2003. Parametric Study of Relative Permeability Effects on Gas-Condensate Core Floods and Wells. M.S. thesis, The University of Texas at Austin, Austin, Texas.

Rannou, G., Voskov, D., and Tchelepi, H.A., 2013. Tie-Line-Based *K*-Value Method for Compositional Simulation. SPEJ, 18(6),1112-1122, doi:10.2118/167257-PA.

Rasmussen, C.P., Krejberg, K., Michelsen, M.L., and Bjurstrom, K. E., 2006. Increasing the Computational Speed of Flash Calculations with Applications for Compositional, Transient Simulations. SPE Res. Eval. and Eng., 9, 32-38.

Rezaveisi, M., Rostami, B., Kharrat, R., Ayatollahi, S., and Ghotbi, C., 2010. Experimental Investigation of Tertiary Oil Gravity Drainage in Fractured Porous Media. Special Topics & Reviews in Porous Media: An International Journal, 1(2), 179-191.

Rezaveisi, M., Sepehrnoori, K., and Johns, R.T., 2014a. Tie-Simplex-Based Phase-Behavior Modeling in an IMPEC Reservoir Simulator. SPE Journal, 19(02), 327-339.

Rezaveisi, M., Javadpour, F., and Sepehrnoori, K., 2014b. Modeling Chromatographic Separation of Produced Gas in Shale Wells. International Journal of Coal Geology, 121, 110-122.

Rezaveisi, M., Johns, R.T., and Sepehrnoori, K., 2015. Application of Multiple-Mixing-Cell Method to Improve Speed and Robustness of Compositional Simulation. SPE Journal, Preprint, doi: http://dx.doi.org/10.2118/169063-PA.

Ruthven, Douglas M. *Principles of Adsorption and Adsorption Processes*. John Wiley and Sons, 1984.

Sahni, A., Burger, J., and Blunt, M., 1998. Measurement of Three Phase Relative Permeability During Gravity Drainage Using CT. Society of Petroleum Engineers. doi:10.2118/39655-MS.

Sapmanee, K., 2011. Effects of Pore Proximity on Behavior and Production Prediction of Gas/Condensate. M.S. thesis, University of Oklahoma, Tulsa, Oklahoma.

Schmall, L., 2013. Development of a Multi-Formulation Compositional Simulator. PhD Dissertation, The University of Texas at Austin, Austin, Texas.

Schmall, L., Varavei, A., and Sepehrnoori, K., 2013. A Comparison of Various Formulations for Compositional Reservoir Simulation. Society of Petroleum Engineers. doi:10.2118/163630-MS.

Shapiro, Alexander A., and Erling H. Stenby, 1997. Kelvin Equation for a Non-Ideal Multicomponent Mixture. Fluid phase equilibria 134.1 (1997): 87-101.

Shapiro, A.A., and Stenby, E.H., 1999. High Pressure Multicomponent Adsorption in Porous Media. Fluid phase equilibria, 158, 565-573.

Shapiro, A.A., and Stenby, E.H., 2001. Thermodynamics of the Multicomponent Vapor–Liquid Equilibrium Under Capillary Pressure Difference. Fluid Phase Equilibria, 178(1), 17-32.

Shoaib, S., and Hoffman, B.T., 2009. CO_2 Flooding the Elm Coulee Field. Society of Petroleum Engineers. doi:10.2118/123176-MS.

Shojaei, H., Rastegar, R., and Jessen, K., 2012. Mixing and Mass Transfer in Multicontact Miscible Displacements. Transport in Porous Media, 94, 837-857, doi: 10.1007/s11242-012-0027-8.

Sigmund, P.M., Dranchuk, P.M., Morrow, N.R., and Purvis, R.A., 1973. Retrograde Condensation in Porous Media. Society of Petroleum Engineers. doi:10.2118/3476-PA.

Singh, H., Javadpour, F., Ettehadtavakkol, A., and Darabi, H., 2014. Nonempirical Apparent Permeability of Shale. SPE Reservoir Evaluation & Engineering, 17(3), 414-424, doi: http://dx.doi.org/10.2118/170243-PA.

Singh, S.K., Sinha, A., Deo, G., and Singh, J.K., 2009. Vapor-Liquid Phase Coexistence, Critical Properties, and Surface Tension of Confined Alkanes. The Journal of Physical Chemistry C, 113(17), 7170-7180.

Skjaeveland, S.M., Siqveland, L.M., Kjosavik, A., Thomas, W.L.H., and Virnovsky, G.A., 2000. Capillary Pressure Correlation for Mixed-Wet Reservoirs. Society of Petroleum Engineers. doi:10.2118/60900-PA.

Stalkup, F.L., 1990. Effect of Gas Enrichment and Numerical Dispersion on Enriched-Gas-Drive Predictions. SPE Reservoir Engineering, 5(04), 647-655. doi:10.2118/18060-PA.

Sun, A.C., and Seider, W.D., 1995. Homotopy-Continuation Method for Stability Analysis in the Global Minimization of the Gibbs Free Energy. Fluid Phase Equilibria. 103, 213–249.

TACC (Texas Advanced Computing Center). 2014. https://www.tacc.utexas.edu/user-services/user-guides/lonestar-user-guide.

Tarahhom, F., 2008. Development of an Implicit Full-Tensor Dual Porosity Compositional Reservoir Simulator. PhD dissertation, The University of Texas at Austin, Austin, Texas.

Tarahhom, F., Sepehrnoori, K., and Marcondes, F., 2009. A Novel Approach to Integrate Dual Porosity Model and Full Permeability Tensor Representation in Fractures. Society of Petroleum Engineers. doi:10.2118/119001-MS.

Tavassoli, S., 2014. Investigation of the Effects of Buoyancy and Heterogeneity on the Performance of Surfactant Floods. PhD Dissertation, The University of Texas at Austin, Austin, Texas.

Tavassoli, S., Lu, J., Pope, G.A., and Sepehrnoori, K. 2014. Investigation of the Critical Velocity Required for a Gravity-Stable Surfactant Flood. SPE Journal. 19(5): 931-942. http://dx.doi.org/10.2118/163624-PA.

Teklu, T.W., Alharthy, N., Kazemi, H., Yin, X., Graves, R.M., and Al Sumaiti, A.M. 2014. Phase Behavior and Minimum Miscibility Pressure in Nanopores. SPE Reservoir Evaluation and Engineering, 17(03), 396-403. doi:10.2118/168865-PA.

Tester, J.W., and Modell, M., 1997. Thermodynamics and Its Applications. Prentice Hall International Series in the Physical and Chemical Engineering Sciences.

Trangenstein, J.A., 1985. Minimization of Gibbs Free Energy in Compositional Reservoir Simulation. Paper SPE 13520, presented at the SPE Reservoir Simulation Symposium, Dallas, TX. SPE doi:10.2118/13520-MS .

Trebin, F.A., and Zadora, G.I., 1968. Experimental Study of the Effect of a Porous Media on Phase Changes in Gas Condensate Systems. Neft i Gaz 8, 37-40.

Udell, K.S., 1982. The Thermodynamics of Evaporation and Condensation in Porous Media. Society of Petroleum Engineers. doi:10.2118/10779-MS.

Varavei, A., 2009. Development of an Equation-of-State Thermal Flooding Simulator. PhD dissertation, The University of Texas at Austin, Austin, Texas.

Varavei, A., and Sepehrnoori, K., 2009. An EOS-Based Compositional Thermal Reservoir Simulator. Society of Petroleum Engineers. doi:10.2118/119154-MS.

Voskov, D., and Tchelepi, H. A., 2007. Compositional Space Parameterization for Flow Simulation. Society of Petroleum Engineers. doi:10.2118/106029-MS.

Voskov D.V., and Tchelepi H.A., 2008. Compositional Space Parameterization for Miscible Displacement Simulation. Transport in Porous Media, 75(1), 111-128.

Voskov D.V., and Tchelepi H.A., 2009a. Compositional Space Parameterization: Theory and Application for Immiscible Displacement. SPEJ, 14(3), 431- 440.

Voskov D.V., and Tchelepi H.A., 2009b. Compositional Space Parameterization: Multicontact Miscible Displacements and Extension to Multiple Phases. SPEJ, 14(3), 441- 449.

Voskov D.V., and Tchelepi H.A., 2009c. Tie-Simplex-Based Mathematical Framework for Thermodynamical Equilibrium Computation of Mixtures with an Arbitrary Number of Phases. Fluid Phase Equilibria, 283, 1-11.

Walsh, B.W., and Orr, F.M., 1990. Prediction of Miscible Flood Performance: the Effect of Dispersion on Composition Paths in Ternary Systems. In Situ 14, 19–47.

Wang, Y., and Orr, F.M., Jr., 1997. Analytical Calculation of Minimum Miscibility Pressure. Fluid Phase Equilibria, 139, 101–124.

Wang, P., Yotov, I., Wheeler, M., Arbogast, T., Dawson, C., Parashar, M., and Sepehrnoori, K., 1997. A New Generation EOS Compositional Reservoir Simulator: Part I - Formulation and Discretization. Society of Petroleum Engineers. doi:10.2118/37979-MS.

Wang, P. and Stenby, E.H., 1994. Non-Iterative Flash Calculation Algorithm in Compositional Reservoir Simulation. Fluid Phase Equilibria 95, 93-108.

Wang, Y., Yan, B., and Killough, J., 2013. Compositional Modeling of Tight Oil Using Dynamic Nanopore Properties. Society of Petroleum Engineers. doi:10.2118/166267-MS.

Wheeler, M.F., Arbogast, T., Bryant, S., Eaton, J., Qin, L., Peszynska, M., and Yotov, I., 1999. A Parallel Multiblock/Multidomain Approach for Reservoir Simulation. Society of Petroleum Engineers. doi:10.2118/51884-MS.

Whitson, C.H., and Michelsen, M.L., 1989. The Negative Flash. Fluid Phase Equilibria, 53, 51-71.

Young, L.C., and Stephenson, R.E., 1983. A Generalized Compositional Approach for Reservoir Simulation. Society of Petroleum Engineers. doi:10.2118/10516-PA.

Yuan, C., and Pope, G.A., 2012. A New Method to Model Relative Permeability in Compositional Simulators to Avoid Discontinuous Changes Caused by Phase-Identification Problems. SPEJ, 17(4): 1221-1230. doi:10.2118/142093-PA

Zarragoicoechea, G.J., and Kuz, V.A., 2004. Critical Shift of a Confined Fluid in a Nanopore. Fluid Phase Equilibria, 220(1), 7-9.

Zaydullin, R., Voskov, D., and Tchelepi H., 2013. Nonlinear Formulation Based on Equation-of-State Free Method for Compositional Flow Simulation. SPEJ 18, 2 (2013) 264-273, DOI: 10.2118/146989-PA.

Zhao, G.B., Adidharma, H., Towler, B., and Radosz, M., 2006. Using a Multiple-Mixing-Cell Model to Study Minimum Miscibility Pressure Controlled by Thermodynamic Equilibrium Tie Lines. Industrial and Engineering Chemistry Research, 45(23), 7913-7923.